

University of New Hampshire

University of New Hampshire Scholars' Repository

Doctoral Dissertations

Student Scholarship

Spring 1995

Reactions of a dimolybdenum cage complex with phosphorus and nitrogen nucleophiles and the synthesis and reactions of heterobimetallic cages

Haiying Yang

University of New Hampshire, Durham

Follow this and additional works at: <https://scholars.unh.edu/dissertation>

Recommended Citation

Yang, Haiying, "Reactions of a dimolybdenum cage complex with phosphorus and nitrogen nucleophiles and the synthesis and reactions of heterobimetallic cages" (1995). *Doctoral Dissertations*. 1852. <https://scholars.unh.edu/dissertation/1852>

This Dissertation is brought to you for free and open access by the Student Scholarship at University of New Hampshire Scholars' Repository. It has been accepted for inclusion in Doctoral Dissertations by an authorized administrator of University of New Hampshire Scholars' Repository. For more information, please contact Scholarly.Communication@unh.edu.

INFORMATION TO USERS

This manuscript has been reproduced from the microfilm master. UMI films the text directly from the original or copy submitted. Thus, some thesis and dissertation copies are in typewriter face, while others may be from any type of computer printer.

The quality of this reproduction is dependent upon the quality of the copy submitted. Broken or indistinct print, colored or poor quality illustrations and photographs, print bleedthrough, substandard margins, and improper alignment can adversely affect reproduction.

In the unlikely event that the author did not send UMI a complete manuscript and there are missing pages, these will be noted. Also, if unauthorized copyright material had to be removed, a note will indicate the deletion.

Oversize materials (e.g., maps, drawings, charts) are reproduced by sectioning the original, beginning at the upper left-hand corner and continuing from left to right in equal sections with small overlaps. Each original is also photographed in one exposure and is included in reduced form at the back of the book.

Photographs included in the original manuscript have been reproduced xerographically in this copy. Higher quality 6" x 9" black and white photographic prints are available for any photographs or illustrations appearing in this copy for an additional charge. Contact UMI directly to order.

UMI

A Bell & Howell Information Company
300 North Zeeb Road, Ann Arbor, MI 48106-1346 USA
313/761-4700 800/521-0600

REACTIONS OF A DIMOLYBDENUM CAGE COMPLEX
WITH PHOSPHORUS AND NITROGEN NUCLEOPHILES
AND THE SYNTHESIS AND REACTIONS OF
HETEROBIMETALLIC CAGES

By

HAIYING YANG

B. S., Zhengzhou University, P. R. C., 1982

M. S., Zhengzhou University, P. R. C., 1985

DISSERTATION

Submitted to the University of New Hampshire in Partial
Fulfillment of the Requirements for the Degree of

Doctor of Philosophy
in
Chemistry

May, 1995

UMI Number: 9528774

UMI Microform 9528774

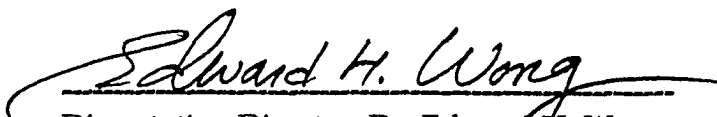
Copyright 1995, by UMI Company. All rights reserved.

**This microform edition is protected against unauthorized
copying under Title 17, United States Code.**


UMI

**300 North Zeeb Road
Ann Arbor, MI 48103**

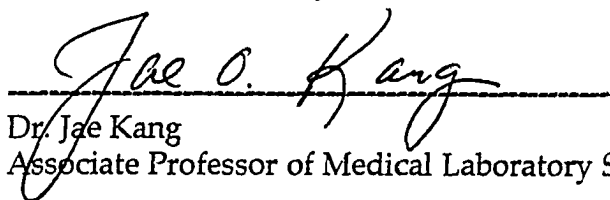
This dissertation has been examined and approved.



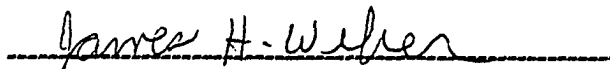
Dissertation Director, Dr. Edward H. Wong,
Professor of Chemistry



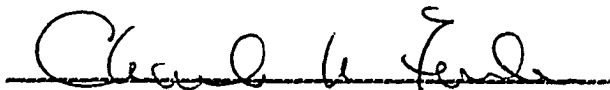
Dr. Kenneth K. Andersen,
Professor of Chemistry



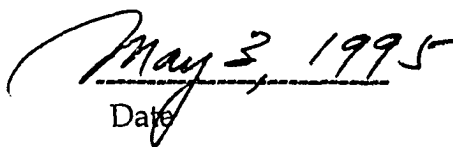
Dr. Jae Kang
Associate Professor of Medical Laboratory Science



Dr. James H. Weber
Professor of Chemistry



Dr. Charles K. Zercher
Assistant Professor of Chemistry



Date

DEDICATION

To the memory of my grandmother, Shuying Miao, for her love.
To my parents XiuLan and Yongli, my parents-in-law Baizing and Yongshun,
for their love and support.

ACKNOWLEDGEMENTS

I would like to thank Dr. Edward H. Wong, my research advisor, for his guidance, encouragement, patience and help. I must say Dr. Wong is a great professor and research advisor. The help that I received from the former member of the Wong group, X. Y. Sun, is greatly appreciated.

I would like to thank the staff of the Instrumentation Center at UNH for their assistance on this project, especially Ms. Kathleen Gallagher for her instruction in the use of NMR and friendship; Mr. Richard Sweet for fixing the instruments; Deanna Cardin and Nancy Cherim for analyzing countless samples for elemental analysis.

I would also like to thank all the professors and graduate students at the chemistry department, especially Dr. Tomellini for his help with the HPLC.

I would like to thank Jerry P. Jasinski, Roman Y. Pozdniakov, Richard Woudenberg at the Keene State College and A L. Rheingold, B E. Owens-Waltermire, B S. Haggerty at the University of Delaware for their solution of the solid-state x-ray crystal structures for this project.

Finally my deepest thanks go to my husband Rongliang Li, my daughters Yangzi and Kathie for their love and support.

TABLE OF CONTENTS

APPROVAL PAGE	ii
DEDICATION.....	iii
ACKNOWLEDGMENTS.....	iv
TABLE OF CONTENTS.....	v
LIST OF TABLES.....	viii
LIST OF FIGURES.....	ix
ABSTRACT.....	xii
INTRODUCTION.....	1
I. REACTIONS OF A DIMOLYBDENUM CYCLO-TETRAPHOSPHOXANE CAGE WITH PHOSPHORUS AND NITROGEN NUCLEOPHILES.....	7
Results and Discussion.....	9
1. Synthesis and Characterization of (CO) ₃ Mo[ⁱ Pr ₂ NPO] ₄ Mo(CO) ₂ PPh ₂ R (R=Ph, Me, H).....	9
2. Synthesis and Characterization of (CO) ₃ (L)Mo[ⁱ Pr ₂ NPO] ₄ Mo(CO) ₃ P(OMe) ₃ [L=CO, P(OMe) ₃].....	24
3. Synthesis and Characterization of (CO) ₃ Mo[ⁱ Pr ₂ NPO] ₄ Mo(CO) ₂ P(OMe) ₃	33
4. Synthesis and Characterization of (CO) ₃ (L)Mo[ⁱ Pr ₂ NPO] ₄ Mo(CO) ₃ PPh ₂ H (L=CO, PPh ₂ H).....	38
5. Synthesis and Characterization of (CO) ₃ Mo[ⁱ Pr ₂ NPO] ₄ Mo(CO) ₂ (L) (L=Py, CO).....	41

6. Relation of Reaction Rates to Steric and Electronic Factors.....	51
Conclusions and Suggestions for Future Work.....	55
Experimental.....	57
II. DEMETALLATION OF A DIMOLYBDENUM CYCLO-TETRAPHOSPHOXANE CAGE COMPLEX AND THE SYNTHESIS OF HETEROBIMETALLIC CAGES AND THEIR CHEMICAL REACTIONS.....	66
Results and Discussion.....	70
1. Synthesis and Characterization of the Monometallic Cage Precursor (CO) ₄ Mo[ⁱ Pr ₂ NPO] ₄	70
2. Synthesis and Characterization of Heterobimetallic Complexes.....	77
2.1 (CO) ₄ Mo[ⁱ Pr ₂ NPO] ₄ Cr(CO) ₄	77
2.2 (CO) ₄ Mo[ⁱ Pr ₂ NPO] ₄ Fe(CO) ₃	78
2.3 (CO) ₄ Mo[ⁱ Pr ₂ NPO] ₄ Cu(CH ₃ CN) ₂ BF ₄	79
2.4 (CO) ₄ Mo[ⁱ Pr ₂ NPO] ₄ AgNO ₃	81
2.5 (CO) ₄ Mo[ⁱ Pr ₂ NPO] ₄ PtCl ₂	83
2.6 (CO) ₄ Mo[ⁱ Pr ₂ NPO] ₄ NiBr ₂	84
2.7 (CO) ₄ Mo[ⁱ Pr ₂ NPO] ₄ Ni(CO) ₂	87
2.8 (CO) ₄ Mo[ⁱ Pr ₂ NPO] ₄ NiX ₂ (X=Cl, I).....	88
2.9 (CO) ₄ Mo[ⁱ Pr ₂ NPO] ₄ PdBr ₂	90
2.10 (CO) ₃ Mo[ⁱ Pr ₂ NPO] ₅ PdCl ₂	94
2.11 (CO) ₃ Mo[ⁱ Pr ₂ NPO] ₅ PdBr ₂	95

3. Structures of $(\text{CO})_4\text{Mo}[\text{iPr}_2\text{NPO}]_4\text{MBr}_2$ (M=Ni, Pd).....	99
4. Reactions of $(\text{CO})_4\text{Mo}[\text{iPr}_2\text{NPO}]_4$ with Alcohols.....	102
5. Miscellaneous Reactions.....	118
6. Evidence for Intracage Influences Due to the Heterometal.....	122
6.1 Comparison of the FT-IR Spectral Data of the $\text{Mo}(\text{CO})_4$ Moiety.....	122
6.2 Comparison of the ^{13}C NMR Chemical Shifts of the $\text{Mo}(\text{CO})_4$ Moiety.....	125
6.3 Comparison of the X-ray Structural Data of the Heterobimetallic Complexes.....	127
7. Expansion of the P_4O_4 Cage to a P_5O_5 Cage.....	129
Conclusions and Suggestions for Future Work.....	133
Experimental.....	136
LIST OF REFERENCES.....	146
APPENDICES.....	152
A. COMPOUND NUMBER ASSIGNMENTS.....	153
B. SELECTED SPECTRA.....	156

LIST OF TABLES

Table I.	$^{31}\text{P}\{^1\text{H}\}$ NMR Data for the Complexes	12
Table II.	Selected Infrared Absorption for the Complexes	14
Table III.	Selected X-ray Structure Data for 2	18
Table IV.	Selected X-ray Structure Data for 7	35
Table V.	Selected X-ray Structure Data for 11	47
Table VI.	Comparison of the Reaction Rates with Ligands Cone Angle	53
Table VII.	Comparison of the Reaction Rates with the Electronic Parameters of the Ligands	53
Table VIII.	Crystal Data for Complexes 2 , 7 and 11	64
Table IX.	Selected X-ray Structure Data for 14	75
Table X.	Selected X-ray Structure Data for 21	86
Table XI.	Selected X-ray Structure Data for 25	93
Table XII.	Selected X-ray Structure Data for 28	109
Table XIII.	^{31}P NMR Data for Complexes	111
Table XIV.	^{13}C NMR Data for Complexes	113
Table XV.	^1H NMR Data for Complexes	115
Table XVI.	IR Spectra Data for the Complexes	117
Table XVII.	The Carbonyl Stretching Frequencies (A_1 mode) in Heterobimetallic Cages	123
Table XVIII.	^{13}C NMR Chemical Shifts for the Carbonyl Resonances of the Complexes	125
Table XIX.	Selected Bond Lengths for Several Complexes	128

LIST OF FIGURES

Figure 1.	Molecular structure of $(\text{CO})_8\text{Mo}_2[\text{iPr}_2\text{NPO}]_4$	2
Figure 2.	$^{31}\text{P}\{^1\text{H}\}$ NMR spectrum of complex 2	10
Figure 3.	IR spectrum in the ν_{CO} region for $\text{cis}-(\text{CO})_4\text{Mo}[\text{P}(\text{OPh}_3)]_2$	15
Figure 4.	CO stretches for $\text{cis}-(\text{CO})_4\text{MoP}_2$	15
Figure 5.	IR spectra in the ν_{CO} region for complexes 1, 2, 3, and 4	16
Figure 6.	Molecular structure of complex 2	17
Figure 7.	Core geometry of complex 2	17
Figure 8.	Structure of $[\text{C}_5\text{H}_5\text{Fe}(\text{PF}_2)_2\text{NCH}_3]_2$	20
Figure 9.	2D COSY $^{31}\text{P}\{^1\text{H}\}$ NMR spectrum of complex 2	23
Figure 10.	Proposed structures for isomers of 5	25
Figure 11.	2D COSY $^{31}\text{P}\{^1\text{H}\}$ NMR spectrum of 5	27
Figure 12.	^{31}P NMR spectrum of 5 (selective methine proton decoupled)	28
Figure 13.	^{31}P NMR spectrum of 5 (selective trimethyl phosphite proton decoupled)	28
Figure 14.	^{31}P NMR spectrum of 5 (full decoupled)	29
Figure 15.	Proposed structures for isomers of 6	29
Figure 16.	2D COSY ^{31}P NMR spectrum of 6	30
Figure 17.	^{31}P NMR spectrum of 6 (selective methine proton decoupled)	31
Figure 18.	^{31}P NMR spectrum of 6 (full decoupled)	31

Figure 19.	HPLC traces for complexes 5 and 6	32
Figure 20.	Molecular structure of complex 7	34
Figure 21.	Core geometry of complex 7	35
Figure 22.	^1H NMR spectrum of (CO) ₂ [P(OMe) ₃]Mo[ⁱ Pr ₂ NPO] ₄ Mo(CO) ₂ [P(OMe) ₃]	38
Figure 23.	Proposed structures for 8 and 9	40
Figure 24.	$^{31}\text{P}\{^1\text{H}\}$ NMR spectra of 10 in CDCl ₃	43
Figure 25.	^1H NMR spectra of 10 and 11	44
Figure 26.	Molecular structure of complex 11	46
Figure 27.	Core geometry of complex 11	46
Figure 28.	Comparison of the phosphido-bridge structure data for complexes 2, 7, 11	50
Figure 29.	$^{31}\text{P}\{^1\text{H}\}$ NMR spectrum for 14	73
Figure 30.	Molecular structure of complex 14	74
Figure 31.	Three conformations for the MoP ₄ O ₄ core	76
Figure 32.	$^{31}\text{P}\{^1\text{H}\}$ NMR spectrum of 19	82
Figure 33.	$^{31}\text{P}\{^1\text{H}\}$ NMR spectrum of 20	84
Figure 34.	Molecular structure of complex 21	85
Figure 35.	The carbonyl regions of the IR spectra for Mo/Ni complexes	89
Figure 36.	Molecular structure of complex 25	92
Figure 37.	IR spectra of the carbonyl regions for 25, 26, 27	96
Figure 38.	$^{13}\text{C}\{^1\text{H}\}$ NMR spectra for 25, 26	97
Figure 39.	$^{31}\text{P}\{^1\text{H}\}$ NMR spectra for 25, 26	98
Figure 40.	Selected structural data for 14, 21, 25	101
Figure 41.	^{31}P NMR spectra of 28	104
Figure 42.	^1H NMR spectrum of 28	105

Figure 43.	^{13}C NMR spectra of 28	106
Figure 44.	Molecular structure of complex 28	108
Figure 45.	Orbital overlap in M-CO bonding	124
Figure 46.	A correlation of the ^{13}C NMR chemical shifts vs the IR frequencies(A_1 mode) for the carbonyl groups in $\text{cis}-(\text{CO})_4\text{MoP}_2$	127

ABSTRACT

REACTIONS OF A DIMOLYBDENUM CAGE COMPLEX WITH PHOSPHORUS AND NITROGEN NUCLEOPHILES AND THE SYNTHESIS AND REACTIONS OF HETEROBIMETALLIC CAGES

By

Haiying Yang

University of New Hampshire, May, 1995

The reactions of the dimolybdenum cage complex $\text{Mo}(\text{CO})_4\text{-}[\text{iPr}_2\text{NPO}]_4\text{Mo}(\text{CO})_4^*$ with phosphorus and nitrogen nucleophiles were studied. This dimolybdenum cage complex reacted with tertiary phosphines of the type PPh_2R ($\text{R}=\text{Ph}, \text{Me}, \text{H}$) in refluxing toluene. In each case, incorporation of a single phosphine led to the loss of three carbonyls to form orange complexes of the type $\text{Mo}(\text{CO})_3[\text{iPr}_2\text{NPO}]_4\text{Mo}(\text{CO})_2\text{PPh}_2\text{R}$ (2, 3, 4). The X-ray molecular structure of **2** has been determined. This revealed that a cage P-O-P bond has been cleaved near the substitution site with the resulting phosphinito oxygen replacing a second CO. Additionally, the phosphido group generated displaced a third CO at the other Mo center to bridge the two metals which are now within bonding distance of each other. Under milder conditions, reactions using phosphite yielded both mono- and disubstituted products $\text{Mo}(\text{CO})_4[\text{iPr}_2\text{NPO}]_4\text{Mo}(\text{CO})_3\text{P}(\text{OMe})_3$ or $\text{Mo}(\text{CO})_3\text{P}(\text{OMe})_3\text{-}[\text{iPr}_2\text{NPO}]_4\text{Mo}(\text{CO})_3\text{P}(\text{OMe})_3$ with the original core structure intact. Both

* See Appendix A for the structure.

products were mixtures of diastereomers and can be transformed to orange $\text{Mo}(\text{CO})_3[\text{iPr}_2\text{NPO}]_4\text{Mo}(\text{CO})_2\text{P}(\text{OMe})_3$.

Treatment of the mixed-valent $\text{Mo}(\text{CO})_4[\text{iPr}_2\text{NPO}]_4\text{Mo}(\text{CO})_2\text{I}_2$ cage complex with sodium dimethyldithiocarbamate selectively removed the divalent molybdenum vertex to give the metalla-ligand $\text{Mo}(\text{CO})_4[\text{iPr}_2\text{NPO}]_4$ (**14**) via an orange intermediate $\text{Mo}(\text{CO})_4[\text{iPr}_2\text{NPO}]_4\text{Mo}(\text{CO})_2(\text{S}_2\text{CNMe}_2)_2$. The metalla-ligand has been characterized spectrally and by X-ray crystallography. It has been used as a precursor to assemble novel heterobimetallic cage complexes of the type $\text{Mo}(\text{CO})_4[\text{iPr}_2\text{NPO}]_4\text{ML}_n$ where ML_n can be $\text{Cr}(\text{CO})_4$, $\text{Fe}(\text{CO})_3$, $\text{Cu}(\text{MeCN})_2\text{BF}_4$, AgNO_3 , PtCl_2 , NiBr_2 and PdBr_2 , or the type $\text{Mo}(\text{CO})_3[\text{iPr}_2\text{NPO}]_5\text{ML}_n$ where ML_n can be PdCl_2 , PdBr_2 . All these heterobimetallic cage complexes have been characterized by elemental analyses and spectral data. In addition, X-ray structures of the heterobimetallic cage complexes $\text{Mo}(\text{CO})_4[\text{iPr}_2\text{NPO}]_4\text{MBr}_2$ [$\text{M}=\text{Ni}$ (**21**), Pd (**25**)] have been determined. Comparison of the well-resolved A_1 carbonyl stretching frequency and the ^{13}C NMR chemical shift of the cis- $\text{Mo}(\text{CO})_4$ moiety in $\text{Mo}(\text{CO})_4[\text{iPr}_2\text{NPO}]_4\text{ML}_n$ and also the X-ray structures of **14**, **21**, **25** suggest a transmission of the increasing electron demand of the second cage metal to the molybdenum vertex.

INTRODUCTION

Transition metal complexes with phosphine ligands have proven to be useful and versatile catalysts in homogeneous reactions^[1]. Mono-phosphine ligands are used to induce chemistry at metal centers through steric and electronic influences. Chelating phosphines are even more successful in this role, and the use of polyphosphine ligands (i. e., those with several P donor sites) is increasingly important^[2].

Recently, binuclear metal complexes, particularly those with bridging phosphine ligands, have begun to attract interest because of their potentially reactive features. The interest in binuclear complexes arose because of anticipation that they can allow for increased versatility in catalyst design^[3]. Complexes with two metal atoms can have several advantages over a catalyst containing only a single metal. For example, the presence of two metal atoms may facilitate multielectron redox reactions which could not be handled by only a single metal atom.

The first bimetallic cage complex of 1,3,5,7-tetraoxa-2,4,6,8-tetraphosphorinane [RPO]₄ with the familiar adamantane structure common to P₄O₆ and P₄O₁₀ was reported in 1983^[4]. It contains the novel cyclic tetramer [RNPO]₄ in a boat-boat conformation serving as a tetradentate ligand chelating two metals as shown in **Figure 1**:

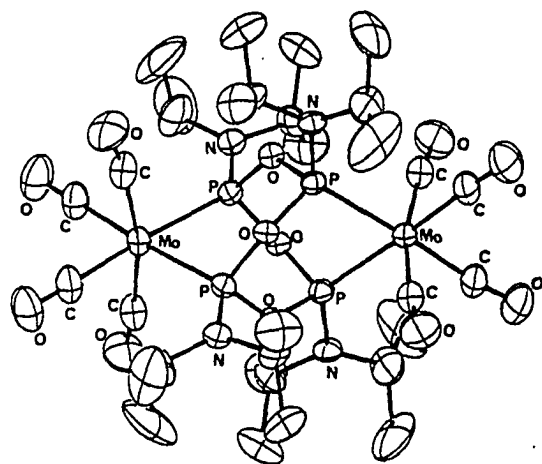
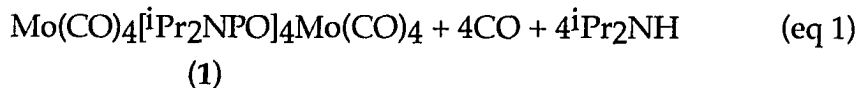
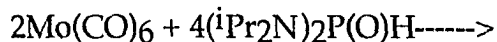


Figure 1. Molecular structure of Cage complex $\text{Mo(CO)}_4[\text{}^i\text{Pr}_2\text{NPO}]_4\text{Mo(CO)}_4$

Before this work, the coordination chemistry of the polydentate ligand $[\text{RPO}]_n$ was not known. The first report of a cyclic phosphoxane $[\text{RPO}]_3$ (where $\text{R}=\text{OEt}$, OBu , and Et_2N) appeared in 1967^[5], but the structures of these compounds were not fully identified. In 1980, Niecke^[6] isolated and characterized the cyclic trimer $[\text{}^i\text{Pr}_2\text{NPO}]_3$. In 1986, Chasar^[7] and co-workers synthesized and identified both $[\text{RPO}]_3$ and $[\text{RPO}]_2$ where R is 2, 6-di-tert-butyl-4-methylphenoxy. Compared to the familiar cyclic condensed metaphosphates and thiophosphates of phosphorus (V), phosphorus-oxygen heterocycles or cyclophosphoxanes of phosphorus (III) are thus relatively rare. These trivalent phosphorus heterocycles can provide multiple donor sites and should have useful coordination chemistry as polydentate ligands leading to polycyclic and cage complexes.

The dimolybdenum cage complex is the first example of a cyclotetraphosphoxane ligand that chelates two metals. It contains two mutually-orthogonal $\text{Mo(CO)}_4\text{P}_2$ centers which are subjected to considerable steric buttressing due to the rigid polycyclic structure^[4]. Complex 1 was

synthesized by the reaction of Mo(CO)₆ and (iPr₂N)₂P(O)H:



Since the serendipitous synthesis of this Mo₂P₄O₄ cage complex **1** in 1983, Wong's group has been studying the mechanism of its formation as well as coming up with alternate methods of preparing other members of this family of compounds. Some reports on the synthesis of phosphoxane complexes have appeared and the reactivity studies of complex **1** were also explored^[8-13]. Prior to the work reported here, the reactivity studies of the parent complex have been limited to halogenation and redox investigations. The substitution chemistry at Mo(CO)₄ with neutral Group V ligands was unexplored. Only one example of a heterobimetallic cage complex of this type was known^[9].

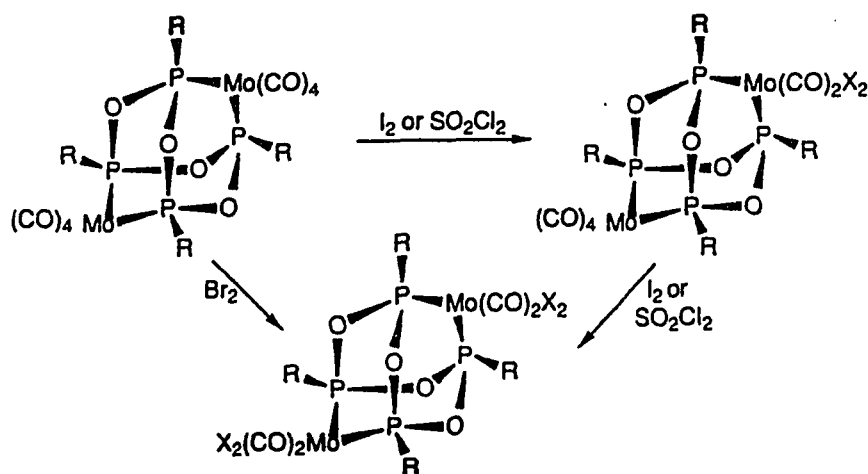
Phosphine substituents at all four cage phosphorus vertices can influence each of the metal sites. For example, the trans CO-Mo-CO angle is compressed to only 167°^[8] due to the diisopropylamino groups on the two remote P's^{**}. Halogenation reactions have already been shown to produce 16-electron trigonal prismatic MoX₂(CO)₂P₂ vertices, possibly as a result of this unique cage environment^[9].

We are interested in the following aspects of cage chemistry: (I) How does the presence of a very rigid and relatively bulky cage ligand affect the inorganic and organometallic chemistry at the Mo⁰(CO)₄ centers? (II) Can

^{**} See page 135.

heterobimetallic cage complexes be synthesized? (III) Is there any intra-cage "communication" or interaction between the metal centers?

Several interesting aspects of cage halogenation chemistry have already been discovered for the parent cage. This is a two-step process, giving $(\text{CO})_4\text{Mo}[\text{iPr}_2\text{NPO}]_4\text{Mo}(\text{CO})_2\text{X}_2$ and then $\text{Mo}(\text{CO})_2\text{X}_2[\text{iPr}_2\text{NPO}]_4\text{Mo}(\text{CO})_2\text{X}_2$ products (Scheme I):



Scheme I

The Mo(II) products are six-coordinate rather than the usual seven-coordinate for non-cage analogues. Seven-coordination is expected for the molybdenum-substituted halocarbonyls if we assume that the effective atomic number rule applies to these complexes. By Kepert's calculations^[14] there are three possible geometries with lowest energies for seven coordinated complexes: the pentagonal bipyramid, the mono-capped octahedron and the mono-capped trigonal prism. For $\text{M}(\text{CO})_3(\text{PR}_3)_2\text{X}_2$ complexes, often stereochemically nonrigid seven-coordinated complexes are isolated^[15]. For example, $\text{Mo}(\text{CO})_3\text{I}_2(\text{dpm})$ [dpm=bis(diphenylphosphino)-methane] has a mono-capped trigonal prism geometry^[16], and

$\text{Mo}(\text{CO})_3\text{I}_2(\text{Ph}_2\text{POPPh}_2)$ adopted a pentagonal bipyramidal structure^[17]. The solution and solid state geometries of the cage halogenation products are unique. In addition, all halogenated cage products are low-spin d^4 and diamagnetic.

The new cage chemistry we shall investigate includes substitution chemistry at $\text{Mo}(\text{CO})_4$ with neutral Group V ligands. Nucleophilic substitutions at this center may also generate unusual coordination chemistry due to cage structure constraints. Tertiary phosphines and phosphites can substitute for one or more of the remaining 4 CO's. The types, geometries, distribution of isomeric products, as well as influence of reaction at one cage metal on the other when compared to normal $\text{Mo}(\text{CO})_4(\text{diphosphine})$ products will reveal any unique features for the cage reactions. Pyridine, acetonitrile and benzonitrile can potentially substitute CO's also.

While attempted synthesis of heterobimetallic cages from the parent cage failed, we reasoned that the Mo^{II} center in the mixed-valent complex $(\text{CO})_4\text{Mo}[\text{iPr}_2\text{NPO}]_4\text{Mo}(\text{CO})_2\text{I}_2$ may provide a potential demetallation site. Dithiocarbamate ion has been found to coordinate to a transition metal both as a bidentate or monodentate ligand^[18,19]. It is a potential candidate for use in removing of the Mo^{II} vertex to give the monometallic cage precursor complex $(\text{CO})_4\text{Mo}[\text{iPr}_2\text{NPO}]_4$. We could then synthesize a series of heterobimetallic cage complexes from this metallo ligand by inserting the second metal into the vacated site.

Since it was known that cage halogenation is a two-step process,

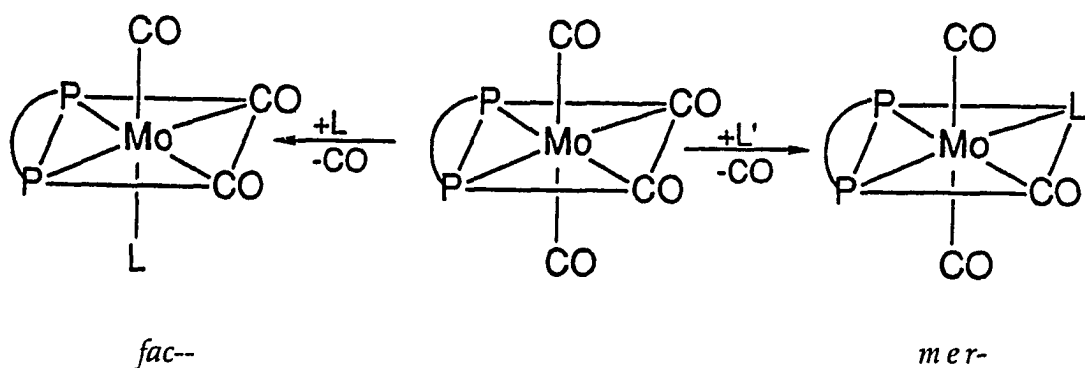
oxidation at one metal makes oxidation at the other more difficult. A series of the heterobimetallic cage complexes with rigidly constrained pairs of metal vertices should be especially interesting for the study of intracage metal-metal interactions. Comparison of the spectral properties of the conserved $\text{Mo}(\text{CO})_4$ moiety in these heterobimetallic cage complexes will give valuable information concerning such interactions.

The first chapter will describe the substitution reactions of the cage complex **1** with phosphine and phosphite ligands, pyridine, acetonitrile and benzonitrile, and the characterization of the products. These results revealed an unusual intramolecular P-O-P bond cleavage with extensive rearrangement of the core structure and formal oxidative addition to both metals, all direct consequences of the replacement of a carbonyl by a single phosphorus or nitrogen donor. Furthermore, the electronic and steric effects of the phosphine ligands were investigated.

In the second chapter, the demetallation of a dimolybdenum cyclotetraphosphoxane cage complex $(\text{CO})_4\text{Mo}[\text{iPr}_2\text{NPO}]_4\text{Mo}(\text{CO})_2\text{I}_2$ by reaction with dithiocarbamates to give the metalla-ligand $(\text{CO})_4\text{Mo}[\text{iPr}_2\text{NPO}]_4$ will be described. The nucleophilic attack by primary alcohols on the precursor and the characterization of the products will be related. The use of this metalla-ligand as a precursor for synthesizing of heterobimetallic cage complexes will also be described. These heterobimetallic cage complexes are among the first examples of a cyclotetraphosphoxane ligand that chelates two different metals. Finally, this chapter will also present a study of the intracage influence between the cage metal sites.

CHAPTER I
REACTIONS OF A DIMOLYBDENUM
CYCLO-TETRAPHOSPHOXANE CAGE WITH PHOSPHORUS
AND NITROGEN NUCLEOPHILES

Nucleophilic substitution reactions at Group VI metal carbonyls have been extensively studied[20]. For tetracarbonylmetal diphosphine chelate complexes like $\text{Mo}(\text{CO})_4(\text{diphos})$, CO substitution reactions with phosphines, phosphites and amines usually yield either axial-substituted *fac*- or equatorial-substituted *mer*- $\text{Mo}(\text{CO})_3\text{L}$ products depending on the ligand used (Scheme II)[21]:



Scheme II

Ligand and carbonyl π -bonding effects are evidently of primary importance for these type of complexes. Thus, the carbonyl group *trans* to the more strongly π -accepting ligand carbonyl is expected to be more labile and more readily replaced, and *fac*- products are anticipated. When considering steric effects, the *mer*- products should be expected because it reduces crowding at a face of the octahedron with the more sterically demanding ligands.

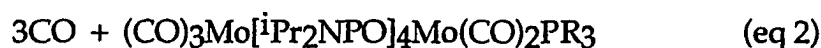
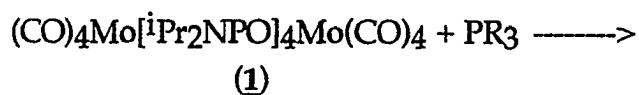
In this chapter, we report the synthesis of the bimetallic cage complexes of the form $(\text{CO})_4\text{Mo}[\text{iPr}_2\text{NPO}]_4\text{Mo}(\text{CO})_3\text{L}$ and $(\text{CO})_3\text{LMo}[\text{iPr}_2\text{NPO}]_4\text{Mo}(\text{CO})_3\text{L}$ where L is one of several phosphines and the complexes $(\text{CO})_3\text{Mo}[\text{iPr}_2\text{NPO}]_4\text{Mo}(\text{CO})_2\text{L}'$ where L' is a phosphine, pyridine or carbonyl ligand. Spectroscopic characterization of these complexes is

reported. Crystallographic investigations of the complexes where L = PPh₃, P(OMe)₃ and CO are also described.

RESULTS AND DISCUSSION

1. Synthesis and Characterization of (CO)₃Mo[iPr₂NPO]₄Mo(CO)₂PPh₂R (R=Ph, Me, H)

Complexes (CO)₃Mo[iPr₂NPO]₄Mo(CO)₂PPh₂R (R=Ph, Me, H) were synthesized by the reactions of triphenylphosphine, diphenylmethylphosphine, and diphenylphosphine with the dimolybdenum cage complex (CO)₄Mo[iPr₂NPO]₄Mo(CO)₄ **1** in refluxing toluene. The equation representing the preparations of these complexes is shown below.



The yields of complexes **2**, **3**, **4** in the reactions above were 40 (isolated yield from **1**), 80 and 80 percent, respectively.

The reactions were monitored by TLC. In each case, at the beginning there were several spots, but after 24 hours, the starting material was completely gone, and only one orange-colored spot showed as product. The reaction solutions were clear red. By routine column chromatography and recrystallization the pure orange-colored products were isolated. These orange compounds were not very soluble in hexane and so were recrystallized from it. Each of the complexes was characterized by ³¹P, ¹H, ¹³C

NMR , IR and elemental analyses.

^{31}P NMR can serve as an important analytical tool for solution structure determination. In addition, P coupling constants provide important information on the nature of bonding and structure in molecules[22]. Compounds that contain two or more coupled phosphorus atoms exhibit very characteristic coupling patterns in the completely proton-decoupled ^{31}P spectra. When this type of information is used in conjunction with other NMR data, the structures of polyphosphorus compounds are often readily elucidated[23].

Compounds 2, 3, 4 have similar ^{31}P NMR, IR spectra. The one- and two-dimensional ^{31}P and ^1H NMR spectra of the product showed that only one attacking phosphine ligand was incorporated even in the presence of excess phosphine and prolonged reaction times. The D_{2d} symmetry of the parent cage is complexly lost upon formation of the orange complexes, since in each case five distinct resonances can be seen(Figure 2):

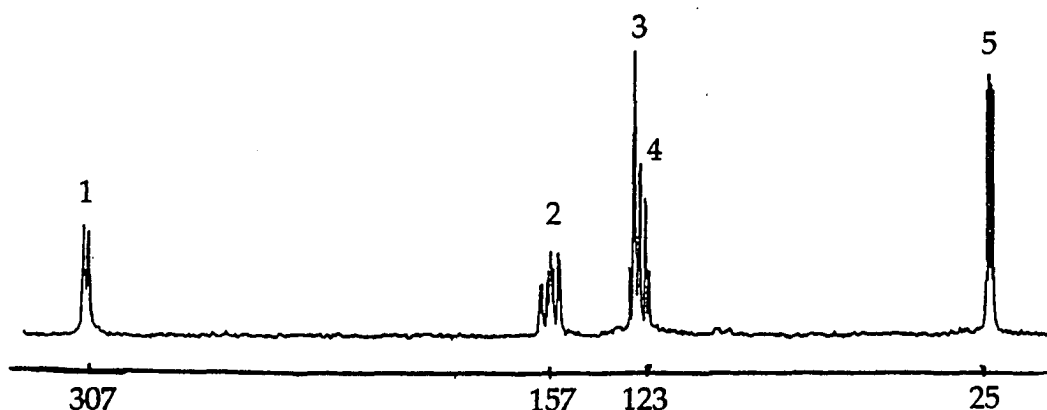


Figure 2. $^{31}\text{P}\{^1\text{H}\}$ NMR spectrum of complex 2

Significantly, one phosphorus (P1) has a chemical shift far downfield (305-307 ppm), and its position is essentially independent of the nature of the entering ligand. This chemical shift is not consistent with Mo-coordinated tertiary phosphines or phosphites, but is in the region of phosphonium cations or phosphido ligands[24]. From literature[25], we know that the two-bond phosphorus-phosphorus coupling constant between the *trans* phosphorus atoms, $^2J_{(P,P)_{trans}}$, should be much greater than $^2J_{(P,P)_{cis}}$. Comparing similar coupling constants, $^2J_{(P,P)}$, ranged 25-53 Hz between the entering phosphine ligands and the cage P's in complexes 2, 3, 4 (Table I), though it is hard to tell whether an equatorial or axial CO has been substituted. Also, from the IR spectra, we know that the *cis*-Mo(CO)₄P₂ coordination sphere at the original cage no longer exists because all of the orange products exhibit metal carbonyl stretches below 2000 cm⁻¹, with four or five well-resolved bands between 1850 and 1980 cm⁻¹ that indicate low symmetry of the products (Table II):

Table I: $^{31}\text{P}\{^1\text{H}\}$ NMR Data for the Complexes

Complex	Chemical Shift, ppm [J, Hz]
1	150.1(s)
2	AJMNX 307.5, 156.9, 124.3, 123.3, 24.9 [J _{AJ} = J _{AN} = 14.7, J _{AM} = 19.1, J _{AX} = 49.8, J _{JM} = 77.7, J _{JN} = 126.0, J _{JX} = 24.9, J _{MN} = 36.7 Hz]
3	AJMNX 305.5, 156.9, 129.3, 125.4, 15.3 [J _{AJ} = 14.7, J _{AN} = 11.7, J _{AM} = 17.6, J _{AX} = 52.8, J _{JM} = 79.1, J _{JN} = 129.0, J _{JX} = 26.4, J _{MN} = 38.1 Hz]
4	AJMNX 305.9, 154.9, 128.8, 127.1, 23.3 [J _{AJ} = J _{AM} = 14.7, J _{AN} = 11.7, J _{AX} = 52.8, J _{JM} = 90.9, J _{JN} = 129.0, J _{JX} = 29.3, J _{MN} = 38.1 Hz]
7	ALMNX 306.8 156.9, 153.7, 149.8, 123.9 [J _{NX} = 38.1, other J's not obtained]
10	AMXY 295.3, 150.7, 134.7, 128.1 [J _{AM} = 14.7, J _{AX} = 12.2, J _{AY} = 17.1, J _{MX} = 125.7, J _{MY} = 80.6, J _{XY} = 36.6 Hz]
11	AMXY 306.3, 149.8, 131.6, 121.4 [J _{AM} = 15.4, J _{AX} = 24.2, J _{AY} = 11.0, J _{MX} = 101.1, J _{MY} = 127.4, J _{XY} = 37.4 Hz]
5	AMNX ₂ 180.0, 164.0, 155.6, 148.2 [J _{AM}

		= 187.1, $J_{AN} = 41.0$, $J_{MN} = 47.5$, $J_{MX} = 10.5$, $J_{NX} = 6.7$ Hz]
	AM ₂ NX	166.9, 155.0, 151.2, 148.2 [J_{AM} = 45.1, $J_{MN} = 10.5$, $J_{MX} = 6.7$, $J_{NX} =$ 48.3 Hz]
6	AMX	179.3, 159.8, 151.6 [$J_{AM} = 185.5$, $J_{AX} = 40.9$, $J_{MX} = 51.1$ Hz]
	AMNX ₂ Y	178.6, 164.7, 158.8, ≈151.1, ≈151.1 [$J_{AN} = 187.1$ Hz, other J's not obtained]
	AMNX ₂ Y	178.1, 163.8, 162.0, ≈153.5, ≈153.5 [$J_{AN} = 190.0$ Hz, other J's not obtained]
	AXY	165.8, ≈151.6, ≈151.6 [J's not obtained]
8	A ₂ M ₂ X	157.1, 149.6, 12.9 [$J_{AM} = 7.0$, $J_{AX} = 32.8$, $J_{MX} = 0$ Hz]
9	A ₂ X	157.3, 13.5 [$J_{AX} = 34.2$ Hz]

^a In CDCl₃ solution.

Table II. Selected Infrared Absorptions for the Complexes

Complex	CO region, cm ⁻¹	POP region, cm ⁻¹
1	2015, 1923, 1906, 1887	875, 849, 809
2	1977, 1925, 1904, 1884, 1854	870, 849, 832, 800
3	1975, 1917, 1896, 1853	875, 845, 805
4	1977, 1921, 1895, 1856	874, 856, 826, 805
7	1979, 1925, 1889, 1856	870, 843, 834, 800
10	1973, 1915, 1889, 1874, 1851	875, 839, 800
11	2011, 1983, 1944, 1921, 1917, 1909, 1903, 1893	877, 847, 810
5	2003, 1988, 1975, 1937, 1916, 1900(sh), 1887	866, 845
6	1985, 1965, 1920(sh), 1877(bd), 1860(sh)	867, 846
8	2013, 1962, 1941, 1927, 1905, 1886, 1861	864, 832
9	1952, 1860	864, 833

^a KBr pellets, Perkin-Elmer 283B Spectrophotometer.

The species *cis*-Mo(CO)₄P₂ has C_{2v} symmetry, so four bands are expected in the CO region of its IR spectrum (Figure 3)^[26]. These four bands are attributed to the four possible CO vibrations depicted in Figure 4:

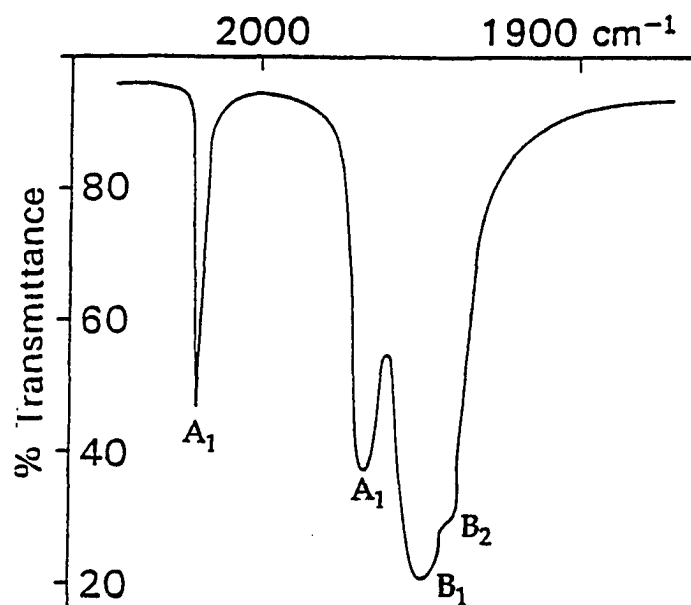


Figure 3. IR spectrum in the ν_{CO} region for $\text{cis}-(\text{CO})_4\text{Mo}[\text{P}(\text{OPh})_3]_2$

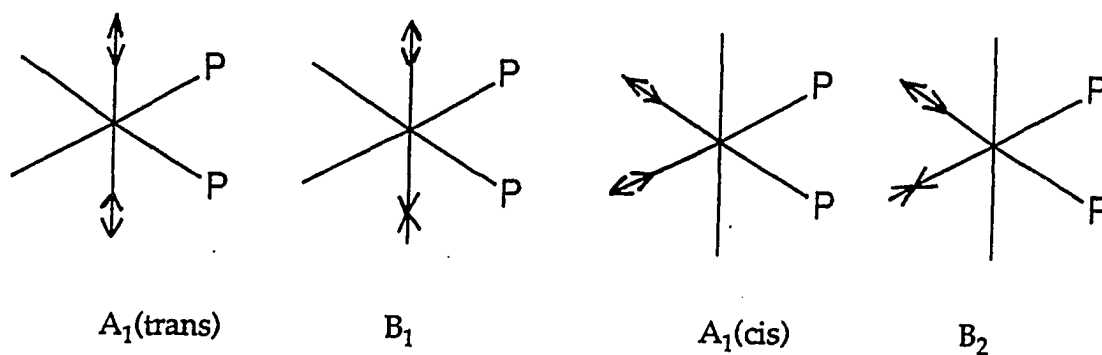


Figure 4. CO Stretches for $\text{cis}-(\text{CO})_4\text{MoP}_2$

The band above 2000 cm^{-1} is due to the $A_1(\text{trans})$ stretch. The bands below 2000 cm^{-1} are attributed to the B_1 , B_2 and $A_1(\text{cis})$ modes. Comparing the IR spectra of the products 2, 3, 4 with the IR spectrum of the original cage 1 (Figure 5), it is clear that the A_1 band at 2014 cm^{-1} had disappeared:

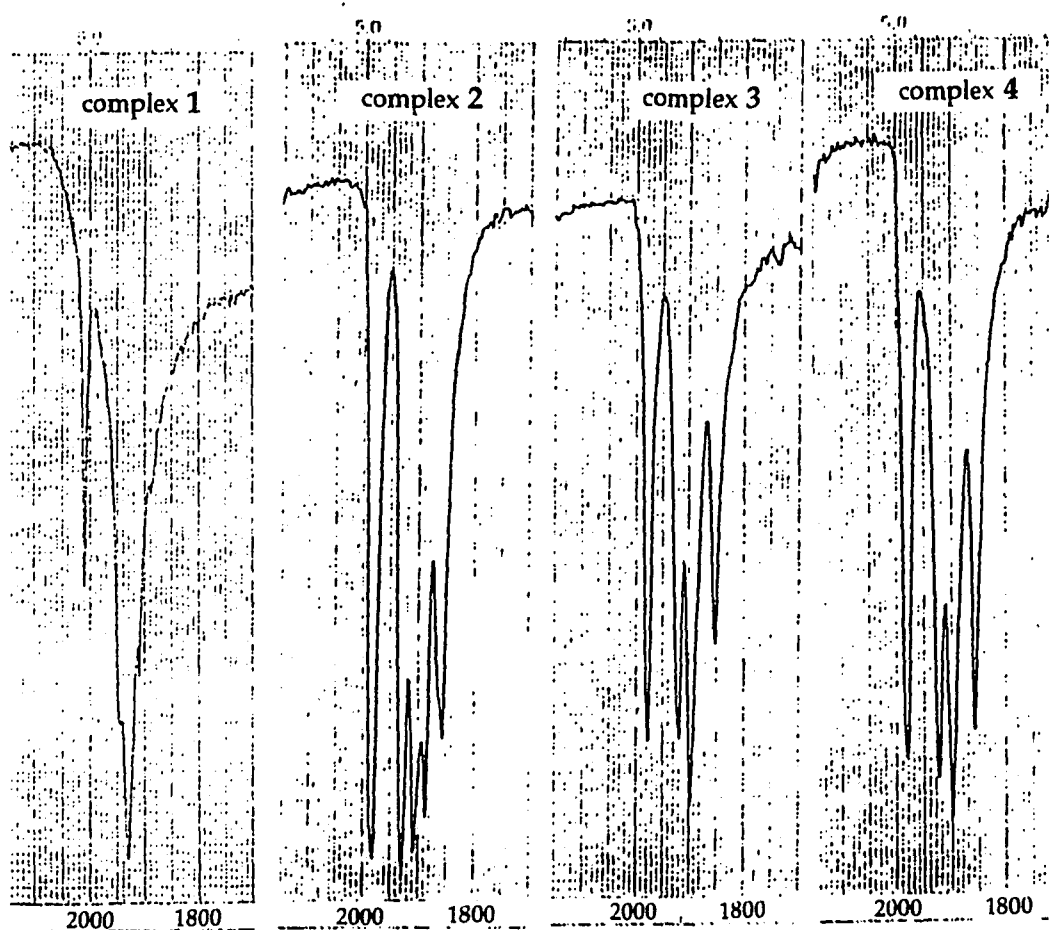


Figure 5. IR spectra in the ν_{CO} region for complexes 1, 2, 3 and 4

Thus, both the IR and NMR spectra gave us the first hint that the product may have a novel structure and that the cage structure was disrupted substantially upon CO replacement. Later the X-ray structure of complex 2 confirmed that the $\text{cis-Mo(CO)}_4\text{P}_2$ coordination spheres at both metal sites are changed. The elemental analyses are fully consistent with the structure (Figures 6 and 7):

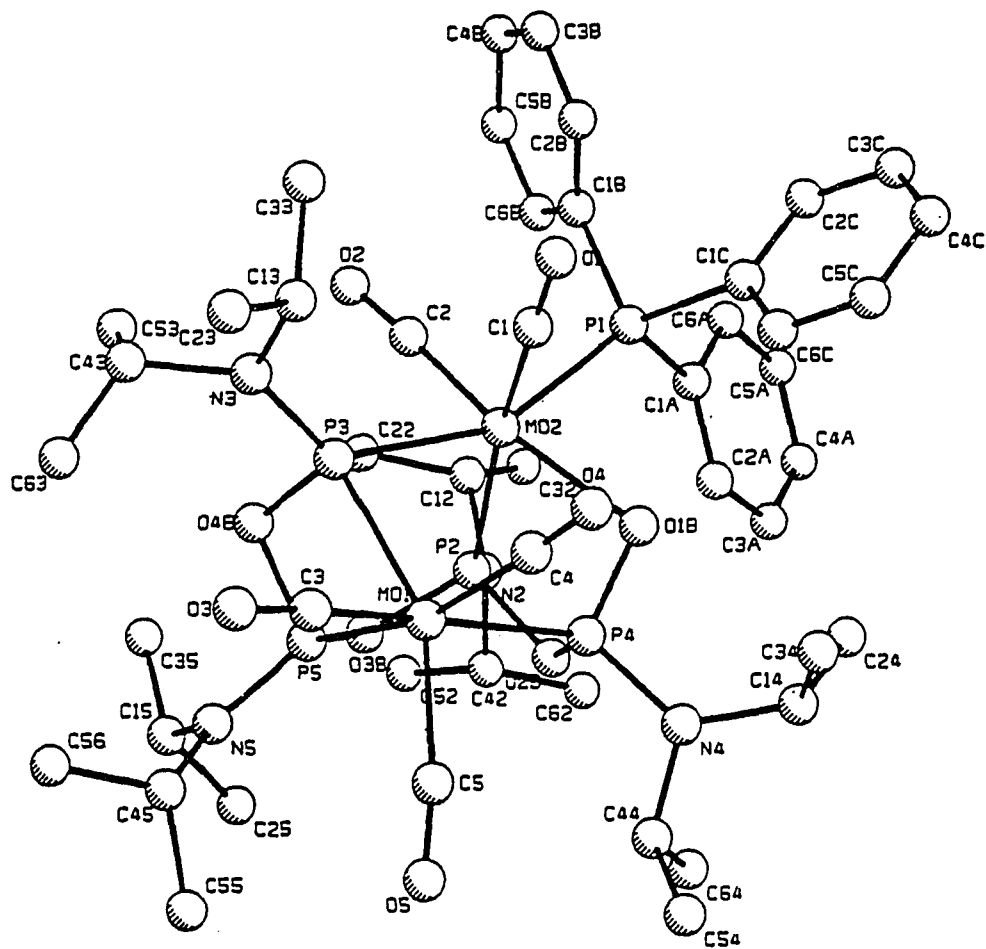


Figure 6. Molecular structure of complex 2
(with hydrogens omitted for clarity)

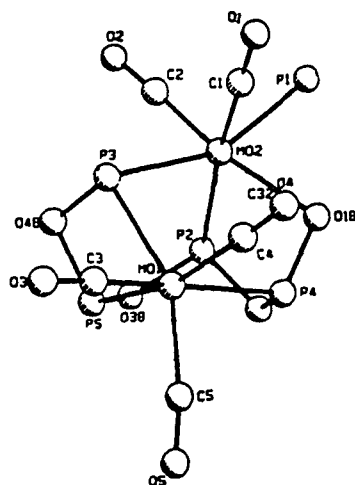


Figure 7. Core geometry of complex 2

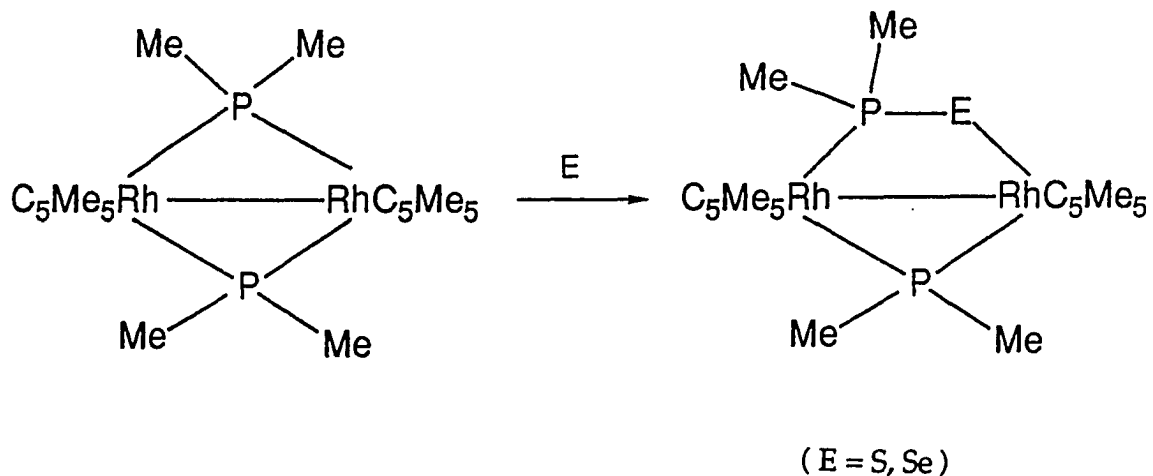
There are extensive alterations in the metal coordination spheres and cage geometry. Upon the addition of trimethylphosphine, there was a P-O-P bond cleaved near the substitution site with formation of one μ -P-O- and one μ -P- bridge, three carbonyls were lost. The first carbonyl at Mo(2) was replaced by the entering ligand. The phosphinito oxygen (P(4)-O(1B)) replaced a second CO while the μ -P- (P3) displaced a third CO at the other Mo center to bridge the two metals. These are now within bonding distance of each other at 3.186(4) Å, a substantial contraction from the Mo-Mo metal separation (6.001(1) Å) in the original parent cage structure. Mo-Mo single bond distances vary depending on ligand constraints, and 3.186(4) Å is well within the 3.057(6)-3.235(1) Å range of weak single bonds reported for the doubly-bridged molecules Mo₂(CO)₈(μ -PEt₂)₂^[27], Mo₂(CO)₆(PEt₃)₂(μ -PMe₂)₂^[28] and Cp₂Mo₂(CO)₆^[29], which all contains direct Mo-Mo bonds. If both Mo(1) and Mo(2) are assigned +1 formal oxidation states, electron counting requires the presence of a single Mo-Mo bond to achieve the noble-gas configuration at both metals.

Table III. Selected Bond Distances (Å) and Angles (deg) for Complex 2

Mo(1)-Mo(2)	3.186(4)		
Mo(1)-P(3)	2.464(4)	P(1)-C(1A)	1.87(1)
Mo(1)-P(4)	2.502(4)	P(1)-C(1B)	1.85(1)
Mo(1)-P(5)	2.455(4)	P(1)-C(1C)	1.84(1)
Mo(1)-C(3)	2.00(1)	P(2)-O(2B)	1.635(8)
Mo(1)-C(4)	2.05(1)	P(2)-O(3B)	1.671(8)
Mo(1)-C(5)	2.08(2)	P(3)-O(4B)	1.672(9)
Mo(2)-P(1)	2.563(4)	P(4)-O(1B)	1.540(8)
Mo(2)-P(2)	2.524(4)	P(4)-O(2B)	1.731(9)

Mo(2)-P(3)	2.362(4)	P(5)-O(3B)	1.624(8)
Mo(2)-O(1B)	2.222(8)	P(5)-O(4B)	1.677(8)
Mo(2)-C(1)	1.1(1)	C(1)-O(1)	1.18(2)
Mo(2)-C(2)	1.92(1)	C(2)-O(2)	1.17(1)
C(3)-O(3)	1.13(2)	C(4)-O(4)	1.10(2)
C(5)-O(5)	1.12(2)		
P(3)-Mo(1)-P(4)	105.7(1)	P(1)-Mo(2)-P(2)	100.2(1)
P(3)-Mo(1)-P(5)	62.8(1)	P(1)-Mo(2)-P(3)	155.4(1)
P(3)-Mo(1)-C(3)	82.1(4)	P(1)-Mo(2)-O(1B)	81.1(2)
P(3)-Mo(1)-C(4)	101.9(4)	P(1)-Mo(2)-C(1)	82.5(4)
P(3)-Mo(1)-C(5)	153.6(4)	P(1)-Mo(2)-C(2)	83.8(4)
P(4)-Mo(1)-P(5)	94.3(1)	P(2)-Mo(2)-P(3)	90.7(1)
P(4)-Mo(1)-C(3)	168.4(5)	P(2)-Mo(2)-O(1B)	78.5(2)
P(4)-Mo(1)-C(4)	82.7(4)	P(2)-Mo(2)-C(1)	172.1(4)
P(4)-Mo(1)-C(5)	91.9(4)	P(2)-Mo(2)-C(2)	94.9(4)
P(5)-Mo(1)-C(3)	96.9(5)	P(3)-Mo(2)-O(1B)	123.0(2)
P(5)-Mo(1)-C(4)	163.1(3)	P(3)-Mo(2)-C(1)	89.8(4)
P(5)-Mo(1)-C(5)	97.0(4)	P(3)-Mo(2)-C(2)	73.2(4)
C(3)-Mo(1)-C(4)	87.4(6)	O(1B)-Mo(2)-C(1)	94.7(5)
C(3)-Mo(1)-C(5)	83.9(6)	O(1B)-Mo(2)-C(2)	162.1(4)
C(4)-Mo(1)-C(5)	99.7(6)	C(1)-Mo(2)-C(2)	92.8(6)
Mo(1)-P(3)-O(4B)	97.4(3)	Mo(2)-P(1)-C(1A)	121.6(4)
Mo(1)-P(4)-O(1B)	107.6(3)	Mo(2)-P(1)-C(1B)	111.8(4)
Mo(1)-P(4)-O(2B)	110.6(3)	Mo(2)-P(1)-C(1C)	113.2(4)
Mo(1)-P(3)-Mo(2)	82.6(1)	Mo(2)-P(2)-O(2B)	103.3(3)
Mo(1)-P(5)-O(3B)	115.3(3)	Mo(2)-P(2)-O(3B)	115.4(3)
Mo(1)-P(5)-O(4B)	97.5(3)	C(1A)-P(1)-C(1B)	103.9(6)
Mo(2)-P(3)-O(4B)	114.5(3)	C(1A)-P(1)-C(1C)	100.0(6)
Mo(2)-O(1B)-P(4)	100.3(4)	C(1B)-P(1)-C(1C)	104.2(3)
O(2B)-P(2)-O(3B)	100.3(4)	O(1B)-P(4)-O(2B)	103.1(4)
O(3B)-P(5)-O(4B)	98.8(4)	P(2)-O(2B)-P(4)	107.1(5)
P(2)-O(3B)-P(5)	117.8(5)	P(3)-O(4B)-P(5)	99.9(5)

Complexes containing metals bridged simultaneously by a phosphido group as well as a P-chalcogen group are known, though they are usually formed by insertion of chalcogens into a metal-phosphido bond^[30] (Scheme III):



Scheme III

Newton and co-workers have reported a P-N-P cleavage reaction in the photolysis of $\text{CH}_3\text{N}(\text{PF}_2)_2$ with $\{\text{CpFe}(\text{CO})_2\}_2$ ^[31]. The structure of the product was found to have a $\mu\text{-PF}_2\text{NMePF}_2$ and a $\mu\text{-PF}_2$ as well as a $\mu\text{-PNMe}$ bridging ligand (Figure 8):

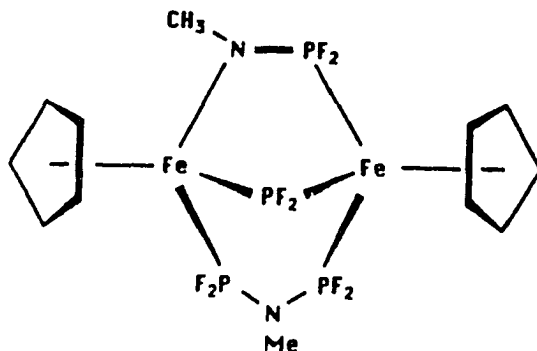


Figure 8. Structure of $[\text{C}_5\text{H}_5\text{Fe}(\text{PF}_2)_2\text{NCH}_3]_2$ (ref. 39)

This triple-bridging by three different ligands is similar to that found in 2, though there is no accompanying metal-metal bond formation in this case.

A short metal-phosphorus distance of 2.362(4) Å is found for Mo(2)-P3 which is approximately trans to the PPh₃ ligand. All other Mo-P bonds are in the 2.46-2.56 Å range, not significantly changed from the value of 2.50 Å in the parent cage complex. The Mo(2)-O(1B) bond length is 2.222(8) Å with the cis-Mo(2)-C(1) and trans-Mo(2)-C(2) bond lengths of 1.91(1) and 1.92(1) Å marginally shorter than all of the other Mo(1)-C bonds (2.00-2.08 Å). Except at P(4), ring P-O distances range from 1.62 to 1.67 Å. The two P(4)-O distances are very different with P(4)-O(1B) at 1.540(8) Å and P(4)-O(2B) at 1.731(9) Å. The data reflect the multiple bond character in the former at the expense of the latter. Corbridge summarized bond length data for phosphates and found an average of 1.54 Å for the reported P-O distances^[32].

Due to the polycyclic ligand system bridging the two metals, substantial deviations from idealized angles are found for both coordination spheres though each is approximately an octahedron. At Mo(1), the four-membered M-P-O-P chelate ring compresses the P(5)-Mo(1)-P(3) angle to only 62.8(1)°. The five-membered Mo(2)-P(3)-Mo(1)-P(4)-O(1B) heterocycle contains a narrow Mo(2)-P(3)-Mo(1) angle of 82.6(1)° while the P(3)-Mo(2)-O(1B) angle is distended to 123.0(2)°. As a result, the angle closest to linearity at Mo(2) is C(1)-Mo(2)-P(2) at 172.1(4)°. The four equatorial ligand atoms P(3), O(1B), P(1), and C(2) then subtend very distorted angles at Mo(2); P(3)-Mo(2)-O(1B) is 123.0(2)°, O(1B)-Mo(2)-P(1) is 81.1(2)°, P(1)-Mo(2)-C(2) is 83.8(4)°, and C(2)-Mo(2)-P(3) is 73.2(4)°. These equatorial angles sum up to 361°. At Mo(1), C(3) and P(4) are approximately axial as C(3)-Mo(1)-P(4) is 168.4(5)°. The corresponding equatorial angles deviate widely from orthogonality ranging from 62.8° to

101.9° but again summing up to 361°.

It is now easy to understand why the ^{31}P NMR spectra of all the orange complexes show one phosphorus chemical shift so far downfield (305-307 ppm). The X-ray structure of **2** (and X-ray structure of **7**, **11**) explicitly showed that the phosphido ligand is indeed present in the orange complexes. Since the phosphido chemical shift is known to be quite sensitive to the M-P-M angle and the extent of metal-metal interaction^[33], the nearly unchanged chemical shift value at around +306 ppm implies that the M-P-M angle as well as the nature of Mo-Mo bonding remain little changed through the series of orange complexes. This is also confirmed by the X-ray structure data of complexes **2**, **7**, **11** (see Part I-5 for a comparison of the structures). The highest-field resonance in **2**, **3**, **4** can be readily assigned to the newly-coordinated phosphine ligands by using typical coordination shifts from the free ligand values^[34]. That is, there is a linear relationship between the coordination chemical shift, $\Delta \delta = \delta_{\text{complex}} - \delta_{\text{free phosphine}}$, and the resonance position of the free phosphine. For compound **4**, a proton-coupled spectrum clearly identifies the high-field multiplet as the PPh_2H resonance with a $^1J_{\text{P-H}}$ of 334 Hz.

In each complex the connectivity between the five resonances can be unambiguously established by ^{31}P COSY (Figure 9):

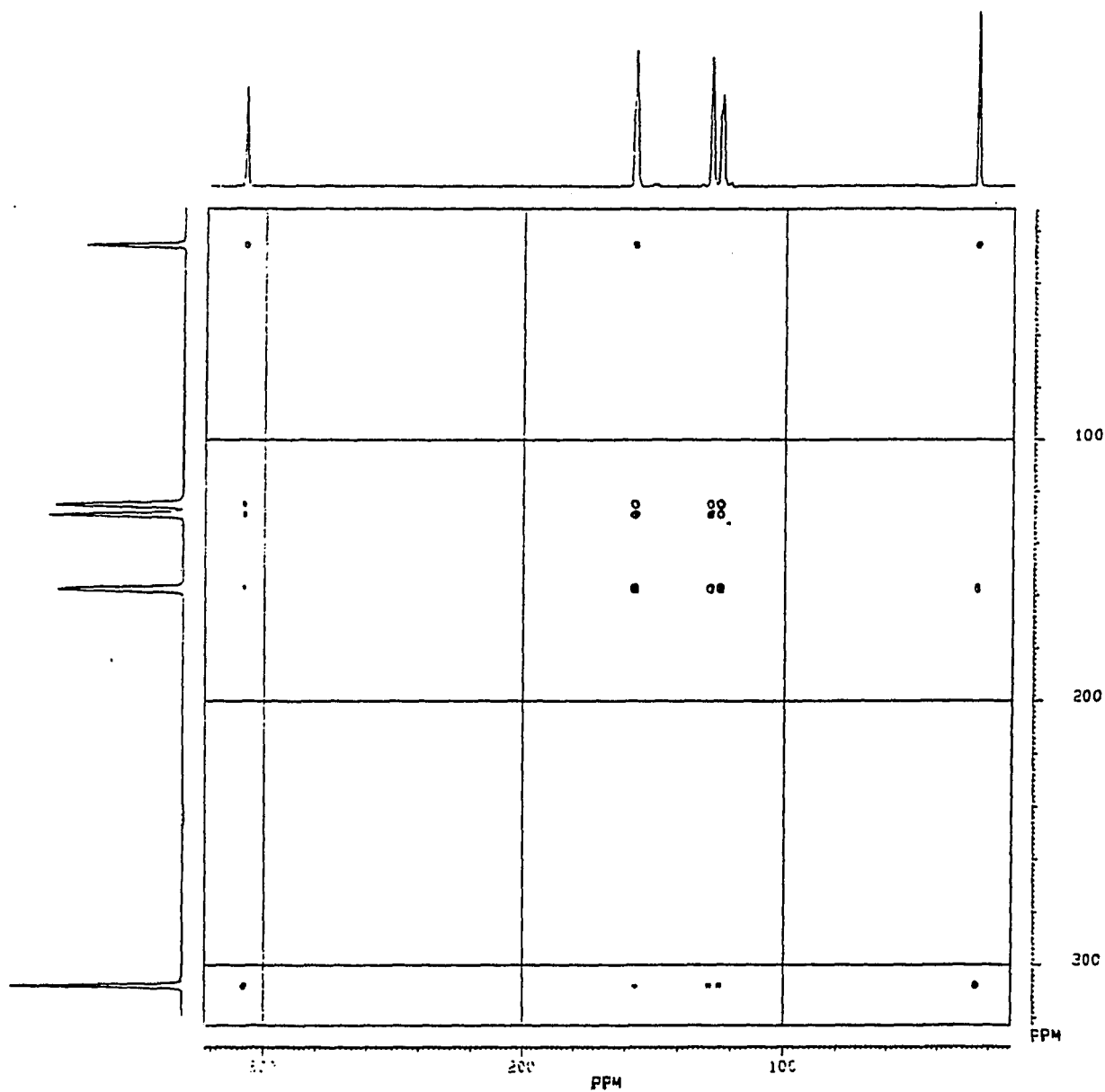


Figure 9. 2D COSY $^{31}\text{P}\{^1\text{H}\}$ NMR spectrum of complex 2

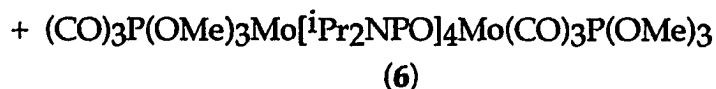
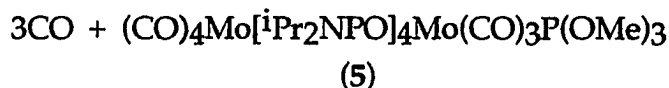
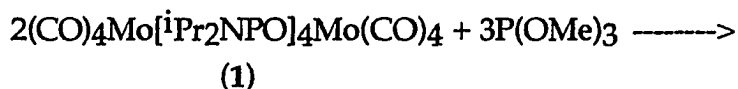
When CO gas was bubbled through the reaction solutions, the orange compounds did not revert to the original cage but another orange compound 11 formed. This new complex has a similar structure to 2 with the difference that the attacking phosphine was replaced by CO.

When compound 2 was first obtained, it was thought that since the attacking ligand was bulky (cone angle of PPh₃ = 145°), it could only substitute one CO. So the two smaller ligands MeP(C₆H₅)₂ (Θ = 136°) and HP(C₆H₅)₂ (Θ = 126°) were used to react with the cage under the same conditions. The same type of products (3 and 4) were obtained. It was therefore thought that a steric threshold might exist for the formation of simple mono- and di- substituted compounds and electronic influences may also play a role for both substitution and rearrangement reactions. In order to verify this, trimethyl phosphite with a smaller cone angle (Θ = 106°) and better π-accepting ability was chosen for reaction with the cage.

2. Synthesis and Characterization of



Complexes (CO)₃(L)Mo[iPr₂NPO]₄Mo(CO)₃P(OMe)₃ [L=CO (5), P(OMe)₃ (6)] were synthesized by the reaction of trimethylphosphite with the dimolybdenum cage complex (1) in refluxing toluene. The equation representing the preparation of these complexes is shown below.



(eq 3)

Thus from this ligand, different results were indeed obtained. After only 6 hrs, a clear, very light-yellow solution was formed while the cage was totally consumed. TLC showed only two colorless product spots. By routine column chromatography compound 5 followed by compound 6 were eluted and isolated. The isolated percent yields after chromatography of complexes 5 and 6 were 32 and 50%, respectively.

The products were characterized by ^{31}P , ^1H , ^{13}C NMR, IR spectra and elemental analyses. The proton-decoupled 1-D and 2D COSY ^{31}P NMR spectra of 5 and 6 and elemental analytical data showed that 5 is a monosubstituted product and compound 6 is a disubstituted compound with the original cage structure intact. Both of these complexes are mixtures of isomers. For example, in complex 5 only one CO was substituted, but it could be an equatorial or axial CO (Figure 10):

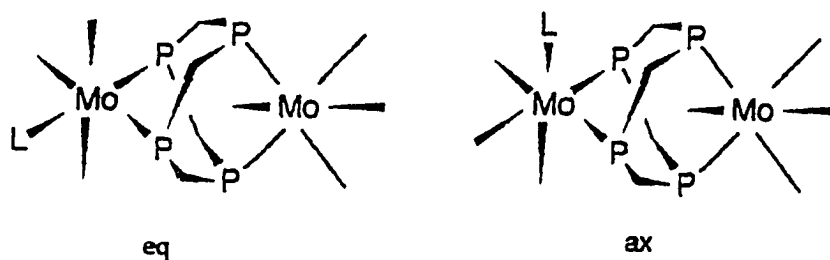


Figure 10. Proposed structures for isomers of complex 5

In order to integrate and calculate the ratio of isomers, we used selective proton decoupling techniques to determine which ^{31}P peaks were phosphite resonances and which were due to the cage phosphorus atoms. If an individual proton resonance is selected and irradiated with sufficient power

to decouple only that proton resonance, it simplifies the spectrum by removing all of the couplings to that proton. For example, if we selectively decouple the trimethyl phosphite protons, the couplings between P and H will disappear. Therefore the decaplets due to the coupling of P with nine H's will be gone and only the P-P couplings will be seen. If the decoupler is set to the center of the proton region and then modulated using a 'noise generator' with a bandwidth wide enough to cover the complete proton region, every proton frequency will be irradiated, resulting in the decoupling of all protons in the molecule^[35].

The composition of complex 5 can be easily assigned as 40% axial-substituted and 60% equatorial-substituted $(\text{CO})_4\text{Mo}[\text{iPr}_2\text{NPO}]_4\text{Mo}(\text{CO})_3\text{-P}(\text{OMe})_3$ by the 2-D COSY ^{31}P NMR spectrum (**Figure 11**) and full-decoupled or selectively-decoupled 1-D ^{31}P NMR spectra (**Figures 12, 13, 14**):

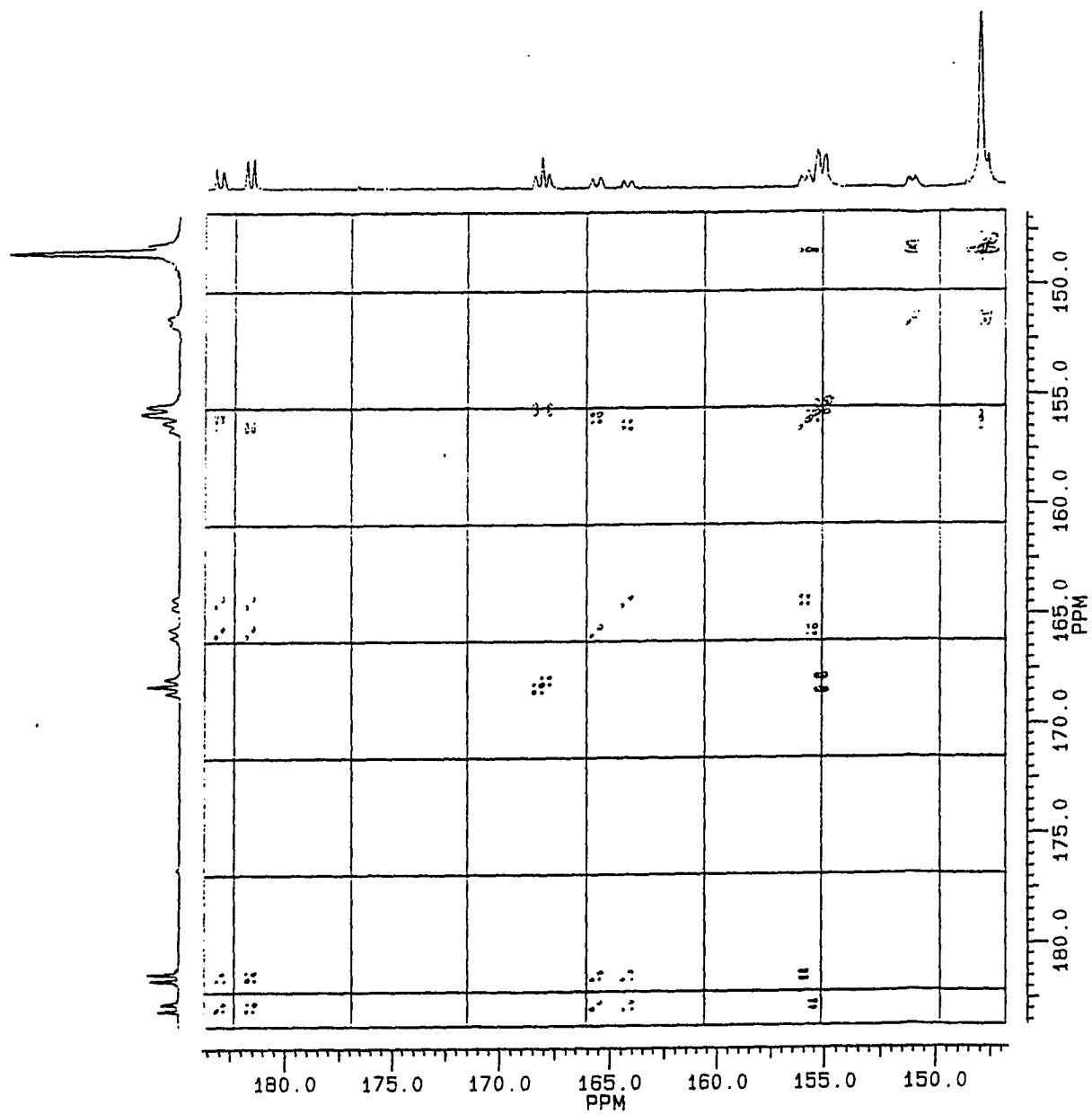


Figure 11. The 2-D COSY $^{31}\text{P}\{^1\text{H}\}$ NMR spectrum of complex 5

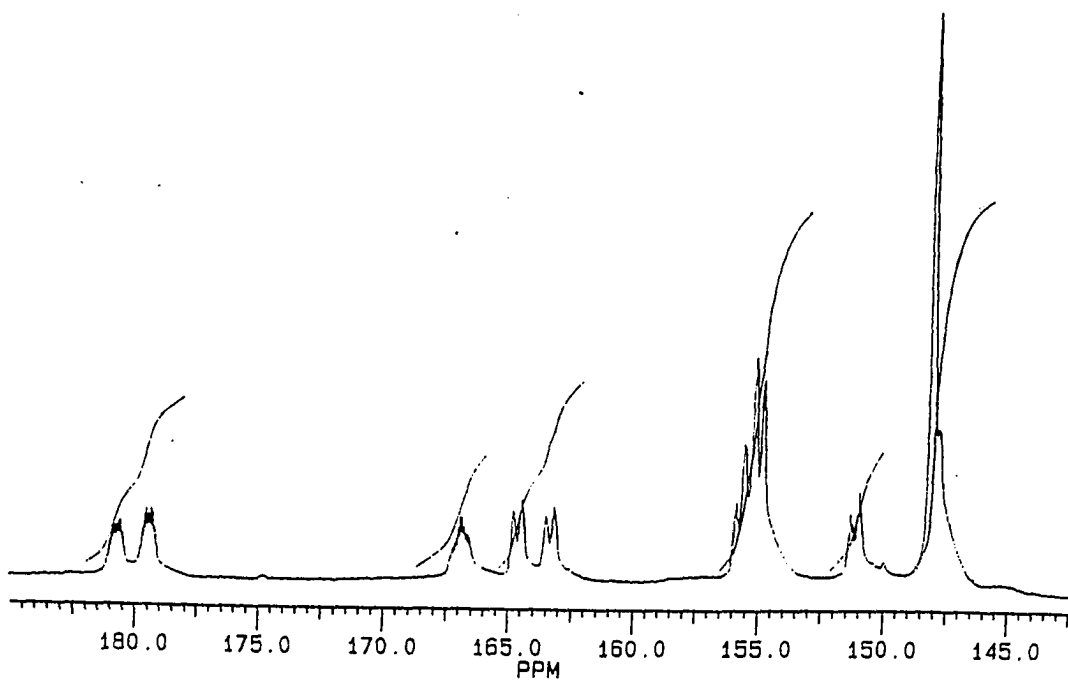


Figure 12. $^{31}\text{P}\{^1\text{H}\}$ NMR spectrum of complex 5
 [Selective methine proton ($\delta = 4.57\text{-}4.38$ ppm) decoupled, DP 16L]

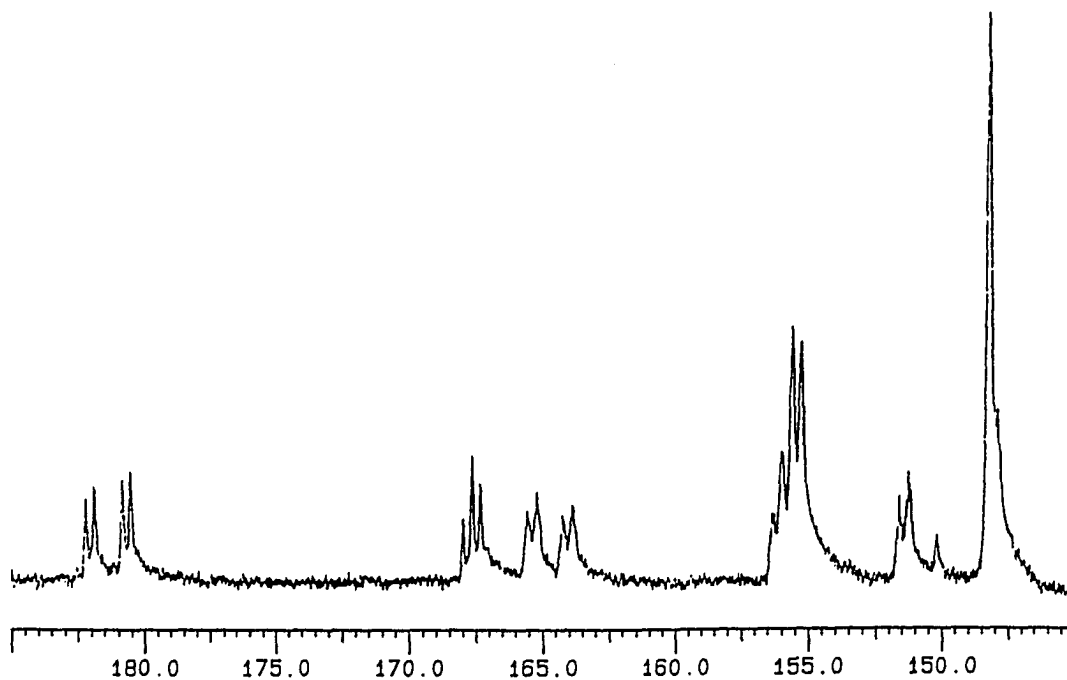


Figure 13. $^{31}\text{P}\{^1\text{H}\}$ NMR spectrum of complex 5
 [Selective trimethyl phosphite proton ($\delta = 3.61\text{-}3.59$ ppm) decoupled, DP 24L]

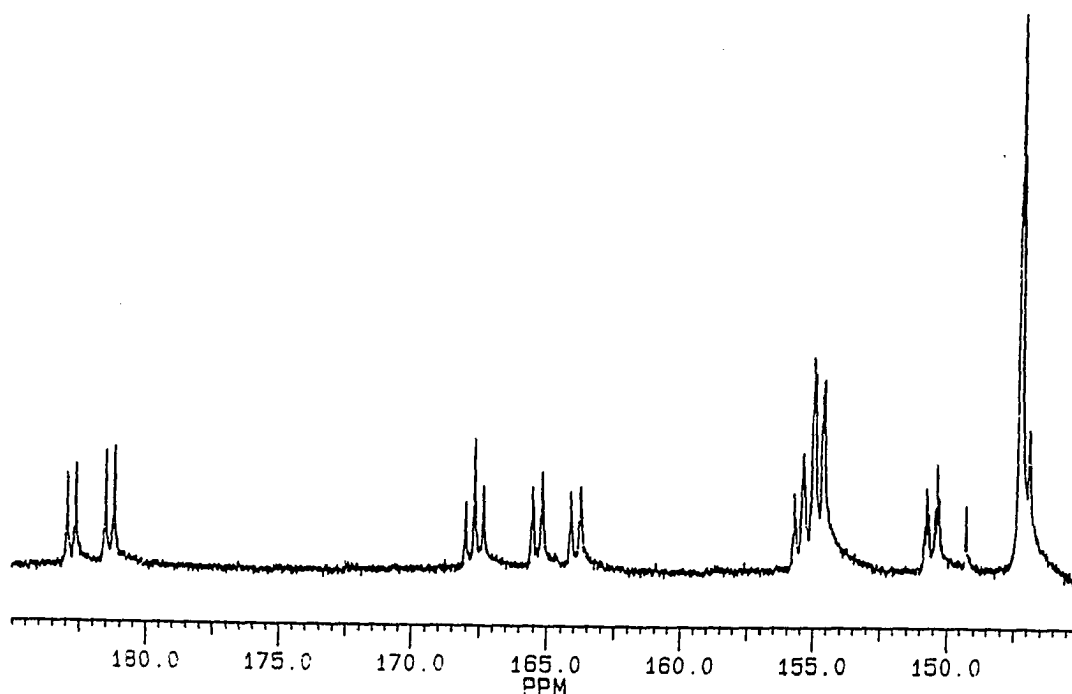


Figure 14. $^{31}\text{P}\{^1\text{H}\}$ NMR spectrum of complex 5

(Full decoupled, DP 12H)

Complex 6 can have four isomers assuming only monosubstitution at each metal (Figure 15):

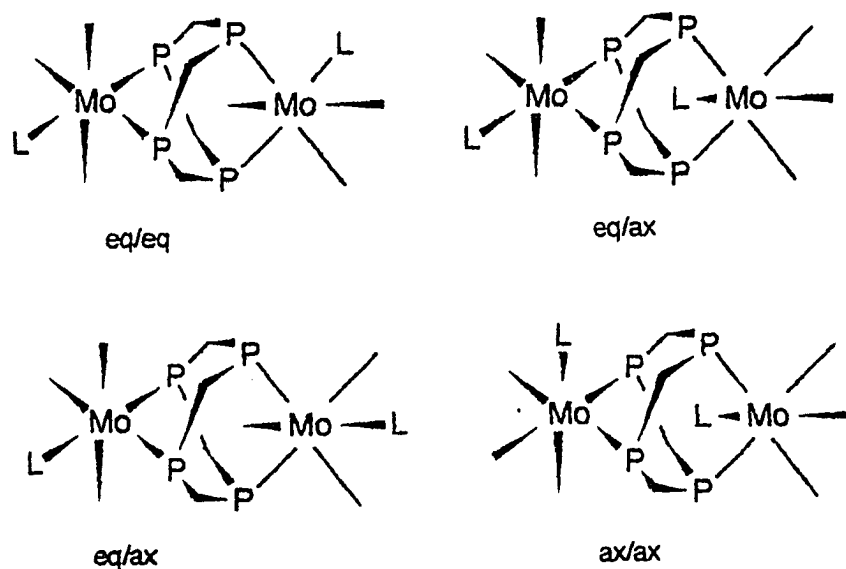


Figure 15. Proposed structures for isomers of complex 6

The extremely complex 1-D ^{31}P spectrum of **6** can similarly be satisfactorily resolved into its four diastereomeric components of equatorial/equatorial, equatorial/axial(trans), equatorial/axial(cis), and axial/axial disubstituted $(\text{CO})_3\text{P}(\text{OMe})_3\text{Mo}[\text{iPr}_2\text{NPO}]_4\text{Mo}(\text{CO})_3\text{P}(\text{OMe})_3$ diastereomers by its 2-D COSY spectrum and the selectively-decoupled 1-D ^{31}P NMR spectrum (Figures 16, 17, 18):

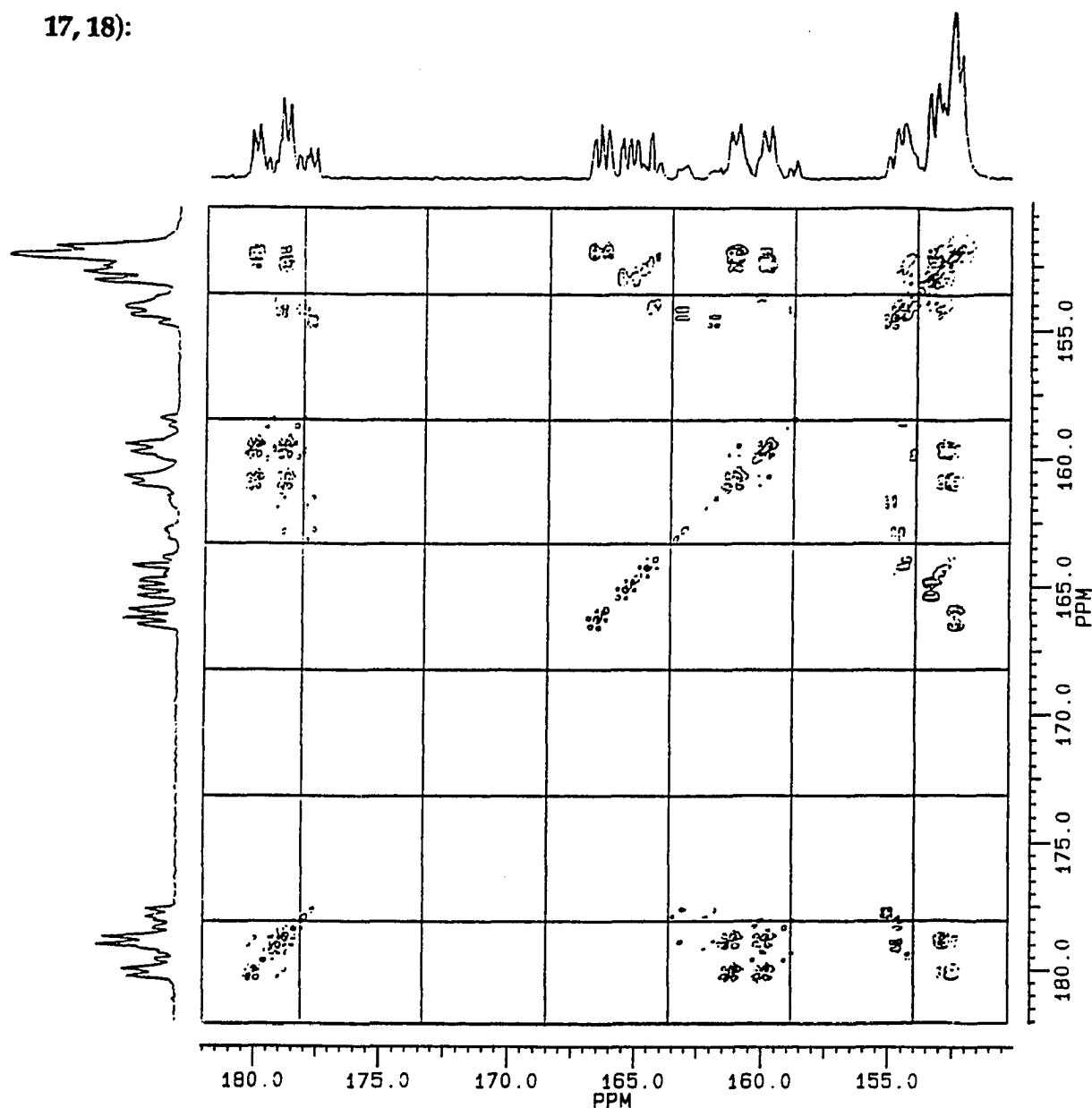


Figure 16. The 2-D COSY $^{31}\text{P}\{^1\text{H}\}$ NMR spectrum of complex **6**

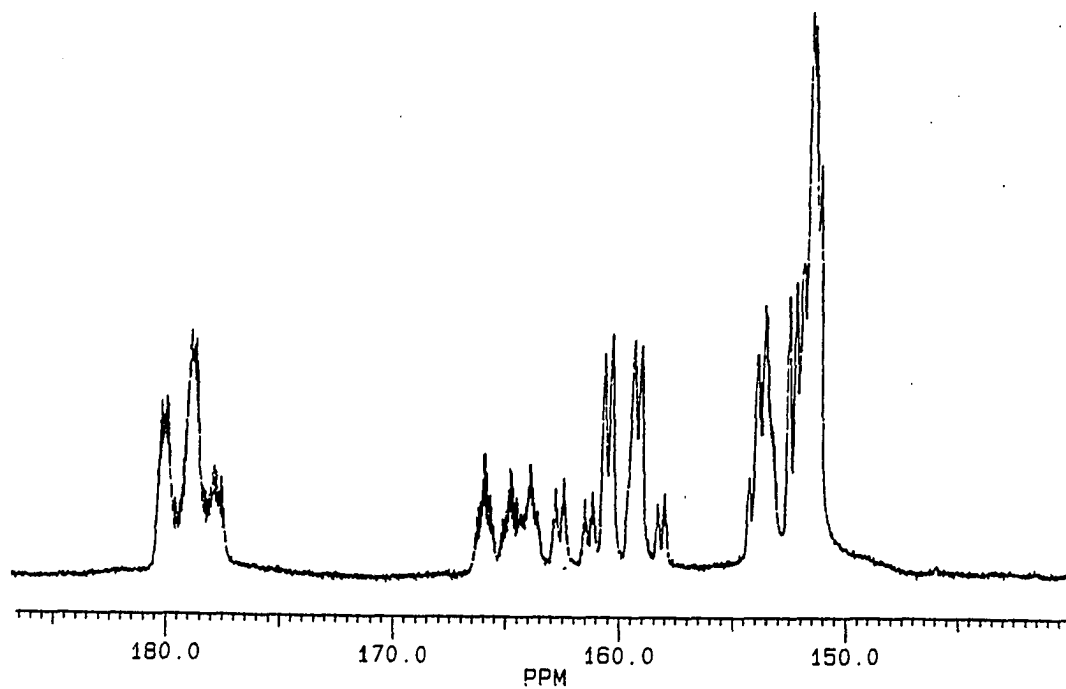


Figure 17. $^{31}\text{P}\{^1\text{H}\}$ NMR spectrum of complex 6
[Selective methine proton ($\delta = 4.66\text{--}4.53$ ppm) decoupled, DP 16L]

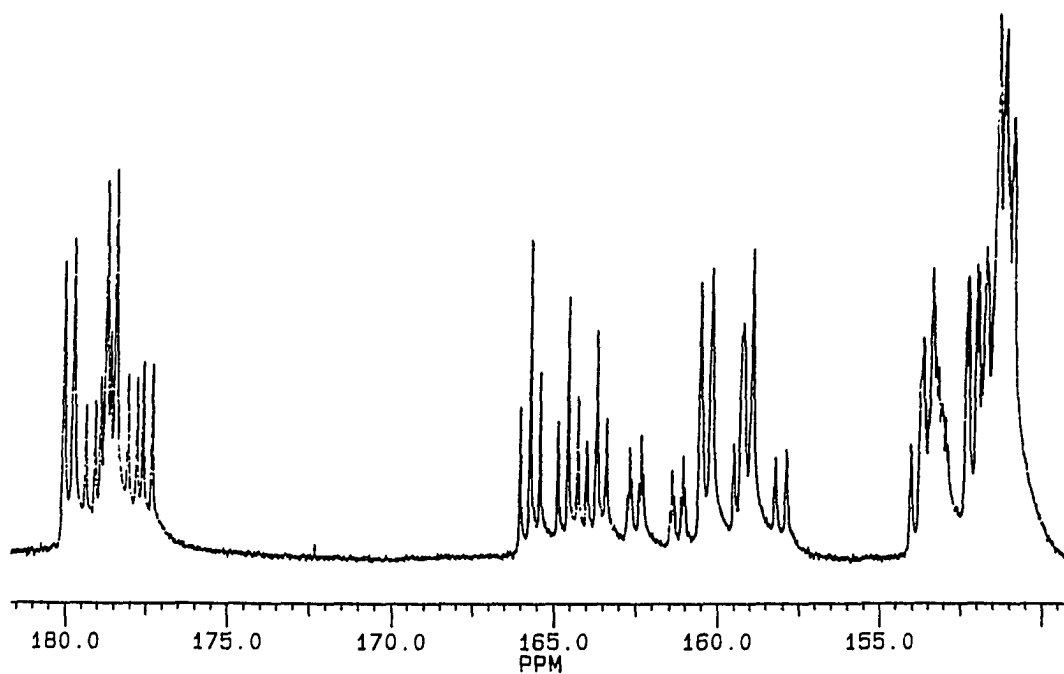


Figure 18. $^{31}\text{P}\{^1\text{H}\}$ NMR spectrum of complex 6
(Full decoupled, DP 12H)

All of the peaks of these isomers can be assigned. The relative proportions of the isomers are approximately 40 : 24 : 18 : 18, again indicating a preference for equatorial substitution and *mer*- stereochemistry at the Mo atoms. In addition, the presence of all diastereomers in complexes 5 and 6 was confirmed by HPLC (Figure 19):

Retention time (min.):

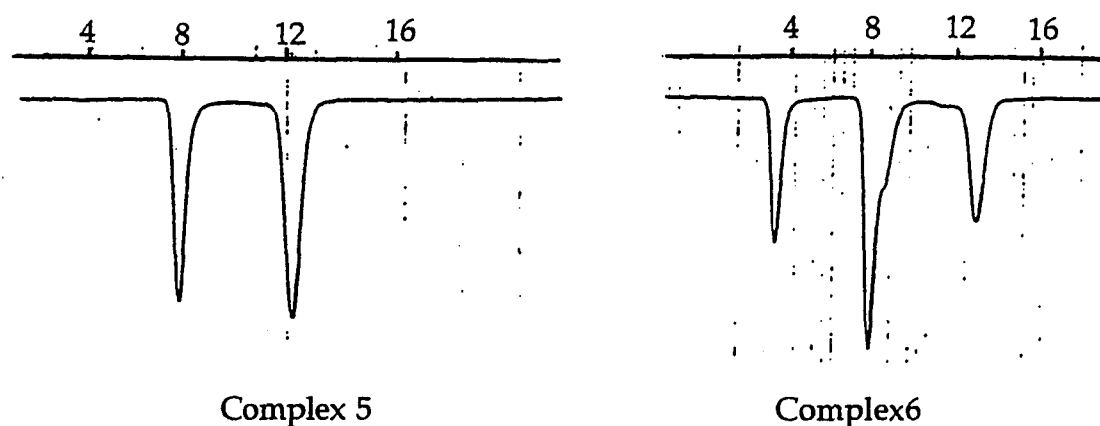


Figure 19. HPLC traces for complexes 5 and 6

Hexane/CH₂Cl₂ (75/25), Al₂O₃ column

Thus, we can see that both complexes 5 and 6 are isomeric mixtures. The HPLC of 5 showed 2 peaks and of 6 showed 3 peaks plus one shoulder. Due to the small capacity of the HPLC column, attempts to separate the diastereometric isomers quantitatively failed.

From the ³¹P NMR spectra of 5 and 6 we can clearly see that the *trans* two-bond P-P coupling constants are larger than the *cis* values (²J(P, P)_{trans}

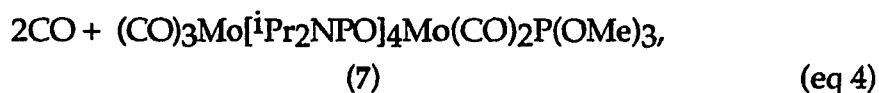
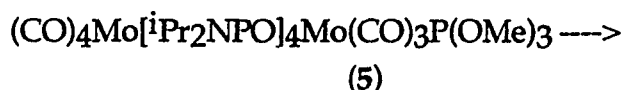
=185 to 189 Hz, $^2J(\text{P}, \text{P})_{\text{cis}} = 41$ to 42 Hz). Both products are white solids with no chemical shifts around 307 ppm. Thus, the ^{31}P NMR spectra of compounds 5 and 6 are distinct from those of orange 2, 3, and 4. Here we can assign peaks from the phosphorus atoms trans and cis to the entering ligands. The chemical shift differences between these two phosphorus atoms are only about 20 ppm.

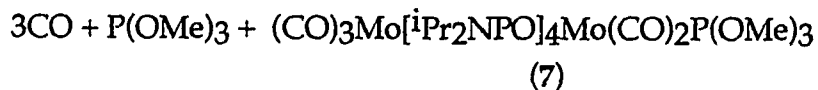
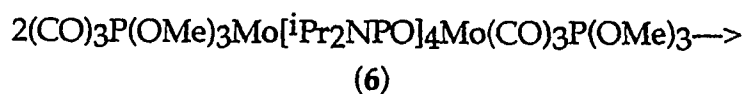
Similar reaction conditions using the phosphines resulted in negligible reaction. Under milder conditions, traces of the conventional substitution products similar to 5 and 6 can also be observed in the reactions generating 2, 3, and 4 (See Part I-4). The bulkier triphenyl phosphite also yielded conventional substitution products similar to 5 and 6 .

3.Synthesis and Characterization of $(\text{CO})_3\text{Mo}[\text{iPr}_2\text{NPO}]_4\text{Mo}(\text{CO})_2\text{P}(\text{OMe})_3$ (7)

Another interesting result we obtained from the $\text{P}(\text{OMe})_3$ reaction was that the compounds 5 and 6 could both thermally rearrange to orange-colored compounds which did show very low-field peaks at around 307 ppm.

Upon refluxing 5 and 6 in toluene for more than 30 hrs, both of these colorless compounds were transformed into orange-red $(\text{CO})_3\text{Mo}[\text{iPr}_2\text{NPO}]_4\text{Mo}(\text{CO})_2\text{P}(\text{OMe})_3$ (7), which is an analog of complexes 2, 3, and 4. Trace amounts of $(\text{CO})_2\text{P}(\text{OMe})_3\text{Mo}[\text{iPr}_2\text{NPO}]_4\text{Mo}(\text{CO})_2\text{P}(\text{OMe})_3$ were detected by ^1H NMR.





The product complex 7 was characterized by ^{31}P , ^1H , ^{13}C NMR, and IR spectra and by elemental analysis. The X-ray structure of complex 7 has been determined. One is shown in Figure 20. Selected bond angles and bond distances are listed in Table IV.

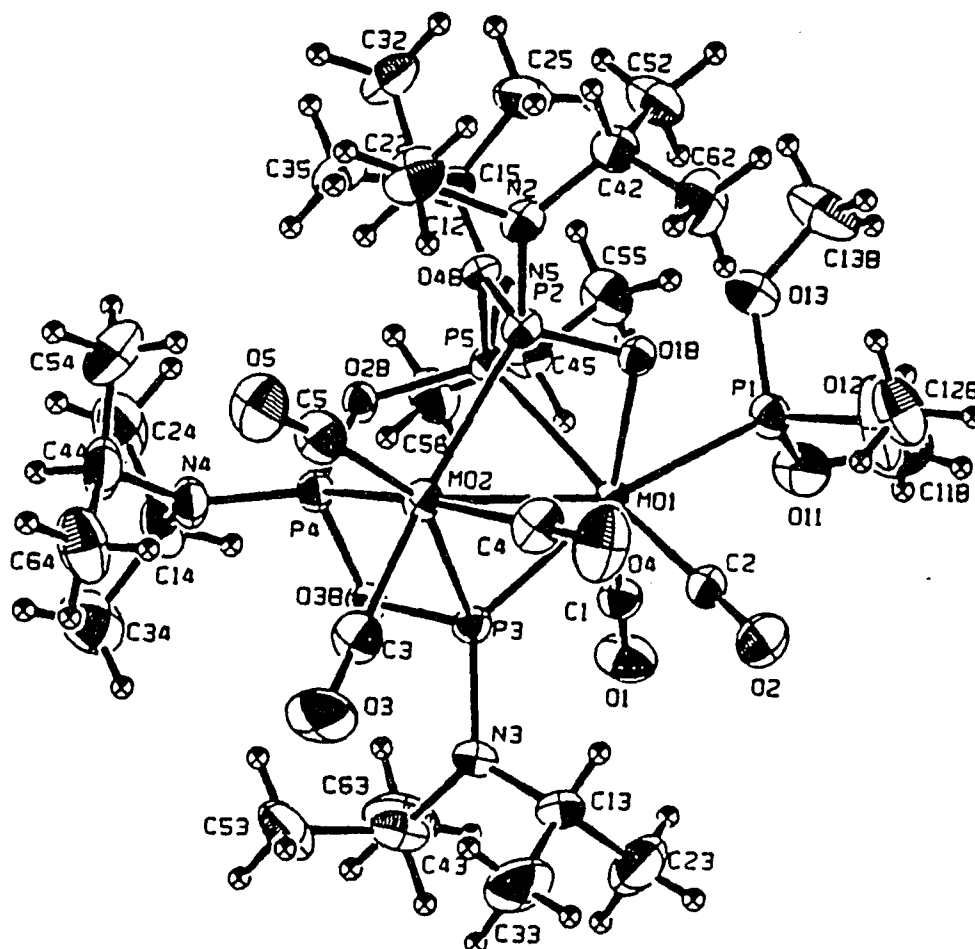


Figure 20. Molecular structure of complex 7

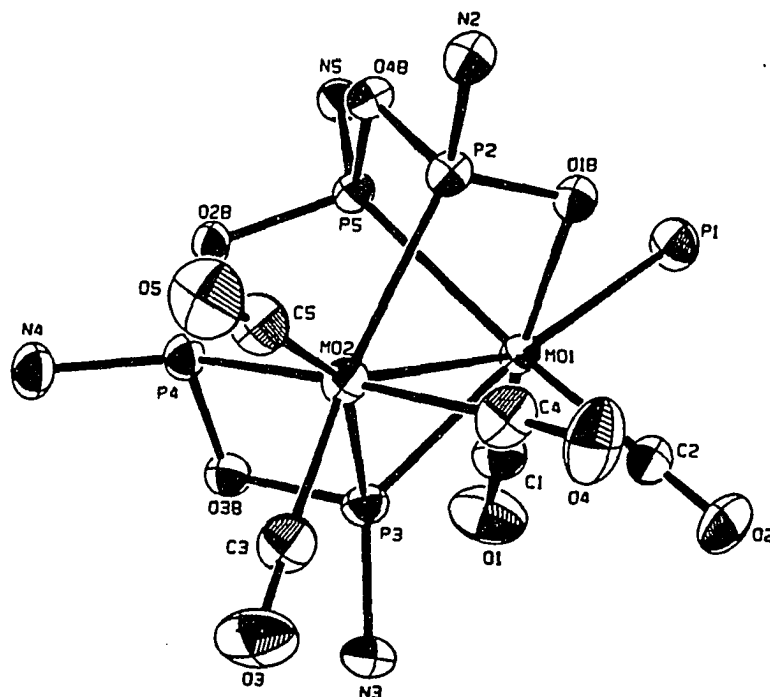


Figure 21. Core geometry of complex 7

Table IV. Selected Bond Distances (Å) and Angles (deg) for Complex 7

Mo(1)-Mo(2)	3.173(1)		
Mo(1)-P(1)	2.465(2)	P(2)-O(1B)	1.537(3)
Mo(1)-P(3)	2.353(2)	P(2)-O(4B)	1.730(3)
Mo(1)-P(5)	2.532(1)	P(3)-O(3B)	1.654(4)
Mo(1)-O(1B)	2.226(3)	P(4)-O(2B)	1.626(3)
Mo(1)-C(1)	1.952(6)	P(3)-O(3B)	1.662(3)
Mo(1)-C(2)	1.969(6)	P(5)-O(2B)	1.670(3)
Mo(2)-P(2)	2.525(2)	P(5)-O(4B)	1.604(3)
Mo(2)-P(3)	2.480(2)	C(1)-O(1)	1.157(6)
Mo(2)-P(4)	2.486(2)	C(2)-O(2)	1.159(6)
Mo(2)-C(3)	1.964(6)	C(3)-O(3)	1.150(7)
Mo(2)-C(4)	2.005(7)	C(4)-O(4)	1.141(7)
Mo(2)-C(5)	1.993(7)	C(5)-O(5)	1.151(7)

Mo(2)-Mo(1)-P(1)	48.83(3)	Mo(1)-Mo(2)-P(3)	47.25(3)
Mo(2)-Mo(1)-P(3)	50.73(4)	Mo(1)-Mo(2)-P(4)	81.01(4)
Mo(2)-Mo(1)-P(5)	78.46(3)	Mo(2)-Mo(1)-O(1B)	74.01(9)
P(1)-Mo(1)-P(3)	155.97(5)	P(2)-Mo(2)-P(3)	103.10(5)
P(1)-Mo(1)-P(5)	93.20(5)	P(2)-Mo(2)-P(4)	93.95(5)
P(1)-Mo(1)-O(1B)	79.30(9)	P(2)-Mo(2)-C(3)	171.0(2)
P(1)-Mo(1)-C(1)	83.1(2)	P(2)-Mo(2)-C(4)	84.3(2)
P(1)-Mo(1)-C(2)	88.7(2)	P(2)-Mo(2)-C(5)	96.0(2)
P(3)-Mo(1)-P(5)	91.09(5)	P(3)-Mo(2)-P(4)	62.33(5)
P(3)-Mo(1)-O(1B)	124.71(9)	P(3)-Mo(2)-C(3)	79.1(2)
P(3)-Mo(1)-C(1)	72.9(2)	P(3)-Mo(2)-C(4)	102.6(2)
P(3)-Mo(1)-C(2)	91.7(2)	P(3)-Mo(2)-C(5)	154.1(2)
P(5)-Mo(1)-O(1B)	78.28(9)	P(4)-Mo(2)-C(3)	95.1(2)
P(5)-Mo(1)-C(1)	98.6(2)	P(4)-Mo(2)-C(4)	163.9(2)
P(5)-Mo(1)-C(2)	168.7(2)	P(4)-Mo(2)-C(5)	102.0(2)
O(1B)-Mo(1)-C(1)	161.9(2)	C(3)-Mo(2)-C(4)	87.0(3)
O(1B)-Mo(1)-C(2)	91.1(2)	C(3)-Mo(2)-C(5)	82.2(3)
C(1)-Mo(1)-C(2)	92.7(2)	C(4)-Mo(2)-C(5)	94.1(3)
Mo(1)-P(1)-O(11)	114.2(2)	Mo(2)-P(2)-O(1B)	108.0(1)
Mo(1)-P(1)-O(12)	119.7(2)	Mo(2)-P(2)-O(4B)	110.5(1)
Mo(1)-P(1)-O(13)	111.8(2)	Mo(2)-P(3)-O(3B)	97.0(1)
Mo(1)-P(3)-Mo(2)	82.02(5)	Mo(2)-P(4)-O(2B)	114.1(1)
Mo(1)-P(3)-O(3B)	115.1(1)	Mo(2)-P(4)-O(3B)	96.5(1)
Mo(1)-P(5)-O(2B)	114.0(1)	O(11)-P(1)-O(12)	98.5(3)
Mo(1)-P(5)-O(4B)	102.2(1)	O(11)-P(1)-O(13)	106.0(3)
Mo(1)-O(1B)-P(2)	99.6(2)	O(12)-P(1)-O(13)	105.0(3)
O(1B)-P(2)-O(4B)	101.9(2)	O(2B)-P(5)-O(4B)	100.9(2)
O(2B)-P(4)-O(3B)	98.7(2)	P(4)-O(2B)-P(5)	119.8(2)
P(3)-O(3B)-P(4)	101.7(2)	P(2)-O(4B)-P(5)	108.9(2)

The structure is similar to that for complex 2. With the replacement of PPh₃ by P(OMe)₃, a few alterations were found in bond angles and lengths.

The Mo(1)-Mo(2) separation is now 3.173(1) Å. A metal-phosphorus distance of 2.352(2) Å is observed for Mo(1)-P(3) with a P(OMe)₃ instead of the P(Ph)₃ ligand approximately trans to it. All other Mo-P bonds are in the range 2.46-2.53 Å. The Mo(1)-O(1B) bond length is 2.226(3) Å and the trans Mo(1)-C(1) bond length is 1.952(6) Å. All other Mo-C bonds are in the range 1.97-2.00 Å. Except at P(2), ring P-O distances range from 1.60 to 1.67 Å. The two disparate P(2)-O distances with P(2)-O(1B) at 1.537 Å and P(2)-O(4B) at 1.730 Å result from the multiple-bond character of the former bond.

Both coordination spheres are similar to those found in **2**. At Mo(2), the P(3)-Mo(2)-P(4) angle was compressed by the four-membered M-P-O-P chelate ring to only 62.33(5)°. The five-membered Mo(1)-P(3)-Mo(2)-P(2)-O(1B) heterocycle has a narrow Mo(1)-P(3)-Mo(2) angle of 82.02(5)° while the P(3)-Mo(1)-O(1B) angle is distended to 124.7(1)°. The angle closest to linearity at Mo(1) is C(2)-Mo(1)-P(5) at only 168.7(2)°. The four equatorial ligand atoms P(1), O(1B), P(3), and C(1) subtend very distorted angles at Mo(1): P(3)-Mo(1)-O(1B) is 124.7(1), O(1B)-Mo(1)-P(1) is 79.3(1)°, P(1)-Mo(1)-C(1) is 83.1(2)°, and C(1)-Mo(1)-P(3) is 72.9(2)°. These equatorial angles do sum up to 360°. At Mo(2), the approximately axial angle C(3)-Mo(2)-P(2) is 171.0(2)°. The four equatorial angles ranged from 62.3° to 102.6°, summing up to 361°.

Complex **6** can also form another orange compound. From its ¹H NMR spectrum (Figure 22), we can see that there are four P(OMe)₃ groups (four doublets for the trimethyl phosphite protons) and they are in two sets which means that it is a disubstituted compound as well as an isomeric mixture of (CO)₂P(OMe)₃Mo[¹Pr₂NPO]₄Mo(CO)₂P(OMe)₃. Unfortunately, due to the trace amount of the sample available, no satisfactory ³¹P NMR spectrum was obtained.

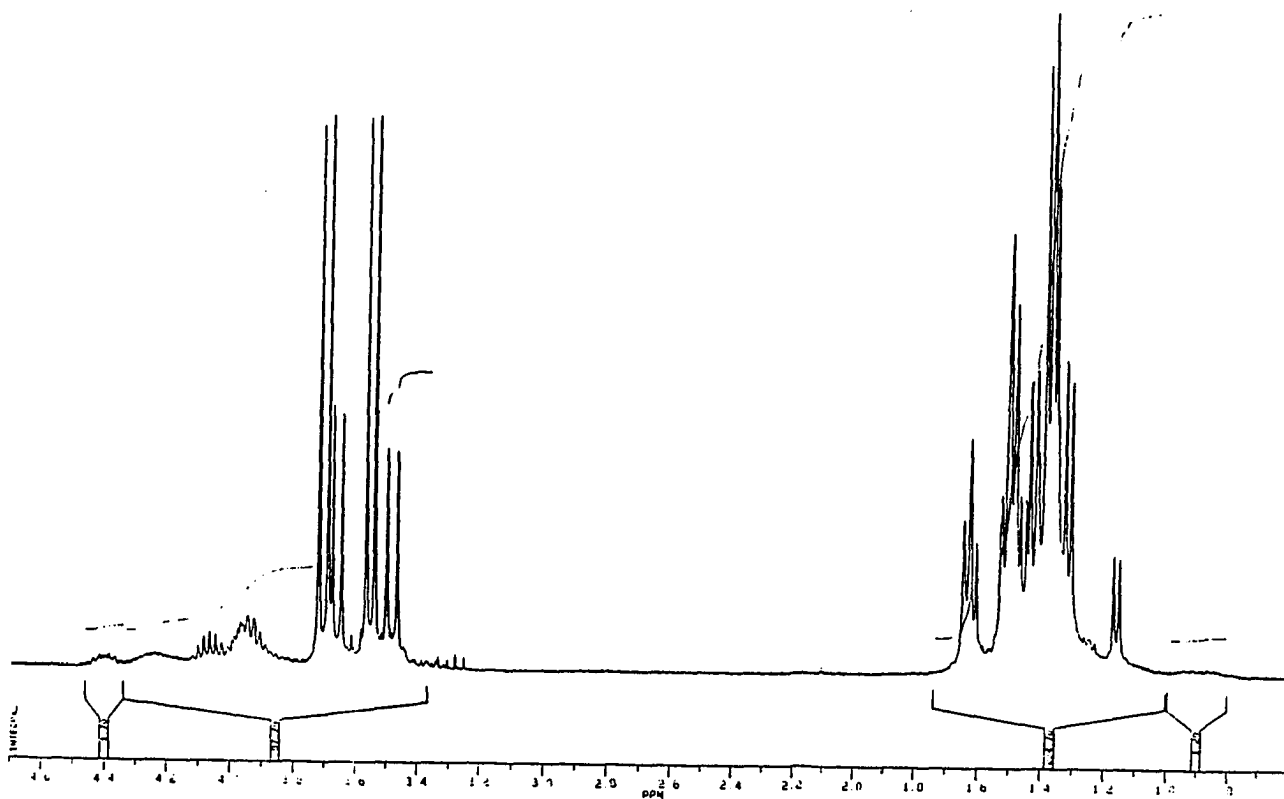


Figure 22. ^1H NMR spectrum for
 $(\text{CO})_2\text{P}(\text{OMe})_3\text{Mo}[\text{iPr}_2\text{NPO}]_4\text{Mo}(\text{CO})_2\text{P}(\text{OMe})_3$

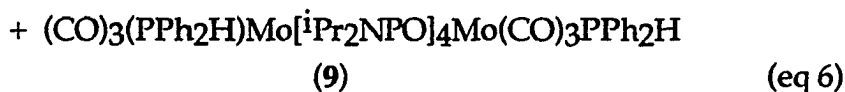
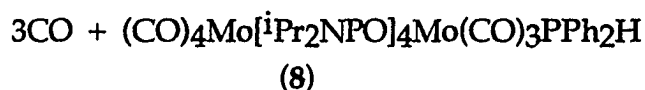
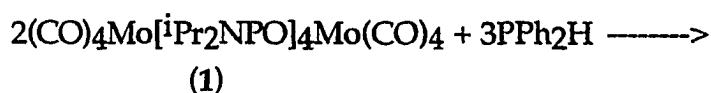
4. Synthesis and Characterization of

$(\text{CO})_3(\text{L})\text{Mo}[\text{iPr}_2\text{NPO}]_4\text{Mo}(\text{CO})_3\text{PPh}_2\text{H}$ (L=CO(8), PPh₂H(9))

When the compounds 2, 3, and 4 were obtained, it was thought that only the phosphines with large enough cone angles could force the cage structural change. Since the trimethyl phosphite ligand with its small cone angle also appeared to give this structure as the thermodynamic product, we realized that reactions described in eq 1 may have also undergone the same initial

substitution. These intermediates may be too unstable with the larger phosphine ligands to allow isolation as they quickly transformed to the more stable Mo-Mo bonded structures. Reactions 1, 2 and 3 were repeated under milder conditions (refluxing hexane). At the lower temperature, the reactions were slow. From the TLC and the ^{31}P NMR spectra of the reaction mixtures we noted that indeed each of these gave simple substitution compounds. Because the reactions were far from complete and the products were not stable, we could only isolate two of these intermediates: $(\text{CO})_3(\text{L})\text{Mo}[\text{iPr}_2\text{NPO}]_4\text{Mo}(\text{CO})_3\text{PPh}_2\text{H}$ ($\text{L}=\text{CO}$ (8), PPh_2H (9)) were obtained from the reaction mixture by column chromatography.

The complexes $(\text{CO})_3(\text{L})\text{Mo}[\text{iPr}_2\text{NPO}]_4\text{Mo}(\text{CO})_3\text{PPh}_2\text{H}$ ($\text{L}=\text{CO}$ (8), PPh_2H (9)) were synthesized by the reaction of diphenylphosphine with the dimolybdenum cage complex $(\text{CO})_4\text{Mo}[\text{iPr}_2\text{NPO}]_4\text{Mo}(\text{CO})_4$ (1) in refluxing hexane. The equation representing the preparation of these complexes is shown below:



After heating the reaction mixture for 72hrs, a clear light-yellow solution formed. TLC showed four products. The second spot was isolated as

compound **8** and the fourth spot as compound **9**. The products were characterized by ^{31}P , ^1H , ^{13}C NMR, and IR spectra, and in addition, the structure of compound **8** was confirmed by elemental analysis. The isolated yields of complexes **8** and **9** were only 11 and 4%, respectively.

Both products are cage-like compounds. One is the monosubstituted isomer with one axial CO replaced by the ligand; the other is the diaxial-substituted isomer, (i. e., monosubstitution at each metal, **Figure 23**):

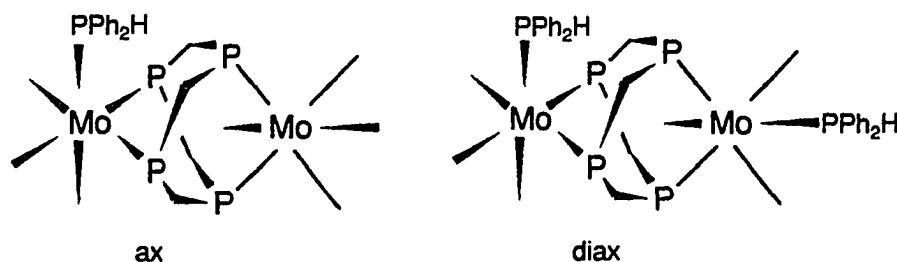


Figure 23. Proposed structures for complex **8** and **9**

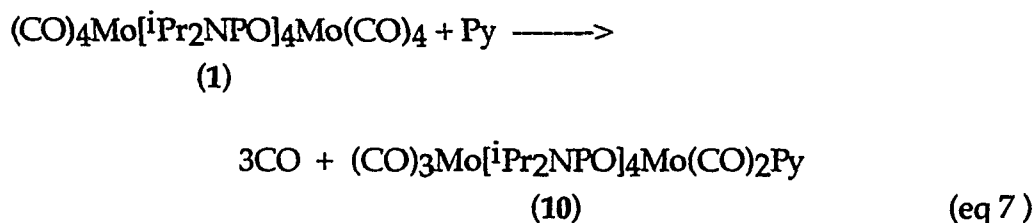
Another expected result yet to be proved is that both of these white-colored complexes, **8** and **9**, can also readily transform to the known orange complex **4** in refluxing toluene.

It seems reasonable to postulate that the colorless cage-like products of simple substitution were formed first in each reaction. These compounds were not very stable and readily rearranged to novel orange complexes by breakage of one P-O bond.

5. Synthesis and Characterization of $(\text{CO})_3\text{Mo}[\text{iPr}_2\text{NPO}]_4\text{Mo}(\text{CO})_2(\text{L})$ (L=Py (10), CO (11))

In order to identify whether it was the electronic or steric factor that forced the structural rearrangement, $\text{P}(\text{OC}_6\text{H}_5)_3$ was used for comparison with $\text{HP}(\text{C}_6\text{H}_5)_2$ since they have similar cone angles (128° and 126°) but different π -acceptor abilities. By following the reaction of $\text{P}(\text{OC}_6\text{H}_5)_3$ with cage 1 by TLC and ^{31}P NMR, a similar result was obtained as for $\text{P}(\text{OCH}_3)_3$. The intermediate substitution product, however, was more stable than that for $\text{HP}(\text{C}_6\text{H}_5)_2$. This suggests that the electronic influence on the rearrangement reaction is more important than the steric influence, and that the stronger π -acceptor ligands can stabilize the simple substitution products.

In order to further verify this observation, a stronger σ -donor ligand, pyridine, was used to react with the cage 1 and to compare with $\text{P}(\text{OCH}_3)_3$. Pyridine has a cone angle very similar to that of $\text{P}(\text{OCH}_3)_3$ ($\Theta=106^\circ$). [Cone angle for the phenyl group is 105° ^[36], pyridine should have essentially the same value.] The reaction of pyridine with the dimolybdenum cage 1 was run in refluxing toluene.



The yield of complex **10** was 76%.

Compared to $P(OCH_3)_3$ from which we can get the substitution intermediates, this result was very different. This product was a red-orange compound with structure similar to the orange compounds 2, 3, 4, and 7. No substitution intermediates showed up at all either on TLC or in the ^{31}P NMR spectra taken during the reaction.

This again suggests that strong π -acceptor ligands can stabilize simple substitution intermediates while good σ -donors make the metal electron rich and facilitate the P-O oxidative addition process.

From this reaction we also observed that:

(A) The product 10 is not stable in the NMR solvent $CDCl_3$, since the 1H and ^{31}P NMR spectra showed that it transformed to another orange complex 11 (Figure 23). The 1H NMR spectrum showed that there was no pyridine in the new complex (Figure 25) and its ^{31}P NMR spectrum is similar to that of the complex 2 after reaction with CO.

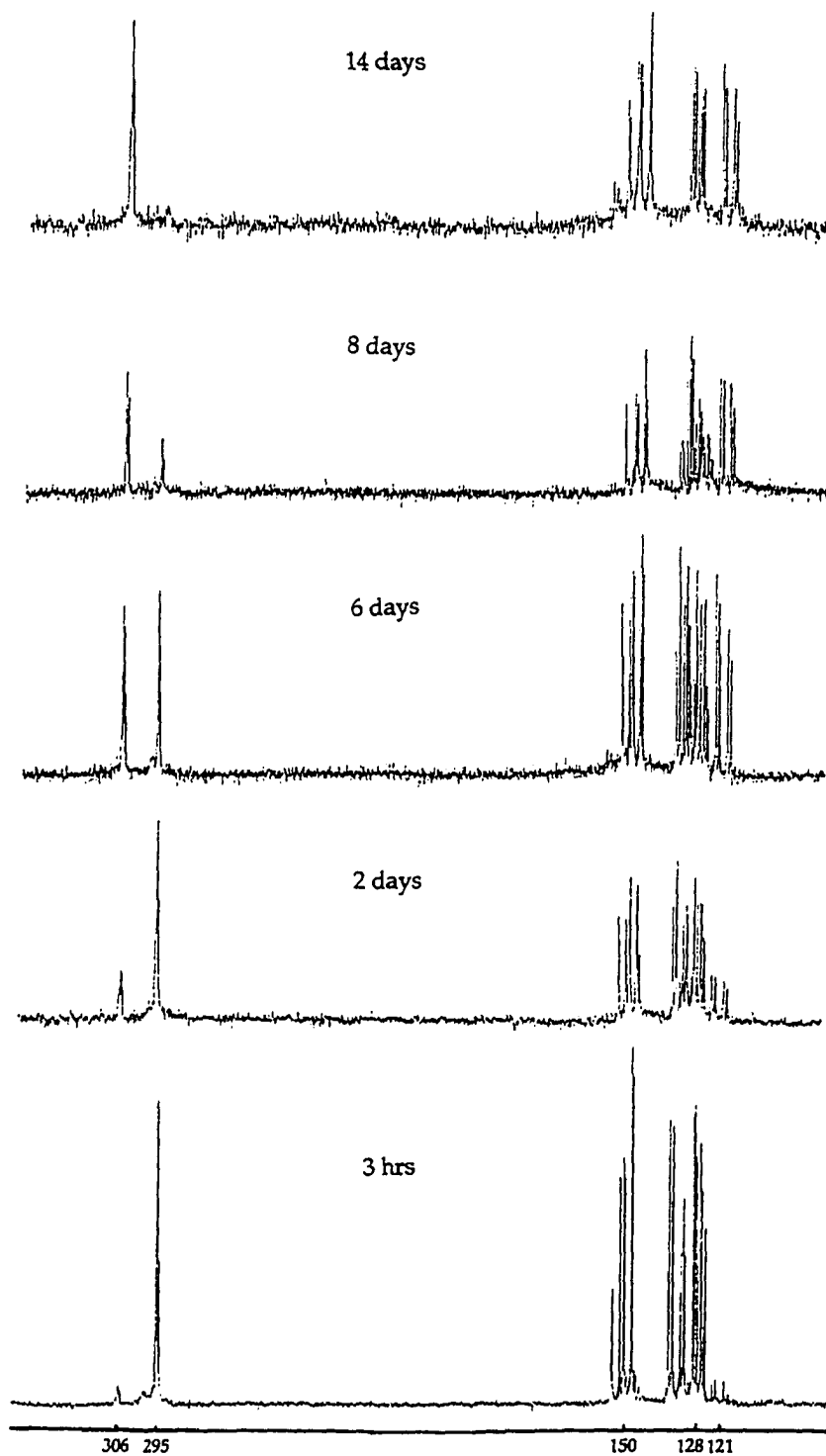


Figure 24. ^{31}P NMR spectra of complex 10 in CDCl_3

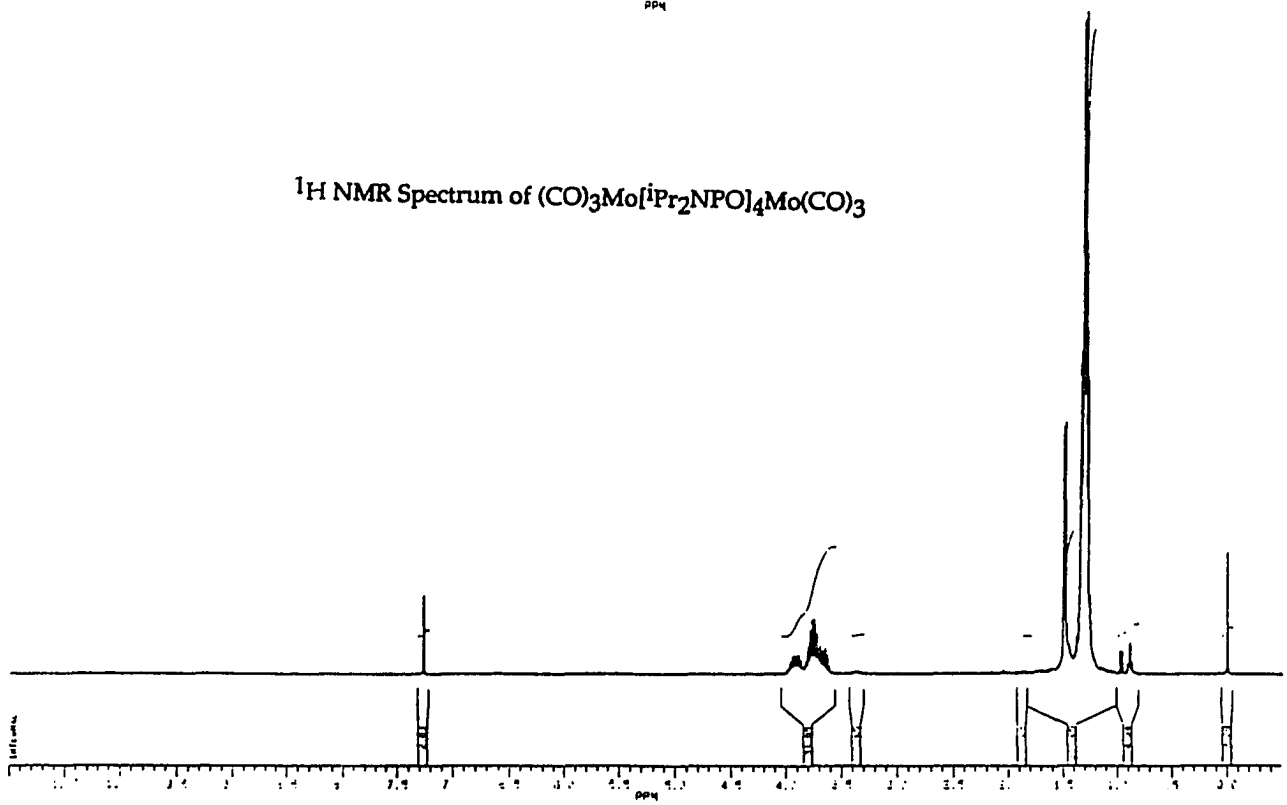
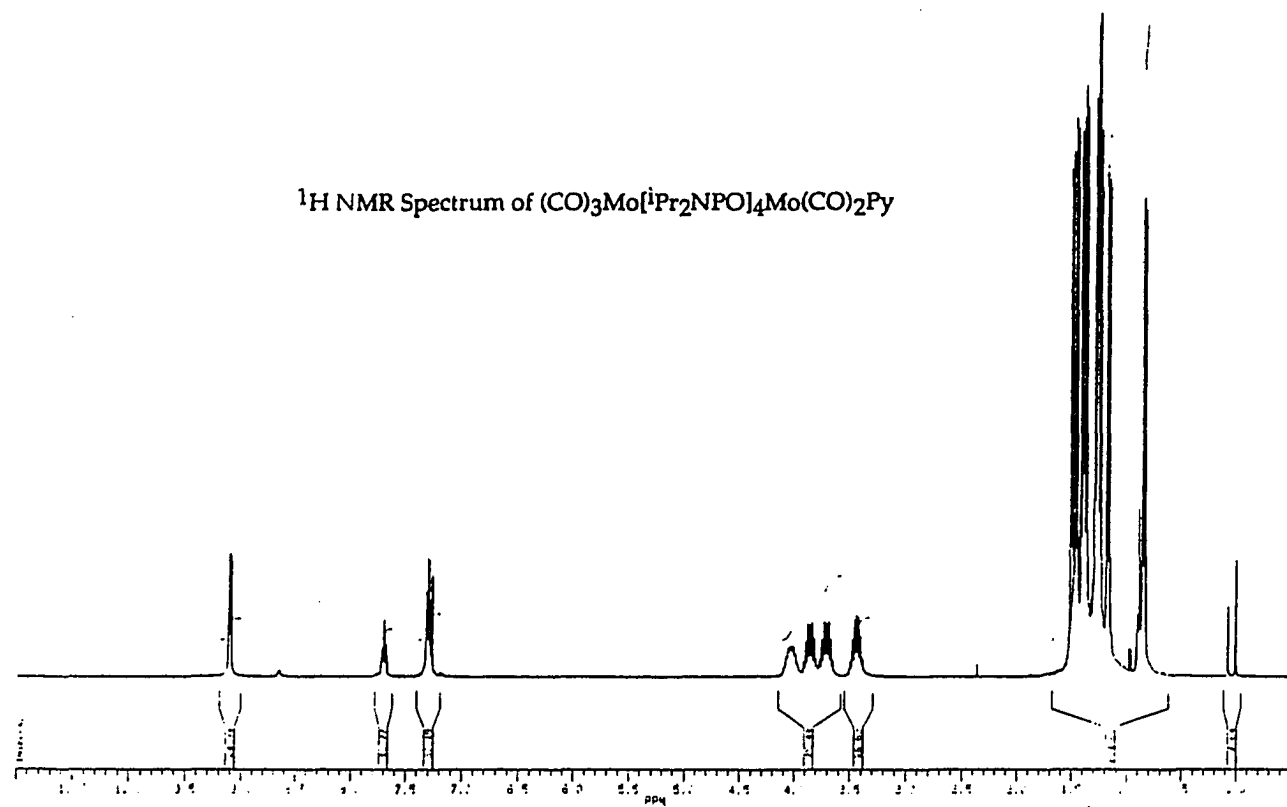
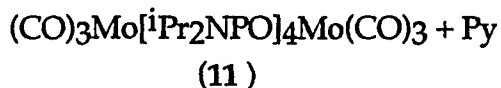
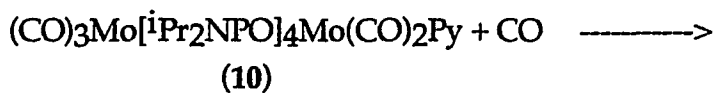


Figure 25. ^1H NMR spectra of complex 10 and 11

Thus, liberated CO from decomposition can displace the Py ligand in **10** to form the new orange complex $\text{Mo}_2[\text{iPr}_2\text{NPO}]_4(\text{CO})_6$. In order to prove this, CO gas was bubbled through a solution of complex **10** at about 60°C. After a few hours, TLC showed that it was completely transformed to orange compound **11**. The new compound showed an orange spot on the top of the spot of complex **10**. ^1H and ^{31}P NMR spectra clearly showed that this new product, $(\text{CO})_3\text{Mo}[\text{iPr}_2\text{NPO}]_4\text{Mo}(\text{CO})_3$ (**11**), is identical to the one obtained from a CDCl_3 NMR solution of **10**. The reaction can be written as:



(eq 8)

(B) Complex **11** is very reactive and easily reacted with pyridine to reform **10**. It can also react with maleic anhydride in warm toluene or refluxing hexane to form a yellow cage-olefin complex. Complex **10** can also react with maleic anhydride in refluxing hexane to form a similar yellow cage-olefin complex. This cage-olefin complex was an inseparable mixture. When complex **10** reacted with $\text{MeP}(\text{C}_6\text{H}_5)_2$ in refluxing toluene, complex **3** was reformed.

Complex **11** was very soluble in warm hexane and hexane solutions under N_2 gave good quality crystals. The X-ray structure of these crystals was determined (Figure 26). Selected bond distances and bond angles are listed in Table V:

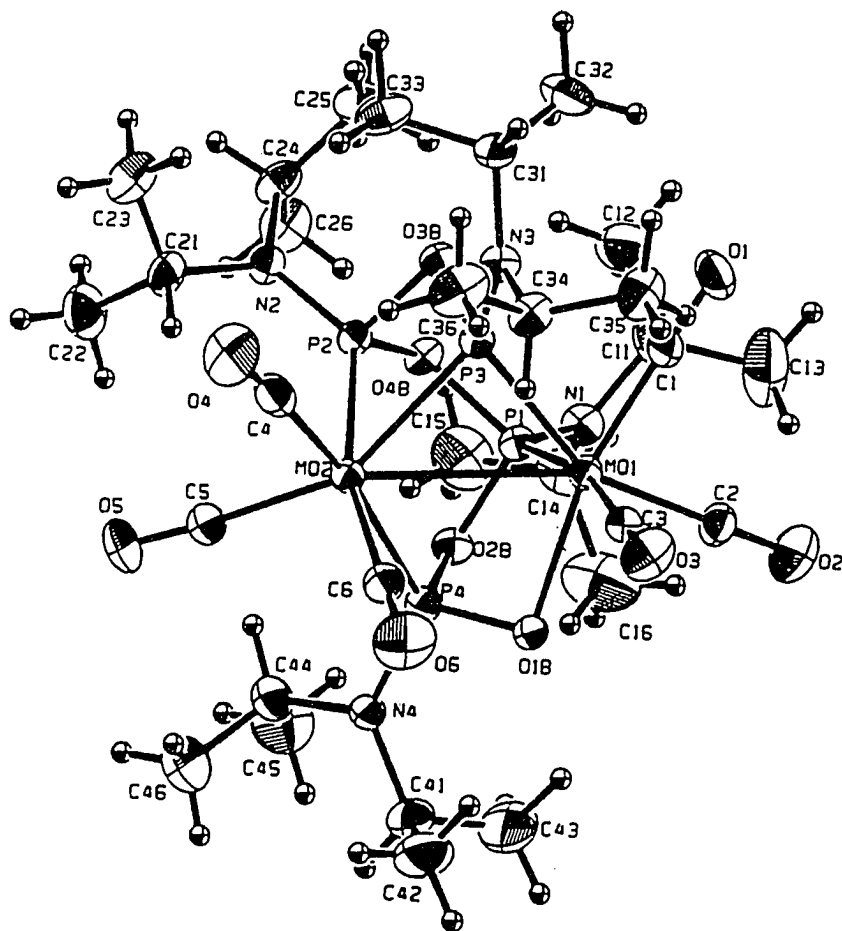


Figure 26. Molecular structure of complex 11

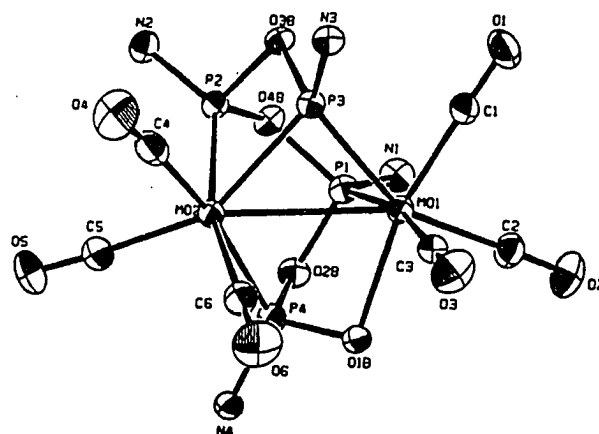


Figure 27. Core geometry of complex 11

Table V. Selected Bond Distances (Å) and Angles (deg) for Mo₂[¹Pr₂NPO]₄(CO)₆ (11)

Mo(1)-Mo(2)	3.143(1)		
Mo(1)-P(1)	2.501(3)	P(2)-O(2B)	1.599(7)
Mo(1)-P(3)	2.403(3)	P(2)-O(4B)	1.676(7)
Mo(1)-O(1B)	2.265(7)	P(2)-P(3)	2.544(4)
Mo(1)-C(1)	1.94(1)	P(2)-O(3B)	1.694(7)
Mo(1)-C(2)	2.04(1)	P(2)-O(4B)	1.621(7)
Mo(1)-C(3)	2.03(1)	P(3)-O(3B)	1.639(7)
Mo(2)-P(2)	2.440(3)	P(4)-O(1B)	1.526(7)
Mo(2)-P(3)	2.443(3)	P(4)-O(2B)	1.742(8)
Mo(2)-P(4)	2.515(3)	C(1)-O(1)	1.16(1)
Mo(2)-C(4)	2.11(2)	C(2)-O(2)	1.13(1)
Mo(2)-C(5)	2.01(1)	C(3)-O(3)	1.13(1)
Mo(2)-C(6)	2.03(1)	C(4)-O(4)	1.10(2)
C(5)-O(5)	1.14(1)	C(6)-O(6)	1.12(1)
Mo(2)-Mo(1)-P(1)	78.42(7)	Mo(1)-Mo(2)-P(2)	81.38(7)
Mo(2)-Mo(1)-P(3)	50.11(7)	Mo(1)-Mo(2)-P(3)	49.00(7)
Mo(2)-Mo(1)-P(4)	49.01(6)	Mo(1)-Mo(2)-P(4)	60.36(7)
Mo(2)-Mo(1)-O(1B)	73.8(2)	Mo(1)-Mo(2)-C(4)	125.2(3)
P(1)-Mo(1)-P(3)	90.6(1)	P(2)-Mo(2)-P(3)	62.8(1)
P(1)-Mo(1)-O(1B)	79.2(2)	P(2)-Mo(2)-P(4)	93.4(1)
P(1)-Mo(1)-C(1)	97.5(4)	P(2)-Mo(2)-C(4)	97.2(1)
P(1)-Mo(1)-C(2)	91.6(4)	P(2)-Mo(2)-C(5)	96.5(4)
P(1)-Mo(1)-C(3)	167.7(3)	P(2)-Mo(2)-C(6)	164.3(4)

P(3)-Mo(1)-O(1B)	123.8(2)	P(3)-Mo(2)-P(4)	107.0(1)
P(3)-Mo(1)-C(1)	72.4(3)	P(3)-Mo(2)-C(4)	81.5(3)
P(3)-Mo(1)-C(2)	153.2(4)	P(3)-Mo(2)-C(5)	151.8(4)
P(3)-Mo(1)-C(3)	93.7(3)	P(3)-Mo(2)-C(6)	103.7(4)
O(1B)-Mo(1)-C(1)	163.2(4)	P(4)-Mo(2)-C(4)	168.7(4)
O(1B)-Mo(1)-C(2)	82.7(4)	P(4)-Mo(2)-C(5)	92.4(4)
O(1B)-Mo(1)-C(3)	88.8(4)	P(4)-Mo(2)-C(6)	82.6(4)
C(1)-Mo(1)-C(2)	80.9(5)	C(4)-Mo(2)-C(5)	82.5(5)
C(1)-Mo(1)-C(3)	94.8(5)	C(4)-Mo(2)-C(6)	88.2(5)
C(2)-Mo(1)-C(3)	89.8(5)	C(5)-Mo(2)-C(6)	98.8(5)
Mo(1)-P(1)-O(2B)	103.1(3)	Mo(2)-P(2)-O(3B)	97.2(3)
Mo(1)-P(1)-O(4B)	116.0(3)	Mo(2)-P(2)-O(4B)	116.7(3)
Mo(1)-P(3)-Mo(2)	80.89(9)	Mo(2)-P(3)-O(3B)	98.6(3)
Mo(1)-P(3)-O(3B)	113.1(3)	Mo(2)-P(4)-O(1B)	108.0(3)
Mo(1)-O(1B)-P(4)	97.7(4)	Mo(2)-P(4)-O(2B)	110.5(3)
O(1B)-P(4)-O(2B)	103.3(4)	P(1)-O(2B)-P(4)	107.9(4)
O(2B)-P(1)-O(4B)	100.3(4)	P(1)-O(4B)-P(2)	116.5(4)
P(2)-O(3B)-P(3)	99.5(2)	O(3B)-P(2)-O(4B)	98.0(4)

Complex 11 has a polycyclic structure similar to complexes 2 and 7. Replacing a phosphine or phosphite ligand by a CO ligand only generated relatively few changes in bonding details. The Mo(1)-Mo(2) bond is now at 3.143(1) Å. The Mo(1)-P(3) bond changed from 2.362(4) in 2 and 2.352(2) in 7 to 2.403(3) Å with a CO instead of the PPh₃ or P(OCH₃)₃ *trans* to it. That is because CO ligand is a better π -acceptor ligand, so the π back-bonding between Mo-CO is stronger and the Mo-P bonding is weakened. The Mo(1)-O(1B) bond distance is changed from 2.222(8) in 2 and 2.226(3) in 7 to 2.260(7) Å. The

Mo(1)-C(1) bond distance *trans* to the Mo(1)-O(1B) bond is 1.94(1) Å. It is indeed shorter than all of the other Mo-C bonds which are in the range 2.01-2.11 Å. The two disparate P(4)-O distances result in a shorter bond P(4)-O(1B) at 1.526(7) Å and a longer bond P(4)-O(2B) at 1.742(8) Å.

Both bond angles and coordination spheres around Mo(2) are similar to those in **2** or **7**. With the replacement of a phosphine or phosphite by a carbonyl ligand, the four-membered Mo(2)-P(2)-O(3B)-P(3) chelate ring and the five-membered Mo(1)-P(3)-Mo(2)-P(4)-O(1B) heterocycle are essentially unchanged. The Mo(2)-P(3)-Mo(1) angle is slightly decreased to 80.9(1)° due to the smaller Mo-Mo distance. At Mo(1), the angle closest to linearity is C(3)-Mo(1)-P(1) at 167.7(3)° while P(4)-Mo(2)-C(4) is 168.7(4)°. The four equatorial ligand atoms P(3), O(1B), C(1), and C(2) have distorted angles at Mo(1); P(3)-Mo(1)-O(1B) is 123.8(2)°, O(1B)-Mo(1)-C(2) is 82.7(4)°, C(1)-Mo(1)-C(2) is 80.9(5)° and C(1)-Mo(1)-P(3) is 72.4(3)°. These angles sum to 359°. At Mo(2), the corresponding equatorial angles deviate widely from orthogonality ranging from 62.8(1) to 103.7(4)°, summing to 362°. The C(3) at Mo(1) now has reasonably orthogonal angles with O(1B), P(3), C(1), and C(2) ranging from 88.9(4) to 94.8(5)° compared to the corresponding angles in **7** ranging from 79.3(1) to 93.20(5)°.

The overall geometries of the complexes **2**, **7**, and **11** are thus quite similar. As mentioned in Part I-2, the phosphido chemical shift is very sensitive to the M-P-M angle and the extent of metal-metal interaction. For the series of orange complexes, the nearly constant phosphido chemical shift at +306 ppm suggests that these geometrical details are very similar in these complexes. A comparison of selected bond details from the X-ray structure of complexes **2**, **7**, **11**, as depicted in Figure 28, demonstrates that the phosphido angle and Mo-

Mo bond indeed remain little changed.

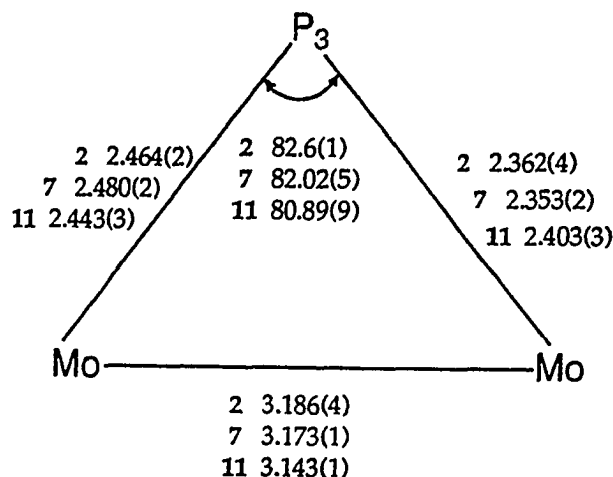
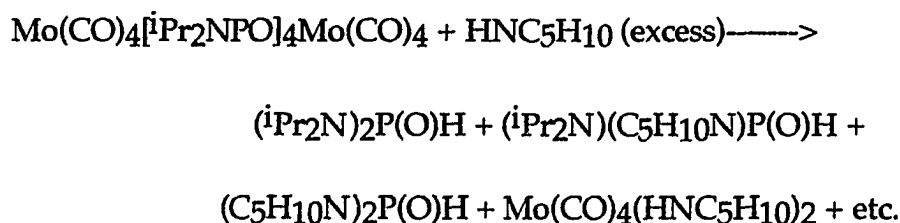


Figure 28. Comparison of the phosphido-bridge structural data for complex **2**, **7**, **11**

For the cage reactions of CH_3CN and $\text{C}_6\text{H}_5\text{CN}$, we deduced from the TLC and the ^{31}P NMR spectra of the reaction solutions that two orange-colored products formed. One of these readily rearranged to the other in CDCl_3 solvent. By comparing the ^{31}P NMR spectra with that of **10** and **11**, it is clear that one of the products is $(\text{CO})_3\text{Mo}[\text{iPr}_2\text{NPO}]_4\text{Mo}(\text{CO})_2(\text{RCN})$ and the other is again complex **11**, $(\text{CO})_3\text{Mo}[\text{iPr}_2\text{NPO}]_4\text{Mo}(\text{CO})_3$. (We tried very hard but unsuccessfully to isolate the pure products.) Since CH_3CN and $\text{C}_6\text{H}_5\text{CN}$ are ligands which have very little π -bonding ability^[37], the substitution intermediates are not very stable.

For the reaction of pyridine, only one substitution product was formed in a fast reaction, but for secondary amines like piperidine and diisopropylamine, the reactions were slow and the cage was degraded via P-O-P cleavage to give bis (dialkylamino) phosphine oxides:



Both transamination and nucleophilic P-O-P cleavage occurred, resulting in essentially a reversal of the cage formation reaction from Mo(CO)_6 and $(\text{iPr}_2\text{N})_2\text{P(O)H}$ [8]. The identities of the products were confirmed by obtaining the proton-decoupled and proton-coupled ^{31}P NMR spectra of the product mixture.

Also, we checked the reactions of the cage compound with tertiary amines such as $[(\text{CH}_3)_2\text{CH}]_2\text{NC}_2\text{H}_5$ and $(\text{C}_2\text{H}_5)_3\text{N}$. Because the bonding between the metal and pure σ -donor ligands is very weak, only negligible cage reactions resulted.

6. Relationship of Reaction Rate to Steric and Electronic Factors

It has long been hoped that the stereoelectronic properties of phosphorus(III) ligands can be parameterized into electronic and steric components. Yet, steric effects can have important electronic consequences and vice versa. Thus, the separation of electronic and steric effects into purely

steric or electronic factors is difficult. Tolman introduced the cone angle^[38] and electronic parameter^[39] (χ values) of phosphorus (III) ligands for this quantification. A measure of steric effects was proposed based on ligand cone angles (θ) of space-filling CPK molecular models and the electronic effect was based on A_1 carbonyl stretching frequencies (ν) in $Ni(CO)_3L$ complexes. Since then, it has been shown that many chemical and spectroscopic properties of organometallic complexes correlate with the cone angle and the χ values, and reflect the collective electronic donor/acceptor properties of the ligands^[36] [40]. It is a practical and useful separation.

In order to distinguish the importance of the electronic and steric influences of the phosphorus ligands in these two-step reactions, we compared the reactions of cage complex **1** with $P(C_6H_5)_3$, $MeP(C_6H_5)_2$, $HP(C_6H_5)_2$, $P(OCH_3)_3$, $P(OC_6H_5)_3$ and pyridine under similar conditions. From the ^{31}P NMR spectra of the reaction mixtures we calculated the percent of cage reacted and also the percent of the orange phosphido- compound formed from the substitution intermediates. The results are listed in Tables VI and VII along with ligand size and electronic parameters derived by Tolman:

Table VI: Comparison of the Reaction Rates with Ligands Cone Angle

Ligand	Θ	%Cage Reacted(4 h)
P(C ₆ H ₅) ₃	145	44(2)
MeP(C ₆ H ₅) ₂	136	56(2)
P(OC ₆ H ₅) ₃	128	56(5)
HP(C ₆ H ₅) ₂	126	95(3)
P(OCH ₃) ₃	106	100(1)
pyridine	105	100(1)

(N. B. % is amount of product relative to the Cage Starting Material)

Table VII: Comparison of the Reaction Rates with the Electronic Parameters of the Ligands

Ligand $PX_1X_2X_3$	$X_1+X_2+X_3$	% orange product formed(4 h)
P(OC ₆ H ₅) ₃	$9.7 \times 3 = 29.1$	0(1)
P(OCH ₃) ₃	$7.7 \times 3 = 23.1$	~10-20(10)*
HP(C ₆ H ₅) ₂	$4.3 \times 2 + 8.3 = 16.9$	49(4)
P(C ₆ H ₅) ₃	$4.3 \times 3 = 12.9$	22(4)
MeP(C ₆ H ₅) ₂	$4.3 \times 2 + 2.6 = 11.2$	33(1)
pyridine		100(1)

* Estimated from the spectra.

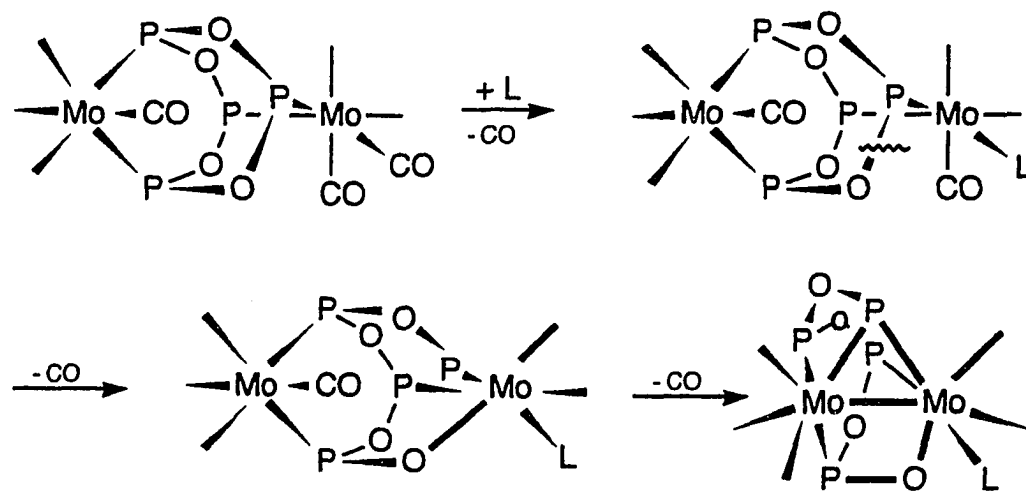
(N. B. % is based on the amount of cage reacted in the reaction mixture.)

From the above results, we can see that as the cone angle of the phosphine ligand decreased, the percent of cage reacted increased. As the π -acceptor ability of ligand decreased, the percent of orange phosphido-product increased. In addition, as the reaction progressed, the fraction of the orange complex to the consumed cage increased. So the ligand steric influence upon the initial substitution step is important. For the second rearrangement step, the steric factor is less important than the electronic influence. The smaller the ligand, the easier it can substitute CO's on the cage, while the stronger the π -acceptor ability of the ligand, the more stable these intermediates proved to be.

Why do strong π -acceptor ligands stabilize the cage-structure? It may be because they can decrease the electron density on the metal by increasing the strength of M->P or M->CO π -bonding, whereas stronger σ -donors will make the metal more electron rich and facilitate P-O-P oxidative addition at the metal.

Conclusions and Suggestions for Future Work

Triphenylphosphine, diphenylmethylphosphine, and diphenylphosphine or pyridine reacted with the molybdenum cage complex, which resulted in the addition of one ligand and loss of three carbonyls to yield the orange products. One P-O-P intercage linkage has been cleaved and oxidatively added to the two molybdenum vertices to create a μ^2 -PO- and a μ^2 -P- bridge. In addition, an intercage metal-metal bond has formed (Scheme IV).



Scheme IV

When trimethylphosphite and triphenylphosphite reacted with the molybdenum cage complex, the simple mono- and disubstituted complexes were obtained. Upon further heating, these substitution products underwent similar P-O-P cleavage and associated transformations to give analogues of the phosphine and pyridine adducts.

When these adducts reacted with CO gas, the attached phosphine was replaced by CO to form complex **11**, $(\text{CO})_3\text{Mo}[\text{iPr}_2\text{NPO}]_4\text{Mo}(\text{CO})_3$. If the weak-

bonding ligands acetonitrile or benzonitrile were used to react with the molybdenum cage, complex 11 formed as the major product even though no CO gas was added to the reaction solution.

The facility for the transformation of simple substitution complexes to the orange complexes appeared to depend on the π -acceptor strength of the attacking nucleophile while the initial substitution itself depended on the steric size of the ligands. A smaller ligand with stronger π -acceptor ability can more easily substitute CO's on the cage and form the substitution intermediates, while ligands with more σ -donor ability can more easily form the orange compound. Also, pure σ -donor ligands such as amines have only weak interactions with the zero-valent metal centers.

Future work in this area might involve studies of the reactivities of analogous cage complexes, cage complexes with different substituents on phosphorus atoms, or different-sized cage such as $M_2(CO)_8[DMP-PO]_4$ ($M=Cr, Mo$), $Ni_2(CO)_4[Cy_2NPO]_4$, $Cr_2(CO)_8[iPr_2NPO]_4$, and $Cr_2(CO)_6[DMP-PO]_6$. The substitution and oxidation-addition rates, the nature of the products or the distribution of the intermediate isomers of these complexes may prove to be very different, because the different metal centers and the different substituents on the phosphorus atoms and even the polyphosphoxane cage size, may all play important roles in these processes.

Strongly nucleophilic species or noncoordinating acids like BF_4^- and HSO_3CF_3 should be reacted with the cage complex. The former may attack the cage phosphorus atoms, whereas the latter can protonate the cage by attacking the P-N sites.

EXPERIMENTAL SECTION

General Procedure: All synthetic procedures were carried out using standard Schlenck technique under an atmosphere of prepurified nitrogen. Chemical reagents were commercial products and were used without further purification. Hexane and methylene chloride were distilled from CaH_2 . Toluene was reagent grade and was dried over Na and freshly distilled before use. Triphenylphosphine, diphenylmethylphosphine, diphenylphosphine, trimethyl phosphite were used as purchased from Strem Chemicals. Pyridine, diisopropylamine, piperidine, ethyl acetate, acetonitrile and benzonitrile were reagent grade obtained from Aldrich Chemical Co. Alumina (Aldrich Chemical Co, Brockmann, I, neutral) was used as received. The cage complex $(\text{CO})_4\text{Mo}(\text{}^i\text{Pr}_2\text{NPO})_4\text{Mo}(\text{CO})_4$ was synthesized as described previously [8]. ^1H , ^{13}C and ^{31}P NMR spectra were recorded on JEOL FX 90Q or Bruker AM360 FT-NMR Spectrometers. For ^1H and ^{13}C , $(\text{CH}_3)_4\text{Si}$ was used as internal standard, whereas for ^{31}P , the chemical shifts were reported in ppm to high frequency of external 85% H_3PO_4 . Spectra were obtained in CDCl_3 solution unless otherwise noted. Infrared spectra were recorded on a Perkin-Elmer 283B Spectrometer. Elemental analyses were performed at the University Instrumentation Center using a Perkin-Elmer 240b or Perkin-Elmer Series CHNS/O Analyzer 2400 elemental analyzer.

X-ray crystal structures were determined by Dr. Jerry P. Jasinski, Roman Y. Pozdnizkov, and Richard Woudenberg, Department of Chemistry, Keene

State College, Keene, New Hampshire.

[(CO)₃Mo(iPr₂NPO)₄Mo(CO)₂(P(C₆H₅)₃)] (2). A 25 mL, round-bottomed flask was charged with 1.0000 g of the cage complex (CO)₄Mo(iPr₂NPO)₄Mo(CO)₄ and 0.5222 g P(C₆H₅)₃, a magnetic stirbar and evacuated. Toluene 10.0 mL was added into the flask under nitrogen. The mixture was stirred and heated to 110 °C. After refluxing for 24 hours (cage completely gone), the clear red-colored reaction solution was evaporated to dryness under reduced pressure. Then 15-mL aliquot of hexane was added to extract the residue. The extract chromatographed on a 1- x 30-cm column of alumina using 2% ethyl acetate in hexane as eluant. Compound 2 was obtained as an orange-red solid in 40% yield (0.4697 g). When 2 was dissolved in hot hexane and the solution cooled, X-ray-quality crystals were obtained. Elemental analyses (calculated/observed for C₄₇H₇₁Mo₂N₄O₉P₅): C% 47.72/47.79, H% 6.05/6.15, N% 4.74/4.68. ¹H NMR: δ 7.86 and 7.24 (m, Ph), 3.86 and 3.68 (m, N-CH), 1.33, 1.32, 1.30, 1.20, 1.19, 1.13, 1.02, 0.87 (d, Me, J=6.7-6.8 Hz). ¹³C NMR: δ 222.7 and 221.7 (m, CO), 218.4 (dd, CO, J=18.8, 54.2 Hz), 137.0-128.1 (m, Ph), 49.1, 48.6, 46.4, 44.8 (d, N-C, J= 12.4, 7.5, 9.3, 8.6 Hz), 23.3 (m, Me).

[(CO)₃Mo(iPr₂NPO)₄Mo(CO)₂(PR₃)] (R₃= MeP(C₆H₅)₂, HP(C₆H₅)₂. 3, 4). A 25 mL, round-bottomed flask was charged with 1.0000 g (1.0000 mmol) of the cage complex, a stirbar, 10 mL of toluene and 2.0000 mmol of the respective phosphine. Similar reaction procedures as 2 were used. Because 3 and 4 were not stable on the column, so after running the reactions for 24 hours (cage completely gone), the clear red-colored reaction solutions were

stripped of the toluene under reduced pressure. Upon standing for one day, the resulting viscous oils afforded red crystals of the products. By washing off $\text{MeP}(\text{C}_6\text{H}_5)_2$ or $\text{HP}(\text{C}_6\text{H}_5)_2$ and other impurities with small portions of cold hexane and dried to give 80% yield of **3** or **4**. Elemental analyses (calculated/observed for $\text{C}_{42}\text{H}_{69}\text{Mo}_2\text{N}_4\text{O}_9\text{P}_5$ **3**): C% 45.01/45.18, H% 6.20/6.27, N% 4.60/5.00. Elemental analyses (calculated/observed for $\text{C}_{41}\text{H}_{67}\text{Mo}_2\text{N}_4\text{O}_9\text{P}_5$ **4**): C% 44.49/44.34, H% 6.10/6.48, N% 5.06/4.72. ^1H NMR (for **3**): δ 7.75-7.30 (m, Ph), 3.97 and 3.70 (m, N-CH), 2.02, 1.45, 1.36, 1.28, 1.23, 1.20 (d, Me, $J=8.3, 6.7, 6.7, 7.7, 6.9, 6.8$ Hz). ^1H NMR (for **4**): δ 7.77-7.32 (m, Ph), 6.51 (dd, P-H, $J=9, 332$ Hz), 4.0-3.55 (m, N-CH), 1.49, 1.32, 1.27, 1.10, 1.00 (d, Me, $J=6.7-6.8$ Hz). ^{13}C NMR (for **3**): δ 224.9 and 221.1 (m, CO), 218.6 (dd, CO, $J=14.6, 36.4$ Hz), 138.0-127.9 (m, Ph), 48.43, 48.38, 46.2, 44.8 (d, N-C, $J=7.5, 10.0, 8.7, 8.7$ Hz), 24.5 (s, Me), 23.3 (m, Me), 15.3 (d, Me, $J=19.3$ Hz). ^{13}C NMR (for **4**): δ 223.2 and 221.2 (m, CO), 218.2 (dd, CO, $J=15.2, 51.3$ Hz), 134.2-128.7 (m, Ph), 48.5, 47.9, 46.5, 44.5 (d, N-C, $J=8.4, 9.2, 9.2, 8.5$ Hz), 24.5 (d, Me, $J=7.8$ Hz), 22.9 (m, Me).



$[(\text{HP}(\text{C}_6\text{H}_5)_2)(\text{CO})_3\text{Mo}(\text{iPr}_2\text{NPO})_4\text{Mo}(\text{CO})_3(\text{HP}(\text{C}_6\text{H}_5)_2)] \text{ (9)}$. A 25 mL, round-bottomed flask was charged with a stirbar, 0.2000 g (0.2000 mmol) of the cage complex, 10.0 mL hexane, and 2.000 mmol of the diphenylphosphine. The mixture was stirred and allowed to heat to reflux. After refluxing for three days, TLC gave four spots. The light-yellow reaction solution was evaporated under reduced pressure and the residue chromatographed on an alumina column as described for **2**. The second complex to elute was complex **8**, isolated in 11% yield (0.025 g), and the fourth was complex **9**, in 4% yield

(0.010 g). Elemental analyses (calculated/observed for $C_{43}H_{67}Mo_2N_4O_{11}P_5$ **8**): C% 44.42/44.19, H% 5.81/5.83, N% 4.82/4.53. Elemental analyses (calculated/observed for $C_{54}H_{78}Mo_2N_4O_{10}P_6$ **9**): C% 49.10/47.36, H% 5.95/6.38, N% 4.38/4.24. Due to the very low yield of **9**, repeated efforts failed to improve on these elemental data. 1H NMR (for **8** in C_6D_6): δ 7.60 and 7.05 (m, Ph), 6.39 (d of t, P-H, $J=4.2$, 309.7 Hz), 4.78 (septet, N-CH, $J=6.4$ Hz), 4.55 and 4.11 (m, N-CH), 1.36 (m, Me), 1.04 (d, Me, $J=7.0$ Hz). ^{13}C NMR (for **8** in C_6D_6): δ 217.7, 217.1, 214.9 (m, CO), 135.0-128.8 (m, Ph), 47.4 (m, N-C), 25.6, 24.3, 23.9 (m, Me). 1H NMR (for **9** in C_6D_6): δ 7.70 and 7.05 (m, Ph), 6.43 (d, P-H, $J=304.9$ Hz), 4.93 and 4.54 (m, N-CH), 1.46, 1.45, 1.15, 1.07 (d, Me, $J=6.9, 7.0, 7.1, 6.9$ Hz). ^{13}C NMR (for **9** in C_6D_6): δ 218.0 (m, CO), 136.1-128.8 (m, Ph), 47.5 (m, N-C), 25.7-24.2 (m, Me).



$[(P(OMe)_3)(CO)_3Mo(iPr_2NPO)_4Mo(CO)_3(P(OMe)_3)](6)$. A 25 mL round-bottomed flask was charged with 1.0000 g (1.00 mmol) of the cage complex, a stirbar, 0.25 mL (2.10 mmol) of $P(OMe)_3$ and 10.0 mL of toluene. The mixture was stirred and allowed to heat to reflux. After refluxing for six hours, a light-yellow solution formed and two colorless spots due to the products showed on the TLC. The solution was evaporated under reduced pressure and the light-yellow residue chromatographed on an alumina column as for **2**. Complex **5** (0.34 g, 0.32 mmol, 32% yield based on the cage) was obtained followed by 0.60 g of complex **6** (0.50 mmol, 50% yield based on the cage). Elemental analyses (calculated/observed for $C_{34}H_{65}Mo_2N_4O_{14}P_5$ **5**): C% 37.10 /36.99, H% 5.95 /6.08, N% 5.09 /4.96. Elemental analyses

(calculated/observed for $C_{36}H_{74}Mo_2N_4O_{16}P_6$ **6**): C% 36.13/36.11, H% 6.23/6.12, N% 4.68/4.72. 1H NMR (for **5**): δ 4.57 and 4.38 (unresolved multiplets, N-CH), 3.61 and 3.59 (d, OMe, $J=11.2, 10.4$ Hz), 1.3-1.5 (overlapping doublets, Me). ^{13}C NMR (for **5**): δ 217.4, 213.6, 210.3, 206.6 (unresolved multiplets, CO), 50.2, 46.0 (unresolved multiplets, N-C and OMe), 23.5 (unresolved multiplets, Me). 1H NMR (for **6**): δ 4.66 and 4.53 (unresolved multiplets, N-CH), ~ 3.6 (unresolved multiplets OMe Hz), ~ 1.35 (overlapping doublets, Me). ^{13}C NMR (for **6**): δ 219.3, 217.8, 214.3, 211.7 (unresolved multiplets, CO), 51.2 and 46.7 (unresolved multiplets, N-C and OMe), 24.7 (unresolved multiplets, Me).

$[(CO)_3Mo(iPr_2NPO)_4Mo(CO)_2(P(OMe)_3)](7)$. The same procedure used for the syntheses of complexes as **5** and **6** was followed except that the reaction solution was refluxed for 34 hours. After chromatography, 0.720 g (0.69 mmol, 69% yield) of **7** was obtained. X-ray-quality crystals were obtained by slow evaporation from a hexane solution. Elemental analyses (calculated/observed for $C_{32}H_{65}Mo_2N_4O_{12}P_5$ **7**): C% 36.79 /36.71, H% 6.27/6.58, N% 5.36 /5.00. 1H NMR (in C_6D_6): δ 4.02, 3.80, 3.65 (m, N-CH), 3.60 (d, OMe, $J=10.6$ Hz), 1.47 and 1.32 (d, Me, $J=6.7$ and 6.8 Hz), 1.39 and 1.21 (m, Me). ^{13}C NMR (in C_6D_6): δ 223.2, 221.8, 220.2 (m, CO), 218.6 (dd, $J=15.6, 50.6$ Hz), 52.2, 48.4, 48.1, 46.5, 44.6 (d, N-C or OMe, $J=5.2, 8.4, 10.6, 9.4, 8.4$ Hz), 23.0, 22.7, 22.6, 22.3 (m, Me).

$[(CO)_3Mo(iPr_2NPO)_4Mo(CO)_2(NC_5H_5)](10)$. A 25 mL round-bottomed flask was charged with 2.0000 g of the cage complex, 2.00 mL pyridine, a

stirbar, 18.0 mL toluene. The mixture was stirred and allowed to heat to reflux, The reaction was followed by TLC. Only one orange-colored spot appeared as the product on the TLC during the reaction. After 9 hours, the cage complex was gone and the reaction mixture was deep red, some brown precipitate formed. A clear deep red solution was obtained after filtering the reaction mixture. The filtrate was evaporated to dryness under reduced pressure and the residue was washed with several portions of hexane to give 1.522 g red compound **10** (1.52 mmol, 76% yield). Elemental analyses (calculated/observed for $C_{34}H_{61}Mo_2N_5O_9P_4$ **10**): C% 40.85/40.87, H% 6.15/6.21, N% 7.01 /6.75. 1H NMR: δ 9.11-7.29 (m, Py), 4.03, 3.85, 3.71, 3.44 (septets, N-CH, $J=6.6, 6.8, 6.9, 6.7$ Hz), 1.51, 1.47, 1.41, 1.38, 1.29, 1.26, 1.19 (d, Me, $J=6.7, 6.7, 6.8, 6.8, 6.9, 6.9, 6.8$ Hz), 1.39 and 1.21 (m, Me). ^{13}C NMR: δ 228.1 (dd, CO, $J=12.1, 44.0$ Hz), 221.4 218.2 (m, CO), 153.4-124.2 (m, Py), 48.4, 47.5, 46.5, 45.2 (d, N-C, $J= 8.4, 10.4, 9.6, 9.2$ Hz), 23.5-22.4 (m, Me).

$[(CO)_3Mo(iPr_2NPO)_4Mo(CO)_3](11)$. Complex **10** (0.6565 g) was dissolved in 20 mL toluene at $60^\circ C$, and CO gas was bubbled through it for 6 hours. Complex **10** was gone, and a new orange-red solution was obtained. The orange red clear solution was evaporated to dryness and an orange residue was obtained. The residue was chromatographed to give 0.3095 g (0.33 mmol, 50% yield) of orange compound **11**. X-ray-quality crystals were obtained by slow evaporation from a hexane solution. Elemental analyses (calculated/observed for $C_{30}H_{56}Mo_2N_4O_{10}P_4$ **11**): C% 37.99/37.57, H% 5.95/6.13, N% 5.91/5.71. 1H NMR: δ 3.92, 3.72 (m, N-CH), 1.50 and 1.35 (d, Me, $J=6.7, 3.0$ Hz), 1.31 (m, Me). ^{13}C NMR: δ 220.8, 217.6, 215.6, 208.0 (m, CO), 48.9, 48.2, 47.4, 45.3 (d, N-C, $J= 8.9, 10.3, 10.4, 8.6$ Hz), 23.0 (m, Me).

X-ray Structural Determination of Complex 2. A summary of crystal data, data collection, and structural refinement details is presented in **Table VIII**. The intensities of a 0.6- x 0.2- x 0.8-mm crystal were collected on a Rigaku AFC6S diffractometer. A total of 11267 unique reflections were measured of which 6097 were considered significant at the 3σ level. The structure was solved using direct methods, and the hydrogens were included at calculated positions^[41]. Final least squares were performed varying 605 parameters. Final RF=0.074 and Rw=0.120 with a goodness-of-fit (GOF) of 3.81. Selected bond distances and bond angles are listed in **Table III**.

X-ray Structural Determination of Complex 7. A summary of crystal data, data collection, and structural refinement details is presented in **Table VIII**. The intensities of a 0.6- x 0.4- x 0.7-mm crystal were collected to yield a total of 11384 unique reflections were measured of which 6070 were considered significant at the 3σ level. The structure was solved using direct methods, and hydrogens were included at calculated positions. Final least squares were performed varying 497 parameters. Final RF=0.042 and Rw=0.044 with a goodness-of-fit (GOF) of 1.32. Selected bond distances and bond angles are listed in **Table IV**.

Table VIII. Crystal Data for Complexes 2, 7 and 11

	2	7	11
formula	Mo ₂ P ₅ O ₉ N ₄ C ₄₇ H ₇₁	Mo ₂ P ₅ O ₁₂ N ₄ C ₃₂ H ₆₅	Mo ₂ P ₄ O ₁₀ N ₄ C ₃₀ H ₅₆
fw	1182.85	1044.63	948.57
space group	<i>P</i> 2 ₁ / <i>c</i>	<i>P</i> 2 ₁ / <i>n</i>	<i>C</i> 2 ₁ / <i>c</i>
	monoclinic	monoclinic	monoclinic
<i>a</i> , Å	12.684(1)	13.026(3)	36.523(7)
<i>b</i> , Å	13.383(3)	21.054(3)	13.287(5)
<i>c</i> , Å	37.109(4)	18.118(3)	20.348(3)
β, deg		103.46(2)	109.48(1)
<i>Z</i>	4	4	8
<i>d</i> _{calc} , g cm ⁻³	1.247	1.436	1.353
μ, mm ⁻¹	5.58	7.22	7.07
cryst dimens, mm	0.6x0.2x0.8	0.6x0.4x0.7	1.0x1.0x1.0
λ(Mo K radiation), Å	0.71069	0.71069	0.71069
data collcd	0° < 2θ < 55.0°	0° < 2θ < 55.0°	0° < 2θ < 55.0°
scan	ω	ω	ω
no. of unique reflcns	11267	11384	11325
no. of obsd reflcns	6097	6070	4770
<i>F</i> (000)	2448	2160	3904
<i>R</i> _{<i>F</i>}	0.074	0.042	0.054
<i>R</i> _{WF}	0.121	0.044	0.074
GOF	3.81	1.32	2.00

X-ray Structural Determination of Complex 11. A summary of crystal data, data collection, and structural refinement details is presented in Table VIII. The intensities of a 1.0- x 1.0- x 1.0-mm crystal were collected to yield a total of 11150 unique reflections were measured of which 4723 were considered significant at the 3σ level. The structure was solved using direct methods, and the hydrogens were included at calculated positions. Final least squares were performed varying 452 parameters. Final $R_f=0.054$ and $R_w=0.074$ with a goodness-of-fit (GOF) of 2.00. Selected bond distances and bond angles are listed in Table V.

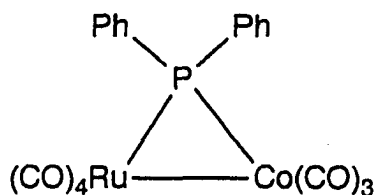
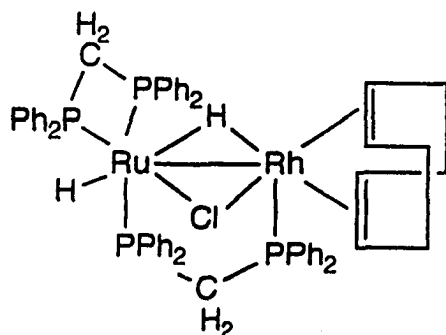
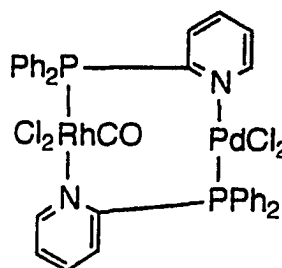
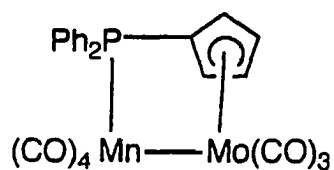
Comparison of the substitution reactions of the cage with different ligands: Each of the six 25 mL round-bottomed Schlenk flasks was charged with the same amount of the cage complex (0.5000 g) and evacuated, and the ligand in toluene was added into the proper flask to make the molar ratio of cage to ligand to be 1 : 2. Then toluene was added to the flasks to make the total volume of solution 5.0 mL. The resulting mixtures were stirred and warmed to dissolve the cage complex. Then 0.5 mL of solution from each of the colorless reaction solutions was removed and added to 0.3 mL of C_6D_6 . The ^{31}P NMR spectrum was obtained. From the integration of the ^{31}P NMR resonances, the beginning molar ratio of the cage to ligand could be calculated. The starting colorless solutions were stirred at reflux for 4 hours. A volume of 3.0 mL reaction solution was removed from each reaction mixture and added to 0.50 mL of C_6D_6 and the ^{31}P NMR spectrum was obtained again. From the ^{31}P NMR spectra we calculated the % of cage reacted and also the % of the orange compound formed from the intermediates.

CHAPTER II

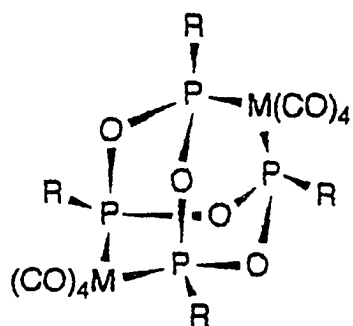
DEMETALLATION OF A DIMOLYBDENUM CYCLO- TETRAPHOSPHOXANE CAGE COMPLEX AND THE SYNTHESIS OF HETEROBIMETALLIC CAGES AND THEIR CHEMICAL REACTIONS

The synthesis and study of heterobimetallic complexes has been the subject of active research over the past decade. Initially studies of complexes containing two different metal atoms from the same or neighboring groups were done^[42]. Later, interest developed in complexes that contained widely divergent transition metals^[43]. Heterobimetallic complexes are of interest because of the potential to promote unique or sequential interactions.

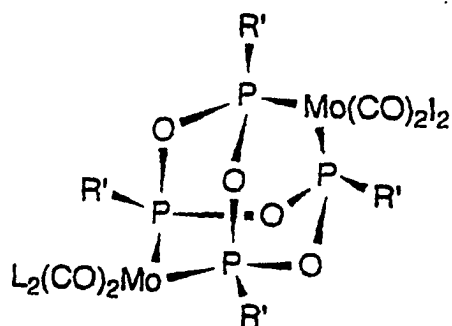
Bifunctional ligands such as 1-(diphenylphosphino)cyclopentadiene^[44] and 2-(diphenylphosphino)pyridine^[45] have proven to be particularly useful in constructing heterobimetallic species. Mixed-metal complexes have also been synthesized by using bidentate diphosphines such as bis(diphenylphosphino)methane^[46], as well as phosphido ligands^[47]. A substantial number of heterobimetallic complexes have now been synthesized. Several typical complexes are shown below:



Wong and coworkers have reported results from our laboratory on the synthesis of several bimetallic cage complexes and mixed-valent bimetallic cage complexes as shown below [8,9,13].

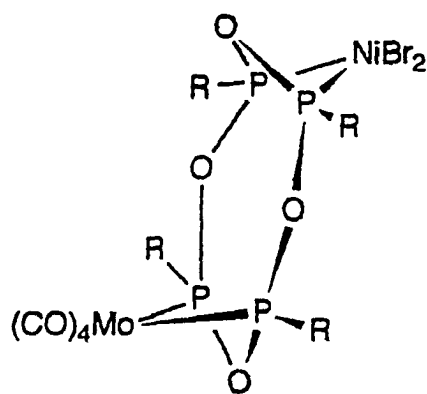


(R=*i*Pr₂N, Ph
M=Mo, Cr)

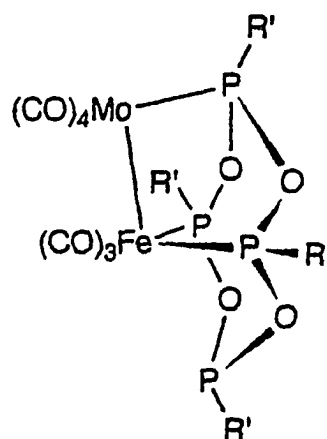


(R'=*i*Pr₂N
X=Cl, Br, I. L=CO, Cl, Br, I)

Before this work, no heterobimetallic cage complexes had been synthesized except (CO)₄Cr[PhFO]₄Mo(CO)₄ which had been detected by ³¹P NMR spectroscopy of a reaction mixture^[48]. Recently, Xiaoyong et al.^[49] reported the synthesis of two novel heterobimetallic complexes of the types:

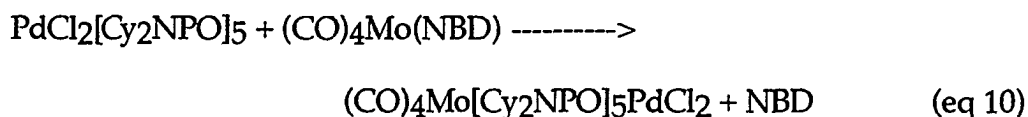
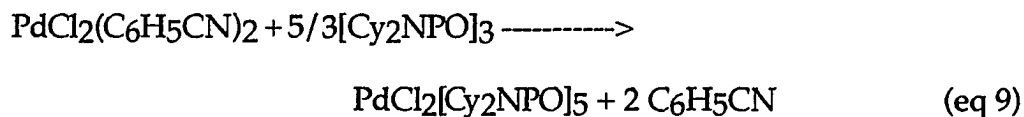


(R=Cy₂N)



R'=*i*Pr₂N

and a P₅O₅ heterobimetallic cage complex (CO)₃Mo[Cy₂NPO]₅PdCl₂. This Mo⁰/Pd^{II} P₅O₅ cage complex was synthesized as shown in eq 9 and eq 10:



Our research goal was also to study the intracage metal-metal interactions in a series of structurally-related heterobimetallic cage complexes. The parent (CO)₄Mo[ⁱPr₂NPO]₄Mo(CO)₄ cage has been shown to exhibit mixed-valent and intracage oxidative-addition reactions. A series of heterobimetallic complexes of this type with rigidly-constrained pairs of metal vertices should be especially interesting for the study of intracage metal-metal interactions. Substituted cages of this type, however, have been elusive due to lack of rational synthetic routes. Although attempted demetallation of the parent cage complex failed, we note that its mixed-valent derivative (CO)₄Mo[ⁱPr₂NPO]₄Mo(CO)₂I₂ contains one Mo(II) center which does present a potential decomplexation site. Successful demetallation should give the precursor complex (CO)₄Mo[ⁱPr₂NPO]₄[50].

In this chapter, we describe the synthesis, characterization and chemistry of this monometallic cage precursor and its use as a metalla-ligand for the synthesis of a series of heterobimetallic cage complexes of the form (CO)₄Mo[ⁱPr₂NPO]₄ML_n. Possible intracage metal-metal interactions have

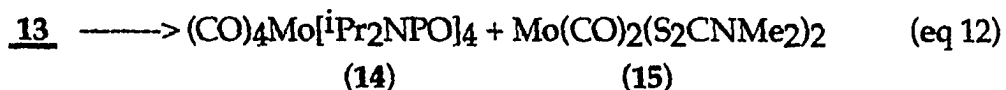
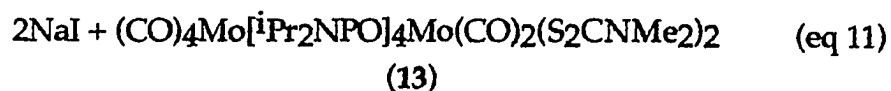
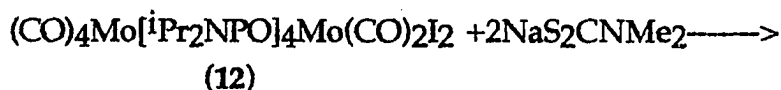
been investigated. In addition, some reactions of both the precursor and heterobimetallic cage complexes are reported.

RESULTS AND DISCUSSION

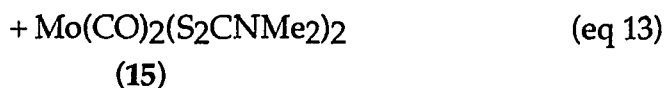
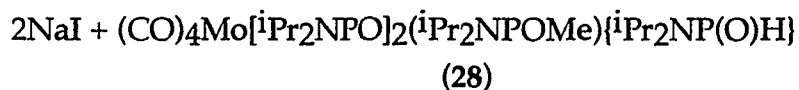
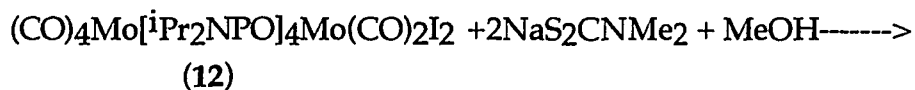
1. Synthesis and Characterization of the Monometallic Cage Precursor

(CO)₄Mo[iPr₂NPO]₄ (14)

Complex (CO)₄Mo[iPr₂NPO]₄ (14) was synthesized by the reaction of (CO)₄Mo[iPr₂NPO]₄Mo(CO)₂I₂ (12) with two equivalents of sodium dimethyldithiocarbamate in CH₂Cl₂ at room temperature via an orange intermediate (CO)₄Mo[iPr₂NPO]₄Mo(CO)₂(S₂CNMe₂)₂ (13). The reaction sequence representing the preparation of 14 is as follows:



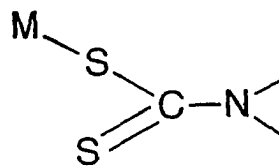
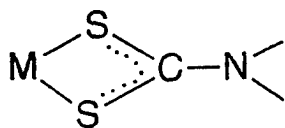
Complex 12 was synthesized by literature methods^[9]. At first, a 2:1 CH₂Cl₂/MeOH mixture was chosen as the solvent since 12 is very soluble in CH₂Cl₂ while sodium dimethyldithiocarbamate easily dissolves in MeOH. The following reaction was obtained by using this solvent system at room temperature:



Thus methanol-decomposed **14** was obtained. Details of this reaction will be discussed in Part II. 5.

When **12** and $\text{NaS}_2\text{CNMe}_2$ were mixed with CH_2Cl_2 at room temperature, a suspension was formed. The white solid, $\text{NaS}_2\text{CNMe}_2$, was suspended in the deep-red mixture of complex **12**. After stirring for 3 hours, a red suspension was obtained. The red suspension contained complex **15** which could be isolated by filtration of the mixture. Complex **15** gave no ^{31}P NMR signal. Its formula was confirmed by ^1H , ^{13}C NMR, IR and elemental analyses. The two major IR carbonyl bands indicated a *cis*-configuration of the carbonyl groups. The band at 1517cm^{-1} was due to the C-N stretching mode^[18]. A ^1H NMR spectrum of **15** showed two methyl resonances of unequal intensities. It is likely that this arose from two of isomers^[51], (one with an octahedral structure and one with a trigonal prismatic structure similar to that found in the solid state for $\text{Mo}(\text{S}_2\text{CN}^i\text{Pr}_2)_2(\text{CO})_2$ ^[52]).

Dithiocarbamate ligands can act as a bidentate or as a monodentate ligand when coordinated to a transition metal^{[18][19]}.



In eq 11, the dithiocarbamate ligand first acted as a monodentate ligand to replace the iodide to give orange 13. This then rearranged to a bidentate mode and replaced the phosphorus donor atoms, removing the molybdenum from the rest of the cage (eq 12).

TLC and the ^{31}P NMR spectrum of the reaction mixture showed that the orange complex 13 is the major product. Complex 14 gave a colorless TLC spot with a high R_f value. By routine column chromatography, complex 13 was isolated in about 30% yield. This complex was very unstable and it decomposed to white complex 14 and red-purple 15 in solution or in the solid state when left at room temperature for several days. The decomposition products were examined by ^1H , ^{31}P NMR and IR spectroscopy. White solid compound 14 was isolated in 59% yield by column chromatography of the decomposition product after one week. Complex 14 has been characterized by ^1H , ^{13}C , ^{31}P NMR, IR spectra, elemental analyses and X-ray crystallography. It is an air-stable white solid with four IR carbonyl absorptions at 2010, 1925, 1908, and 1882 cm^{-1} which is consistent with a $\text{cis-Mo}(\text{CO})_4\text{P}_2$ of C_{2v} symmetry. Its proton-decoupled ^{31}P NMR spectrum exhibited the expected A_2X_2 pattern with one sharp (150.6 ppm, coordinating P's) and one broad (126.0 ppm, uncoordinating P's) triplet with a coupling

constant of about 2 Hz (Figure 29). The ^{13}C NMR spectrum showed two triplets for carbonyl resonances at 215.8 ppm ($^2J_{\text{pc}}=14$ Hz) and at 209.5 ppm ($^2J_{\text{pc}}=12$ Hz).



Figure 29. $^{31}\text{P}\{^1\text{H}\}$ NMR spectrum of **14**

The X-ray structure of **14** is shown in **Figure 30** and selected bond distances and bond angles are listed in **Table IX**:

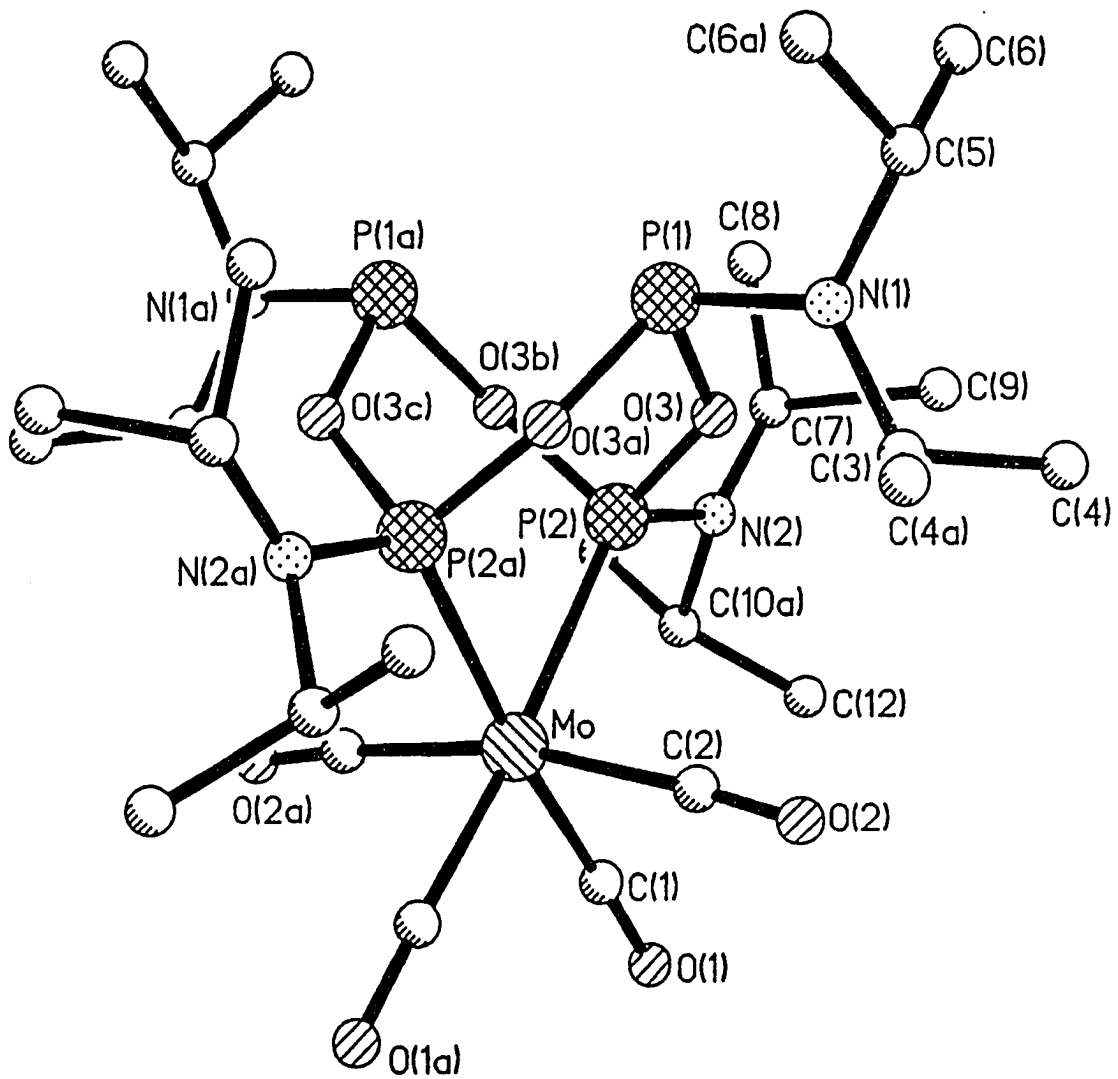


Figure 30. Molecular Structure of 14

Table IX. Selected Bond Distances (Å) and Angles(deg) for (CO)₄Mo^IPr₂NPO₁₄

Mo-P(2) = Mo-P(2A)	2.512(2)
Mo-C(2) = Mo-C(2A)	2.027(10)
Mo-C(1) = Mo-C(1A)	1.978(9)
P(1)-O(3) = P(1)-O(3A) = P(1A)-O(3B) = P(1A)-O(3C)	1.671(4)
P(2)-O(3) = P(2)-O(3B) = P(2A)-O(3A) = P(2A)-O(3C)	1.623(4)
P(1)-N(1) = P(1A)-N(1A)	1.655(6)
P(2)-N(2) = P(2A)-N(2A)	1.642(7)
P(2)-Mo-P(2A)	75.1(1)
C(1)-Mo-C(1A)	87.5(5)
C(2)-Mo-C(2A)	169.8(5)
P(2)-Mo-C(1) = P(2A)-Mo-C(1A)	98.7(3)
P(1)-O(3)-P(2) = P(1)-O(3A)-P(2A)	131.6(2)
P(1A)-O(3B)-P(2) = P(1A)-O(3)-P(2A)	131.6(2)
Mo-P(2)-O(3) = Mo-P(2)-O(3B)	112.1(1)
Mo-P(2A)-O(3A) = Mo-P(2A)-O(3C)	112.1(1)
O(3)-P(1)-O(3A) = O(3B)-P(1A)-O(3C)	97.6(3)
O(3)-P(2)-O(3B) = O(3A)-P(2A)-O(3C)	102.1(3)

The molecule has perfect C_{2v} symmetry with the expected vacant metal vertex. Complex **14** retains the parent P_4O_4 boat-boat ring conformation with significant modifications in the phosphorus-oxygen bond lengths. Comparing to the average of 1.646(4) Å found in complex **1**, the four coordinated (Mo)-P-

O bonds are shortened to 1.623(4) while the uncoordinated phosphorus-oxygen bonds are lengthened to 1.671(4) Å. These data indicate that the P-O bonding at the coordinated sites are enhanced at the expense of the uncoordinated P-O bonds^[53]. This structure represents the third configurational isomer (boat-boat) of the MoP₄O₄ moiety to be structurally characterized. Previously, chair-boat and chair-chair forms were described but this third geometry has not been accessible by direct synthesis^[13]. These three conformations are showed in **Figure 31**:

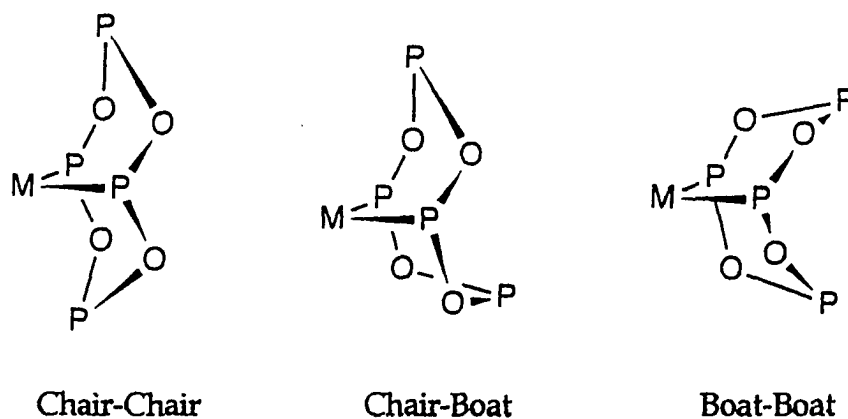


Figure 31. Three Conformations for the MoP₄O₄ Core

By the temperature-independent NMR spectral behavior of complex 14 up to 110°C and from previous work^[13], it can be seen that a substantial barrier to phosphorus inversion exists.

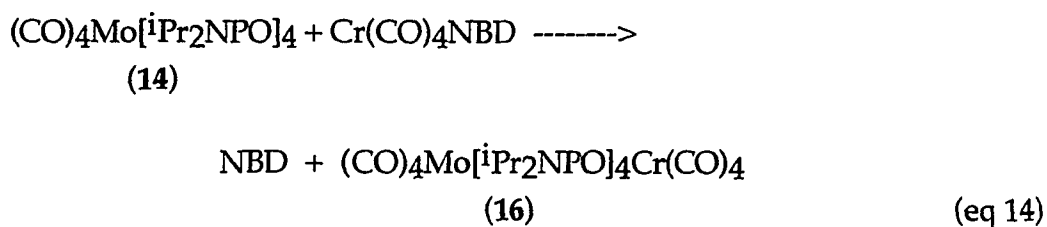
Unlike the MoP₄O₄ complex with chair-chair or chair-boat forms, complex 14 in the boat-boat form has convergent phosphorus lone pairs that make it a promising metalla-ligand for the formation of novel bimetallic cage complexes.

2. Synthesis and Characterization of Heterobimetallic Complexes

In this section, the synthesis and characterization of heterobimetallic cage complexes from complex 14 are described.

2.1. $(\text{CO})_4\text{Mo}[\text{iPr}_2\text{NPO}]_4\text{Cr}(\text{CO})_4$ (16):

Complex 16 was synthesized by the reaction of complex 14 with $\text{Cr}(\text{CO})_4\text{NBD}$ (NBD = norbornadiene) in refluxing heptane:

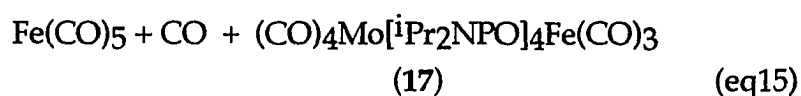
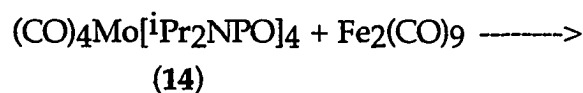


This reaction was monitored by ^{31}P NMR spectroscopy. After one day, the reaction mixture showed that only 32% of complex 16 had formed. When the reaction was run for an additional 3 days, 84% Mo-Cr cage 16 and 9% Mo-Mo cage 1 were found. Because the reaction was slow, some of the precursor decomposed, and some complex 1 formed. By routine column chromatography, pure complex 16 was isolated. The isolated yield of complex 16 was around 35%. This product was identified by ^1H , ^{13}C , ^{31}P NMR, IR spectra and elemental analyses. Its proton-decoupled ^{31}P NMR spectrum exhibits the expected A_2X_2 pattern with two triplets at 175.0 ppm and at 147.9 ppm. The coupling constant is equal to 6 Hz. Both the resonances of the coordinated P's and uncoordinated P's of complex 14 are shifted downfield upon bonding of the chromium. These downfield shifts can be rationalized by the decrease in electron density around the phosphorus atoms coordinated to the chromium.

The ^{13}C NMR spectrum of **16** showed four carbonyl resonances with the $\text{Cr}(\text{CO})_4\text{P}_2$ group at 224.5 ppm ($J_{\text{PC}}=9$ Hz) and 218 ppm ($J_{\text{PC}}=18$ Hz) and the $\text{Mo}(\text{CO})_4\text{P}_2$ moiety at 214.0 ppm ($J_{\text{PC}}=16$ Hz) and 207.2 ppm ($J_{\text{PC}}=13\text{Hz}$). The IR spectrum in the carbonyl stretch region was slightly different from that of complex **14**. Here the *cis*- $\text{Cr}(\text{CO})_4$ group shows a sharp A_1 mode at 2023 cm^{-1} . The higher energy absorption at 2009 cm^{-1} is assigned to the A_1 mode of *cis*- $\text{Mo}(\text{CO})_4$, because the (Cr)C-O bond is typically stronger than the (Mo)C-O bond^[54].

2.2. $(\text{CO})_4\text{Mo}[\text{iPr}_2\text{NPO}]_4\text{Fe}(\text{CO})_3$ (**17**):

Complex **17** was synthesized by the reaction of complex **14** with $\text{Fe}_2(\text{CO})_9$ in refluxing hexane as shown below:

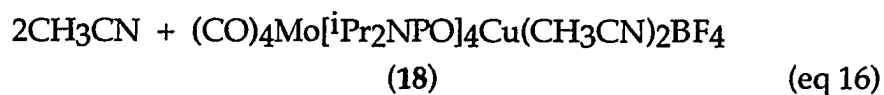
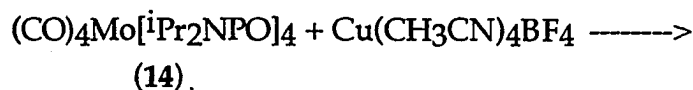


This reaction was monitored by ^{31}P NMR spectroscopy. After one day, ^{31}P NMR spectroscopy of the reaction mixture showed that only 51% of complex **17** had formed while 13% Mo-Mo cage had formed as a side product. When the reaction was allowed to run for an additional 15 hours, ^{31}P NMR spectroscopy showed that 68% of complex **17** had formed. In order to decrease the percentage of the undesired Mo-Mo cage, the reaction was stopped after 39

hours. The product was not easy to purify, because both the Mo-Mo cage and green $\text{Fe}_3(\text{CO})_{12}$ were hard to remove. By routine column chromatography, a 28% yield of complex **17** was isolated. The product was identified by ^1H , ^{13}C , ^{31}P NMR, and IR spectra and by elemental analyses. The ^{31}P NMR spectrum of the complex showed a familiar A_2X_2 pattern with two triplets at 165.2 ppm and 152.1 ppm ($^2J = 14$ Hz). In the ^{13}C NMR spectrum, the $\text{Fe}(\text{CO})_3$ group shows only one resonance, a triplet at 217.3 ppm with the P-C coupling constant equal to 7 Hz. This is consistent with the well-known fluxional property of the $\text{P}_2\text{Fe}(\text{CO})_3$ moiety^[55]. Carbonyl ligands in a wide variety of ligand-substituted iron pentacarbonyls have been observed with this property, as stereochemical nonrigidity is a very common phenomenon in molecules with five coordination. We also tried the reaction of **14** with $\text{Fe}(\text{CO})_5$, but after 5 days in refluxing hexane, only some Mo-Mo cage formed.

2.3 $(\text{CO})_4\text{Mo}[\text{iPr}_2\text{NPO}]_4\text{Cu}(\text{CH}_3\text{CN})_2\text{BF}_4$ (**18**):

Complex **18** was synthesized by the reaction of complex **14** with $\text{Cu}(\text{CH}_3\text{CN})_4\text{BF}_4$ in hexane/ CH_2Cl_2 (2:1 v:v) solution. The equation representing the preparation of the complex is shown below.



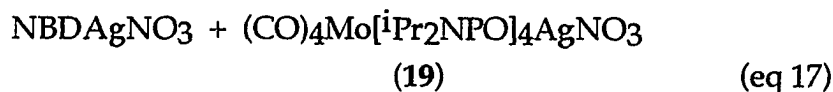
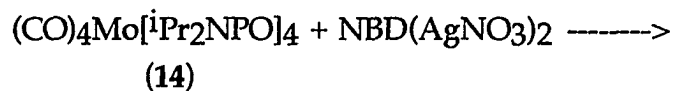
The percent yield of complex **18** in the reaction above was more than

95%. This reaction was very fast, being complete after refluxing for one hour. After evaporating the CH_2Cl_2 , a white suspension was obtained. After filtration, a few portions of hexane were used to wash the product, and pure complex **18** was obtained. The product was not stable due to the ready loss of CH_3CN ligands. When the product was dried under reduced pressure, it changed color from white to light yellow. A ^1H NMR spectrum of the sample confirmed that some CH_3CN ligand was lost from the sample. Hence, the reaction was run using excess **14** and all of the NMR, IR spectra and CHN analyses had to be done within 24 hours after isolating the pure sample.

Complex **18** was identified by ^1H , ^{13}C , ^{31}P NMR, and IR spectra and by elemental analyses. Its ^{31}P NMR spectrum showed a sharp triplet at 155.6 ppm and a broad triplet at 90.0 ppm with a coupling constant of 10 Hz. The broad resonance was assigned to phosphorus atoms coordinated to copper. Since ^{63}Cu and ^{65}Cu both have spin $I=3/2$, the nuclear charge distribution around the metal is not symmetrical, thus giving rise to broad peaks due to quadrupolar relaxation[56]. The ^{13}C NMR spectrum showed a singlet resonance at 120.4 for $\text{CH}_3\text{C}\underline{\text{N}}$ and a singlet at 2.2 for $\underline{\text{C}}\text{H}_3\text{CN}$. The ^1H NMR spectrum showed a singlet at 2.35 ppm for the $\text{C}\underline{\text{H}}_3\text{CN}$ group. The IR spectrum showed the usual C_{2v} symmetry in the carbonyl region with one sharp peak at 2019 cm^{-1} and a broad peak at 1905 cm^{-1} . In addition, it also showed peaks in the CN region at 2303 and 2273 cm^{-1} [57].

2.4. (CO)₄Mo[ⁱPr₂NPO]₄AgNO₃(19):

Complex **19** was synthesized by the reaction of complex **14** with NBD(AgNO₃)₂ in hexane at room temperature:



The percent yield of complex **19** in the reaction above was 54%. White solid NBD(AgNO₃)₂ was suspended in hexane. When the reaction was run at room temperature for one hour, the ³¹P NMR spectrum of the mixture showed that the reaction was already complete. A white suspension was obtained, and after filtration, a white solid resulted. A few portions of hexane were used to wash this product to give pure white solid complex **19**. This product is not stable due to the decomposition of Ag (I). The reaction was therefore run using excess **14** and all of the NMR and IR spectra and CHN analyses were done within a few hours after obtaining a pure sample.

When complex **14** reacted with (AgNO₃)₂NBD, no matter whether the ratio of Mo to Ag was 1:1, 2:1 or 1:2, the same product resulted. Integration of the ³¹P NMR peaks of starting material and the product reaction mixtures from the different reagent ratios confirmed the 1:1 complex. This cage compound was not stable and changed color to brown even under nitrogen and in the absence of light. It was characterized by ³¹P, ¹H, ¹³C NMR and IR spectroscopy, but no satisfactory CHN data were obtained even after repeated

attempts.

The ^{31}P NMR spectrum for complex **19** exhibited a unique pattern due to the coupling between phosphorus and silver nuclei. Silver exists as a combination of two isotopes, ^{107}Ag and ^{109}Ag . Both isotopes are NMR-active and have nuclear spins of one half with natural abundances of 51.82% and 48.18%, respectively. In contrast to the quadrupolar copper nuclei discussed for complex **18**, the ^{31}P NMR spectrum of **19** clearly displayed Ag-P couplings. It showed a triplet at 154.3 ppm, and a doublet of triplets at both 103.6 ppm and 103.5 ppm [$^2J_{\text{pp}} = 13$ Hz, $^1J_{\text{AgP}} = 568, 492$ Hz] (Figure 32).

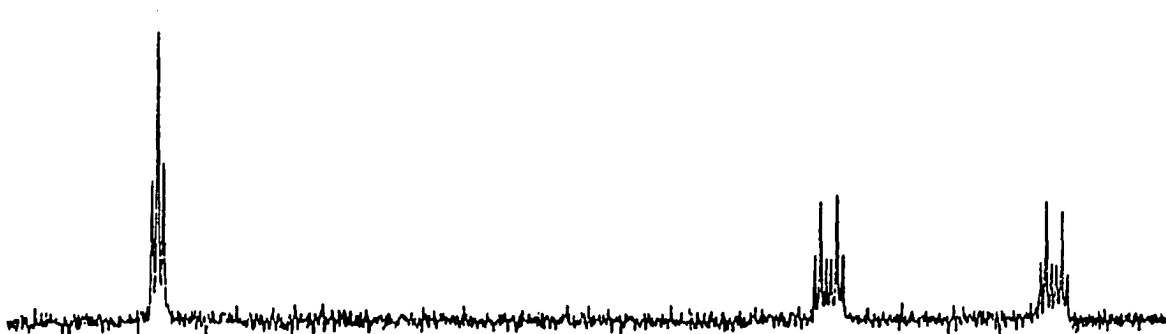
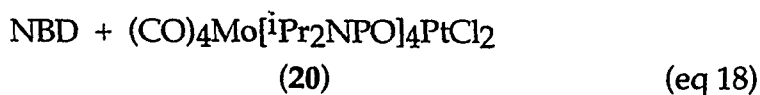
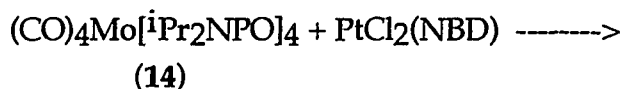


Figure 32. $^{31}\text{P}\{^1\text{H}\}$ NMR spectrum for **19**

One-bond coupling between ^{31}P and silver isotopes range from about 210 to more than 1100 Hz^[56]. Several groups have reported $^1J_{\text{PAg}}$ values for $\text{Ag}(\text{L}_2)\text{NO}_3$ complexes of about 500 Hz^[58]. The $^1J_{\text{PAg}}$ of complex **19** is consistent with these literature values. The IR spectrum of complex **19** indicated the expected C_2v symmetry in the carbonyl region.

2.5. (CO)₄Mo[iPr₂NPO]₄PtCl₂(20):

Complex **20** was synthesized by the reaction of complex **14** with PtCl₂(NBD) in toluene at 60°C:



The yield of complex **20** was quantitative. Since PtCl₂(NBD) is not very soluble in hot toluene, the white reaction suspension was stirred at 60 °C and monitored by TLC. After 4 hours, this showed that no starting **14** was left. This reaction was fast and clean, and the product (CO)₄Mo[iPr₂NPO]₄PtCl₂ was easily isolated pure by filtration of the suspension to give a white solid. After washing this product with toluene, pure complex **20** was obtained. Complex **20** was identified by ¹H, ¹³C, ³¹P NMR and IR spectroscopy and elemental analyses. The ¹⁹⁵Pt isotope is NMR-active and has a nuclear spin of one half and a natural abundance of 33.8%. Thus the ³¹P NMR spectrum of this product showed an A₂X₂ pattern with a triplet at 147.4 ppm and a triplet at 56.6 ppm (J_{pp}=10 Hz) together with a doublet of triplets of ¹⁹⁵Pt satellites (Figure33). The value of the coupling between phosphorus and platinum (J¹⁹⁵PtP=5520 Hz) is typical of phosphorus trans to halogen ligands^[59]. Complex **20** shows a similar IR carbonyl spectrum as for complex **14** and **19**.

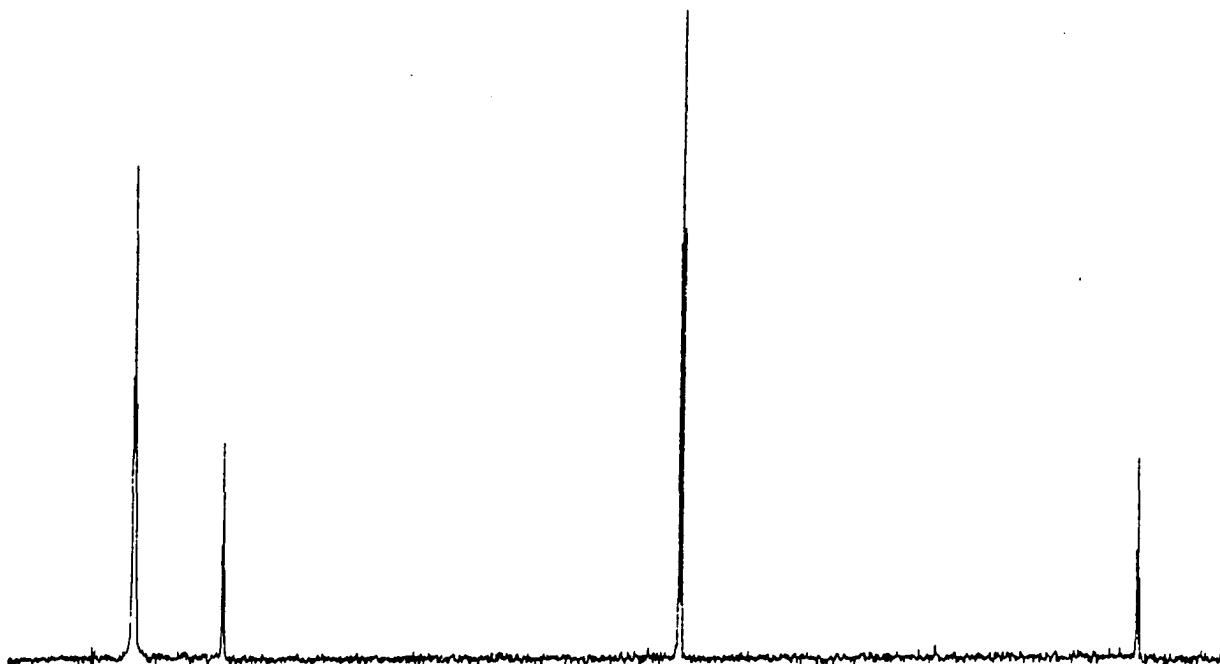
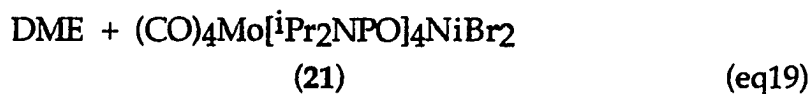
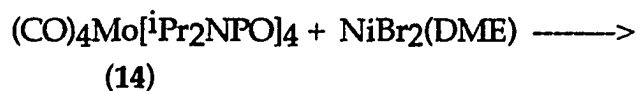


Figure 33. $^{31}\text{P}\{^1\text{H}\}$ NMR spectrum for 20

2.6. $(\text{CO})_4\text{Mo}[\text{iPr}_2\text{NPO}]_4\text{NiBr}_2$ (21):

Complex 21 was synthesized by the reaction of complex 14 with $\text{NiBr}_2(\text{DME})$ in refluxing hexane for 5 hours:



The yield of complex 21 in the reaction above was around 80%. When compound 14 reacted with $\text{NiBr}_2(\text{DME})$, the deep-red Mo-NiBr₂ cage formed. This product has no NMR signal and its formulation has been confirmed by X-ray study and IR spectroscopy. The pseudo-tetrahedral coordination geometry around the nickel is consistent with its paramagnetic behavior. The X-ray structure of this complex is shown in Figure 34 and the selected bond

distances and angles are listed in Table X:

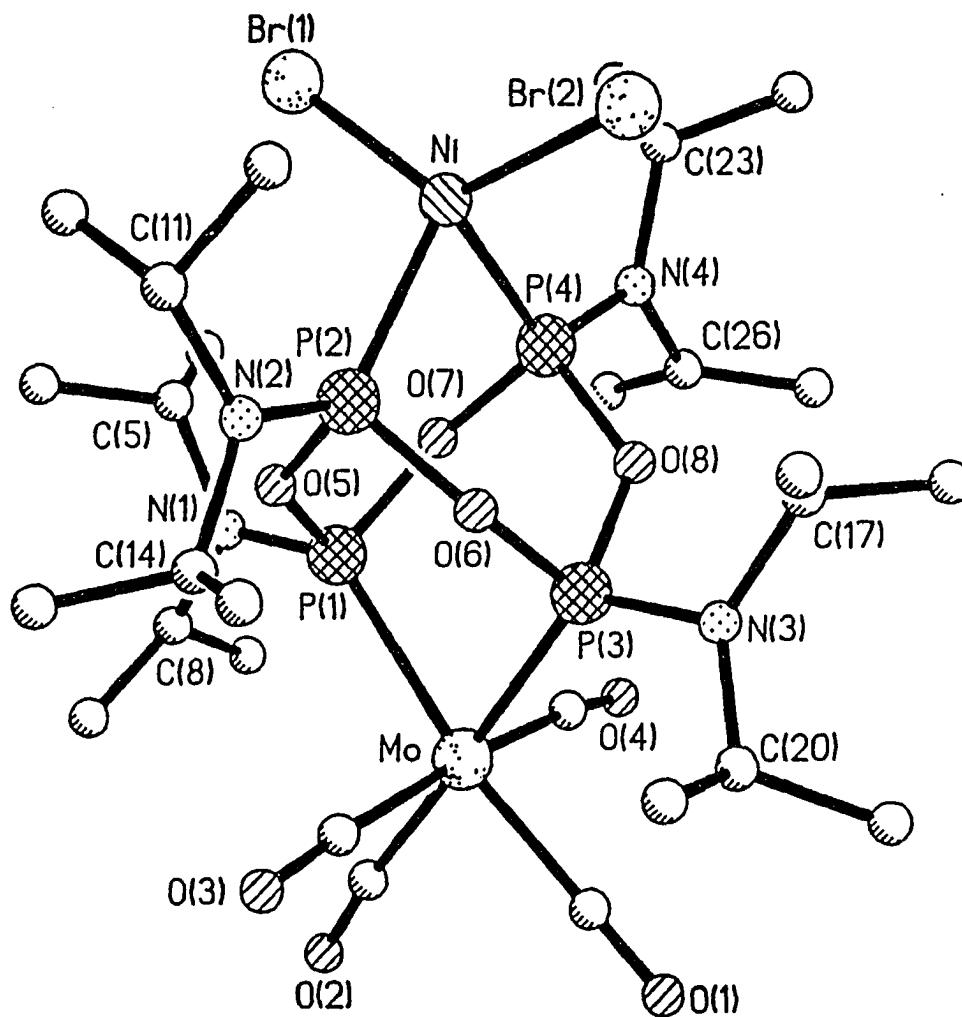


Figure 34. Molecular Structure of 21

Comparing the X-ray structure of 21 with the precursor 14, the data clearly show that the eight cage phosphorus-oxygen bonds have readjusted to the new coordination mode: the four (Ni^{II})P-O distances now average $1.633(8)\text{\AA}$ while the four (Mo^0)-P-O lengths average to a marginally longer $1.650(9)\text{\AA}$. Again, this shows intracage communication between the two metals. In Part II 3 this structure will be discussed further.

This cage compound is not very stable in refluxing hexane, and some of it transformed to a Mo-Ni(CO)₂ cage compound by the reduction of Ni(II) and the replacement of Br⁻ by CO from the decomposition of the parent cage. This was verified by its facilitation by adding a CO source as well as a reducing reagent, Fe(CO)₅. (See Part II 2.7 for detail).

Table X. Selected Bond Distances (Å) and Angles(deg) for 21

Mo-P(1)	2.493(4)	Mo-P(3)	2.493(4)
Mo-C(1)	2.004(15)	Mo-C(2)	1.987(17)
Mo-C(3)	2.047(17)	Mo-C(4)	2.019(17)
Ni-Br(1)	2.320(3)	Ni-Br(2)	2.318(3)
Ni-P(2)	2.254(4)	Ni-P(4)	2.266(4)
P(1)-O(5)	1.639(9)	P(1)-O(7)	1.661(9)
P(1)-N(1)	1.587(11)	P(2)-O(5)	1.654(9)
P(2)-O(6)	1.627(8)	P(2)-N(2)	1.614(12)
P(3)-O(6)	1.659(9)	P(3)-O(8)	1.649(9)
P(3)-N(3)	1.660(11)	P(4)-O(7)	1.623(9)
P(4)-O(8)	1.631(8)	P(4)-N(4)	1.609(12)
O(1)-C(1)	1.125(19)	O(2)-C(2)	1.162(21)
O(3)-C(3)	1.140(21)	O(4)-C(4)	1.130(21)
P(1)-Mo-P(3)	77.9(1)	P(1)-Mo-C(1)	171.9(4)
P(3)-Mo-C(1)	96.4(4)	P(1)-Mo-C(2)	100.8(5)
P(3)-Mo-C(2)	177.7(4)	C(1)-Mo-C(2)	85.2(6)
P(1)-Mo-C(3)	94.3(4)	P(3)-Mo-C(3)	92.2(5)
C(1)-Mo-C(3)	91.6(6)	C(2)-Mo-C(3)	85.9(6)
P(1)-Mo-C(4)	89.0(4)	P(3)-Mo-C(4)	94.9(5)
C(1)-Mo-C(4)	85.7(6)	C(2)-Mo-C(4)	87.0(6)
C(3)-Mo-C(4)	172.7(6)	Br(1)-Ni-Br(2)	128.9(1)
Br(1)-Ni-P(2)	110.6(1)	Br(2)-Ni-P(2)	111.3(1)
Br(1)-Ni-P(4)	106.4(1)	Br(2)-Ni-P(4)	104.4(1)
P(2)-Ni-P(4)	85.7(1)	Mo-P(1)-O(5)	112.7(3)
Mo-P(1)-O(7)	108.8(3)	O(5)-P(1)-O(7)	98.9(4)
Ni-P(2)-O(5)	109.3(3)	O(5)-P(2)-O(6)	100.6(4)
Ni-P(2)-O(6)	106.7(3)	O(6)-P(3)-O(8)	98.4(4)
Ni-P(4)-O(7)	110.0(3)	O(7)-P(4)-O(8)	100.7(4)
Ni-P(4)-O(8)	111.3(3)	P(1)-O(5)-P(2)	131.7(5)
Mo-P(3)-O(6)	112.8(3)	P(1)-O(7)-P(4)	132.1(5)
Mo-P(3)-O(8)	111.8(3)	P(2)-O(6)-P(3)	133.6(5)
P(3)-O(8)-P(4)	127.8(5)		

2.7. $(\text{CO})_4\text{Mo}[\text{iPr}_2\text{NPO}]_4\text{Ni}(\text{CO})_2$ (22):

Complex 22 was synthesized by the reaction of complex 21 with $\text{Fe}(\text{CO})_5$ in refluxing hexane for 1 hour:



(21)



(22)

(eq 20)

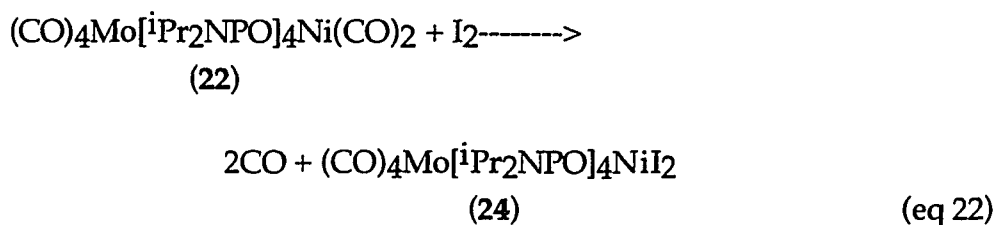
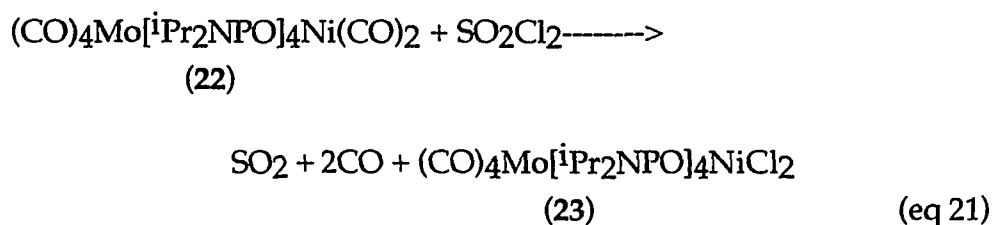
The yield of complex 22 in the reaction above was 85%. When the red reaction suspension was refluxed for one hour, the color disappeared and a yellow suspension formed. By routine column chromatography, pure white complex 22 was isolated. The formulation of complex 22 has been confirmed by NMR and IR spectroscopy and by elemental analyses. A large crystal of 22 was obtained by recrystallization from hot hexane but unfortunately, this crystal was twined. It will be very interesting to obtain an X-ray structure of 22 for comparing with the structure of 21.

The ^{13}C NMR spectrum of 22 exhibits a triplet (198.4 ppm, $^2J_{\text{PC}}=4$ Hz) resonance associated with the two equivalent carbonyls. This can be compared with the chemical shift of carbonyl carbons in typical $\text{Ni}(\text{CO})_2\text{P}_2$ complexes at 197.9 ppm for $\text{P}=\text{P}(\text{OMe})_3$, 198.3 ppm for $\text{P}=\text{P}(\text{OEt})_3$, and 198.9 ppm for $\text{P}=\text{P}(\text{O}^i\text{Pr})_3$ [60]. $^2J_{\text{PC}}$ spin-spin couplings are negligible in $\text{Ni}(\text{CO})_2[\text{P}(\text{OCH}_2)_3\text{CMe}_2]_2$ [61], and only a few Hz in $(\text{PR}_3)_2\text{Ni}(\text{CO})_2$ (R=Ph, Bu, OMe, OPh)[62]. The ^{31}P NMR spectrum of 22 shows an A_2X_2 pattern

with a triplet at 154.5 ppm and a triplet at 128.0 ppm. The P-P coupling constant is 3 Hz. This small value is consistent with the literature values^[62].

2.8. (CO)₄Mo[ⁱPr₂NPO]₄NiX₂ (X=Cl (23), X=I (24)):

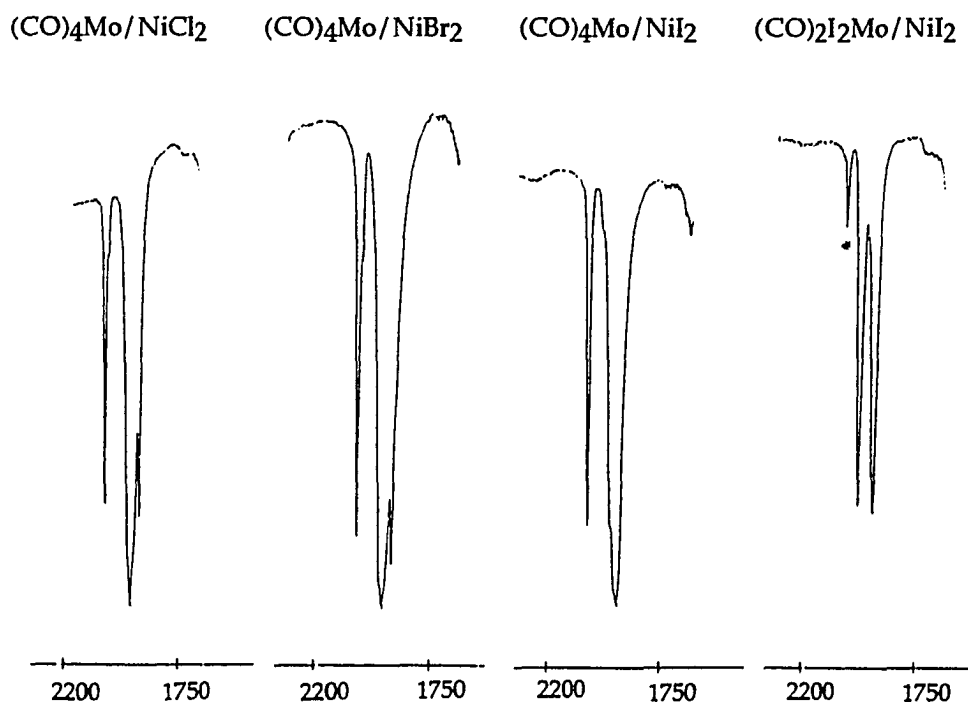
Substituted nickel carbonyl complex **22** was oxidized by halogens to give the corresponding nickel dihalide derivatives. Complexes **23** and **24** were isolated from the reactions of complex **22** with SO₂Cl₂ in hexane at -78 °C or with I₂ in CH₂Cl₂ at room temperature, respectively.



The yields of complexes **23** and **24** in the reactions above were 84% and 76%, respectively.

When a SO₂Cl₂ solution in CH₂Cl₂ was added to a hexane solution of (CO)₄Mo[ⁱPr₂NPO]₄Ni(CO)₂, this colorless solution immediately changed to yellow. After 5 minutes, it became an orange suspension. The TLC of this solution showed that no complex **21** remained. An orange solid complex **23** was obtained after work up. This product was identified by its IR spectrum and elemental analyses. Its IR spectrum showed four carbonyl absorptions consistent with a C_{2v} symmetry for the cis-Mo(CO)₄P₂ moiety.

When a CH_2Cl_2 solution of I_2 was added to the colorless solution of complex **22** and stirred at room temperature for 2 hours, a deep-red solution formed. TLC of this solution showed no starting material **22**. The deep-red solution was allowed to dry under reduced pressure to give a deep-red residue. This solid was washed with CH_3CN and vacuum dried, to give complex $(\text{CO})_4\text{Mo}[\text{iPr}_2\text{NPO}]_4\text{NiI}_2$. It was identified by IR spectroscopy which gave spectra similar to those of complexes **21** and **23**. For the reaction of **22** with I_2 , if the excess I_2 was used, the product showed two major carbonyl bands in the IR spectrum, indicating that $(\text{CO})_2\text{I}_2\text{Mo}[\text{iPr}_2\text{NPO}]_4\text{NiI}_2$ had formed. The carbonyl regions of the IR spectra for these Mo/Ni compounds are shown in Figure 35:



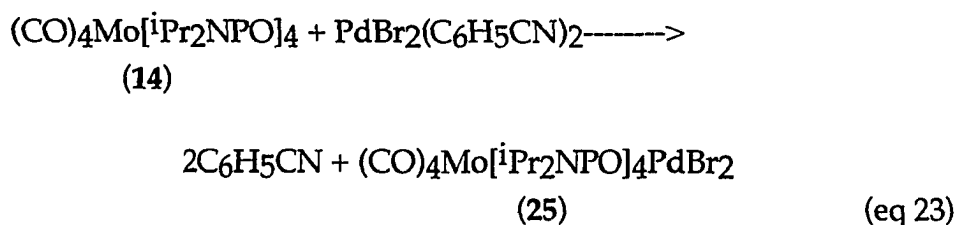
* peak of $(\text{CO})_4\text{Mo}/\text{NiI}_2$

Figure 35. The carbonyl regions of the IR spectra for Mo/Ni complexes

Both complexes **23** and **24** were found to react with $\text{Fe}(\text{CO})_5$ to produce complex **22** in 80% yield.

2.9. $(\text{CO})_4\text{Mo}[\text{iPr}_2\text{NPO}]_4\text{PdBr}_2$ (**25**):

Complex **25** was synthesized by the reaction of complex **14** with $\text{PdBr}_2(\text{C}_6\text{H}_5\text{CN})_2$ in toluene at 70 °C for 16 hours:



The yield of complex **25** in the reaction above was 83%. ^{31}P NMR spectroscopy was used to monitor the reaction. After 16 hours, there was 95% $\text{Mo}^0\text{P}_4\text{O}_4\text{PdBr}_2$ cage and minute amounts of $\text{Mo}^0\text{P}_4\text{O}_4\text{Mo}^0$ cage and $\text{Mo}^0\text{P}_5\text{O}_5\text{PdBr}_2$ cage, but no starting material. Workup by filtration and purification yielded a yellow solid $(\text{CO})_4\text{Mo}[\text{iPr}_2\text{NPO}]_4\text{PdCl}_2$. Small crystals were formed by recrystallization from hot toluene. This product was identified by ^1H , ^{13}C , ^{31}P NMR, and IR spectroscopy and by elemental analyses. In addition, an X-ray crystal structure determination was completed. The IR spectrum again confirms C_{2v} symmetry for cis- $\text{Mo}(\text{CO})_2\text{P}_2$ in the carbonyl region with four absorptions at 2045.8 cm^{-1} , 1961.0 cm^{-1} , 1943.0 cm^{-1} , and 1921.8 cm^{-1} . The ^{31}P NMR spectrum of **25** showed a triplet at 147.6 ppm and a triplet at 82.6 ppm ($^2J_{\text{PP}} = 6$ Hz). The ^{13}C NMR spectrum in the carbonyl

region shows a multiplet at 211.8 ppm and a triplet at 205.1 ppm ($J_{pc}=13\text{Hz}$) in the carbonyl region.

We observed some interesting phosphorus chemical shift changes. For the precursor complex **14**, the coordinated phosphorus atoms resonate at 150.6 ppm and the uncoordinated phosphorus atoms at 126.0 ppm. When the uncoordinated phosphorus atoms coordinated to the second metal in complexes **16**, **17**, **18**, **19**, **20**, **22** and **25**, large chemical shifts of +26.1 to -69.5 resulted, While the chemical shifts for the phosphorus atoms bound to Mo^0 shifted by +24.4 to -3.2 ppm. $\text{Cr}(0)$, $\text{Fe}(0)$, $\text{Ni}(0)$ moved the phosphorus shifts to lower field in the order: $\text{Cr}^0 > \text{Fe}^0 > \text{Ni}^0$ while $\text{Cu}(I)$, $\text{Ag}(I)$, $\text{Pt}(II)$ $\text{Pd}(II)$ metals shifted the resonances upfield in the order: $\text{Pt}(II) > \text{Pd}(II) > \text{Cu}(I) > \text{Ag}(I)$. These large changes can be explained by the differences between the metals and the ancillary ligands on the metals. The upfield shifts for $\text{Cu}(I)$, $\text{Ag}(I)$, $\text{Pt}(II)$ and $\text{Pd}(II)$ metals are consistent with the typical coordination shifts in the phosphine complexes[63]. For example, ^{31}P chemical shifts for free ligands PMe_3 and PPh_3 are at +62 ppm and +6ppm, while in complexes $\text{cis-PtCl}_2(\text{PMe}_3)_2$, $\text{cis-PdBr}_2(\text{PMe}_3)_2$, AgClPPh_3 and $\text{Cp}^*\text{Cu}(\text{PMe}_3)_3$, ^{31}P chemical shifts are at -24, -17, +3 and -49 ppm[63].

The structure of complex **25** is shown in **Figure 36** and selected bond distances and angles are listed in **Table XI**:

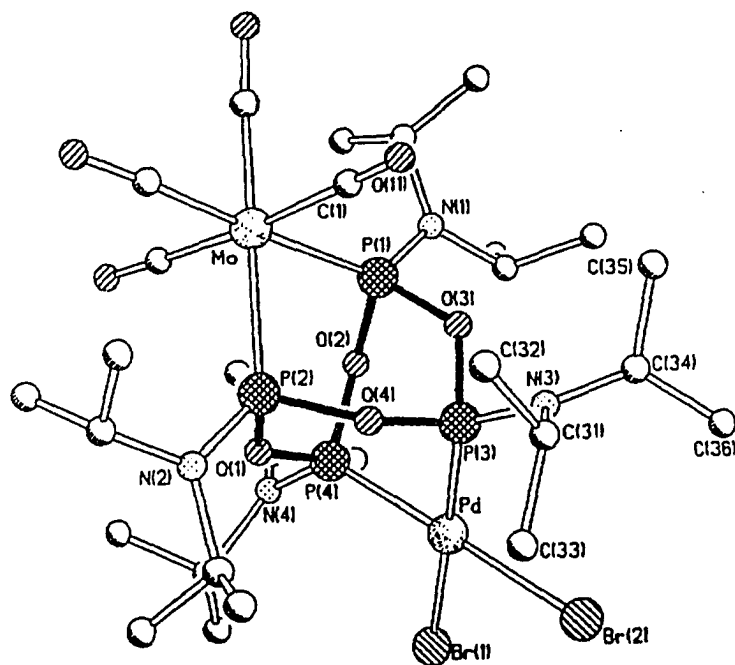


Figure 36. Molecular structure of 25

In complex 25, a square-planar geometry has been adopted by the Pd(II) vertex. The energy ordering of the d orbitals in a square-planar ligand field is $d_{x^2-y^2} > d_{xy} > d_{xz}, d_{yz} > d_{z^2}$. Since the pairing energy is less than the difference between the energy of the $d_{x^2-y^2}$ and the d_{xy} orbitals, the eight 4d-electrons in Pd(II) completely fill the four lowest energy orbitals, leaving the $d_{x^2-y^2}$ empty. Thus complex 25 is diamagnetic and gives useful NMR spectra.

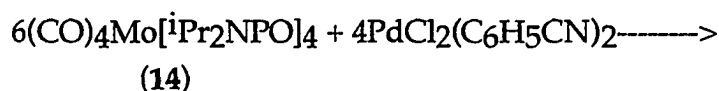
From the x-ray structural data, we can see that similar to complex 21, the eight cage P-O bonds are readjusted to the new coordination mode: the four (Pd^{II})P-O distances now average 1.599(12) (comparing to 1.633(8) Å in 21) while the four (Mo⁰)-P-O lengths average to 1.672(13) (even longer than that of 1.650(9) Å in complex 21). Once again this suggests intracage transmission of electron density.

Table XI. Selected Bond Distances (Å) and Angles(deg) for 25

Mo-P(1)	2.475(5)	Mo-P(2)	2.495(5)
Mo-C(1)	2.026(25)	Mo-C(2)	1.996(26)
Mo-C(3)	2.027(26)	Mo-C(4)	1.970(25)
Pd-Br(1)	2.456(3)	Pd-Br(2)	2.474(5)
Pd-P(3)	2.233(5)	Pd-P(4)	2.233(5)
P(1)-O(2)	1.660(13)	P(1)-O(3)	1.694(12)
P(1)-N(1)	1.631(15)	P(2)-O(1)	1.654(12)
P(2)-O(4)	1.679(12)	P(2)-N(2)	1.642(14)
P(3)-O(3)	1.616(12)	P(3)-O(4)	1.575(11)
P(3)-N(3)	1.625(15)	P(4)-O(1)	1.616(12)
P(4)-O(2)	1.594(12)	P(4)-N(4)	1.627(17)
O(11)-C(1)	1.183(30)	O(22)-C(2)	1.189(31)
O(33)-C(3)	1.152(32)	O(44)-C(4)	1.178(31)
Br(1)-Pd-Br(2)	87.8(1)		
P(1)-Mo-P(2)	80.0(2)	P(1)-Mo-C(1)	89.8(7)
P(2)-Mo-C(1)	92.3(7)	P(1)-Mo-C(2)	99.3(7)
P(2)-Mo-C(2)	178.5(7)	C(1)-Mo-C(2)	89.0(10)
P(1)-Mo-C(3)	92.9(7)	P(2)-Mo-C(3)	90.3(7)
C(1)-Mo-C(3)	176.6(10)	C(2)-Mo-C(3)	88.4(10)
P(1)-Mo-C(4)	177.7(7)	P(2)-Mo-C(4)	100.5(7)
C(1)-Mo-C(4)	87.9(10)	C(2)-Mo-C(4)	80.2(10)
C(3)-Mo-C(4)	89.4(10)	P(3)-Pd-P(4)	85.0(2)
Br(1)-Pd-P(3)	178.5(2)	Br(2)-Pd-P(3)	93.5(2)
Br(1)-Pd-P(4)	93.7(2)	Br(2)-Pd-P(4)	177.4(2)
Mo-P(1)-O(3)	110.2(4)	O(2)-P(1)-O(3)	96.2(6)
Mo-P(2)-O(4)	110.1(4)	O(1)-P(2)-O(4)	98.5(6)
Pd-P(3)-O(3)	109.8(5)	O(3)-P(3)-O(4)	104.7(6)
Pd-P(3)-O(4)	109.5(5)	O(1)-P(4)-O(2)	104.6(6)
Pd-P(4)-O(1)	107.1(3)	P(2)-O(1)-P(4)	132.1(7)
Pd-P(4)-O(2)	110.4(5)	P(1)-O(2)-P(4)	129.7(8)
Mo-P(1)-O(2)	113.7(4)	P(1)-O(3)-P(3)	129.8(7)
Mo-P(2)-O(1)	109.3(5)	P(2)-O(4)-P(3)	129.6(7)

2.10. (CO)₃Mo[iPr₂NPO]₅PdCl₂ (26):

Complex **26** was synthesized by the reaction of complex **14** with PdCl₂(C₆H₅CN)₂ in toluene at 70 °C for 66 hours.



³¹P NMR spectra were used to monitor the reaction. When the reaction was run for 66 hours, a red-brown suspension formed. Its ³¹P NMR spectrum showed a mixture of complexes **1** and **26** in about a 1: 2 ratio while the spectrum of the suspended gray yellow solid showed that it was the Mo-PdCl₂P₅O₅ cage complex. Work-up of the solid by recrystallization from chloroform gave pure yellow needle crystals of complex **26**. Evaporating the solution followed by washing the residue with acetone and hexane gave more pure **26**. Acetone removed the brown color and hexane removed complex **1** since complex **26** is not very soluble in either solvent. The combined yield of complex **26** was 52%.

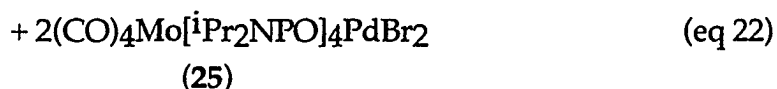
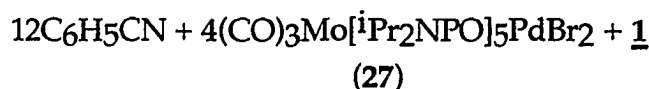
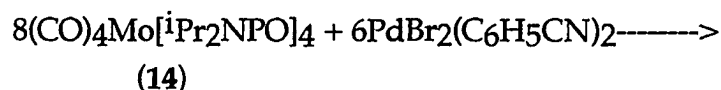
Complex **26** was identified by its ¹H, ¹³C, ³¹P NMR, and IR spectra and by elemental analyses. Its spectra are very different from those of complex **25**. The ³¹P NMR spectrum shows an AM₂X₂ pattern with the three phosphorus atoms coordinated to Mo⁰ giving two resonances: a triplet of triplet at 154.7 ppm, and a doublet at 134.9 ppm. The two phosphorus atoms bonded to Pd(II) gave rise to a doublet at 86.0 ppm (J_{AM}=31 Hz, J_{AX}=11 Hz, J_{MX}=0 Hz). The IR spectrum showed three absorptions in the carbonyl region at 1981.6 cm⁻¹,

1910.4 cm⁻¹ and 1880.1 cm⁻¹ consistent with the fac-Mo(CO)₃P₃ group. The ¹³C NMR spectrum in the carbonyl region showed two sets of doublets of triplets at 218.1 ppm (J_{PC}=39, 14 Hz) and 216.1 ppm (J=41, 10 Hz). These data are consistent with the previously-reported spectra of P₅O₅ cage complexes^[49].

No trace of the expected Mo-Pd P₄O₄ cage was detected.

2.11. (CO)₃Mo[ⁱPr₂NPO]₅PdBr₂ (27):

Complex **27** was synthesized by the reaction of complex **14** with PdBr₂(C₆H₅CN)₂ in toluene at 70 °C for 72 hours.



Again, ³¹P NMR spectroscopy was used to monitor the reaction. To optimize the synthesis of the P₅O₅ cage complex **27**, we used starting materials in a 5 : 1 ratio of P to Pd. When the reaction was run for 72 hours, a brown yellow suspension formed. Whose ³¹P NMR spectrum showed it to be a mixture of complexes **1**, **25** and **27** in about a 1 : 2 : 4 ratio. The spectrum of the solid (gray yellow color) showed only the Mo-PdBr₂P₅O₅ cage complex. Workup of the solid by recrystallization from chloroform gave yellow

crystalline solid 27. Work-up of the solution mixture by vacuum drying and washing the residue with acetone followed by hexane yielded more pure complex 27. The combined yield of complex 27 was 48%. Complex 25 is soluble in acetone. Small amounts of complex 1 can be removed by hexane since complex 27 is not very soluble in either solvent.

The product was identified by ^1H , ^{13}C , ^{31}P NMR, and IR spectroscopy and by elemental analyses. The spectra of complex 27 are very similar to those of complex 26. These data are listed in Tables XII, XIII, XIV and XV. Selected spectra for 25, 26, and 27 are shown in Figures 37, 38 and 39 for comparison:

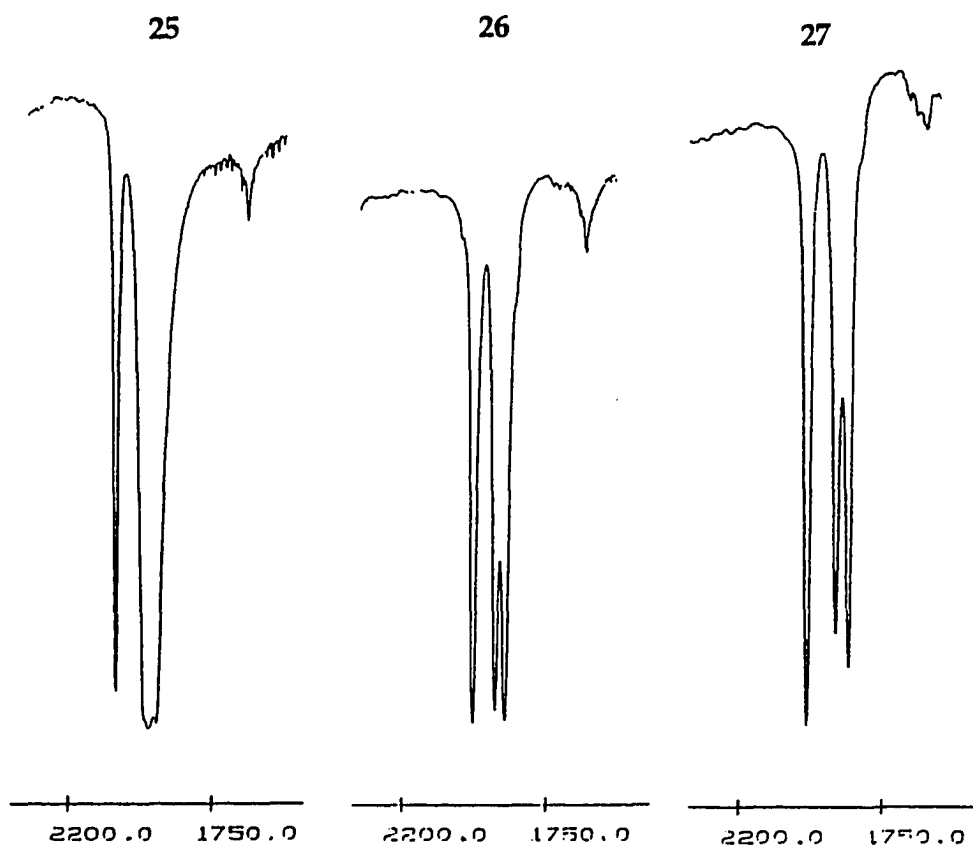
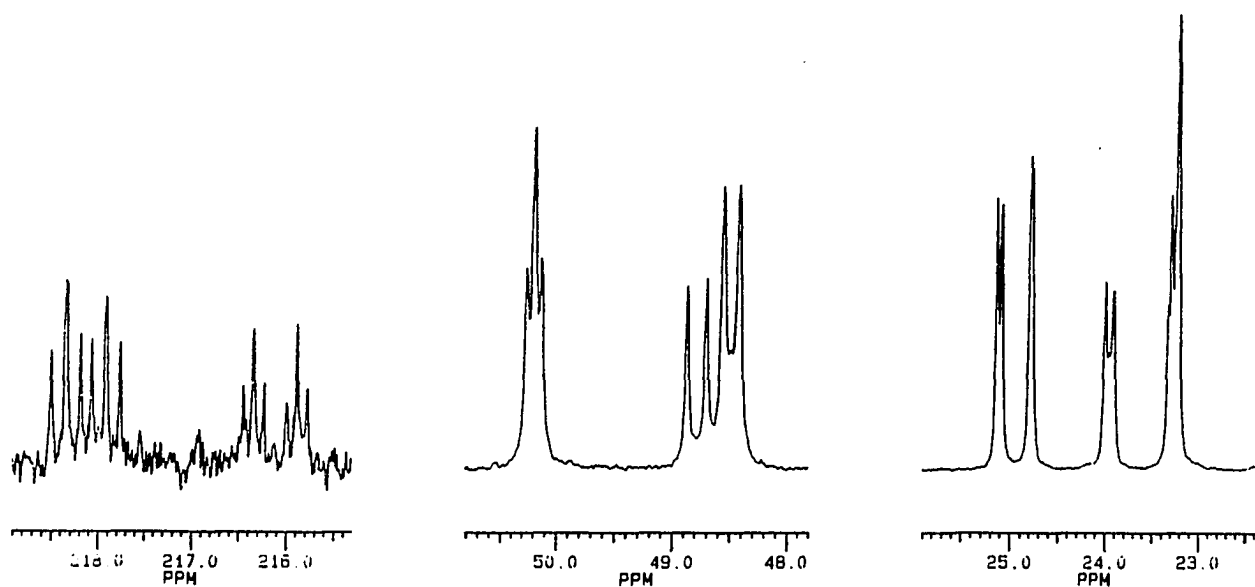


Figure 37. IR spectra of the carbonyl region for 25, 26 and 27

Complex 26



Complex 25

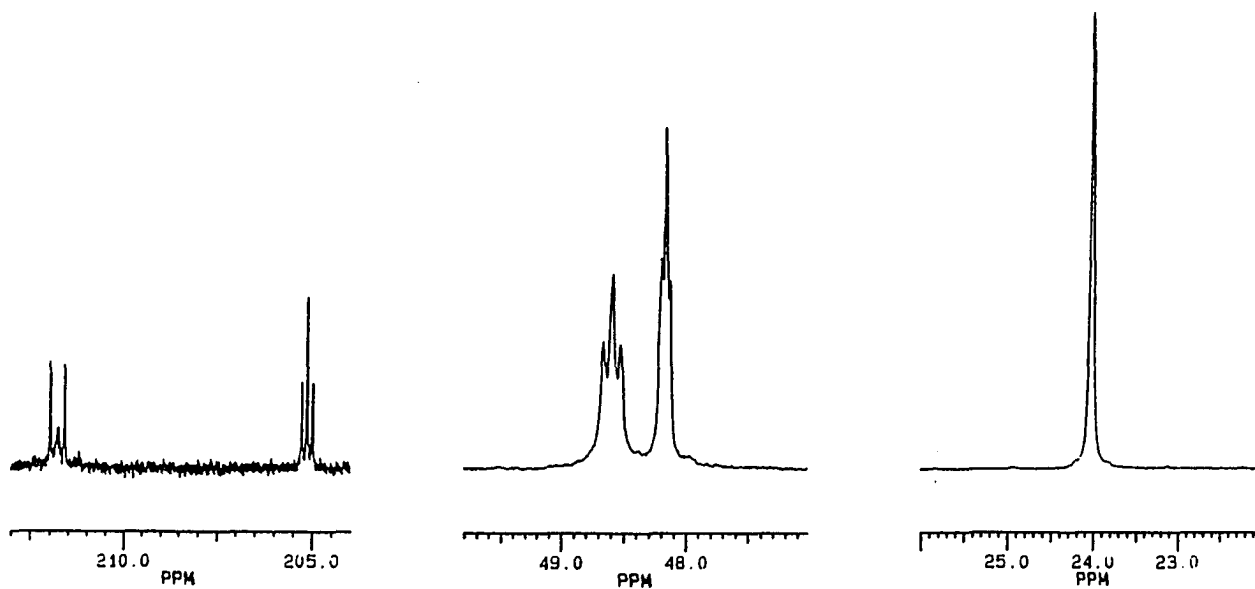
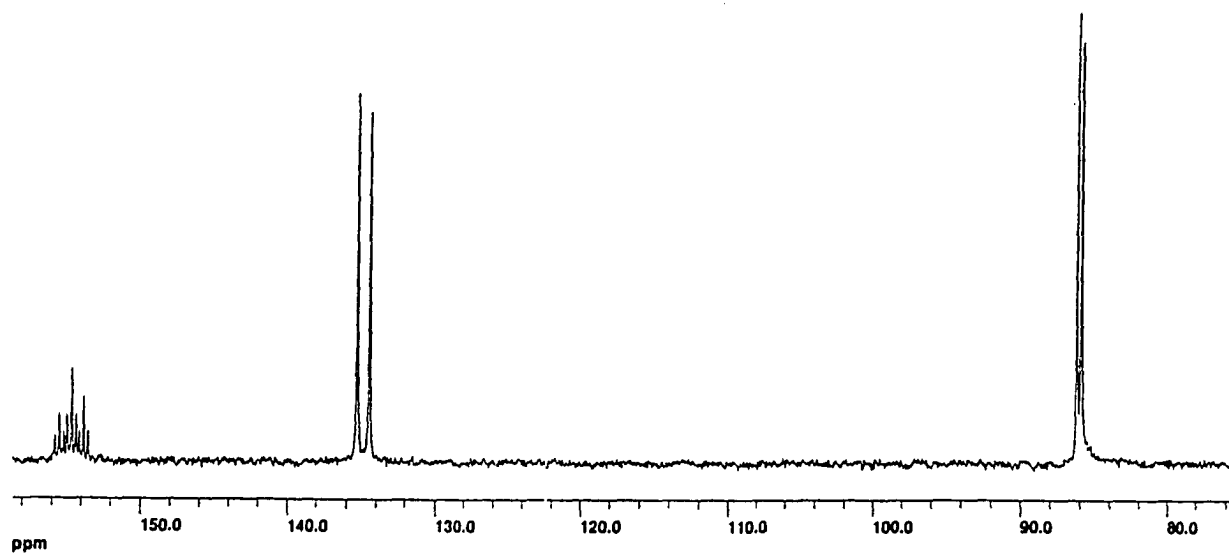


Figure 38. ^{13}C $\{^1\text{H}\}$ NMR spectra for 25, 26

Complex 26



Complex 25

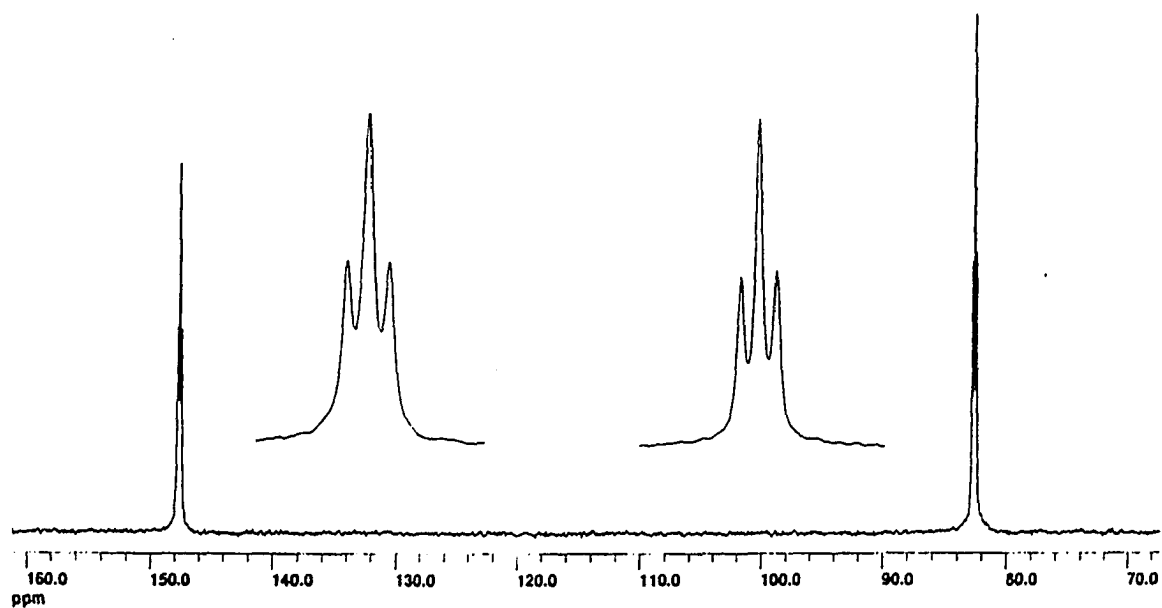


Figure 39. $^{31}\text{P}\{^1\text{H}\}$ NMR spectra for 25, 26

From the similarity of the spectral data between 26 and 27, we can see that the influence of the halide ligands is negligible.

The reaction shown by equation 22 is very different from that shown by equation 21. For the reaction of complex 14 with $\text{PdBr}_2(\text{C}_6\text{H}_5\text{CN})_2$, both P_4O_4 and P_5O_5 cage complexes formed. When complex 25 and phosphine oxide $(i\text{Pr}_2\text{N})_2\text{P}(\text{O})\text{H}$ were heated in 70 °C toluene for one day, a ^{31}P NMR spectrum of the reaction mixture showed that the P_4O_4 cage had totally disappeared while the P_5O_5 cage and some complex 14 had formed in about a 4:1 ratio. When only complex 25, or complex 25 with $\text{PdBr}_2(\text{C}_6\text{H}_5\text{CN})_2$, or complex 14 with phosphine oxide were heated in toluene, no complex 27 formed. This expansion of a P_4O_4 cage to a P_5O_5 cage was discussed in detail in Part II-7.

3. Structure of $(\text{CO})_4\text{Mo}[i\text{Pr}_2\text{NPO}]_4\text{MBr}_2$ (M=Ni, Pd).

The X-ray crystal structures of complexes $(\text{CO})_4\text{Mo}[i\text{Pr}_2\text{NPO}]_4\text{NiBr}_2$ (21) and $(\text{CO})_4\text{Mo}[i\text{Pr}_2\text{NPO}]_4\text{PdBr}_2$ (25) are shown in Figures 34 and 36, and the bond data listed in Tables IX and X. By comparing the data for these two structures, it can be seen that even though both Ni(II) and Pd(II) are formally of d^8 electronic configuration and both are four-coordinate, there are major differences between their coordination modes. In complex 21, the four-coordinate nickel(II) center adopts a pseudo-tetrahedral geometry. This geometry is consistent with its paramagnetic behavior^[64]. In complex 25, the Pd(II) center adopts a square-planar geometry which is consistent with its diamagnetism. With few exceptions^[65], four-coordinate d^8 Pd(II) complexes

form square-planar complexes while four-coordinate Ni(II) complexes can form either tetrahedral D_{2d} , or square-planar complexes. Generally, weak-field ligands such as the halides and bulky ligands tend to form tetrahedral complexes, while strong-field ligands such as phosphines favor the square-planar geometry. In the latter geometry, the metal to phosphorus $d\pi$ - $d\pi$ back bonding exists and the alignment of the participating orbitals is better, making the $d\pi$ - $d\pi$ back bonding more efficient.

X-ray analysis of complex **21** showed the deviations from idealized angles are found in both metal coordination spheres though there is approximately a tetrahedral geometry around the Ni vertex and an octahedral geometry at the Mo center. At Mo, the angle closest to linearity is P(3)-Mo-C(2) at $177.7(4)^\circ$. The four equatorial ligand atoms P(1), C(1), C(3), and C(4) have angles at Mo from $85.7(6)^\circ$ to $94.3(4)^\circ$ which sum up to 361° . The P(1)-Mo-P(3) bond angle is compressed by the chelate ring to $77.9(1)^\circ$. The two Mo-P bond distances are similar at $2.493(3) \text{ \AA}$ which is within the bonding range of the P-Mo(CO)_n bonds^[66]. The Mo-C bond distance of the equatorial carbonyls are now at $1.987(17)$ and $2.004(15) \text{ \AA}$, shorter than the Mo-C bond length of the axial carbonyls at $2.019(17)$ and $2.047(17) \text{ \AA}$. This is because the carbonyls trans to the phosphorus (good σ -donor compared to CO) can form better π back-bonding.

The bond angles around nickel deviate widely from 109.5° : the P-Ni-P angle is compressed to only $85.7(1)^\circ$. The Br(1)-Ni-Br(2) angle is distorted to $128.9(1)^\circ$, and the other angles are in the range of $104.4(1)$ to $111.3(1)^\circ$. The Ni-P bond distances at 2.254 \AA and 2.266 \AA are consistent with the literature values^{[66][67]}.

Replacing NiBr₂ by PdBr₂ in complex **25** generated relatively few changes in bonding data at Mo where the angle closest to linearity is P(2)-Mo-C(2) at 178.5(7)° and in **21** it is at 177.7(4)°. The four equatorial angles range from 87.9(10) to 92.9(7), but sum to 360°. In complex **21** these angles are in the range of 85.7(6)° to 94.3(4)°. The chelate ring compresses the P(1)-Mo-P(2) angle to 80.0(2)° compared with 77.9(1)° in **21**, the Mo-P bond distances are changed from 2.493(3) Å in complex **21** to 2.475(5) Å and 2.495(5) Å. The Mo-C bond distances of the equatorial carbonyls are 1.996(26) and 1.970(25) Å, again, smaller than the Mo-C bond length of the axial carbonyls at 2.026(25) and 2.027(26) Å. The four bond angles around palladium deviate from orthogonality; the P-Pd-P angle is the most distorted one at 85.0°, Br(1)-Pd-Br(2), 87.8(1)°; Br(2)-Pd-P(3), 93.5(2)°; Br(1)-Pd-P(4), 93.7(2)°. These orthogonal angles sum to 360°. The P-Pd bond distances at 2.233 Å are consistent with literature values^[66].

The P-O distances of complex **14**, **21** and **25** are compared in **Figure 40**:

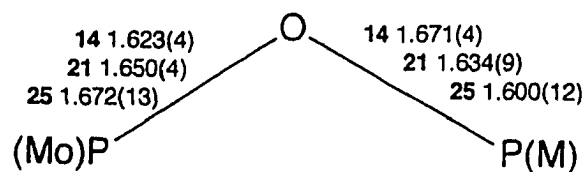
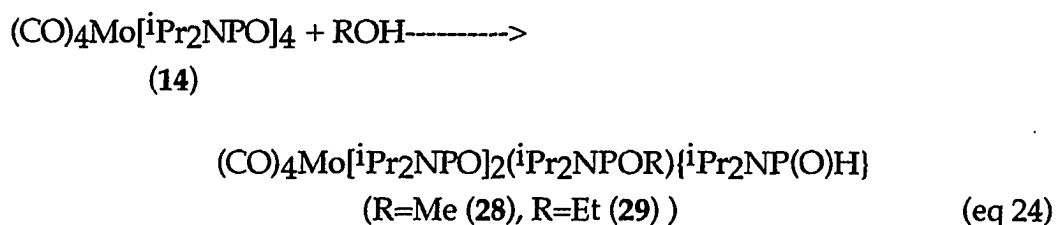


Figure 40. Selected Structural Data for **14**, **21** and **25**

The eight cage P-O bond distances in **14**, **21**, **25** are different; in each case, they are adjusted to the respective coordination needs.

4. Reactions of $(\text{CO})_4\text{Mo}[\text{iPr}_2\text{NPO}]_4$ (14) with Alcohols:

In Part II 1, we mentioned the reaction of complex 14 with MeOH; in this section, we will discuss details of this reaction. The reactions of complex 14 with MeOH and EtOH can be written as follows:



The respective yields of complexes 28 and 29 in these reactions were 75 and 72%, respectively. Complex 28 was synthesized by the reaction in refluxing MeOH/hexane solution, and complex 29 was synthesized in refluxing EtOH/hexane solution.

Nucleophilic attack by primary alcohols such as MeOH and EtOH on complex 14 led to cleavage of a single P-O-P bond to give complexes 28 and 29, $(\text{CO})_4\text{Mo}[\text{iPr}_2\text{NPO}]_2(\text{iPr}_2\text{NPOR})\{\text{iPr}_2\text{NP}(\text{O})\text{H}\}$. Both 28 and 29 have been identified by ^1H , ^{13}C , and ^{31}P NMR and IR spectroscopy and by elemental analyses. In addition, the postulated monocyclic structure of complex 28 has been confirmed by X-ray crystallography. From ^1H , ^{13}C , and ^{31}P NMR and IR spectra of compound 28, we deduced that it was a monomolybdenum compound. The IR spectrum showed a P=O stretching band at 1241 cm^{-1} . The ^1H -decoupled ^{31}P NMR spectrum showed an ABMX pattern and the ^1H NMR and proton-coupled ^{31}P NMR spectra showed that one phosphorus was bonded directly to a proton to give a -P(H)O group (Chemical shift of P=-1.5

ppm, chemical shift of H = 7.56 ppm, $J_{PH} = 635.2$ Hz) The coupling relationships among the four phosphorus atoms also indicated that one P-OP bond was broken. The ^1H NMR showed a P-OCH₃ group (3.41 ppm, $J_{PH} = 12$ Hz). Proton-coupled and decoupled ^{13}C NMR spectra confirmed this, since POCH₃ showed a ^{13}C singlet in the proton-decoupled spectrum changing to a quartet in the proton-coupled spectrum ($J_{CH} = 145$ Hz, the coupling constant between phosphorus and carbon in -POCH₃ was not detected). Selected spectra are shown in **Figures 41, 42 and 43**.

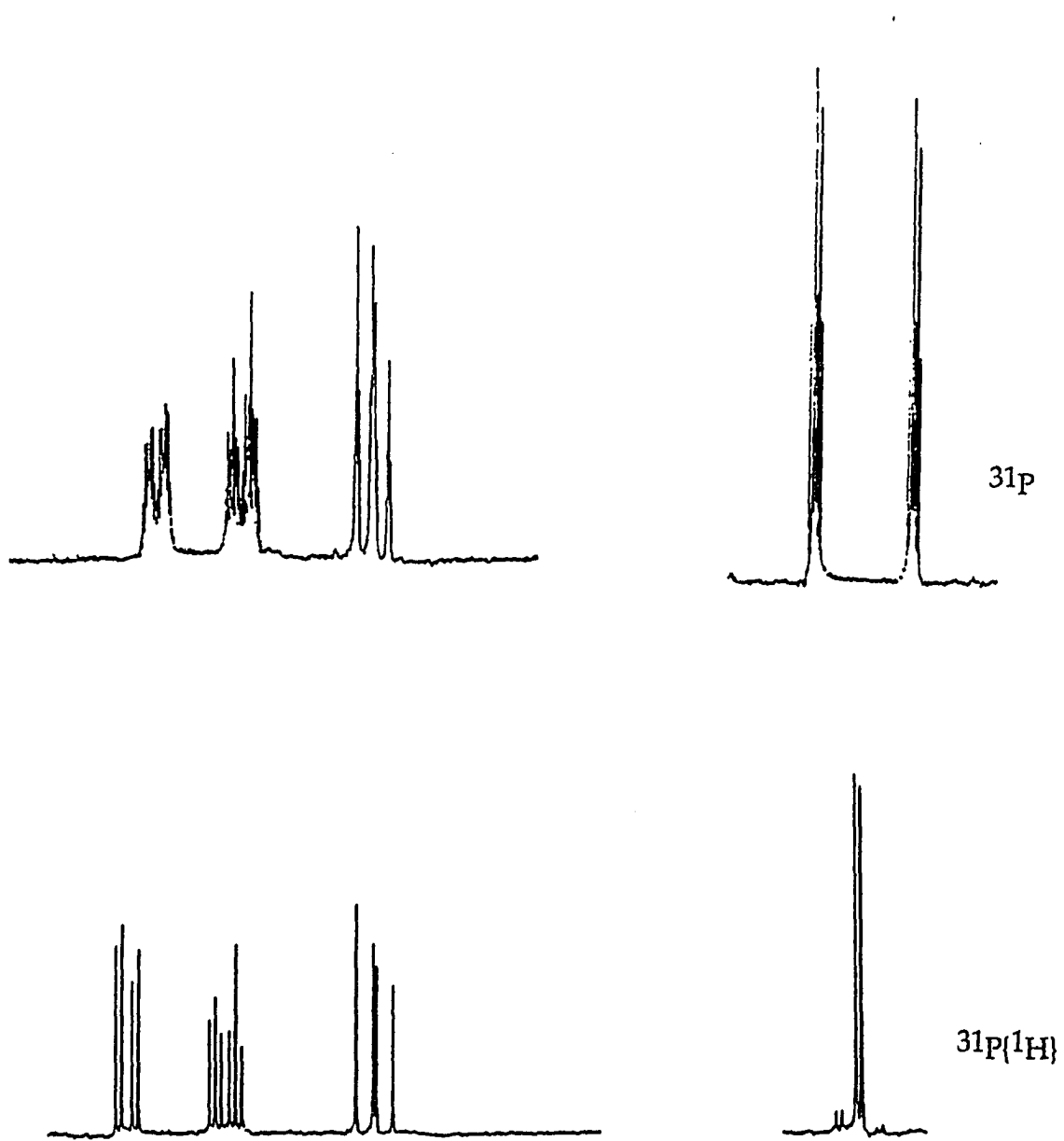


Figure 41. Proton-coupled and decoupled ^{31}P NMR spectrum for 28

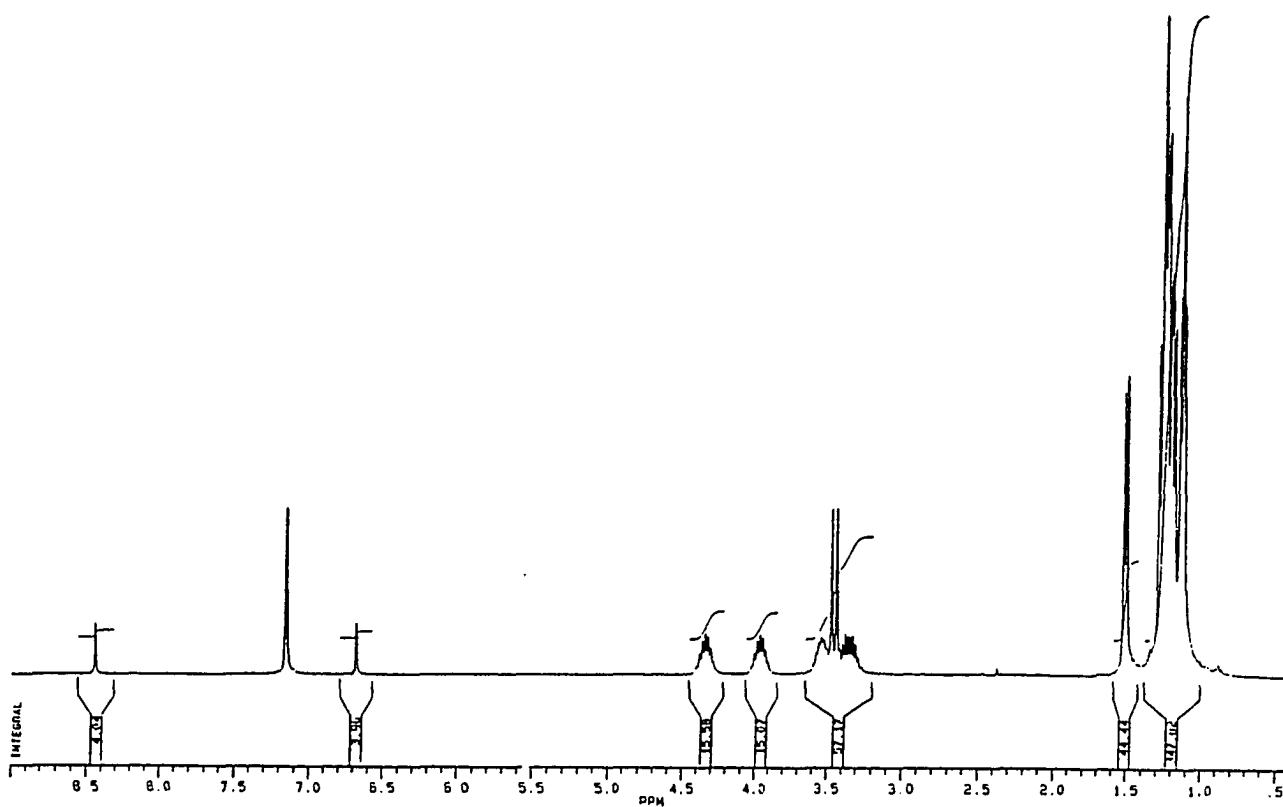


Figure 42. ^1H NMR spectrum for 28

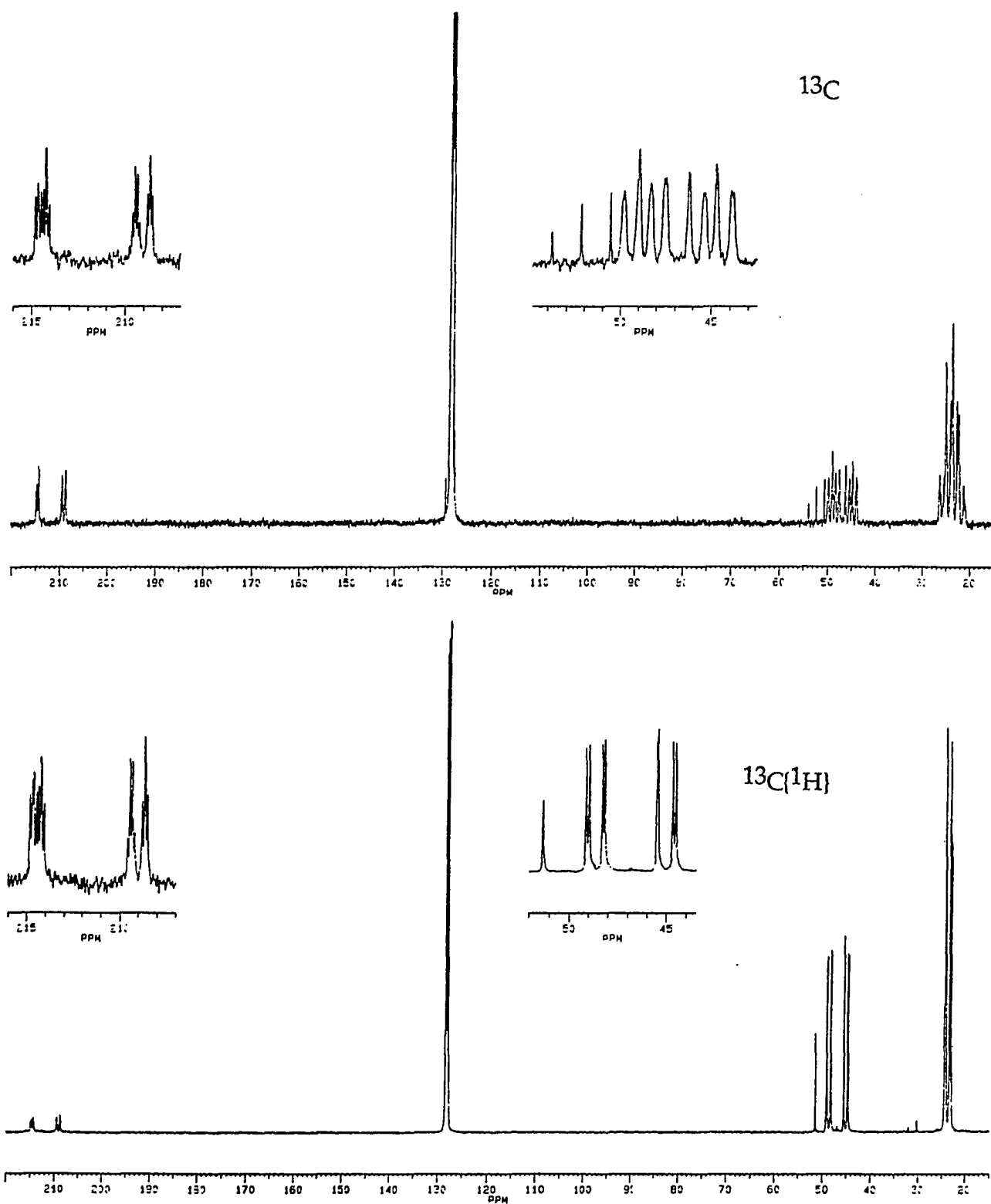
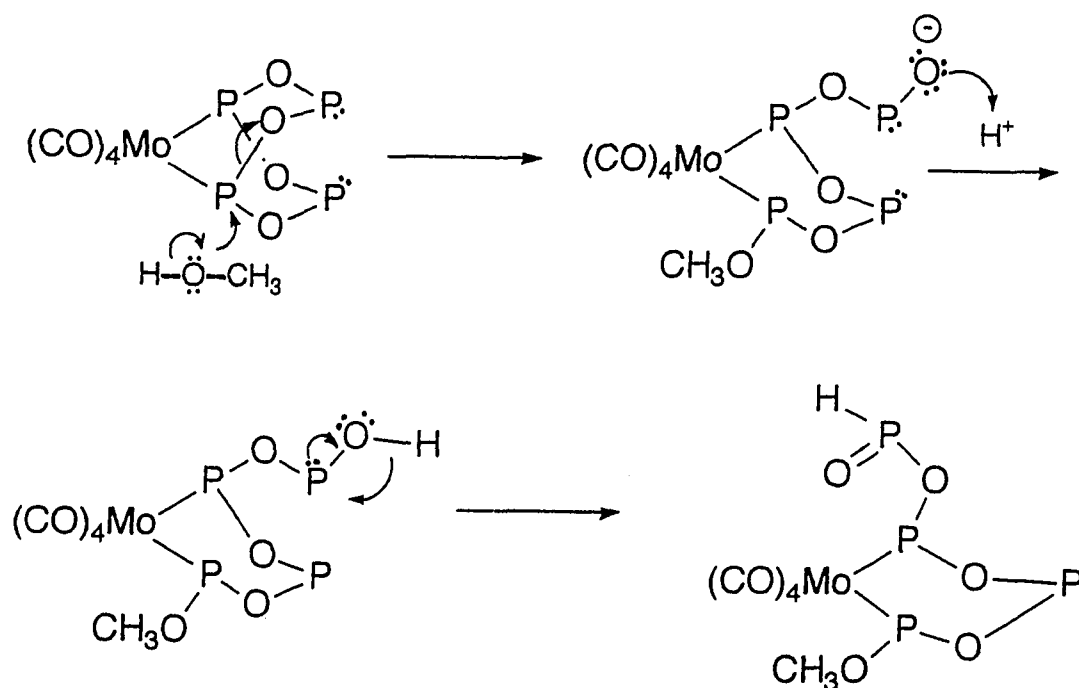


Figure 43. Proton-coupled and decoupled ^{13}C NMR spectrum for 28

The bonding relationship of atoms in complex **28** can be deduced by an analysis of all of the spectra. Complex **28** may form following this mechanism (Scheme V):



Scheme V

Later, the structure of **28** was determined by X-ray crystallography which confirmed the proposed structure. This X-ray structure is shown in **Figure 44** with the relevant structural data listed in **Table XII**.

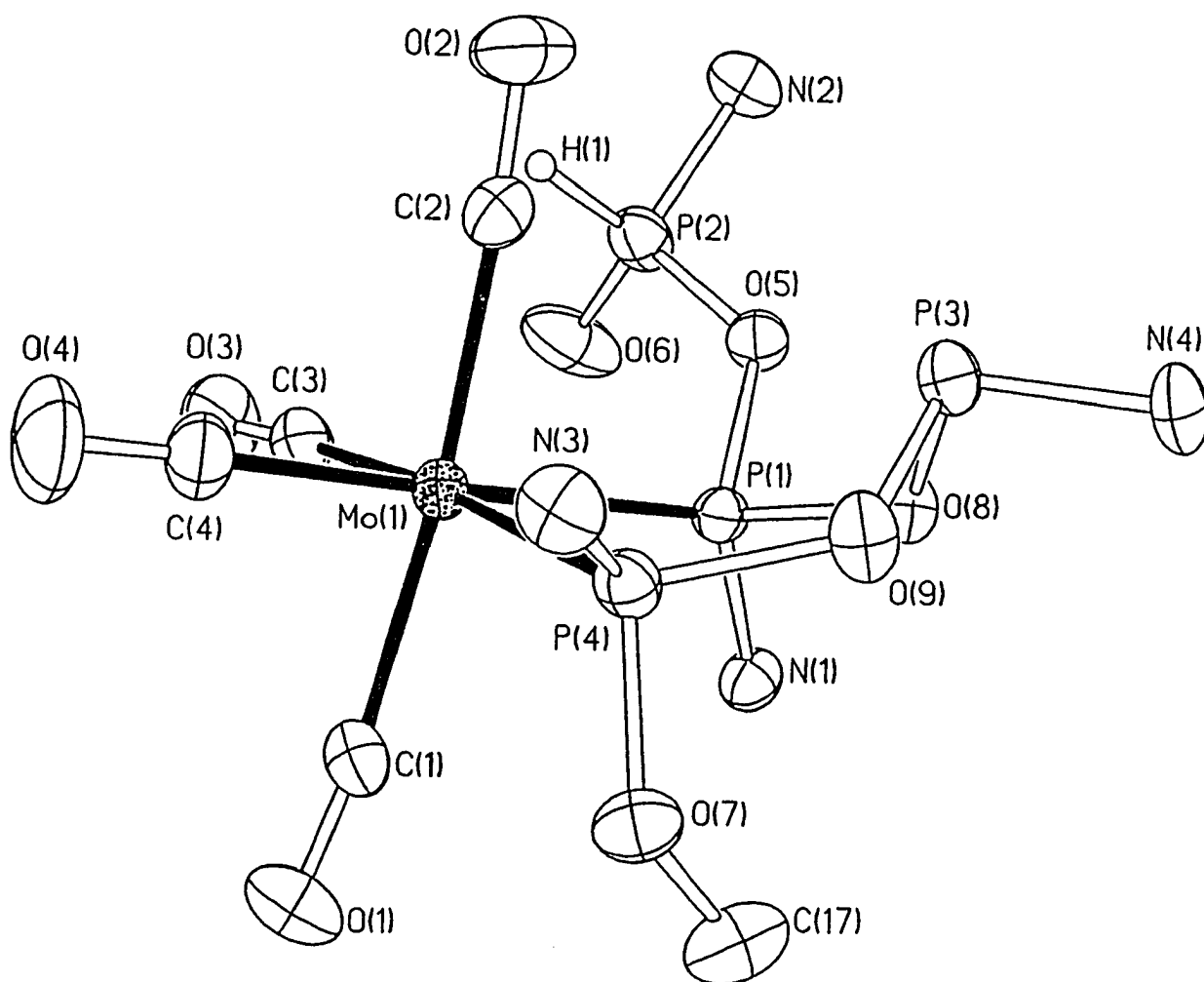


Figure 44. Molecular structure of 28

Table XII. Selected Bond Distances (Å) and Angles(deg) for 28

Mo(1)-P(1)	2.521(2)	Mo(1)-P(4)	2.501(2)
Mo(1)-C(1)	2.029(5)	Mo(1)-C(2)	2.030(5)
Mo(1)-C(3)	1.998(5)	Mo(1)-C(4)	1.992(6)
P(1)-O(5)	1.668(3)	P(1)-O(8)	1.616(3)
P(1)-N(1)	1.644(4)	P(2)-O(5)	1.604(3)
P(2)-O(6)	1.452(5)	P(2)-N(2)	1.609(4)
P(3)-O(8)	1.679(3)	P(3)-O(9)	1.649(3)
P(3)-N(4)	1.648(4)	P(4)-O(7)	1.602(3)
P(4)-O(9)	1.644(3)	P(4)-N(3)	1.655(4)
O(1)-C(1)	1.144(7)	O(2)-C(2)	1.145(6)
O(3)-C(3)	1.142(7)	O(4)-C(4)	1.142(7)
O(7)-C(17)	1.422(6)		
<hr/>			
P(1)-Mo(1)-P(4)	89.1(1)	P(1)-Mo(1)-C(1)	98.3(2)
P(4)-Mo(1)-C(1)	87.1(2)	P(1)-Mo(1)-C(2)	88.7(1)
P(4)-Mo(1)-C(2)	92.2(1)	C(1)-Mo(1)-C(2)	172.9(2)
P(1)-Mo(1)-C(3)	92.3(2)	P(4)-Mo(1)-C(3)	175.5(1)
C(1)-Mo(1)-C(3)	88.4(2)	C(2)-Mo(1)-C(3)	92.1(2)
P(1)-Mo(1)-C(4)	177.8(2)	P(4)-Mo(1)-C(4)	91.0(2)
C(1)-Mo(1)-C(4)	83.9(2)	C(2)-Mo(1)-C(4)	89.1(2)
C(3)-Mo(1)-C(4)	87.8(2)	Mo(1)-P(1)-O(5)	113.4(1)
Mo(1)-P(1)-O(8)	114.2(1)	O(5)-P(1)-O(8)	95.6(2)
Mo(1)-P(4)-O(7)	115.4(2)	O(5)-P(2)-O(6)	113.5(2)
Mo(1)-P(4)-O(9)	113.9(1)	O(8)-P(3)-O(9)	96.5(2)
P(1)-O(5)-P(2)	131.5(2)	O(7)-P(4)-O(9)	99.0(2)
P(1)-O(8)-P(3)	121.8(2)	P(3)-O(9)-P(4)	125.1(2)
P(4)-O(7)-C(17)	120.7(3)		

This shows that indeed a P-O-P was cleaved. One phosphorus, P(2), has a

new P=O double bond, and the other phosphorus, P(4), has a new P-OCH₃ bond. The lone remaining chelate ring shows a boat conformation with changes in ring angles and bond distances upon P-O-P cleavage. The P-Mo-P angle opened to 89.1(1)° from 75.1° in **14**. The P-O-P angles in the ring are compressed to 121.8(2)° and 125.1(2)° compared to 131.0° in **14**. This may be due to the repulsion of the two lone pairs flattening the P-O-P bond angles. The O-P-O angle in the ring is 96.5(2)°, similar to the O-P-O angles in **14** (97.7°). The geometry around molybdenum is unexceptional. It is pseudo-octahedral with a compressed axial C-Mo-C angle of 172.9(2) with the axial carbonyls bent away from the bidentate phosphorus ligand. The four equatorial angles are 87.8(2)°, 91.0(2)°, 89.1 (1)° and 92.3(2)°, summing nicely to 360°. The C(3)-Mo-P(4) [175.5(1)°] and C(4)-Mo-P(1) [177.8(2)°] angles are close to orthogonal values. The bonds distances of Mo-P (2.521 and 2.501 Å), P=O (1.452 Å) and P-O (1.602-1.668 Å) are typical literature values^{[69][69]}. The Mo-C bond distances of the two equatorial carbonyls (trans to the phosphorus) are 1.99 Å, shorter than the Mo-C bond lengths of the two axial carbonyls (cis to the phosphorus) at 2.03 Å for the previously-discussed reasons (part II. 3).

Complex **29** has ¹H, ¹³C, and ³¹P NMR and IR spectra very similar to those of **28**. These spectra data are listed in the Tables XIII, XIV, XV and XVI. Therefore complexes **29** should has a structure similar to that of complex **28** also.

Table XIII. $^{31}\text{P}\{^1\text{H}\}$ NMR Data for Cage Complexes

Complex		Chemical Shift, ppm [J, Hz]
13	ABXY	201.1(d), 180.52(d) [$^2J = 146\text{Hz}$] 154.9(d), 151.0(d) [$^2J = 39\text{ Hz}$]
14	A ₂ X ₂	150.6(t), 126.0(t, bd) [$^2J = 2\text{ Hz}$]
16	A ₂ X ₂	175.0(t), 147.9(t) [$^2J = 6\text{ Hz}$]
17	A ₂ X ₂	165.2(t), 152.1(t) [$^2J = 14\text{ Hz}$]
18	A ₂ X ₂	155.6(t), 90.9(t, bd) [$^2J = 10\text{ Hz}$]
19	A ₂ X ₂	154.3(t), 103.6 and 103.5(d of t) [$^2J = 13\text{ Hz}$, $^1J_{\text{AgP}} = 568\text{ and }492\text{Hz}$]
20	A ₂ X ₂	147.4(t), 132.6(t), 56.5(t) -19.4(t) [$^2J = 10\text{ Hz}$, $^1J_{\text{PtP}} = 5,520\text{Hz}$]
21		paramagnetic
22	A ₂ X ₂	154.5(t), 128.0(t) [$^2J = 3\text{ Hz}$]
23		paramagnetic
24		paramagnetic
25	A ₂ X ₂	147.6(t), 82.6(t) [$^2J = 6\text{ Hz}$]
26	AM ₂ X ₂	154.7(t of t), 134.9(d), 86.0(d) [$^2J_{\text{AM}} = 30\text{ Hz}$, $^2J_{\text{AX}} = 11\text{ Hz}$]
27	AM ₂ X ₂	154.0(t of t), 134.7(d), 85.4(d) [$^2J_{\text{AM}} = 30\text{ Hz}$, $^2J_{\text{AX}} = 10\text{ Hz}$]
28	ABMX	169.1(d of d) [$^2J_{\text{AB}} = 34\text{ Hz}$, $^2J_{\text{AM}} = 92\text{ Hz}$] 154.4(d of d of d) [$^2J_{\text{BX}} = 32\text{ Hz}$, $^2J_{\text{BA}} = 34\text{ Hz}$, $^2J_{\text{BM}} = 111\text{ Hz}$]

		131.3(d of d)
		$[^2J_{MA} = 92 \text{ Hz}, ^2J_{MB} = 111 \text{ Hz}]$
		-1.50(d) $[^2J_{BX} = 32 \text{ Hz}]$
29	ABMX	164.4(d of d)
		$[^2J_{AB} = 34 \text{ Hz}, ^2J_{AM} = 98 \text{ Hz}]$
		153.1(d of d of d) $[^2J_{BX} = 29 \text{ Hz},$
		$^2J_{BA} = 34 \text{ Hz}, ^2J_{BM} = 115 \text{ Hz}]$
		131.2(d of d)
		$[^2J_{MA} = 98 \text{ Hz}, ^2J_{MB} = 115 \text{ Hz}]$
		-2.86(d) $[^2J_{BX} = 29 \text{ Hz}]$

^a Spectra were run in CDCl₃ solutions (d = doublet, t = triplet, bd = broad).

Table XIV. ^{13}C NMR Data for Cage Complexes

Complex	Chemical Shift (assignment, J)
13	241.1 (m, $\text{S}_2\text{C}\underline{\text{N}}\text{Me}_2$), 215.0 (s, CO), 210.0, 209.1, 207.2 (bs, CO), 48.3, 47.8, 46.9 (bs, NC), 39.4 (bs, $\text{S}_2\text{CN}(\underline{\text{C}}\text{H}_3)_3$), 24.2 (bs, Me)
14	215.8 (t, CO, $^2J_{\text{PC}} = 14$ Hz), 209.5 (t, CO, $^2J_{\text{PC}} = 12$ Hz), 48.0 (t, NC, $^2J_{\text{PC}} = 7$ Hz), 44.3 (t, NC, $^2J_{\text{PC}} = 8$ Hz), 24.2 (s, Me), 23.2 (s, Me)
16	224.5 (t, CO, $^2J_{\text{PC}} = 9$ Hz), 218.0 (t, CO, $^2J_{\text{PC}} = 18$ Hz), 214.0 (t, CO, $^2J_{\text{PC}} = 16$ Hz), 207.2 (t, CO, $^2J_{\text{PC}} = 13$ Hz), 47.0 (t, NC, $^2J_{\text{PC}} = 7$ Hz), 46.8 (t, NC, $^2J_{\text{PC}} = 5$ Hz), 24.3 (s, Me), 24.0 (s, Me)
17	217.3 (t, CO, $^2J_{\text{PC}} = 7$ Hz), 214.5 (t, CO, $^2J_{\text{PC}} = 15$ Hz), 207.6 (t, CO, $^2J_{\text{PC}} = 13$ Hz), 48.1, 47.7 (t, NC, $^2J_{\text{PC}} = 6, 7$ Hz), 24.1 (s, Me), 24.0 (s, Me)
18	213.3 (t, CO, $^2J_{\text{PC}} = 16$ Hz), 207.2 (t, CO, $^2J_{\text{PC}} = 12$ Hz), 120.4 (s, $\underline{\text{C}}\text{N}$), 48.3 (t, NC, $^2J_{\text{PC}} = 6$ Hz), 45.3 (t, NC, $^2J_{\text{PC}} = 6$ Hz), 23.6 and 23.1 (s, Me's), 2.2 (s, $\underline{\text{C}}\text{H}_3\text{CN}$)
19	213.2 (t, CO, $^2J_{\text{PC}} = 16$ Hz), 207.5 (t, CO, $^2J_{\text{PC}} = 12$ Hz), 48.6, 45.4 (t, NC, $^2J_{\text{PC}} = 6, 7$ Hz), 23.9 (s, Me), 23.1 (s, Me)
20	212.1 (t, CO, $^2J_{\text{PC}} = 17$ Hz), 205.1 (t, CO, $^2J_{\text{PC}} = 12$ Hz), 48.2, 47.3 (t, NC, $^2J_{\text{PC}} = 6, 3$ Hz), 23.9 (s, Me), 23.6 (s, Me)
21	paramagnetic

22	215.0 (t, CO, $^2J_{PC} = 15$ Hz), 208.0 (t, CO, $^2J_{PC} = 12$ Hz), 198.4 (t, CO, $^2J_{PC} = 4$ Hz), 48.0, 46.3 (t, NC, $^2J_{PC} = 6$ Hz), 23.7(s, Me), 23.6 (s, Me)
23	paramagnetic
24	paramagnetic
25	211.8 (m, CO), 205.1 (t, CO, $^2J_{PC} = 13$ Hz), 48.0, 48.2 (t, NC, $^2J_{PC} = 6, 3$ Hz), 24.0(s, Me)
26	218.1 (d of t, CO, $^2J_{PC} = 39, 14$ Hz), 216.1 (d of t, CO, $^2J_{PC} = 41, 10$ Hz), 50.2 (t, NC, $^2J_{PC} = 6$ Hz), 48.8, 48.5 (d, NC, $^2J_{PC} = 15, 12$ Hz), 25.1 (d, Me, $J = 4$ Hz), 24.8 (s, Me), 24.0 (d, $J = 7$ Hz), 23.3 (t, $J = 3$ Hz), 23.2 (s, Me)
27	218.2 (d of t, CO, $^2J_{PC} = 39, 14$ Hz), 216.3 (d of t, CO, $^2J_{PC} = 41, 10$ Hz), 50.2 (t, NC, $^2J_{PC} = 5$ Hz), 48.7, 48.3 (d, NC, $^2J_{PC} = 15, 12$ Hz), 25.3 (d, Me, $J = 4$ Hz), 25.0 (s, Me), 24.0 (d, $J = 7$ Hz), 23.2 (s, Me), 23.0 (t, $J = 3$ Hz),
28	214.7 (d of d, CO, $^2J_{PC} = 12, 18$ Hz), 214.3 (t, CO, $^2J_{PC} = 14$ Hz), 209.4 (m, CO), 208.7 (t, CO, $^2J_{PC} = 12$ Hz), 51.3 (s, POCH_3), 49.0 (d, NC, $^2J_{PC} = 14$ Hz), 48.2, 45.5, 44.6 (d, NC, $^2J_{PC} = 14, 11, 6, 15$ Hz), 24.3-22.9 (m, Me)
29	214.1 (d of d, CO, $^2J_{PC} = 7, 11$ Hz), 213.6 (t, CO, $^2J_{PC} = 11$ Hz), 208.8 (m, CO), 207.9 (t, CO, $^2J_{PC} = 12$ Hz), 60.4 (s, POCH_2CH_3), 48.7 (d, NC, $^2J_{PC} = 14$ Hz), 47.9, 45.1, 44.3 (d, NC, $^2J_{PC} = 14, 11, 6, 14$ Hz), 24.1-22.8 (m, Me), 15.7 (d, POCH_2CH_3 , $J = 9$ Hz)

^a All spectra were run in CDCl_3 solution (t = triplet, d = doublet, s = singlet, bs = broad singlet)

Table XV. ¹H NMR Data for the Cage Complexes

Complex	Chemical Shift (multiplicity, assignment, J)
13	4.50 (bd, NCH), 4.30(septet, NCH, J = 7 Hz), 3.40, 3.30 (bd, S ₂ CN(CH ₃) ₃), 1.30 (bd, Me)
14	4.01(septet, NCH), 3.77 (bd, NCH), 1.30 and 1.12 (d, Me, J = 6.8 Hz)
16	4.47 and 4.14 (septets, NCH), 1.29 (t, Me, J = 7.0 Hz)
17	4.38 and 4.27 (septets, NCH, J = 7 Hz), 1.30 (m, Me)
18	4.03 and 3.83 (septets, NCH), 2.35 (s, MeCN) 1.29 (d, Me, J = 7.1 Hz)
19	3.99 and 3.83 (septets, NCH), 1.28 (d, Me, J = 6.8 Hz)
20	4.30 and 3.69 (septets, NCH), 1.46 and 1.40 (d, Me, J = 6.9 Hz)
21	paramagnetic
22	4.04 and 3.97 (septets, NCH), 1.30, 1.27 (d, Me, J = 7.0 Hz)
23	paramagnetic
24	paramagnetic

- 25 4.29 and 3.79 (septets, NCH, J = 7.3, 6.8 Hz),
1.48 and 1.45 (d, Me, J = 7.2 and 6.8 Hz)
- 26 4.64, 4.17 and 4.14 (septets, NCH, J = 6.9, 7.2
and 7.1 Hz), 1.43--1.38 (m, Me), 1.32 (d, Me, J =
6.9 Hz)
- 27 4.68, 4.18 and 4.14 (septets, NCH, J = 6.7, 7.1
and 6.7 Hz), 1.42--1.38 (m, Me), 1.33 (d, Me, J =
6.9 Hz)
- 28 7.56 (d, P(O)H, $J_{PH} = 635.2$ Hz), 4.34, 3.96 and
3.47 (septets, NCH, J = 6.8, 7.1 and 6.4 Hz),
3.41 (d, POCH₃, $J_{POCH_3} = 12.36$ Hz), 3.36 and
3.32 (septets, NCH, J = 6.7 Hz), 1.51 (d, Me, J =
6.8 Hz), 1.27--1.12 (m, Me)
- 29 7.58 (d, P(O)H, $J_{PH} = 634.9$ Hz), 4.35 (septet,
NCH, J = 6.9 Hz), 3.97 (m, NCH and
POCH₂CH₃), 3.54, 3.35 and 3.34 (septets, NCH,
J = 5.9, 6.8 and 6.7 Hz), 1.45 (d, Me, J = 6.8 Hz),
1.27 (m, Me and POCH₂CH₃)
-

Table XVI. Infrared Absorptions for the Complexes

Complex	CO region, cm ⁻¹	POP region, cm ⁻¹
1	2025.8, 1945.0, 1905.3, 1886.5 2015, 1923, 1906, 1887	880.4, 858.5, 820.6 ^b 875, 849, 809 ^c
12	2035.1, 1979.3, 1916.2	898.5, 857.7, 824.7 ^b
13	2013, 1912	871, 843, 792 ^c
14	2022.8, 1925.1, 1908.1, 1982.5 2010, 1925, 1908, 1882	891.5, 873.5, 860.2, 838.4 ^b 879, 861, 847, 828 ^c
15	2000, 1932, 1869, 1843, 1837	1517(C-N) ^c
16	2035.3, 2020.8, 1930.5, 1900.6 2023, 2009, 1925, 1901	879.0, 854.4, 805.3 ^b 869, 843, 786 ^c
17	2021, 2014, 2000, 1937, 1907	867, 847, 795 ^c
18	2031.3, 1908.0 2019, 1905	885.9, 860.0, 814.1 ^b 874, 850, 795 ^c
19	2029.7, 1936.2, 1908.2 2015, 1931, 1910	887.3, 861.5, 834.6, 815.0 ^b 870, 852, 822, 804 ^c
20	2045.1, 1958.7, 1948.1, 1917.6 2033, 1950, 1940, 1914	894.1, 873.0, 847.1, 831.0 ^b 879, 861, 835, 818 ^c
21	2036.7, 1946.9, 1936.9, 1899.8 2024, 1949, 1937, 1899	861.0, 830.1 ^b 852, 813 ^c
22	2022.9, 1968.8, 1931.3, 1919.5, 1905.6 2010, 1968, 1928, 1915, 1903	881.3, 854.6, 797.7 ^b 869, 842, 792 ^c
23	2035.7, 1947.4, 1936.3, 1900.0 2025, 1928,	862.1, 831.8 ^b 874, 855 ^c
24	2037.4, 1950.5, 1932.2, 1921.0 2025, 1925	886.5, 859.7, 823.0 ^b 875, 850, 815 ^c
25	2045.8, 1961.0, 1943.0, 1921.8	871.7, 845.2, 820.9 ^b
26	1981.6, 1910.4, 1880.1	888.3, 867.6, 858.9, 834.8 ^b
27	1981.2, 1910.9, 1880.1	887.1, 866.5, 858.2, 833.3 ^b
28	2027.2, 1928.0, 1909.8, 1895.8 2014, 1923, 1907, 1895	895.6, 881.7, 859.4, 845.5 ^b 884, 871, 850, 834 ^c
29	2027.5, 1942.9, 1919.3, 1903.6	896.9, 883.2, 859.6, 839.9 ^b

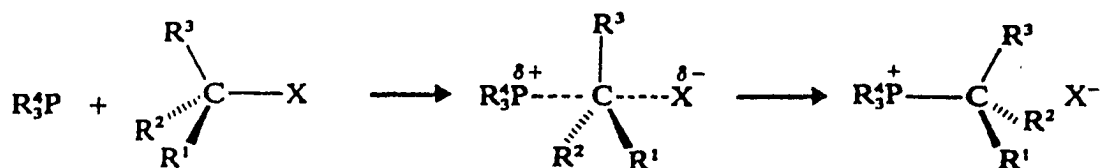
^a KBr pellets, ^b FT-IR: Nicolet MX-1, ^c IR: Perkin-Elmer 283B

5. Miscellaneous Reactions:

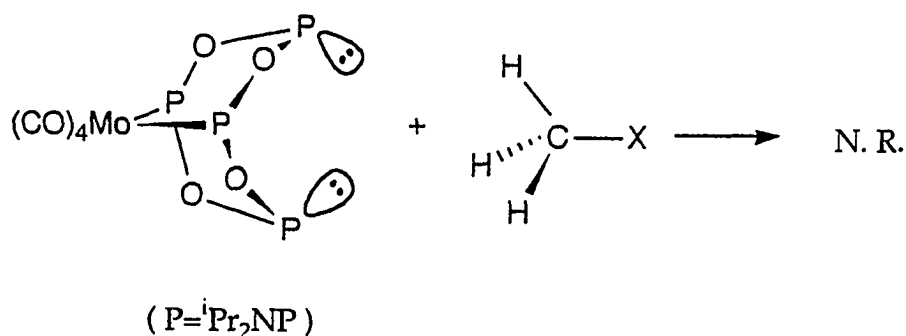
5.1. Reaction of $(\text{CO})_4\text{Mo}[\text{iPr}_2\text{NPO}]_4$ with MeI

Compound $(\text{CO})_4\text{Mo}[\text{iPr}_2\text{NPO}]_4$ has two uncoordinated phosphorus atoms each with an available lone pair. We studied its reaction with the alkylating reagent MeI to see if it could be mono-alkylated which might lead to the formation of a bond between these two phosphorus atoms. Di-alkylation products might also form. However, no reaction occurred. At first, we used hexane as a solvent with MeI in large excess. We expected that the alkylation product salt would precipitate easily in this nonpolar solvent. After running the reaction at room temperature for 3 days, the ^1H , and ^{31}P NMR spectra of the reaction mixture showed that no reaction had occurred. Next, we tried the more polar solvent THF. In THF, even after three days, again no alkylated products had formed. The ^1H NMR spectrum of the reaction mixture showed that some $(\text{CO})_4\text{Mo}[\text{iPr}_2\text{NPO}]_4$ had reacted with the THF to form unidentified products. This was confirmed by comparing the ^1H NMR spectrum of the control reaction of $(\text{CO})_4\text{Mo}[\text{iPr}_2\text{NPO}]_4$ with THF. We also checked the reaction in a 1 : 1 $\text{CH}_3\text{CN}/\text{CH}_2\text{Cl}_2$ solvent mixture (the precursor complex is insoluble in neat CH_3CN); again no reaction resulted.

Tertiary phosphines generally react with alkyl halides by an $\text{S}_{\text{N}}2$ process to form a phosphonium salt. Displacement at a chiral carbon center occurs with inversion of configuration, consistent with a bimolecular transition state, as shown in the following equation^[70]:



We think the unsuccessful alkylation of these phosphorus atoms may be due to the special structure of the compound (Scheme VI). The two electron lone pairs on the phosphorus atoms are convergent, and can not approach the carbon center to form the appropriate transition state; therefore, no alkylation products formed. Also, by its temperature-independent ^{31}P NMR spectral behavior up to 110 °C, we know that the inversion barrier at the phosphorus center is quite high, which prevents the lone pair from becoming accessible in the exo conformation.

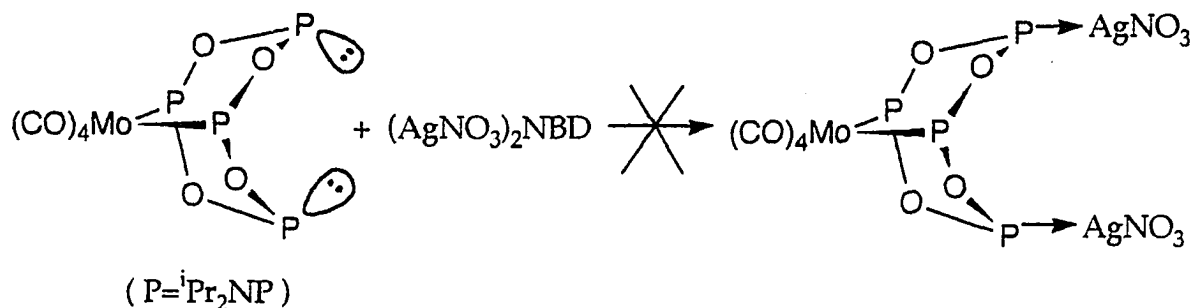


Scheme VI

From this reaction, we recognized that the precursor may only act as a bidentate donor. Thus, only the 1 : 1 Mo-Ag heterobimetallic cage product

$(\text{CO})_4\text{Mo}[\text{iPr}_2\text{NPO}]_4\text{AgNO}_3$ formed (Scheme VII) regardless of excess Ag^+

(See Part II 2.4).



Scheme VII

5.2. The Reaction of $(\text{CO})_4\text{Mo}[\text{iPr}_2\text{NPO}]_4$ with $\text{Ni}(\text{COD})_2$

We attempted to use $(\text{CO})_4\text{Mo}[\text{iPr}_2\text{NPO}]_4\text{Cu}(\text{CH}_3\text{CN})_2\text{BF}_4$ to react with $(\text{CO})_4\text{Mo}[\text{iPr}_2\text{NPO}]_4$ in order to make a trimetallic 2 : 1 (2Mo : Cu) complex. Unfortunately, the reaction was not clean, and it was hard to tell whether the major product was $(\text{CO})_4\text{Mo}[\text{iPr}_2\text{NPO}]_4\text{CuBF}_4$ or $(\text{CO})_4\text{Mo}[\text{iPr}_2\text{NPO}]_4\text{Cu}[\text{iPr}_2\text{NPO}]_4\text{Mo}(\text{CO})_4\text{BF}_4$, since no pure product was isolated. We also attempted the reaction of $(\text{CO})_4\text{Mo}[\text{iPr}_2\text{NPO}]_4\text{Ni}(\text{CO})_2$ with $(\text{CO})_4\text{Mo}[\text{iPr}_2\text{NPO}]_4$, but also failed to produce the desired tri-metallic complex. It may be because the bonds between the carbonyls and Ni are too strong to be replaced. Hence we synthesized $\text{Ni}(\text{COD})_2$ from $\text{Ni}(\text{py})_4\text{Cl}_2$ and used it as a starting material to react with the Mo precursor, but this reaction also failed. As the bonding between Ni and COD may be too weak and at the

same time the substitution reaction was very slow, after three hours the ^1H NMR spectrum of the reaction mixture showed no desired product and the $\text{Ni}(\text{COD})_2$ had decomposed. If the reaction was run in refluxing CH_2Cl_2 , a black murky mixture formed in only 20 minutes as the $\text{Ni}(\text{COD})_2$ decomposed. Since $\text{Ni}(\text{COD})_2$ is very reactive with oxygen and is pyrophoric, we need to find a better nickel compound to use as the starting material.

5.3. Other Reactions of $(\text{CO})_4\text{Mo}[\text{iPr}_2\text{NPO}]_4$

Boron trifluoride is a strong Lewis acid and the Mo precursor (**14**) has several sites (O, N, P) with lone pairs that can act as donors. Thus, we ran the reaction of $(\text{CO})_4\text{Mo}[\text{iPr}_2\text{NPO}]_4$ with $(\text{CH}_3\text{CH}_2)_2\text{O}\cdot\text{BF}_3$ in CH_2Cl_2 at room temperature. After 1 hour, ^1H and ^{31}P NMR spectra of the reaction mixture showed that the starting complex had decomposed. We also attempted the reaction of **14** with sulfur. ^{31}P NMR spectra showed that the products were mixtures, as one or both of the uncoordinated phosphorus atoms had reacted with S to form mono-P=S or di-P=S compounds. No pure products were obtained.

The reactions of complex **14** with nucleophiles such as iPrOH , ArCHO , $(\text{iPr}_2\text{N})_2\text{P}(\text{O})\text{H}$, PCl_3 or electrophiles such as SnCl_2 , SnCl_4 , SnMeCl_3 were also attempted; either no reaction was observed or no products were isolated.

Numerous attempts were made to synthesize Mo/Rh and Mo/Ru heterobimetallic cage compounds which would be possible catalysts. For example, $\text{Ru}(\text{DMSO})_4\text{Cl}_2$, $[(\text{NBD})\text{RhCl}]_2$, $[\text{Rh}(\text{NBD})(\text{CH}_3\text{CN})_2]\text{Cl}$,

[Rh(NBD)(PPh₃)₂]PF₆ were all tried, but no desired products were obtained.

6. Evidence for Intracage Influences Due to the Heterometal

The rigidly conserved structures of the heterobimetallic cage complexes provided a useful setting for the study of intracage metal-metal interactions. By examining the variation of the Mo carbonyl ¹³C NMR shift values and the IR stretching frequencies of the carbonyls of the cis-Mo(CO)₄ group in a series of bimetallic cage complexes of the type (CO)₄Mo[ⁱPr₂NPO]₄ML_n (M=Cr(0), Fe(0), Mo(0), Ni(0), Ag(I), Cu(I), Pt(II), Pd(II) and Ni(II)), it has been found that there are two trends. One is the correlation between the well-resolved A₁ carbonyl stretching frequencies of the cis-Mo(CO)₄ group and the formal charge on the second cage metal M. As the charge of the second metal increases, the A₁ carbonyl stretching frequencies for the cis-Mo(CO)₄P₂ moiety increases. Such a shifting of this carbonyl stretching frequency is in accord with decreasing electron donation to cis-Mo(CO)₄.

A second correlation is that the ¹³C NMR chemical shift of the Mo carbonyl carbon in the heterobimetallic cage compounds moves to higher field with increasing charge on the second cage metal. These observations suggest a transmission of intracage influence from the heterometal. Examination of the X-ray data of several bimetallic cage complexes further supports this conclusion (see Part II 6.3).

6.1. Comparison of the FT-IR Spectral Data of the Mo(CO)₄ Moiety.

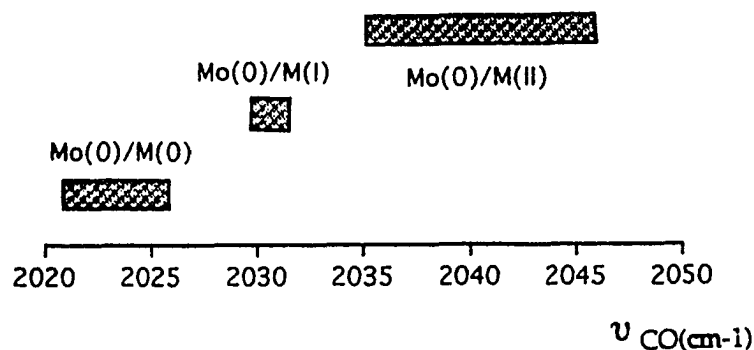
The infrared stretching frequencies for the carbonyl A₁ mode are given in Table XVII and Scheme VIII.

Table XVII. The Carbonyl Stretching Frequencies (A_1 mode) in $(CO)_4Mo[iPr_2NPO]_4ML_n$ Heterobimetallic Cage Complexes

compounds	$\nu_{CO}(cm^{-1})$ (IR)	$\nu_{CO}(cm^{-1})$ (FT-IR)	metals
14	2010	2022.8	Mo/
22	2010	2022.9	Mo/Ni(0)
1	2015	2025.8	Mo/Mo(0)
16	2009	2020.8	Mo/Cr(0)
19	2015	2029.7	Mo/Ag(I)
18	2019	2031.3	Mo/Cu(I)
12	2025	2035.1	Mo/Mo(II)
23	2025	2035.7	Mo/Ni(II)
21	2024	2036.7	Mo/Ni(II)
24	2025	2037.4	Mo/Ni(II)
20	2033	2045.1	Mo/Pt(II)
25	2034	2045.8	Mo/Pd(II)

IR: Perkin-Elmer 283B (KBr pellet). FT-IR: Nicolet MX-1 (KBr pellet).

The data in Table XVII suggest that there is indeed a correlation between the carbonyl stretching frequency of the cis-Mo(CO)₄P₂ group and the charge of the second metal in Mo-M cage complexes.



In metal carbonyl complexes, the carbonyl ligand donates its sigma electron density to an empty metal orbital while the metal returns its d electron density to the empty π^* orbital of the carbonyl by π back-bonding (Figure 45)[71].

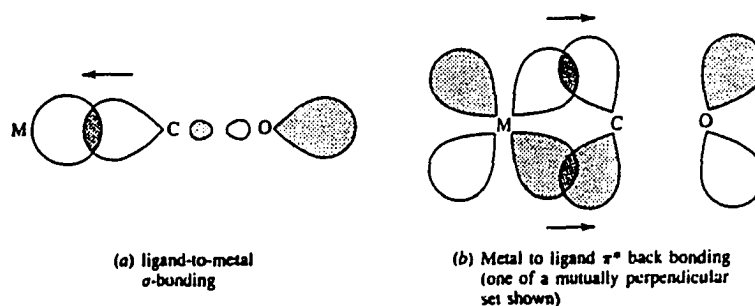


Figure 45. Orbital overlap in M-CO bonding

According to molecular orbital theory, the highest-occupied molecular orbital of CO, which acts as the electron-pair donor to a metal, is slightly antibonding between C and O, donating electron density from this orbital to the metal. This should make the C-O bond slightly stronger and raise ν_{CO} . However, the back π -bonding by donation of metal d electron density into the CO antibonding π^* orbital should significantly weaken the C-O bond[72]. Thus, the most electron-deficient carbonyl has the strongest C-O bond and gives the highest stretching frequency.

The listed infrared frequencies of these complexes indicate an intracage influence between the two metals: As the second metal increases its electron demand by increasing its formal charge, electron density flows along the

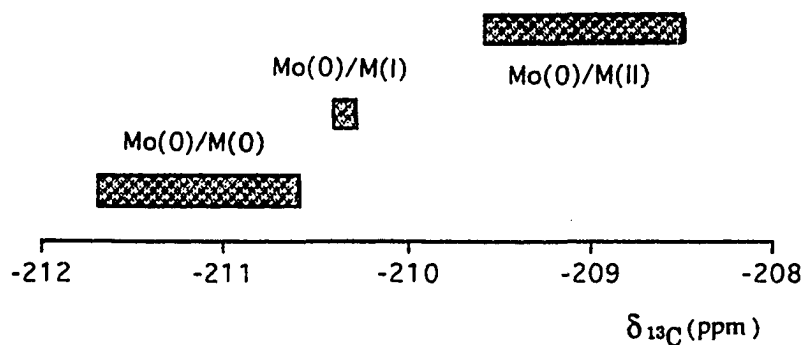
(Mo)P-O-P(M) bonds. This makes the phosphorus atoms bonded to Mo⁰ less basic, so the P → Mo donation decreases, decreasing electron density at the metal Mo⁰. As a result, the Mo → carbonyl π back-donation is also decreased; therefore, the C-O bonds are stronger, and the ν_{CO}'s are raised.

6.2. Comparison of the ¹³C NMR Chemical Shifts of the Mo(CO)₄ Moiety

The ¹³C NMR chemical shift data for the *cis*-Mo(CO)₄P₂ moiety of the complexes are presented in Table XVIII and Scheme IX. The ¹³C NMR spectra of all of these compounds were run in chloroform. The general trend observed is that ¹³C resonances of the carbonyl carbons are shifted to a higher field with increasing formal charge at the second cage metal.

Table XVIII. ¹³C NMR Chemical Shifts for the Carbonyl Resonances of the Complexes

Compounds	δ _{CO} (ppm) (average)	metals
14	212.7	Mo/
22	211.7	Mo/Ni(0)
17	211.2	Mo/Fe(0)
1	210.7	Mo/Mo(0)
16	210.6	Mo/Cr(0)
19	210.4	Mo/Ag(I)
18	210.3	Mo/Cu(I)
12	209.6	Mo/Mo(II)
20	208.6	Mo/Pt(II)
25	208.5	Mo/Pd(II)



Scheme IX

Examination of the data trend in Table XVIII again suggests that there is a transmission of intracage influence between the heterometals. Bodner^[73] and Braterman^[74] have attributed these shieldings of the carbonyl resonance to a decreasing of electron density at the metal center. They suggest that the variations in the M-CO π back bonding are chiefly responsible for the observed changes. Their hypothesis is supported by Bodner's observation that the carbonyl resonance in $(\eta^5\text{-C}_5\text{H}_5)\text{M}(\text{CO})_3$ complexes ($\text{M}=\text{Cr}^-, \text{Mn}^0, \text{Fe}^+$) is shielded with increasing positive charge^[73].

Not surprisingly, the ^{13}C NMR chemical shifts of these carbonyl carbons go to higher field as their CO stretching frequencies increase. A plot of ^{13}C NMR carbonyl chemical shifts in ppm downfield from TMS versus corresponding infrared stretching frequencies is shown in Figure 46 for 8 of the 12 known bimetallic complexes (complexes 21, 23 and 24 are paramagnetic, and the ν_{CO} value for $(\text{CO})_4\text{Mo}$ group in complex 17 is obscured by the $\text{Fe}(\text{CO})_3$ group.).

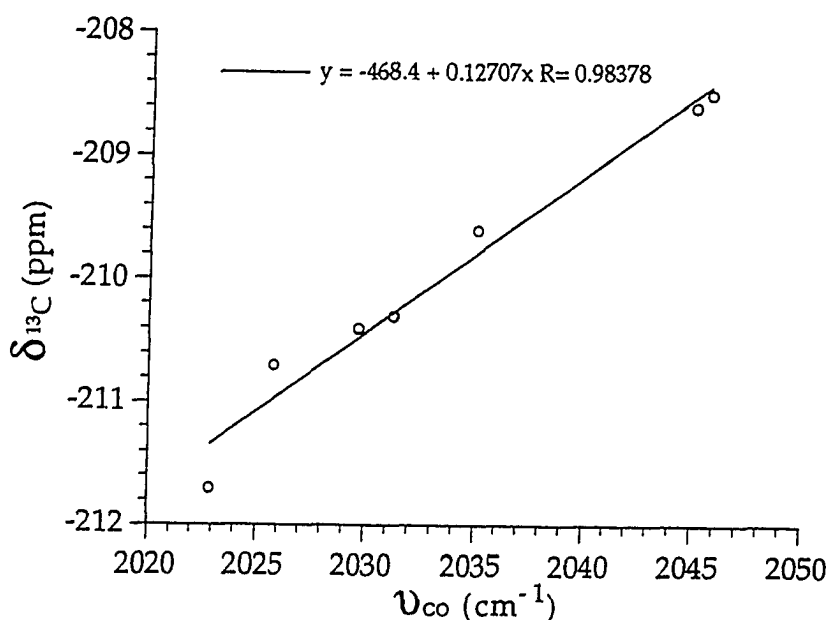


Figure 46. A correlation of the ^{13}C NMR chemical shifts vs the IR frequencies (A_1 mode) for the carbonyl groups in $\text{cis}-(\text{CO})_4\text{MoP}_2$

Similar correlations between ^{13}C NMR chemical shifts of carbonyl carbon atoms and their infrared stretching frequencies have been found for $\text{LW}(\text{CO})_5$ and $\pi\text{-CpFe}(\text{CO})_2\text{X}$ derivatives by Gansow and coworkers^[75], and for $\text{LNi}(\text{CO})_3$, $\text{LM}(\text{CO})_5$, $\text{M}=\text{Cr}$, and Mo and $(\text{C}_6\text{H}_5\text{X})\text{Cr}(\text{CO})_3$ by Bodner and coworkers^[76].

Although suppositive of intracage effects, the NMR and IR shifts we observe are relatively small and may well be sensitive to steric as well as electronic influences. A broader range of structural and spectral data are still needed to affirm this premise.

6.3. Comparison of the X-ray Structural Data of the Complexes

From the comparison of ^{13}C NMR chemical shifts and the IR stretching

frequencies of the *cis*-Mo(CO)₄P₂ vertices in the bimetallic cage complexes in Part II 6.1 and 6.2, it appears that there are interactions between the two metals within the cage.

The same conclusion can be reached from a comparison of X-ray crystallographic bond data of the representative complexes. In Table XVIII the average bond distances of Mo-P, (Mo⁰)P-O and (M)P-O bonds are listed:

Table XIX. Selected Bond Lengths (Å) for Several Complexes

compounds	Mo-P(O)	(Mo ⁰)P-O	(M)P-O
14 (Mo/)	2.512(2)	1.623(4)	1.671(1)
1 (Mo/Mo(0))	2.501(1)	1.646(4)	1.646(4)
21 (Mo/Ni(II))	2.493(4)	1.650(9)	1.633(8)
12 (Mo/Mo(II))	2.486(5)	1.66(1)	1.63(1)
25 (Mo/Pd(II))	2.485(5)	1.672(13)	1.600(12)

The most interesting differences among the complexes **14**, **1**, **21**, **12** and **25** are the P-O bond lengths. When there is only one metal (molybdenum) in complex **14**, the four coordinated P-O bond are much shorter at 1.623(4) Å than the uncoordinated P-O bonds at 1.671(4) Å. This suggests that the P-O bonding at the coordinated sites is enhanced at the expense of the latter. When a second metal is introduced into the cage, the (M)P-O bonds are significantly modified. For example, the four formerly uncoordinated P-O bonds readjust and decrease from 1.671(4) Å in **14** to 1.646(4) Å, 1.633(8) Å,

1.63(1) Å, and 1.600(12) Å in Mo⁰-Mo⁰, Mo⁰-Ni^{II}, Mo⁰-Mo^{II} and Mo⁰-Pd^{II} cages, respectively. The four P-O bonds that are bonded to the original metal Mo⁰ are lengthened at the same time. This changing of bond lengths correlates with the electron demand of the new metals introduced. These data once again support the conclusion that there is a transmission of intracage influence from the heterometal to the Mo center.

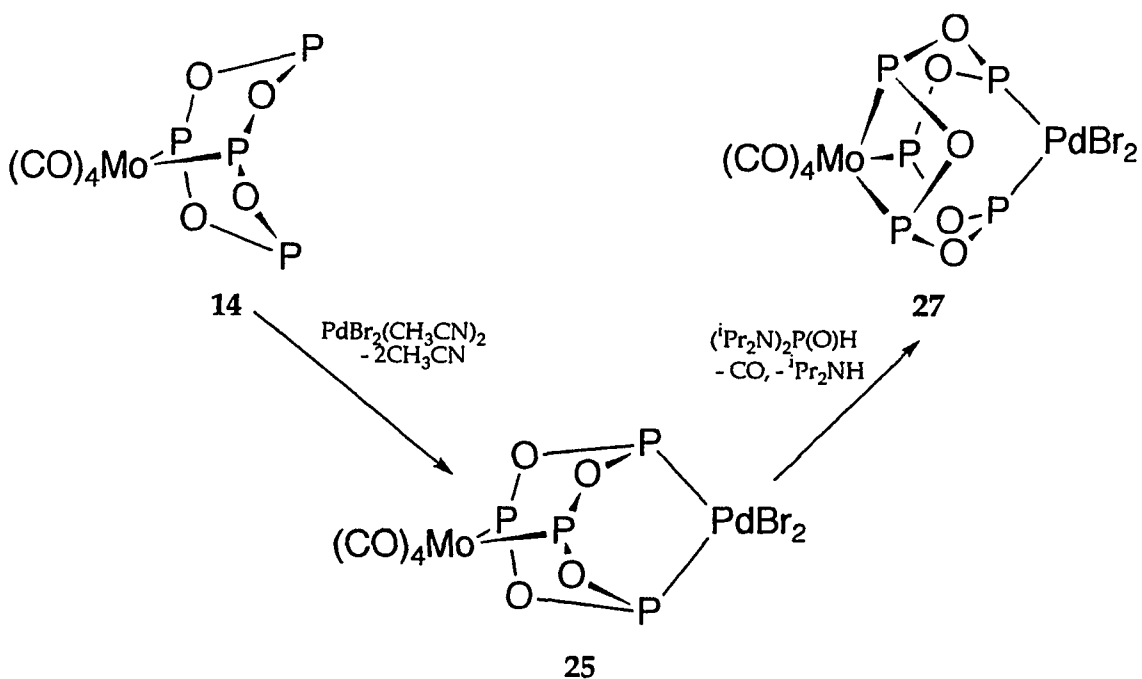
7. Expansion of the P₄O₄ Cage to a P₅O₅ Cage

While attempting to synthesize Mo/Pd heterobimetallic cage complexes from (CO)₄Mo[ⁱPr₂NPO]₄ (**14**) and PdX₂(C₆H₅CN)₂ (X=Cl, Br), it was found that not only the P₄O₄ cage complex, but also the P₅O₅ cage complex, formed depending on the halide ligand of the starting PdX₂(C₆H₅CN)₂. Reaction of PdCl₂(C₆H₅CN)₂ with complex **14** only gave a P₅O₅ cage, but PdBr₂(C₆H₅CN)₂ formed both P₄O₄ and P₅O₅ cage complexes. The Mo/PdBr₂ P₅O₅ cage could be obtained by either thermal reaction of **14** with PdBr₂(C₆H₅CN)₂ or by heating the Mo/Pd P₄O₄ cage with phosphine oxide (ⁱPr₂N)₂P(O)H. It was also found that the Mo/Pd P₅O₅ cage always formed in the company of some Mo/Mo P₄O₄ cage. In addition, when pure Mo/PdBr₂ P₄O₄ cage was heated alone, no P₅O₅ cage formed. Furthermore, pure **14** did not react with excess phosphine oxide. By the distribution of the product complexes **1** and **26**, or **1** and **27**, it can be noted that their ratios were about 1:4. This number may hint at the mechanism of this cage expansion reaction. The expansion requires an extra P-O unit, which may come from the added phosphine oxide or come from the decomposition of the MoP₄O₄ precursor.

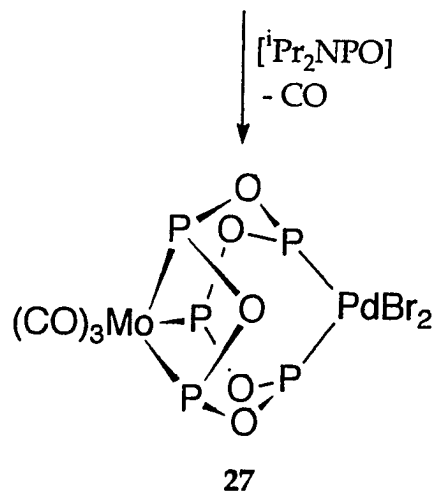
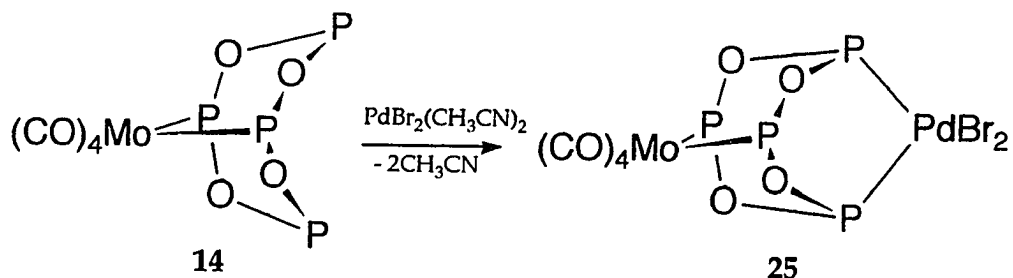
Clearly, the PdX₂ unit plays an important role: it provided the second metal vertex for forming the P₅O₅ cage and it might also assist in the decomposition of the precursor to generate new P-O units.

Three mechanisms may be involved in this expansion reaction:

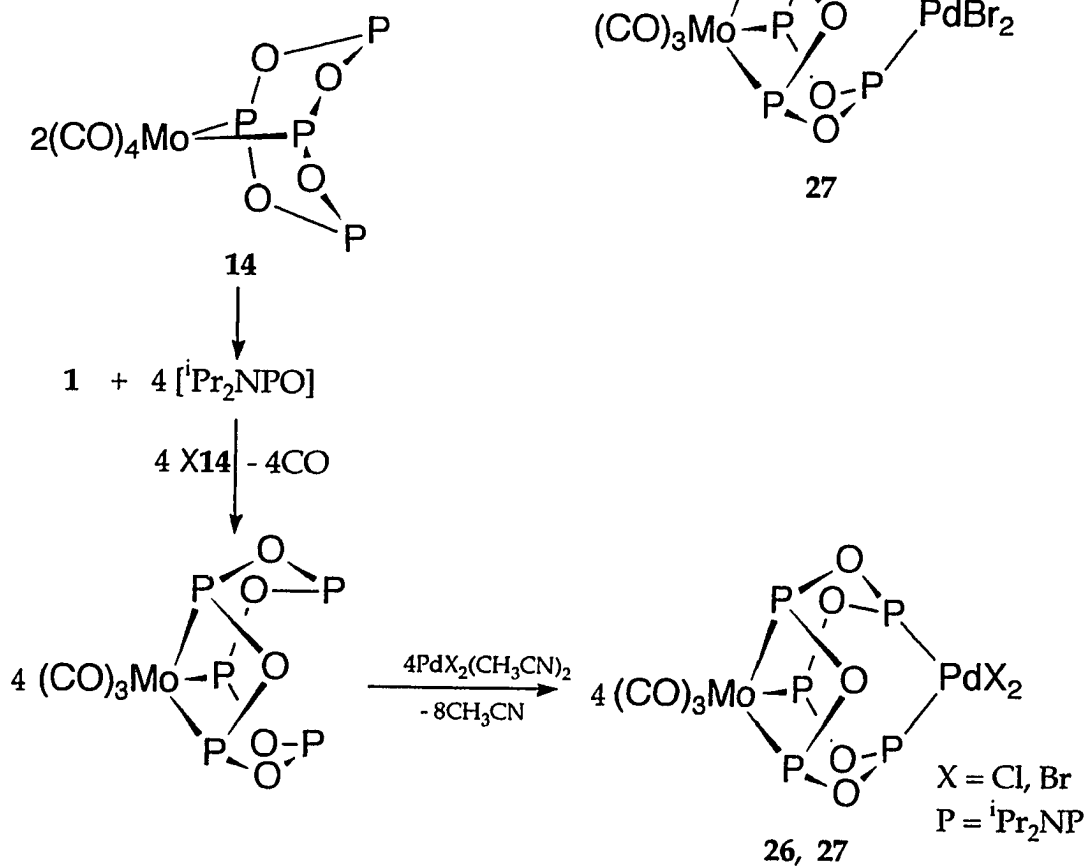
Mechanism 1



Mechanism 3



Mechanism 2



Scheme X

Mechanism 1 involves the direct thermal expansion of the Mo/PdBr₂ P₄O₄ cage to a P₅O₅ cage by incorporation of a phosphine oxide unit. Addition of (iPr₂N)₂NP(O)H to the MoP₄O₄Pd cage and loss of a CO from the cis-Mo(CO)₄ moiety and loss of iPr₂NH from phosphine oxide can lead to a Mo/PdBr₂ P₅O₅ cage complex. Mechanism 2 requires the thermal decomposition of (CO)₄Mo[iPr₂NPO]₄ and the formation of a transient [iPr₂NPO] unit along with the Mo-Mo P₄O₄ cage. Addition of the [iPr₂NPO] unit to 14 and CO loss from (CO)₄Mo can generate a monometallic P₅O₅ intermediate, (CO)₃Mo[iPr₂NPO]₅. This intermediate can be a ligand and react with PdX₂(C₆H₅CN)₂ to form the bimetallic Mo/Pd P₅O₅ cage complex. The P₅O₅ cage may also form from mechanism 3 by reaction of preformed Mo/PdBr₂ P₄O₄ cage with the similarly-liberated [iPr₂NPO] unit. Which of these is the likely mechanism remains to be determined.

Conclusions and Suggestions for Future Work

The metalla-ligand complex $(\text{CO})_4\text{Mo}[\text{iPr}_2\text{NPO}]_4$ (**14**) has been synthesized by the reaction of the mixed-valent, adamantanoid cage complex $(\text{CO})_4\text{Mo}[\text{iPr}_2\text{NPO}]_4\text{Mo}(\text{CO})_2\text{I}_2$ with sodium dimethyldithiocarbamate. X-ray structural data as well as solution NMR spectra of **14** showed that the $[\text{iPr}_2\text{NPO}]_4$ ring in this monometallic cage precursor remains in the boat-boat conformation.

This precursor behaved as a bidentate ligand, reacting with suitable metal complexes with labile ligands to provide heterobimetallic cages of the type $(\text{CO})_4\text{Mo}[\text{iPr}_2\text{NPO}]_4\text{ML}_n$ ($\text{ML}_n = \text{Cr}(\text{CO})_4, \text{Fe}(\text{CO})_3, \text{Cu}(\text{CH}_3\text{CN})_2\text{BF}_4, \text{AgNO}_3, \text{PtCl}_2, \text{NiBr}_2, \text{PdBr}_2$), and the type $(\text{CO})_3\text{Mo}[\text{iPr}_2\text{NPO}]_5\text{PdX}_2$ ($\text{X} = \text{Cl}, \text{Br}$). These heterobimetallic products were obtained in moderate to high yields and have been characterized by elemental analyses and spectral data. In addition, the structures of $(\text{CO})_4\text{Mo}[\text{iPr}_2\text{NPO}]_4\text{NiBr}_2$ (**21**) and $(\text{CO})_4\text{Mo}[\text{iPr}_2\text{NPO}]_4\text{-PdBr}_2$ (**25**) have been determined by X-ray.

X-ray structural data from **14**, **21**, **25** and complexes **1** and **12** showed that the P_4O_4 core readjusted to the electronic demands of the new metal centers, and comparison of the FT-IR and NMR spectral properties of the conserved $\text{cis-Mo}(\text{CO})_4\text{P}_2$ moiety also suggested a transmission of intracage influence between the heterometals.

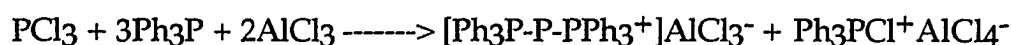
The paramagnetic heterobimetallic cage complex $(\text{CO})_4\text{Mo-}$

$[\text{iPr}_2\text{NPO}]_4\text{NiBr}_2$ reacted with $\text{Fe}(\text{CO})_5$, leading to reduction of Ni(II) to Ni(0) and the carbonylation of the nickel vertex to form a diamagnetic cage complex $(\text{CO})_4\text{Mo}[\text{iPr}_2\text{NPO}]_4\text{Ni}(\text{CO})_2$ (**22**). Chlorination and iodination of complex **22** resulted in preferential halogenation at the nickel site.

Primary alcohols reacted with $(\text{CO})_4\text{Mo}[\text{iPr}_2\text{NPO}]_4$ by nucleophilic attack, leading to cleavage of a single P-O-P bond and formation of a monocyclic product.

Use of the metallo-ligand $(\text{CO})_4\text{Mo}[\text{iPr}_2\text{NPO}]_4$ as a nucleophile towards main group electrophiles like S, SnCl_2 , SnCl_4 have been studied in preliminary work. Although the products could not be isolated at this time, the results were encouraging. Reactions of $(\text{CO})_4\text{Mo}[\text{iPr}_2\text{NPO}]_4$ with main group reagents such as SiCl_4 , MeSiCl_3 may also give very interesting results.

Triphenylphosphine and aluminum chlorides reacting together with phosphorus chloride can form a chlorophosphonium and a triphosphenium ion^[77]:



It may be possible to bond the two uncoordinated phosphorus atoms of complex **14** together the same way to form the analogous cage triphosphenium cation. This reaction was tried using anhydrous SnCl_2 with PCl_3 . Though no product was isolated, the spectral results were encouraging.

Heterobimetallic cage products can be used in CO substitution and redox

reactions. Reduction using NaBH₄/MeOH may give hydride complexes; halogenation of (CO)₄Mo[iPr₂NPO]₄NiX₂ and (CO)_nMo[iPr₂NPO]_mPdX₂ (n=3, 4; m=4, 5) cages may give Mo(II)/M(II) cage products.

** It is of interest to compare the P-Mo-P chelate bite angles of the cage complexes with other known diphosphine complexes. The bond angles for several cis-Mo(CO)₄L₂ complexes are presented in the following table:

cage complexes	P-Mo-P (°)	six-membered ring complexes	P-Mo-P (°)
cis-Mo(CO) ₄ [iPr ₂ NPO] ₄	76.0 ^a	cis-Mo(CO) ₄ [(Ph ₂ PO) ₂ P(O)Me]	91.5 ^b
cis-Mo(CO) ₄ [PhPO] ₄	77.7 ^a	cis-Mo(CO) ₄ [(Ph ₂ PO) ₂ P(O)R] (R=C ₆ H ₄ -P-OMe)	91.3 ^b
bis(diphosphino) Complexes	P-Mo-P (°)	Five-membered ring complexes	P-Mo-P (°)
cis-Mo(CO) ₄ (PMe ₃) ₂	97.5 ^c	cis-Mo(CO) ₄ [Me ₂ PCHF ₂ CF ₂ PMe ₂]	82.0 ^d
cis-Mo(CO) ₄ (PBu ₃) ₂	99.3 ^c	cis-Mo(CO) ₄ (Ph ₂ P-P(O)Ph-OPPh ₂)	82.3 ^e

As shown in the table, the P-Mo-P bond angles of the cage complexes are constrained to be substantially less than the "normal" value of 90°. The angles are significantly smaller than for the monocyclic six-membered chelate ring complexes. They are even smaller than those for the five-membered chelate ring compounds. The effect of the polycyclic cage structure is therefore clearly observed.

a) Wong, E. H.; Turnbull, M. M.; Hutchinson, K. D.; Valdez, C.; Gabe, E. J.; Lee, F.L.; LePage, Y. J. *Am. Chem. Soc.* **1988**, 110, 8422.

b) Gray, G. M.; Zhang, Y. J. *Crystallogr. Spectrosc. Res.* **1993**, 23, 909.

c) Cotton, F. A.; Darensbourg, D. J.; Klein, S. *Inorg. Chem.* **1982**, 21, 2661.

d) Nowell, I. W.; Rettig, S.; Trotter, J. *J. Chem. Soc. Dalton Trans.* **1972**, 2381.

e) Wong, E. H.; Bradley, F. C.; Gabe, E. J. *J. Organomet. Chem.* **1983**, 244, 235.

Experimental section

General Procedure: All manipulations were carried out using standard Schlenck techniques under an atmosphere of prepurified nitrogen. Chemical reagents were commercial products and were used without further purification. Hexane and methylene chloride were distilled from CaH_2 . Reagent grade toluene was dried over Na and freshly distilled before use. Norbornadiene, diisopropylamine, ethyl acetate, CHCl_3 , MeOH, EtOH, $\text{NaS}_2\text{CN}(\text{Me})_2$, and acetonitrile were purchased from Aldrich Chemical Co. and used without further purification. Alumina (Aldrich Chemical Co., Brockmann, I, neutral) was used as received. The cage complex $(\text{CO})_4\text{Mo}(\text{iPr}_2\text{NPO})_4\text{Mo}(\text{CO})_4$ ^[8] (1) and $(\text{CO})_4\text{Mo}(\text{iPr}_2\text{NPO})_4\text{Mo}(\text{CO})_2\text{I}_2$ ^[9] (12) were prepared according to previously reported methods. $\text{Cr}(\text{CO})_4(\text{NBD})$ ^[78], $(\text{AgNO}_3)_2(\text{NBD})$ ^[79], $\text{NiBr}_2(\text{DME})$ ^[80], $\text{PdCl}_2(\text{C}_6\text{H}_5\text{CN})_2$ ^[81], $\text{PdBr}_2(\text{C}_6\text{H}_5\text{CN})_2$ ^[82], $\text{PtCl}_2(\text{NBD})$ ^[83] and $\text{Cu}(\text{CH}_3\text{CN})_4\text{BF}_4$ ^[84] $\text{Ni}(\text{COD})_2$ ^[85] were prepared according to the literature. ^1H , ^{13}C and ^{31}P NMR spectra were recorded on JEOL FX 90Q or Bruker AM360 FT-NMR spectrometers. ^1H and ^{13}C shifts were referenced to internal TMS, ^{31}P shifts were referenced to external 85% H_3PO_4 . Spectra were obtained in CDCl_3 solution unless otherwise noted. Infrared spectra were recorded on a Perkin-Elmer 283B or Nicolet MX-1 FT-IR Spectrometer using KBr disks. Elemental analyses were performed at the University Instrumentation Center using a Perkin-Elmer 240b or Perkin-Elmer 2400 elemental analyzer.

X-ray crystal structures were determined by Dr. Arnold L. Rheingold and Beth E. Owens-Waltermire, Department of Chemistry, University of Delaware, Newark, Delaware.

(CO)₄Mo[iPr₂NPO]₄ (14) and (CO)₄Mo[iPr₂NPO]₄Mo(CO)₂(SCNMe₂)₂ (13): A 250 mL round bottomed flask with a magnetic stirbar was charged with 5.000 g of complex **12** (4.158 mM) and 1.252 g (8.400 mM) of sodium dimethyl-dithiocarbamate. A 100 mL amount of CH₂Cl₂ was added to dissolve the mixed-valent complex, resulting in a burgundy red suspension. After the mixture had been stirred for three hours at room temperature, a red suspension solution had formed. TLC (15% ethyl acetate in hexane, neutral alumina) revealed a colorless and a yellow component. Filtering yielded a red-purple solid identified as [(CO)₂Mo(S₂CNMe₃)₂] (IR, CHN analysis) and a red solution. Evaporation of the filtrate gave a red solid which was allowed to stand at room temperature for one week. This residue was then extracted three times with hexane to give an orange-yellow extract solution. After evaporation, the residue was chromatographed on an alumina column using 15% ethyl acetate in hexane as the eluant. The colorless complex **14** was the first to elute and isolated in 60% yield (1.950 g). Next to elute was the unstable orange complex **13** (0.870 g). Elemental analyses (calculated/observed for C₂₈H₅₆MoN₄O₈P₄ **14**): C% 42.21/42.00 , H% 7.10/7.10, N% 7.03/6.91. Elemental analyses (calculated/observed for C₃₄H₆₈Mo₂N₆O₈P₄S₂ **13**): C% 36.36/36.37, H% 5.76/6.20, N% 7.10/6.73.

(CO)₄Mo[iPr₂NPO]₄Cr(CO)₄ (16): A 100 mL round bottomed flask with a magnetic stirbar was charged with 1.5210 g of compound **14** (1.9091 mM) and

0.9176 g (3.8182 mM) $\text{Cr}(\text{CO})_4(\text{NBD})$. Heptane (40 mL) was added to the mixture resulting in a golden-yellow solution. The mixture was refluxed for three days; a yellow suspension was obtained. After evaporation of the volatiles under reduced pressure, a bright yellow residue was obtained. The residue was washed three times with 10 mL hexane to give a light yellow solid. This was chromatographed on alumina using 5% ethyl acetate in hexane as the eluant to give a colorless solution. This solution was evaporated to dryness to give a white solid complex **16** (0.5755 g, 35%). Elemental analyses (calculated/observed for $\text{C}_{32}\text{H}_{56}\text{MoN}_4\text{O}_{12}\text{P}_4\text{Cr}$ **16**): C% 40.01/40.31, H% 5.88/6.06, N% 5.83/5.74.

$(\text{CO})_4\text{Mo}[\text{iPr}_2\text{NPO}]_4\text{Fe}(\text{CO})_3$ (**17**): A 100 mL round bottomed flask with a magnetic stirbar was charged with 2.83 g of compound **14** (3.55 mM) and 1.75 g (9.59 mM) $\text{Fe}_2(\text{CO})_9$. Hexane (60 mL) was added and the mixture was stirred under N_2 in reflux for 39 hours. A black green residue was obtained when the mixture was dried under reduced pressure. The residue was chromatographed on an alumina column using 2% ethyl acetate in hexane eluant to give 0.9510 g (28%) of **17** as a white solid. Elemental analyses (calculated/observed for $\text{C}_{31}\text{H}_{56}\text{MoN}_4\text{O}_{11}\text{P}_4\text{Fe}$ **17**): C% 39.76/39.50, H% 6.03/6.30, N% 5.98/6.04.

$(\text{CO})_4\text{Mo}[\text{iPr}_2\text{NPO}]_4\text{Cu}(\text{CH}_3\text{CN})_2(\text{BF}_4)$ (**18**): A 50 mL round bottomed flask with a magnetic stirbar was charged with 0.1170 g of compound **14** (0.1468 mM) and 0.0231 g (0.0734 mM) $\text{Cu}(\text{CH}_3\text{CN})_4(\text{BF}_4)$. Hexane (8 mL) and CH_2Cl_2 (4 mL) were added to the mixture resulting in a colorless solution. The mixture was stirred under N_2 in refluxing solvent for one hour. After

evaporation of most of the CH_2Cl_2 , the reaction suspension was refluxed for another 3 hours. Filtration gave a white solid, which was washed with hexane and dried to give 0.0720 g (95.3% based on Cu) of **18**. Elemental analyses (calculated/observed for $\text{C}_{32}\text{H}_{62}\text{MoN}_6\text{O}_8\text{P}_4\text{Cu}$): C% 37.35/37.10, H% 6.07/6.16, N% 8.16/7.55.

(CO)₄Mo[iPr₂NPO]₄AgNO₃ (19): A 50 mL round bottomed flask with a magnetic stirbar was charged with 0.4400 g of compound **14** (0.5522 mM) and 0.0592 g $\text{NBD}(\text{AgNO}_3)_2$ (0.276 mM Ag) and 20 mL hexane. The white suspension solution was stirred at room temperature in the absence of light. After one hour, the white suspension was filtered and the solid washed with hexane and dried to give 0.143 g (54%) of complex **19**. Due to the instability of the product, no satisfactory elemental analyses were obtained.

(CO)₄Mo[iPr₂NPO]₄PtCl₂(20): A 50 mL round bottomed flask with a stirbar was charged with 0.3059 g of compound **14** (0.3839 mM) and 0.1375 g (0.3839 mM) $\text{PtCl}_2(\text{NBD})$. Toluene (10 mL) was added to the mixture resulting in a suspension [$\text{PtCl}_2(\text{NBD})$ was not very soluble in toluene]. The suspension was stirred at 60 °C for 4 hours. After cooling and filtration, a white solid and a clear light yellow filtrate were obtained. The solid was washed with toluene, then with hexane, and dried to give 0.3585 g (88%) of complex **20**. Workup of the light yellow solution gave more complex **20** (0.0490 g, 12%). Elemental analyses (calculated/observed for $\text{C}_{28}\text{H}_{56}\text{MoN}_4\text{O}_8\text{P}_4\text{PtCl}_2$): C% 31.65/31.94, H% 5.31/5.45, N% 5.27/5.36.

(CO)₄Mo[iPr₂NPO]₄NiBr₂(21): A 50 mL round bottomed flask with a

magnetic stirbar was charged with 1.20 g of compound **14** (1.51 mM) and 0.40 g (1.51 mM) NiBr₂(DME). Hexane (10 mL) was added to the mixture. The mixture was refluxed for 5 hours to give a brown-red suspension. This was concentrated to about 5 mL, and the red crystalline precipitate was filtered, washed twice with 5 mL of cold hexane, and dried to give 1.23 g. (80%) of complex **21**. X-ray-quality crystals were grown from a hot hexane solution. Elemental analyses [calculated/observed for C₂₈H₅₆MoN₄O₈P₄-NiBr₂·0.7(hexane)]: C% 35.95/35.92, H% 6.17/6.24, N% 5.21/5.31.

(CO)₄Mo[ⁱPr₂NPO]₄Ni(CO)₂ (**22**): A 50 mL round bottomed flask with a magnetic stirbar was charged with 0.64 g of compound **21** (0.63 mM); 10 mL hexane and 0.5 mL of Fe(CO)₅ were added to give a red suspension. This mixture was stirred in refluxing hexane for one hour to give a yellow suspension. Upon cooling the suspension to room temperature, a light yellow clear solution with a yellow precipitate was formed. The top clear solution was removed by pipette to another flask and evaporated to dryness to give a light yellow residue. The residue was chromatographed on alumina using 5% ethyl acetate in hexane to afford a clear colorless solution from which a white complex **22** was obtained (0.49 g, 85%). Elemental analyses (calculated/observed for C₃₀H₅₆MoN₄O₁₀P₄Ni): C% 39.53/39.40 , H% 6.19/6.23, N% 6.15/6.05.

(CO)₄Mo[ⁱPr₂NPO]₄NiCl₂(**23**): A 50 mL round bottomed flask with a stirbar was charged with 0.320 g of complex **22** (0.3511 mM) and 20.0 mL of hexane. The solution was cooled to -78°C, and a solution of 0.50 mL of SO₂Cl₂ in 40.0 mL of CH₂Cl₂ was made; 3.18 mL of this was added dropwise

to the hexane solution of **22** (Ni : Cl₂ = 1 : 1.1). The colorless solution immediately changed to yellow, and within 5 minutes, an orange suspension then formed. The reaction mixture was concentrated to half its volume. The top clear yellow solution was removed by a pipet, and dried to give 0.2730 g (84%) of complex **23** as an orange solid. Elemental Analyses (calculated/observed for C₂₈H₅₆N₄P₄MoNiO₈Cl₂): C% 36.31/36.54, H% 6.09/6.50, N% 6.05/5.54.

Synthesis of (CO)₄Mo[iPr₂NPO]₄Ni(CO)₂ from (CO)₄Mo[iPr₂NPO]₄-NiCl₂: A 50 mL round bottomed flask with a magnetic stirbar was charged with 0.2040 g of complex **23**, 20.0 mL of hexane and 0.5 mL of Fe(CO)₅. The solution was refluxed for 1 hour to give a yellow suspension. After filtration and evaporation of the volatiles from the filtrate, the residue was chromatographed on alumina using 5% ethyl acetate in hexane to give a colorless solution from which white solid complex **22** was obtained (0.1650 g, 80%).

(CO)₄Mo[iPr₂NPO]₄NiI₂(24) : A 25 mL round bottomed flask with a magnetic stirbar was charged with 0.1542 g of complex **22** (0.1691 mM) and 5 mL of CH₂Cl₂. A solution of 0.472 g (0.186 mM) of iodine in 2.0 mL of CH₂Cl₂ was added and the mixture was stirred at room temperature for 2 hours to give a deep red solution. This was evaporated to dryness under reduced pressure to give a dark red residue. The solid was washed with 2x1mL of CH₃CN and dried to give 0.1425 g (76%) of complex **24**. Satisfactory elemental analyses were not obtained due to its instability.

Synthesis of $(\text{CO})_4\text{Mo}[\text{iPr}_2\text{NPO}]_4\text{Ni}(\text{CO})_2$ (22) from $(\text{CO})_4\text{Mo}[\text{iPr}_2\text{NPO}]_4\text{NiI}_2$ (24): A 25 mL round bottomed flask with a magnetic stirbar was charged with 0.1425 g of complex 24, 8.0 mL of hexane and 0.5 mL of $\text{Fe}(\text{CO})_5$. The mixture was stirred at room temperature for 2 hour to give a yellow suspension. A yellow residue was obtained after filtration and evaporation of the volatiles from the filtrate. The solid was chromatographed on alumina using 5% ethyl acetate in hexane to give a colorless solution from which white solid complex 22 was obtained (0.0935 g, 80%).

$(\text{CO})_4\text{Mo}[\text{iPr}_2\text{NPO}]_4\text{PdBr}_2$ (25): A 50 mL round bottomed flask with a magnetic stirbar was charged with 0.4270 g of complex 14 (0.5359 mM) and 0.2513 g $\text{PdBr}_2(\text{C}_6\text{H}_5\text{CN})_2$ (0.4872 mM, P's : Pd = 4.4 : 1). Toluene (20 mL) was added to the mixture and the resulting solution was stirred at 70°C for 16 hour. After cooling and removal of the volatiles, a yellow-brown residue solid was obtained. This was washed three times with 5 mL hexane to give 0.4490 g of a greenish yellow solid. The solid was dissolve in 5ml of CHCl_3 , the solution filtered, and the clear yellow filtrate evaporated to give 0.4320 g of complex 25 (83% based on Pd). X-ray-quality crystals were obtained upon cooling and slow evaporation of a hot toluene solution. Elemental Analyses (calculated/observed for $\text{C}_{28}\text{H}_{56}\text{N}_4\text{P}_4\text{MoPdO}_8\text{Br}_2$): C% 31.64/31.71, H% 5.31/5.32, N% 5.27/5.18.

$(\text{CO})_3\text{Mo}[\text{iPr}_2\text{NPO}]_5\text{PdCl}_2$ (26): A 50 mL round bottomed flask with a stirbar was charged with 0.7120 g of complex 14 (0.8936 mM) and 0.2741 g $\text{PdCl}_2(\text{C}_6\text{H}_5\text{CN})_2$ (P's : Pd = 5 : 1). Toluene (20 mL) was added to the mixture

and the resulting solution was stirred at 70 °C for 66 hour. The red-brown suspension was cooled to room temperature and filtered to give a gray yellow solid (0.4210 g) and a red-brown solution. The solid was dissolved in 8 mL of CHCl₃, the solution filtered, and the clear yellow filtrate allowed to evaporate slowly. A yellow needle crystalline solid was obtained. The solid was collected by filtration and dried to give 0.3452 g of complex 26. The red-brown solution was evaporated to dryness and the residue washed three times with 2 mL of acetone to give a yellow solid which was a 2:1 mixture of 26 and complex 1 according to the ³¹P NMR spectrum. This mixture was washed three times with 1 mL portions of hexane to give additional 26, for a combined yield of 0.504 g (52% based on Pd). Elemental Analyses (calculated/observed for C₃₃H₇₀N₅P₅MoPdO₈Cl₂): C% 36.26/36.27, H% 6.41/6.48, N% 6.46/6.10.

(CO)₃Mo[ⁱPr₂NPO]₅PdBr₂ (27): A 50 mL round bottomed flask with a magnetic stirbar was charged with 0.6840 g of complex 14 (0.8585 mM) and 0.3239 g PdBr₂(C₆H₅CN)₂ (P's : Pd = 5 : 1). Toluene (20 mL) was added to the mixture and the resulting solution was stirred at 70 °C for 72 hour. The yellow-brown suspension was cooled to room temperature and filtered to give a grayish yellow solid and a clear brown solution. The solid was dissolve in 4 mL of CHCl₃, the solution filtered, and the filtrate allowed to evaporate slowly. A yellow crystalline complex 27 formed which was collected and dried (0.3598 g). The brown solution was evaporated to give a brown residue, which was found to be a 1 : 2 : 4 mixture of complexes (CO)₄Mo[ⁱPr₂NPO]₄Mo(CO)₄, 25, and 27 according to the ³¹P NMR. The residue was washed twice with 5 mL of a 1:1 mixture of acetone and hexane,

followed by 2x2 mL hexane to give 0.1244 g of 27. The combined yield was 48% based on Pd. Elemental Analyses (calculated/observed for $C_{33}H_{70}N_5P_5MoPdO_8Br_2$): C% 33.53/33.88, H% 5.97/6.33, N% 5.93/5.83.

$(CO)_4Mo(iPr_2NPO)_2(iPr_2NPOMe)(iPr_2NP(O)H)$ (28):

Method A [From complex 12 $(CO)_4Mo(iPr_2NPO)_4Mo(CO)_2I_2$]: A 50 mL round bottomed flask with a stirbar was charged with 0.4025 g of complex 12 (0.3347 mM) and 0.0959 g (0.669 mM) sodium dimerhydithiocarbamate. CH_2Cl_2 (20 mL) was added to dissolve 12; the ligand was suspended in the burgundy red mixture. Addition of 10 mL of MeOH gave a clear red solution, which was stirred for three hours. The resulted red suspension was filtered to remove $(CO)_2Mo(S_2CNMe_2)_2$ (0.0834 g) and the filtrate was evaporated to give a brown red residue. This was extracted with 20 mL of hexane, and the extract was evaporated to give a white solid complex 28 (0.2104 g, 70%).

Method B [From complex 14 $(CO)_4Mo(iPr_2NPO)_4$]: A 50 mL round bottomed flask with a magnetic stirbar was charged with 0.3390 g of complex 14 (0.4255 mM). MeOH (6 mL) and 4 mL of hexane were added into the flask to give a clear colorless solution. Which was stirred under refluxing for 9 hours to give a clear light yellow solution. After evaporation of the solution to dryness, a very light yellow solid was obtained. A white suspension was formed after adding 5 mL of MeOH to the filtrate, which was filtered to give a white solid. This was washed twice with 1 mL portions of cold hexane and dried to yield 0.2644 g (75%) of complex 28. X-ray quality flake crystals were obtained by recrystallization from hot hexane. Elemental analysis (calculated/observed for $C_{29}H_{60}O_9P_4N_4Mo$): C% 42.02/41.74, H% 7.31/7.62, N% 6.76/6.77.

(CO)₄Mo[(ⁱPr₂NPO)₂(ⁱPr₂NPOEt){ⁱPr₂NP(O)H}] (29): A 25 mL round bottomed flask with a magnetic stirbar was charged with 0.6950 g of complex **14** (0.8723 mM), 10.0 mL of absolute EtOH and 4.0 mL of hexane. After being refluxed for 24 hours, the light orange solution was cooled and concentrated to about 5 mL to give a suspension which was filtered to give a white solid (0.100 g, identified as unreacted **14**) and a light orange filtrate. Addition of 4 mL of EtOH to the light orange filtrate led to the precipitation of a white solid which was filtered, washed twice with 2 mL portions of EtOH and dried to give 0.4521 g (72% based on reacted **14**) of complex **29**. Elemental Analyses (calculated/observed for C₃₀H₆₂N₄P₄MoO₉): C% 42.75/42.59, H% 7.41/7.64, N% 6.65/6.51.

LIST OF REFERENCES

[1] See for examples: (a) Ziegler, K.; Holzkamp, H.; Breil, H.; Martin, H. *Angew. Chem.* **1955**, 67, 541. (b) Natta, G.; *Polymer Sci.* **1955**, 16, 143. (c) Young, J. F.; Osborn, J. A.; Jardine, F. H.; Wilkinson, G. J. *Chem. Soc., Chem. Comm.* **1965**, 131. (d) Kagan, H. B.; Dang, T. P. *J. Am. Chem. Soc.* **1972**, 94, 6429.

[2] See for examples: (a) DuBois, D. L.; Meek, D. W. *Inorg. Chim. Acta* **1976**, 19, L29. (b) Niewahner, J.; Meek, D. W. *Inorg. Chim. Acta* **1982**, 64, L123. (c) Letts, J. B.; Mazanec, T. J.; Meek, D. W. *J. Am. Chem. Soc.* **1982**, 104, 3898. (d) Hughes, O. R.; Young, D. A. *J. Am. Chem. Soc.* **1982**, 103, 6636. (e) Jia, G. C.; Meek, D. W. *Inorg. Chem.* **1991**, 30, 1953; *Organometallics*, **1991**, 10, 1444.

[3] Balch, A. L. Homogeneous Catalysis with Metal Phosphine Complexes; Plenum Press: New York, **1983**, p.167.

[4] Wong, E. H.; Turnbull, M. M.; Gabe, E. J.; Lee, F. L.; Le Page, Y. J. *Chem. Soc., Chem. Commun.* **1983**, 776.

[5] Nifant'ev, E. E.; Koroteev, M. P.; Ivanov, N. L.; Gudkova, I. P.; Predvoditelev, D. A. *Dokl. Chem.. (Engl. Transl.)* **1967**, 173, 398.

[6] Niecke, E.; Zorn, H.; Krebs, B.; Henkel, G. *Angew. Chem., Int. Ed. Engl.* **1980**, 19, 709.

[7] Chasar, D. W.; Fackler, J. P.; Mazany, A. M.; Komoroski, R. A.; Kroenke, W. J. *J. Am. Chem. Soc.* **1986**, 108, 5956; *J. Am. Chem. Soc.* **1987**, 109, 5690.

[8] Wong, E. H.; Turnbull, M. M.; Hutchinson, K. D.; Valdez, C.; Gabe, E. J.; Lee, F. L.; LePage, Y. J. *Am. Chem. Soc.* **1988**, 110, 8422.

[9] Turnbull, M. M.; Valdez, C.; Wong, E. H.; Gabe, E. J.; Lee, F. L. *Inorg. Chem.* **1992**, 31, 208.

[10] Wong, E. H.; Prasad, L.; Gabe, E. J.; Bradley, F. C. *J. Organomet. Chem.* **1982**, 236, 321.

[11] Wong, E. H.; Gabe, E. J.; Charland, J. P. *J. Chem. Soc., Chem. Commun.* **1988**, 1632.

[12] Wong, E. H.; Gabe, E. J.; Lee, F. L. *J. Chem. Soc., Chem. Commun.* **1989**, 1236.

[13] Wong, E. H.; Sun, X. Y.; Gabe, E. J.; Lee, F. L.; Charland, J. P.

Organometallics, 1991, 10, 3010.

[14] Kepert, D. L. *Inorganic Stereochemistry*; Springer Verlag: New York, 1982, p.130.

[15] Colton, R.; Kevekordes, J. *Aust. J. Chem.* 1982, 35, 895.

[16] Colton, R. *Coord. Chem. Rev.* 1971, 6, 269.

[17] Bradley, F. C.; Wong, E. H.; Gabe, E. J.; Lee, F. L.; LePage, Y. *Polyhedron* 1987, 5, 1103.

[18] Colton, R. *Aust. J. Chem.* 1968, 21, 15, and 1968, 21, 1427.

[19] Abrahamson, H. B.; Freeman, M. L.; Hussain, M. B.; Van der Helm, D. *Inorg. Chem.* 1984, 23, 2286.

[20] See for example: (a) Howell, J. A. S.; Burkinshaw, P. M. *Chem. Rev.* 1983, 83, 557. (b) Atwood, J. D.; Wovkulich, M. J.; Sonnenberger, D. C. *Acc. Chem. Res.* 1983, 16, 350. (c) Poliakoff, M.; Weitz, E. *Adv. Organomet. Chem.* 1986, 25, 277.

[21] See for example: (a) Dobson, G. R.; Houk, L. W. *Inorg. Chim. Acta* 1967, 1, 287. (b) Faber, G. C.; Dobson, G. R. *Inorg. Chim. Acta* 1968, 2, 479. (c) Dobson, G. R.; Rettenmaier, A. J. *Inorg. Chim. Acta* 1972, 6, 507. (d) Dobson, G. R.; Asali, K. A.; Marshall, J. L.; McDaniel, C. R., Jr. *J. Am. Chem. Soc.* 1977, 99, 8100. (e) Dobson, G. R.; Asali, K. A. *Inorg. Chem.* 1981, 20, 3563. (f) Isaacs, E. E.; Graham, W. A. G. *Inorg. Chem.* 1975, 14, 2560. (g) Cohen, M. A.; Brown, T. L. *Inorg. Chem.* 1976, 15, 1417.

[22] Gorenstein, D. G. *P-31 NMR: Principles and applications* ; Academic Press: Orlando, 1984, Chapter 1, Chapter 2.

[23] Verkade, J. G.; Quin, L. D. *P-31 NMR Spectroscopy in Stereochemical Analysis*; VCH: New York, 1987, Chapter 8.

[24] Verkade, J. G.; Quin, L. D. *P-31 NMR Spectroscopy in Stereochemical Analysis*; VCH: New York, 1987, Chapter 16, Chapter 17.

[25] Pregosin, P. S.; Kunz, R. W. *31P and 13C NMR of Transition Metal Phosphine Complexes*; Springer-Verlag: Berlin, 1979. p. 46, pp 115-123.

[26] (a) Darensbourg, M.Y.; Darensbourg, D.J. *J.Chem. Educ.*, 1970, 47, 33. (b) Cotton, F. A. *Chemical Application of Group Theory* , 2nd Edition; Wiley-Interscience: New York, 1971.

[27] Nassimbeni, L. R. *Inorg. Nucl. Chem. Lett.* 1971, 7, 909.

- [28] Mais, R. H. B.; Owston, P. G.; Thompson, D. T. *J. Chem. Soc. A* **1967**, 1735.
- [29] Adams, R. D.; Collins, D. M.; Cotton, F. A. *Inorg. Chem.* **1974**, 13, 1086.
- [30] Klingert, B.; Werner, H. J. *Organomet. Chem.* **1983**, 252, C47.
- [31] Newton, M. G.; King, R. B.; Chang, M.; Gimeno, J. *J. Am. Chem. Soc.* **1978**, 100, 1632.
- [32] Corbridge, D. E. C. Phosphorus: An Outline of its Chemistry, Biochemistry, and Technology, 3rd ed.; Elsevier: Amsterdam, **1985**; Chapter 1.
- [33] Petersen, J. L.; Stewart, R. P. *Inorg. Chem.* **1980**, 19, 186. Carty, A. J.; Maclaughlin, S. A.; Taylor, N. J. *J. Organomet. Chem.* **1981**, 204, C27.
- [34] Pregosin, P. S.; Kunz, R. W. 31P and 13C NMR of Transition Metal Phosphine Complexes; Springer-Verlag: Berlin, **1979**, pp 49-50.
- [35] Abraham, R. J.; Fisher, J.; Loftus, P. Introduction to NMR Spectroscopy; John Wiley & Sons: New York, **1988**, Chapter 6.
- [36] Tolman, C. A. *Chem. Rev.* **1977**, 77, 313.
- [37] Cotton, F. A. *Inorg. Chem.* **1964**, 3, 702.
- [38] Tolman, C. A. *J. Am. Chem. Soc.* **1970**, 92, 2956.
- [39] Tolman, C. A. *J. Am. Chem. Soc.* **1970**, 92, 2953.
- [40] Bartik, T.; Himmler, T.; Schulte, H. G.; Seevogel, K. *J. Organomet. Chem.* **1984**, 272, 29.
- [41] Gilmore, C. J. *J. Appl. Cryst.* **1984**, 17, 42.
- [42] (a) Bruce, M. I. *J. Organomet. Chem.* **1982**, 242, 147. *J. Organomet. Chem.* **1985**, 283, 339. (b) Geoffroy, G. L.; Roberts, D. A. in *Comprehensive Organometallic Chemistry*; Wilkinson, G., Stone, F. G. A., E. W., Eds.; Pergamon: Oxford, England, **1982**; vol.6, Chapter 40. (c) Rosseenberg, S.; Whittle, R. R.; Geoffroy, G. L. *J. Am. Chem. Soc.* **1984**, 106, 5934.
- [43] See for examples: (a) Casey, C. P.; Bullock, R. M.; Nief, F. *J. Am. Chem. Soc.* **1983**, 105, 7574. (b) Casey, C. P.; Jordan, R. F.; Rheingold A. L. *J. Am. Chem. Soc.* **1983**, 105, 665. (c) Casey, C. P.; Palermo, R. E.; Jordan, R. F.; Rheingold A. L. *J. Am. Chem. Soc.* **1985**, 107, 4597. (d) Casey, C. P.; Palermo, R. E. *J. Am. Chem. Soc.* **1986**, 108, 549. (e) Casey, C. P.; Jordan, R. F.; Rheingold A.

L. *Organometallics* 1984, 3, 504. (f) Gelmini, L.; Stephan, D. W. *Inorg. Chem.* 1986, 25, 1222. (g) Ortiz, J. V. *J. Am. Chem. Soc.* 1986, 108, 550. (h) Schumann, H.; Albrecht, I.; Hahn, E. *Angew. Chem., Int. Ed. Engl.* 1985, 11, 985.

[44] Casey, C. P.; Bullock, R. M.; Nief, F. *J. Am. Chem. Soc.* 1983, 105, 7574.

[45] Farr, J. P.; Olmstead, M. M.; Balch, A. L. *J. Am. Chem. Soc.* 1980, 102, 6654.

[46] Delavaux, B.; Chaudret, B.; Dahan, F.; Poilblanc, R. *Organometallics* 1985, 4, 935.

[47] Regragui, R.; Dixneuf, P. H.; Talor, N. J.; Carty, A. J. *Organometallics* 1984, 3, 814.

[48] Hutchinson, K. D.; M. S. Thesis, University of New Hampshire, Durham, New Hampshire, 1987.

[49] Sun, X.; Ph. D. Thesis, University of New Hampshire, Durham, New Hampshire, 1993.

[50] Yang, H. Y.; Wong, E. H.; Rheingold, A. L.; Owens-Waltermire, B. E. *J. Chem. Soc., Chem. Commun.* 1993, 35.

[51] Broomhead, J. A.; Young, C. G. *Aust. J. Chem.* 1982, 35, p.277.

[52] Templeton, J. L.; Ward, B. C. *J. Am. Chem. Soc.* 1980, 102, 6568.

[53] Corbridge, D. E. C. Phosphorus, An Outline of its Chemistry, Biochemistry, and Technology, 3rd edn.; Elsevier: Amsterdam, 1985, pp.37-40.

[54] Purcell, K. F.; Kotz, J. C. Inorganic chemistry; W. B. Saunders Co.: Philadelphia, 1977, p.865.

[55] (a) Casey, C. P.; Whiteker, G. T.; Campana, C. F.; Powell, D. R. *Inorg. Chem.* 1990, 29, 3376. (b) Akhtar, M.; Ellis, P. D.; Macdiarmid, A. G.; Odom, J. D. *Inorg. Chem.* 1972, 11, 2917.

[56] (a) Verkade, J. G.; Quin, L. D. P-31 NMR Spectroscopy in Stereochemical Analysis; VCH: New York, 1987, p.441. (b) Johnson, D. K.; Pregosin, P. S.; Venanzi, L. M. *Helv. Chim. Acta.* 1976, 59, 2691.

[57] Wilkinson, G.; Gillard, R. D.; McCleverty, J. A. Comprehensive Coordination Chemistry; Pergamon Press: New York, 1987, Vol. 2, p.264.

[58] (a) Muttterties, E. L.; Alegranti, C. W. *J. Am. Chem. Soc.*, 1972, 94, 6386. (b) Goel, R. G.; Pilon, P. *Inorg. Chem.* 1978, 17, 2876. (c) Socol, S. M.; Jacobson,

- R. A.; Verkade, J. G. *Inorg. Chem.*, **1984**, 23, 88.
- [59] Pidcock, A.; Waterhouse, C. R., *J. Chem. Soc. A*, **1970**, 2087.
- [60] Bodner, G. M. *Inorg. Chem.*, **1975**, 14, 1932.
- [61] Ogilvie, F. B.; Jenkins, J. M.; Verkade J. G. *J. Am. Chem. Soc.*, **1970**, 92, 1916.
- [62] Bodner, G. M. *Coord. Chem. Rev.*, **1972**, 9, 1. *Inorg. Chem.* **1975**, 14, 1932.
- [63] Verkade, J. G.; Quin, L. D. P-31 NMR Spectroscopy in Stereochemical Analysis; VCH: New York, **1987**, Chapter 14.
- [64] Cotton, F. A.; Wilkinson, G. Advanced Inorganic Chemistry, 5th edn.; Wiley Interscience: New York, **1988**, pp. 746-748.
- [65] Wilkinson, G.; Stone, F. G. A.; Abel, E. W. Comprehensive Organometallic Chemistry; Pergamom Press: New York, **1982**, V. 6, p. 234.
- [66] Corbridge, D. E. C. The structural Chemistry of Phosphorus; Elsevier: New York, **1974**, p. 300.
- [67] Corbridge, D. E. C. Phosphorus, an outline of its Chemistry, Biochemistry, and Technology, 3rd edn.; Elsevier: Amsterdam, **1985**, p.545.
- [68] Corbridge, D. E. C. The Structural Chemistry of Phosphorus; Elsevier: New York, **1974**, p. 65.
- [69] Corbridge, D. E. C. The Structural Chemistry of Phosphorus; Elsevier: New York, **1974**, p. 215, p. 301.
- [70] Barton, D.; Ollis, W. D. Comprehensive Organic Chemistry, The Synthesis and reactions of Organic Compounds; Pergamon Press: New York, **1979**, p. 1146.
- [71] Douglas, B. E.; McDaniel, D. H.; Alexander, J. J. Concepts and models of Inorganic Chemistry, 3rd edn.; John Wiley & Sons: New York, **1994**, p. 562.
- [72] Douglas, B. E.; McDaniel, D. H.; Alexander, J. J. Concepts and models of Inorganic Chemistry, 3rd edn.; John Wiley & Sons: New York, **1994**, p. 600.
- [73] Bodnor, G. M. *Inorg. Chem.* **1974**, 13, 1335.
- [74] Braterman, P.S.; Milne, D, W.; Randall, E. W.; Rosenberg, E. *J. Chem. Soc., Dalton* , **1973**, 1027.

[75] Gansow, O. A.; Kimura, B. Y.; Dobson, G. R.; Brown, R. A. *J. Amer. Chem. Soc.*, **1971**, 93, 5922; Gansow, O. A.; Schexnayder, D. A.; Kimura, B. Y. *J. Amer. Chem. Soc.*, **1972**, 94, 3406.

[76] (a) Bodner, G. M.; Todd, L. J. *Inorg. Chem.*, **1974**, 13, 360. (b) Bodner, G. M. *Inorg. Chem.*, **1974**, 13, 2563, (c) Bodner, G. M. *Inorg. Chem.*, **1975**, 14, 1932, and 2694; (d) Bodner, G. M.; May, M. P.; McKinney, L.E. *Inorg. Chem.*, **1980**, 19, 1951.

[77] (a) Schmidpeter A.; Lochschmidt S.; Sheldrick W. S. *Angew. Chem. int. Ed. Engl.* **1985**, 24, 226. (b) Lochschmidt S.; Schmidpeter A. *Z. Naturfor.* **1985**, 40B, 765.

[78] King, R. B. *Organometallic Synthesis*; Academic Press: New York, **1965**, Vol. 1, p.122.

[79] Abel, E. W.; Bennett, M. A.; Wilkinson, G. J. *J. Chem. Soc.*, **1959**, 3178.

[80] Ward, L. G. L. *Inorg. Synth.*, **1972**, 13, 154.

[81] Doyle, J. R.; Slade, P. E.; Jonassen, H. B., *Inorg. Synth.*, **1960**, 6, 218.

[82] McGindle, R.; Alyea, E. C.; Ferguson, G.; Dias, S. A.; McAlees, J. J. *Chem. Soc.; Dalton Trans.*, **1980**, 1, 137.

[83] Drew, D.; Doyle, J. R. *Inorg. Synth.*, **1990**, 28, 346.

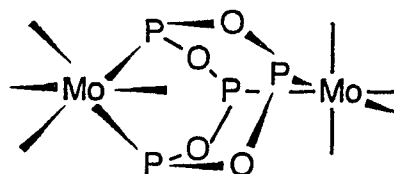
[84] Kubas, G. J. *Inorg. Synth.* **1990**, 28, 68.

[85] Belderrain, T. R., Knight, D. A.; Irvine, D. J.; Paneque, M.; Poveda, M. L.; Carmona, E. J. *Chem. Soc. Dalton*, **1992**, 1491.

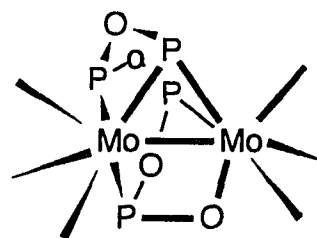
APPENDICES

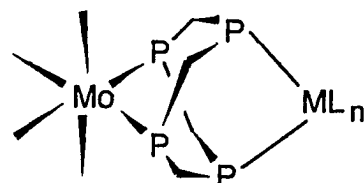
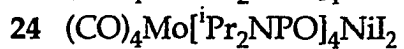
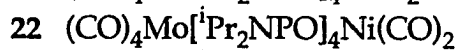
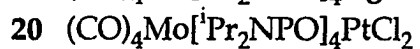
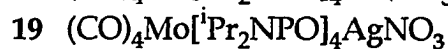
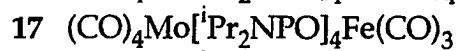
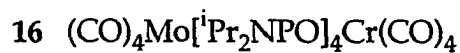
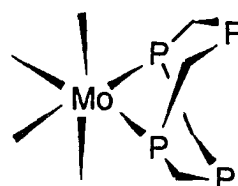
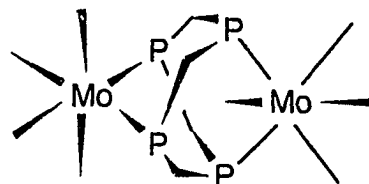
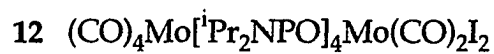
A. COMPOUND NUMBER ASSIGNMENTS

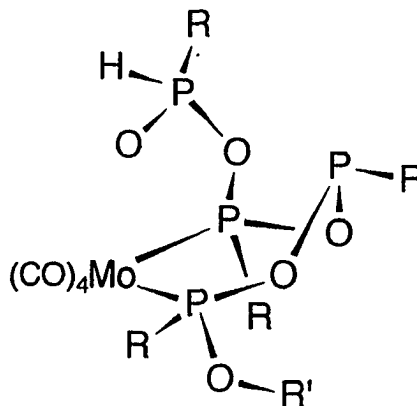
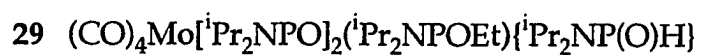
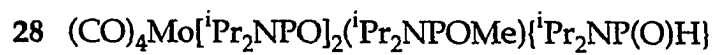
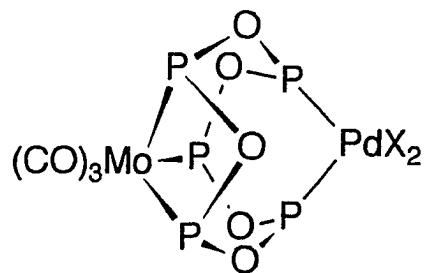
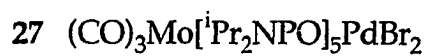
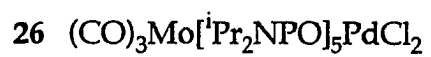
- 1 $(\text{CO})_4\text{Mo}[\text{iPr}_2\text{NPO}]_4\text{Mo}(\text{CO})_4$
 5 $(\text{CO})_4\text{Mo}[\text{iPr}_2\text{NPO}]_4\text{Mo}(\text{CO})_3\text{P}(\text{OMe})_3$
 6 $(\text{CO})_3\text{P}(\text{OMe})_3\text{Mo}[\text{iPr}_2\text{NPO}]_4\text{Mo}(\text{CO})_3\text{P}(\text{OMe})_3$
 8 $(\text{CO})_4\text{Mo}[\text{iPr}_2\text{NPO}]_4\text{Mo}(\text{CO})_3(\text{PPh}_2\text{H})$
 9 $(\text{CO})_3(\text{PPh}_2\text{H})\text{Mo}[\text{iPr}_2\text{NPO}]_4\text{Mo}(\text{CO})_3(\text{PPh}_2\text{H})$



- 2 $(\text{CO})_3\text{Mo}[\text{iPr}_2\text{NPO}]_4\text{Mo}(\text{CO})_2\text{PPh}_3$
 3 $(\text{CO})_3\text{Mo}[\text{iPr}_2\text{NPO}]_4\text{Mo}(\text{CO})_2\text{PPh}_2\text{Me}$
 4 $(\text{CO})_3\text{Mo}[\text{iPr}_2\text{NPO}]_4\text{Mo}(\text{CO})_3\text{PPh}_2\text{H}$
 7 $(\text{CO})_3\text{Mo}[\text{iPr}_2\text{NPO}]_4\text{Mo}(\text{CO})_2\text{P}(\text{OMe})_3$
 10 $(\text{CO})_3\text{Mo}[\text{iPr}_2\text{NPO}]_4\text{Mo}(\text{CO})_2\text{Py}$
 11 $(\text{CO})_3\text{Mo}[\text{iPr}_2\text{NPO}]_4\text{Mo}(\text{CO})_3$

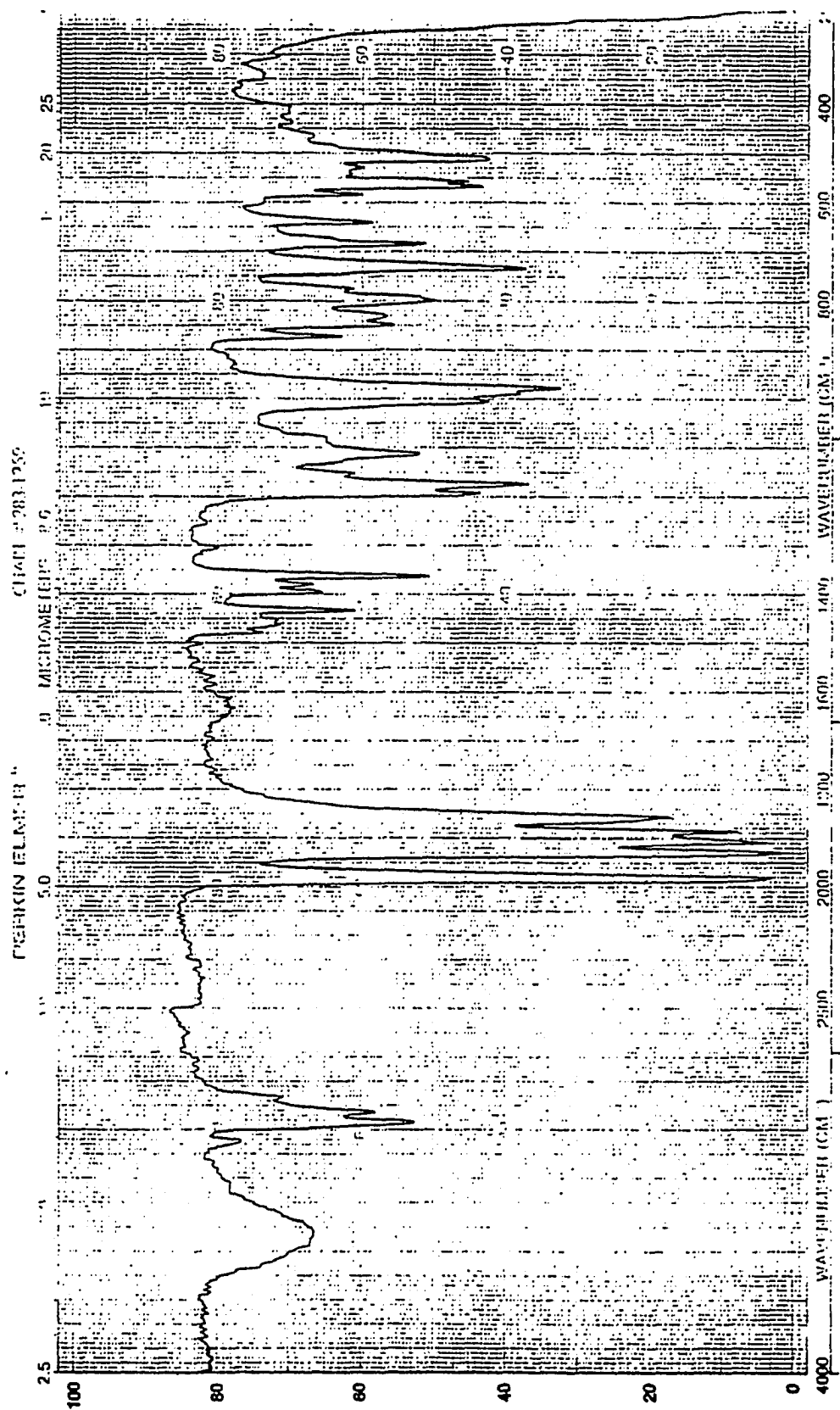




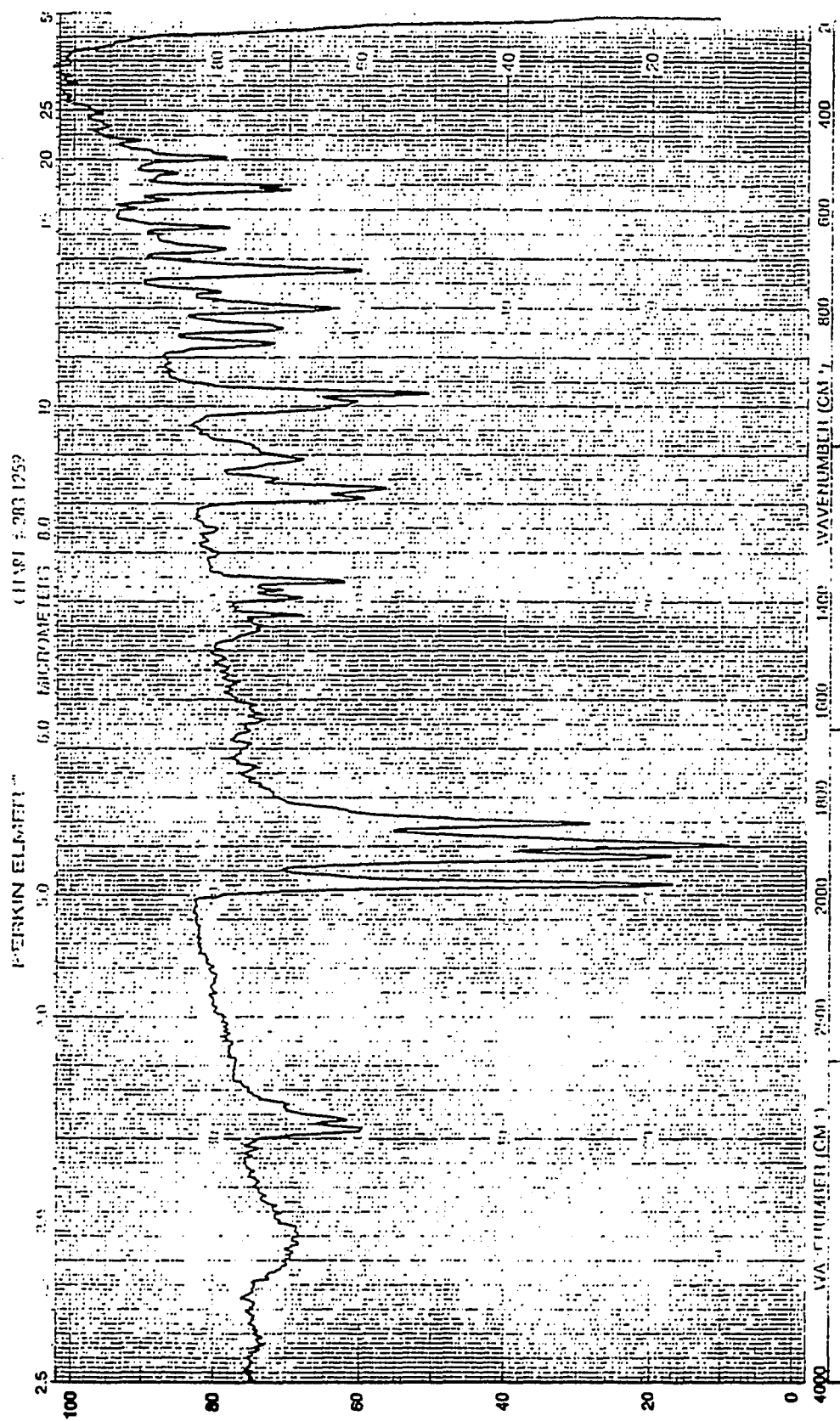


B. SELECTED SPECTRA

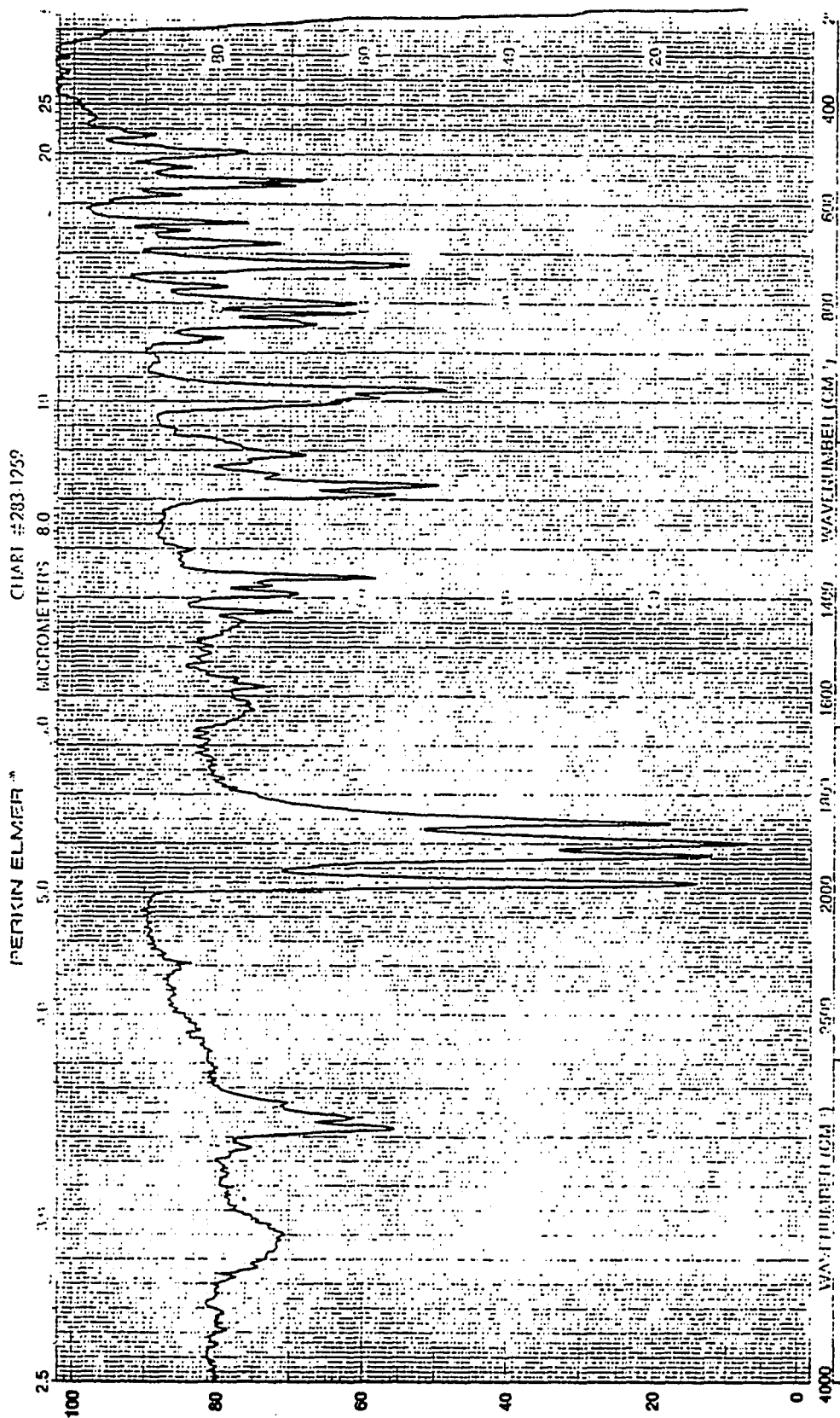
IR Spectrum of $(\text{CO})_3\text{Mo}^i\text{Pr}_2\text{NPO}^{14}\text{Mo}(\text{CO})_2(\text{PPh}_3)$



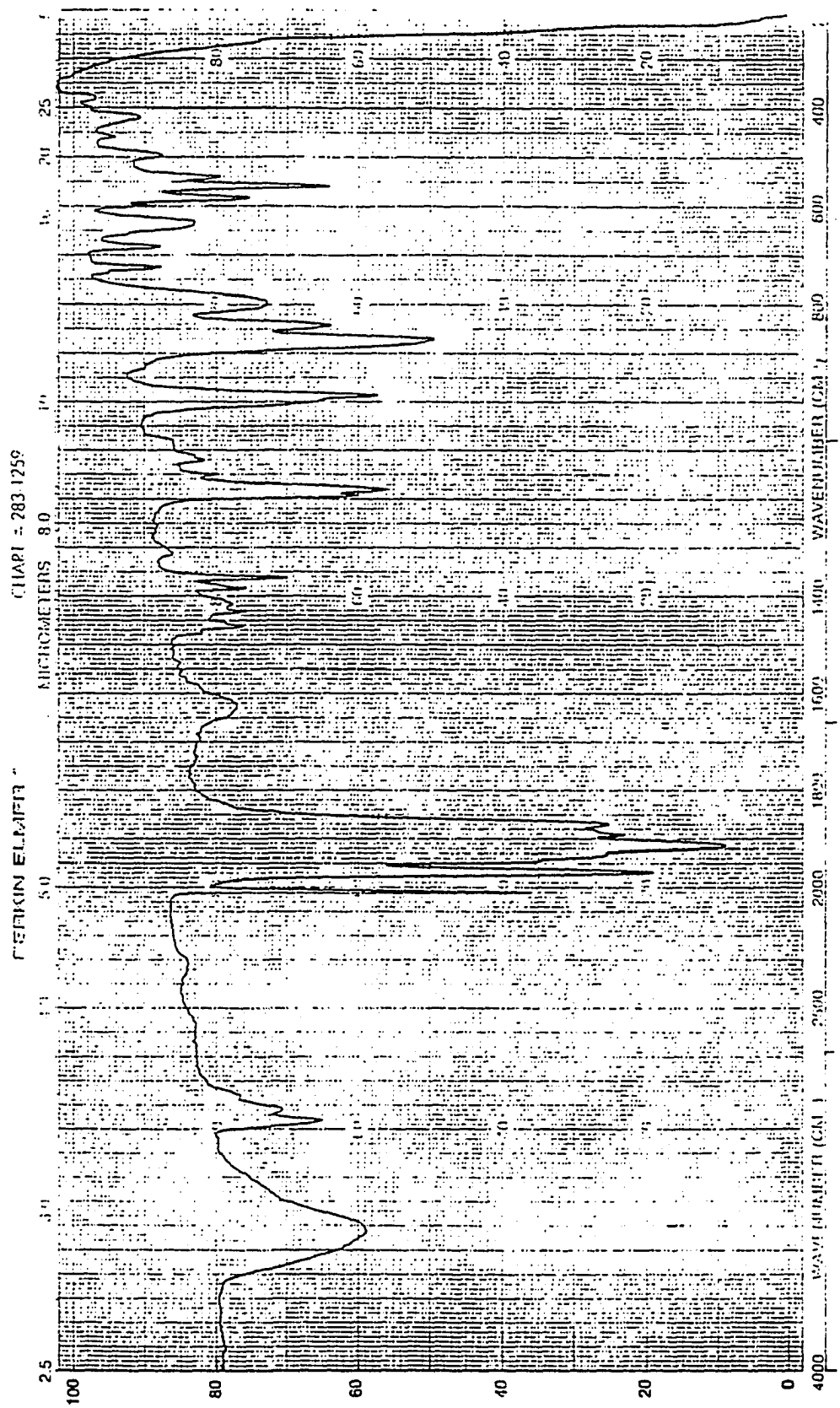
IR Spectrum of $(\text{CO})_3\text{Mo}[\text{Pr}_2\text{NPO}]_4\text{Mo}(\text{CO})_2(\text{PPh}_2\text{Me})$



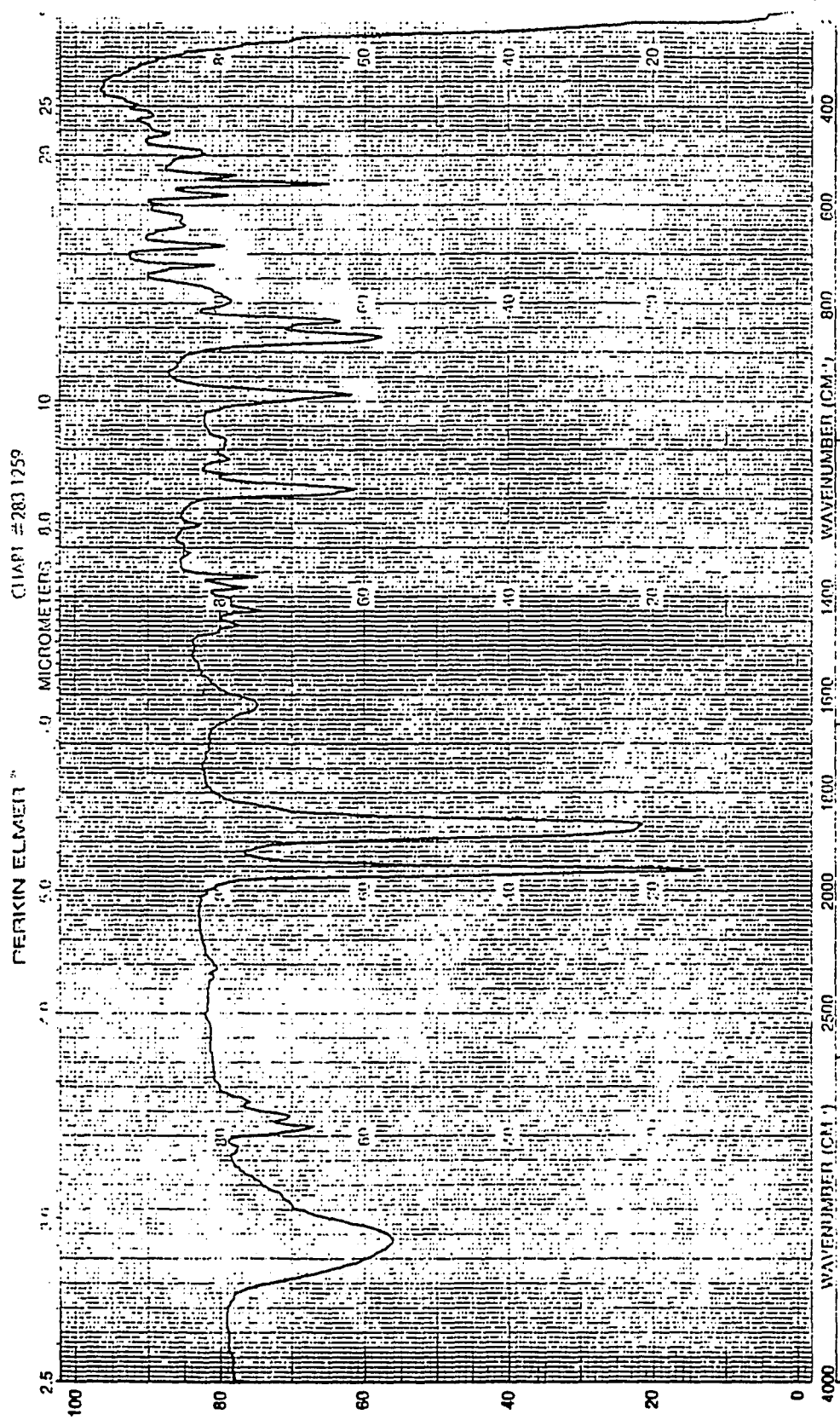
IR Spectrum of $(\text{CO})_3\text{Mo}[\text{Pr}_2\text{NPO}]_4\text{Mo}(\text{CO})_2(\text{PPh}_2\text{H})$



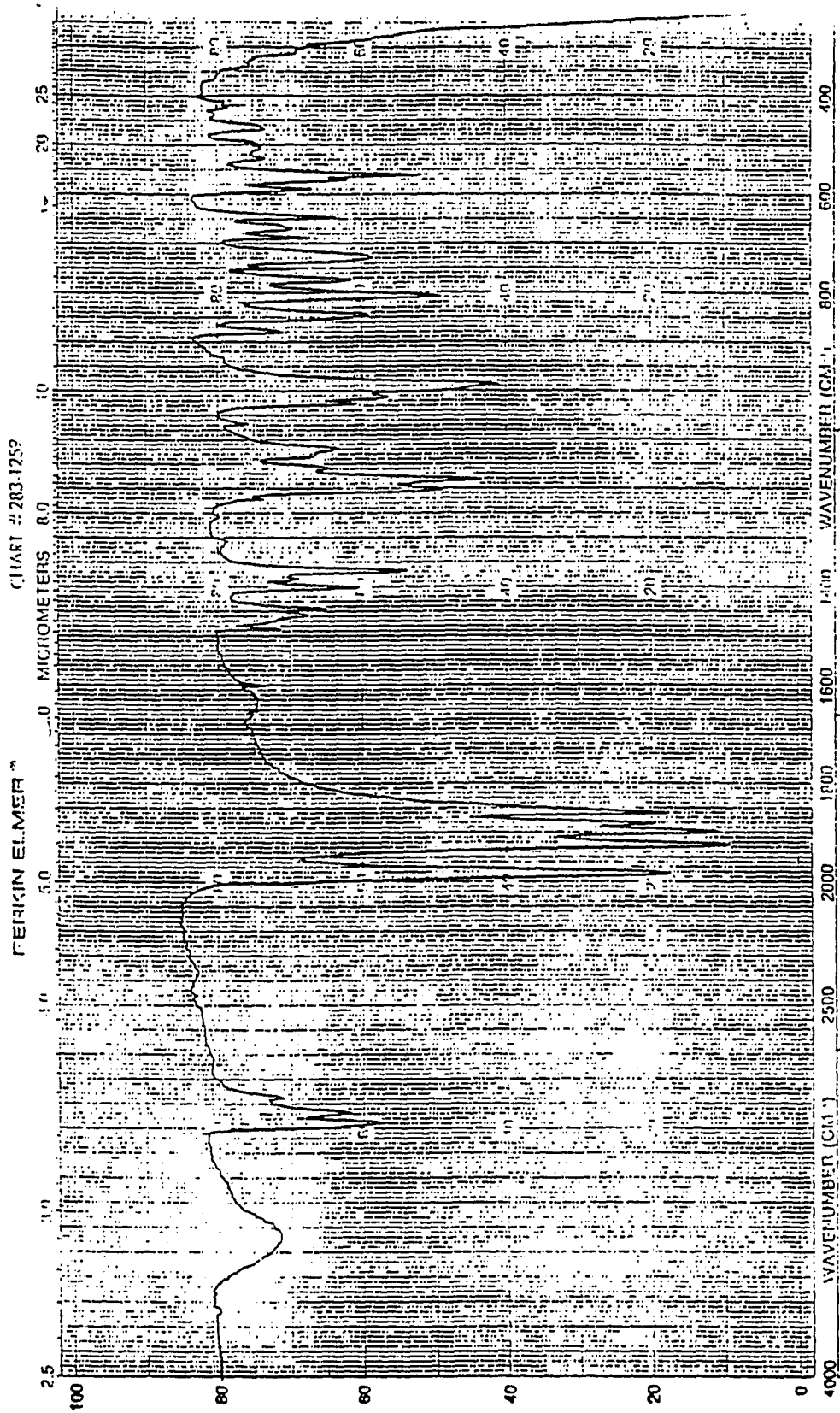
IR Spectrum of $(\text{CO})_4\text{Mo}[\text{Pr}_2\text{NPO}]_4\text{Mo}(\text{CO})_3(\text{PPh}_2\text{H})$



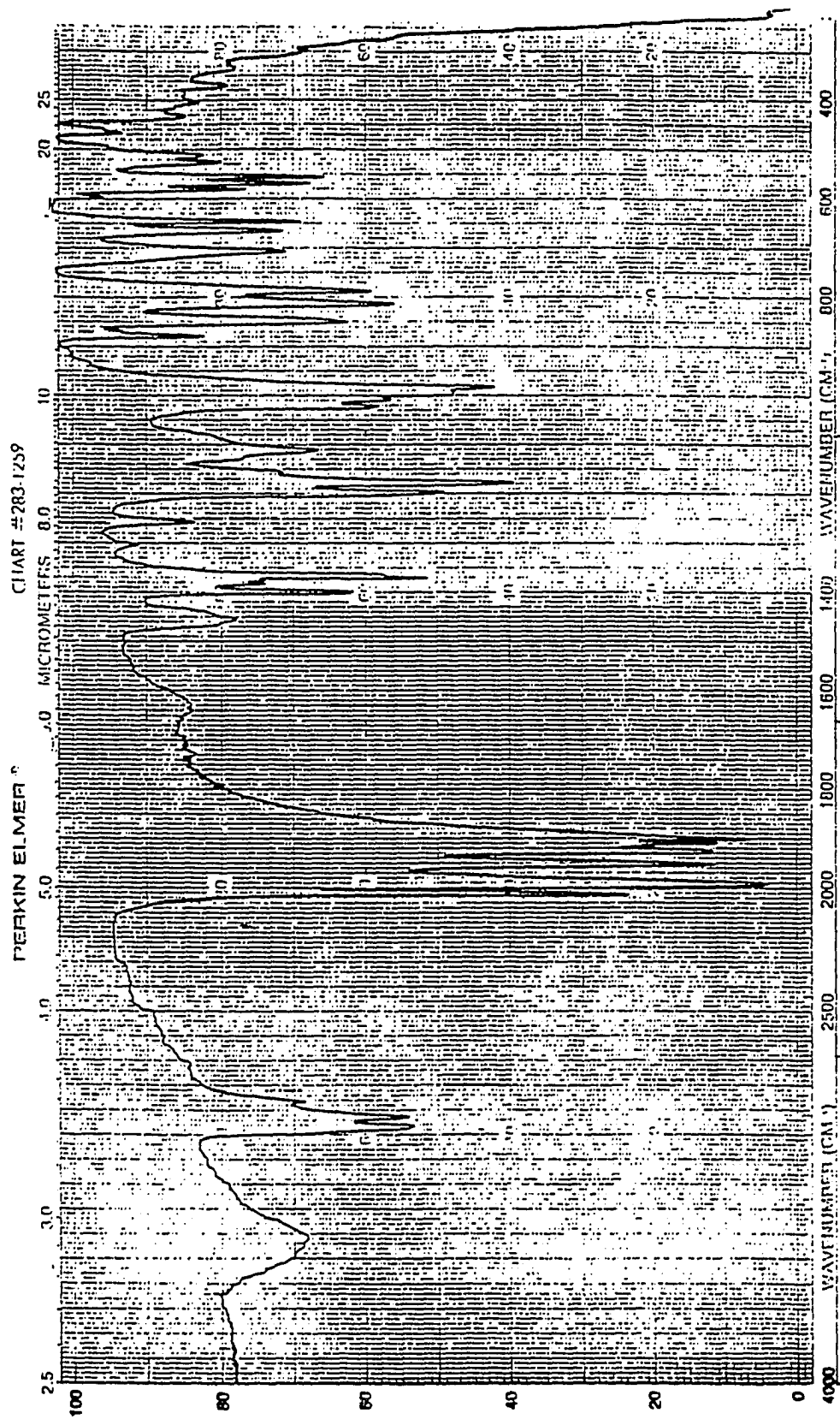
IR Spectrum of $(CO)_3(PPh_2H)Mo[Pr_2NPO]_4Mo(CO)_3(PPh_2H)$



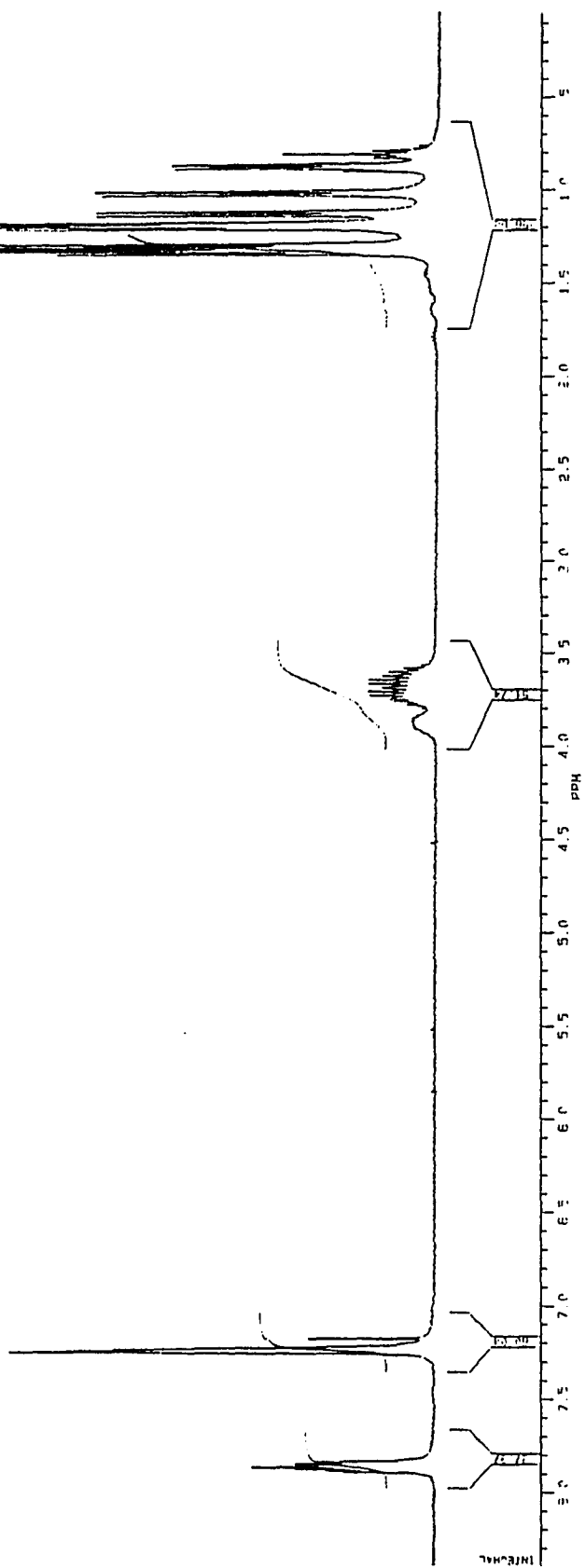
IR Spectrum of $(\text{CO})_3\text{Mo}(\text{iPr})_2\text{NPOl}_4\text{Mo}(\text{CO})_2\text{Py}$



IR Spectrum of $(\text{CO})_3\text{Mo}(\text{tPr}_2\text{NPO})_4\text{Mo}(\text{CO})_3$



^1H NMR Spectrum of $(\text{CO})_3\text{Mo}[\text{iPr}_2\text{NPO}]_4\text{Mo}(\text{CO})_2(\text{PPh}_3)$

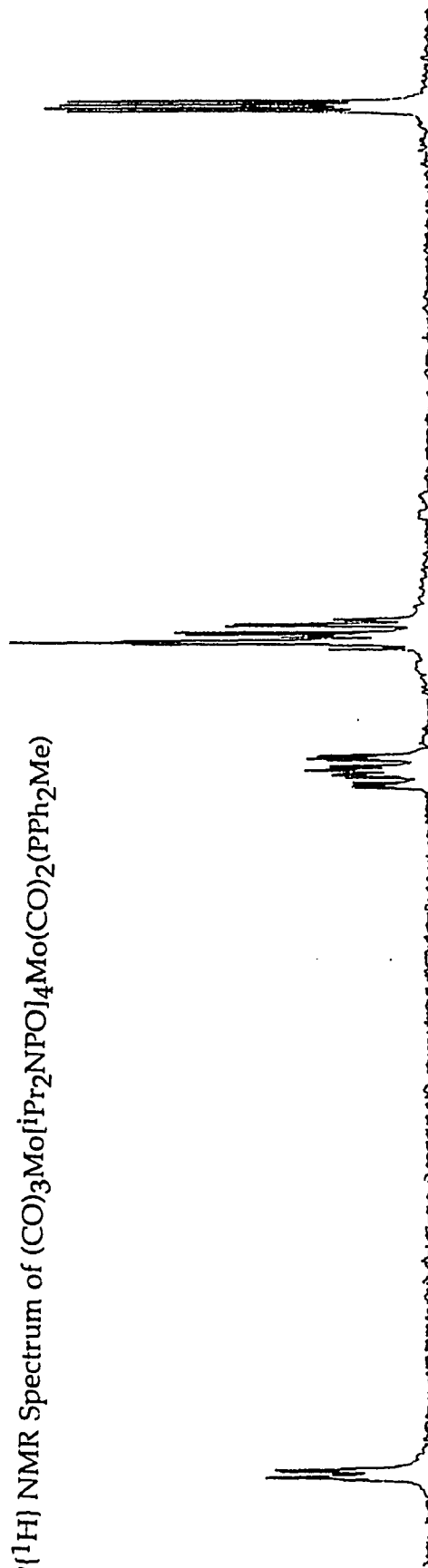


$^{31}\text{P}\{^1\text{H}\}$ NMR Spectrum of $(\text{CO})_3\text{Mo}[\text{iPr}_2\text{NPO}]_4\text{Mo}(\text{CO})_2(\text{PPh}_2\text{H})$

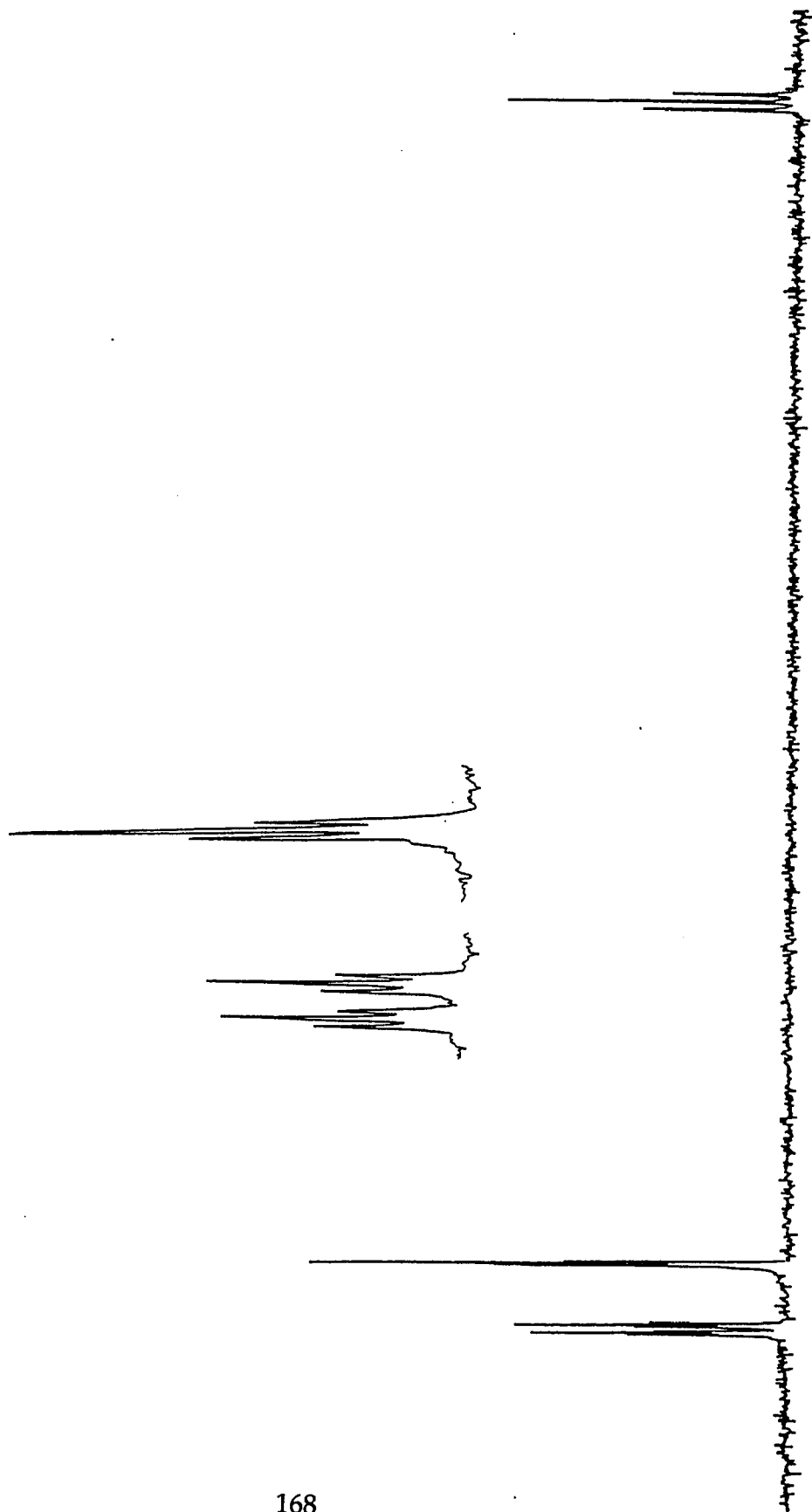


167

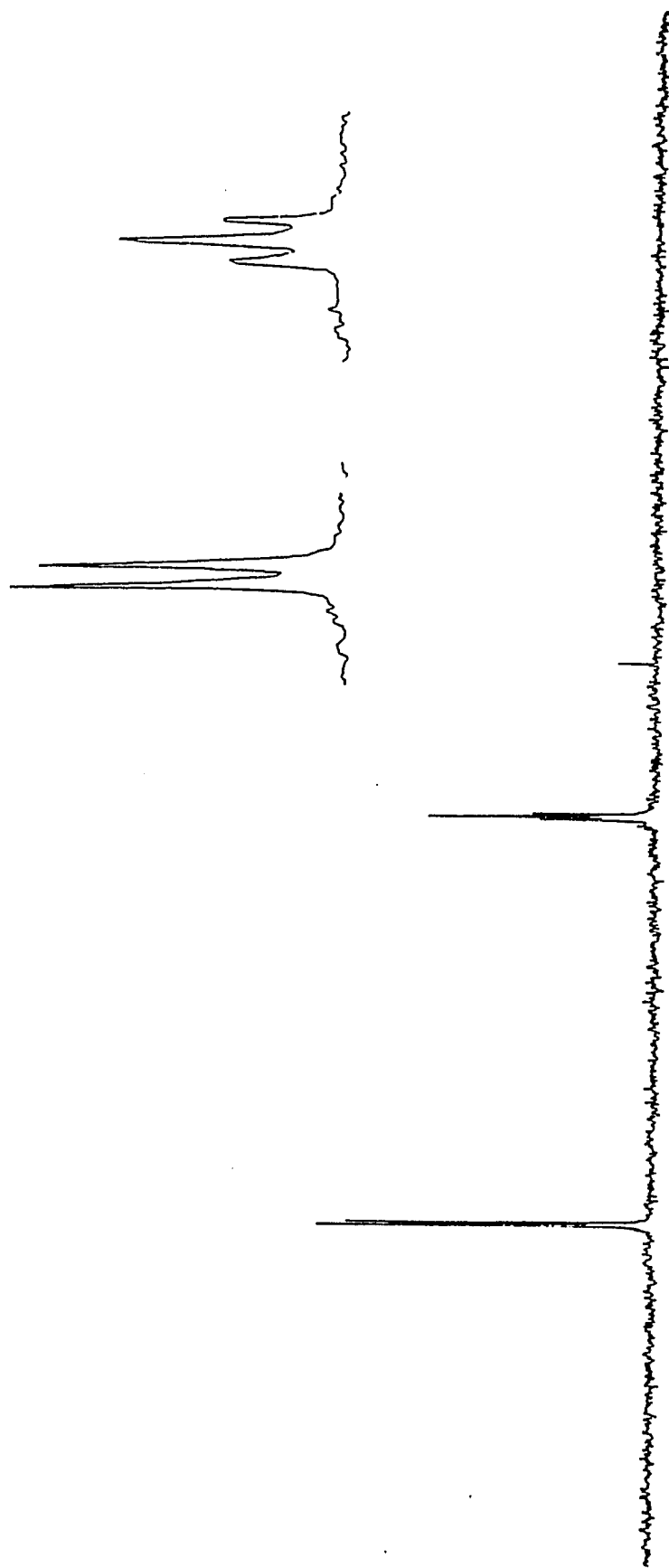
$^{31}\text{P}\{^1\text{H}\}$ NMR Spectrum of $(\text{CO})_3\text{Mo}[\text{iPr}_2\text{NPO}]_4\text{Mo}(\text{CO})_2(\text{PPh}_2\text{Me})$



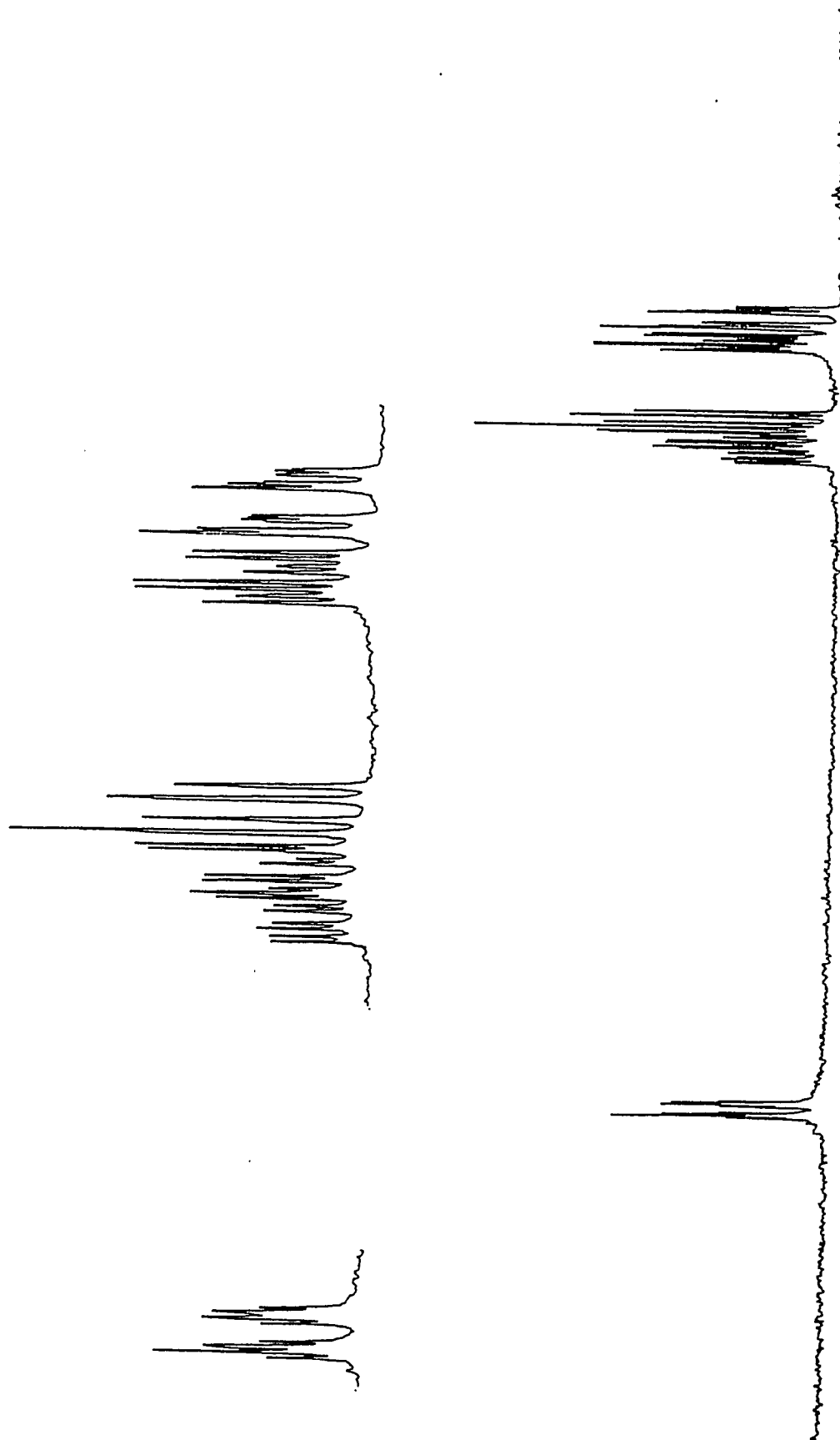
$^{31}\text{P}\{^1\text{H}\}$ NMR Spectrum of $(\text{CO})_4\text{Mo}[\text{iPr}_2\text{NPO}]_4\text{Mo}(\text{CO})_3(\text{PPh}_2\text{H})$



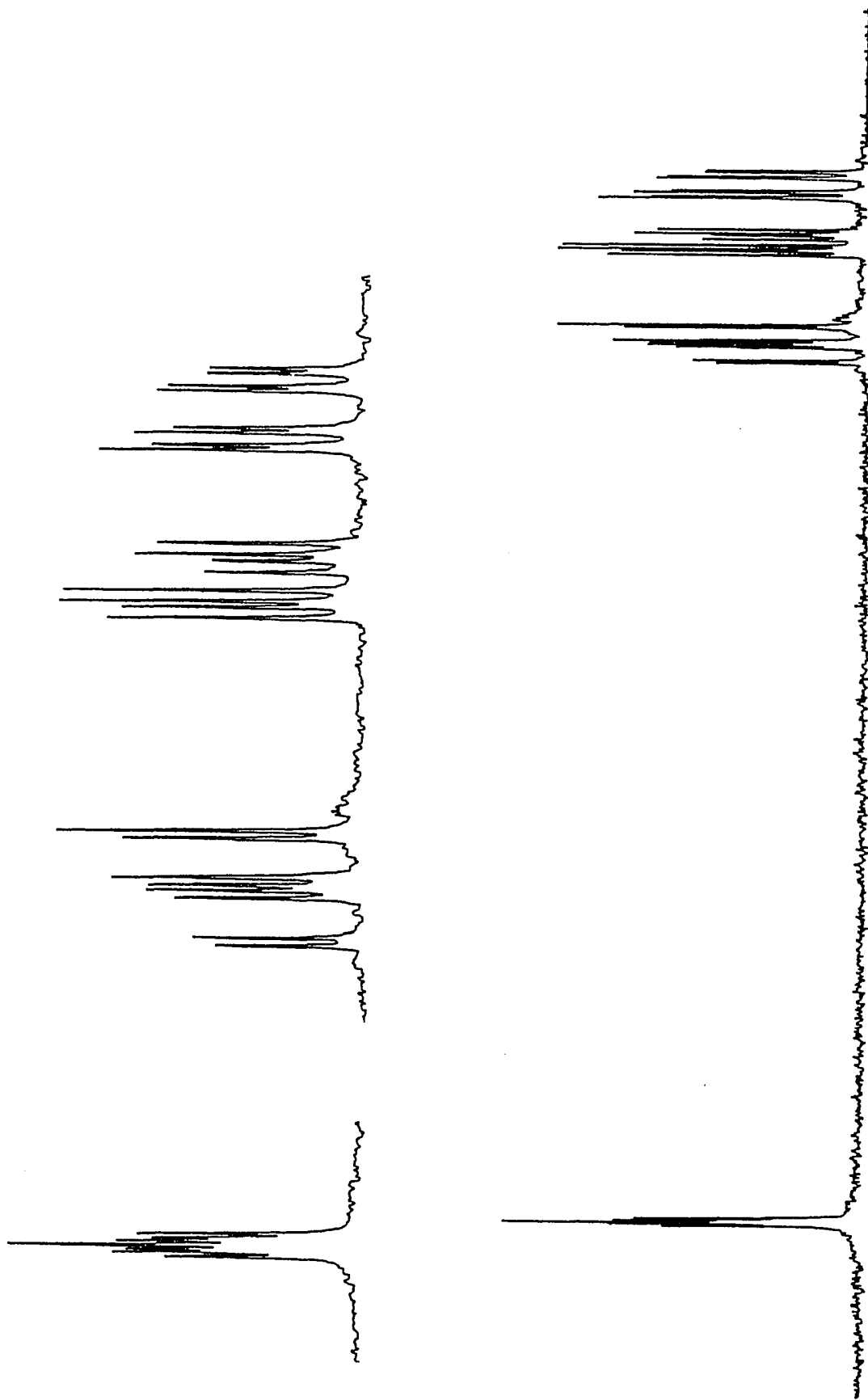
$^{31}\text{P}\{^1\text{H}\}$ NMR Spectrum of $(\text{CO})_3(\text{PPh}_2\text{H})\text{Mo}[\text{Pr}_2\text{NPO}]_4\text{Mo}(\text{CO})_3(\text{PPh}_2\text{H})$



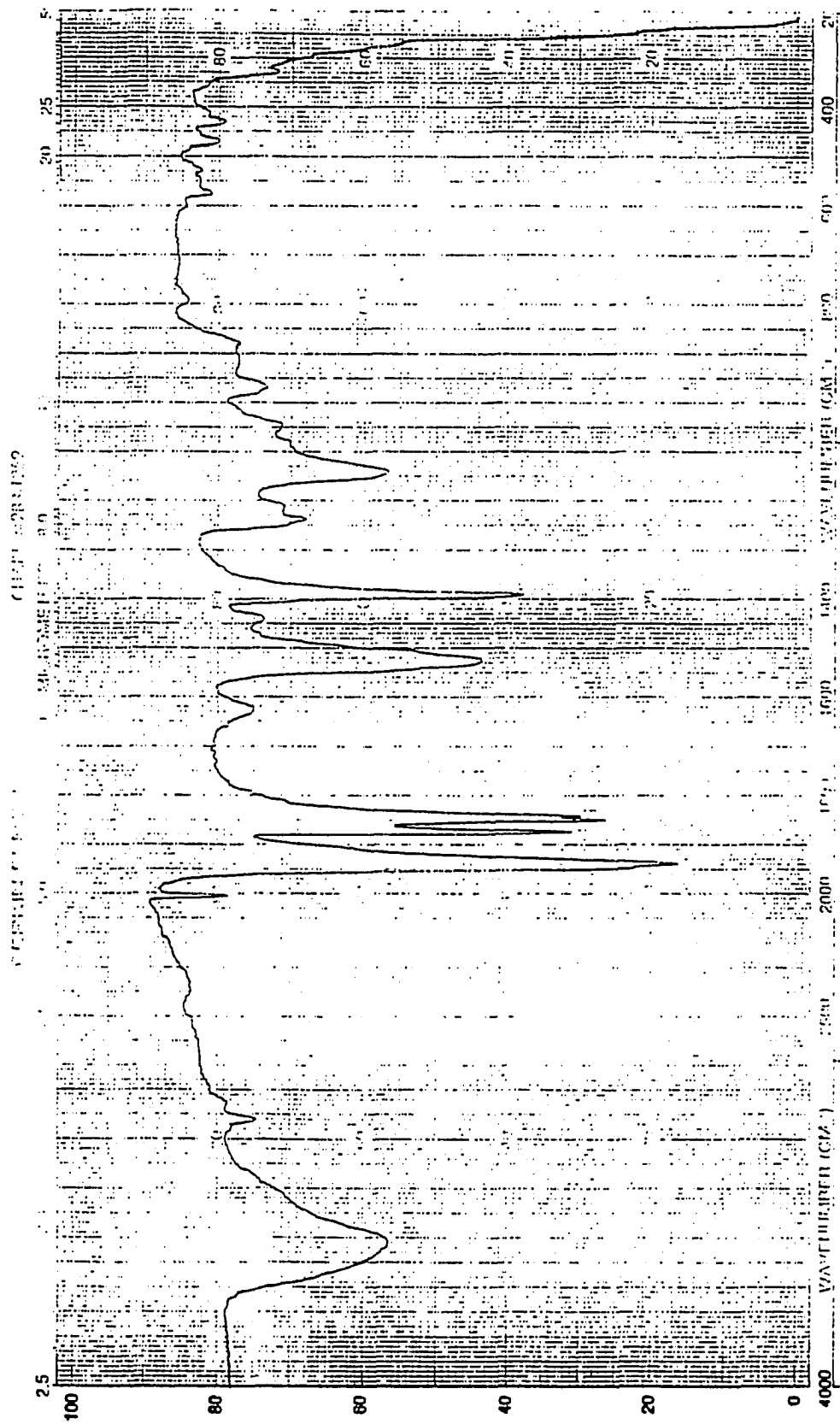
$^{31}\text{P}\{^1\text{H}\}$ NMR Spectrum of $(\text{CO})_3\text{Mo}[\text{iPr}_2\text{NPO}]_4\text{Mo}(\text{CO})_2\text{P}(\text{OMe})_3$



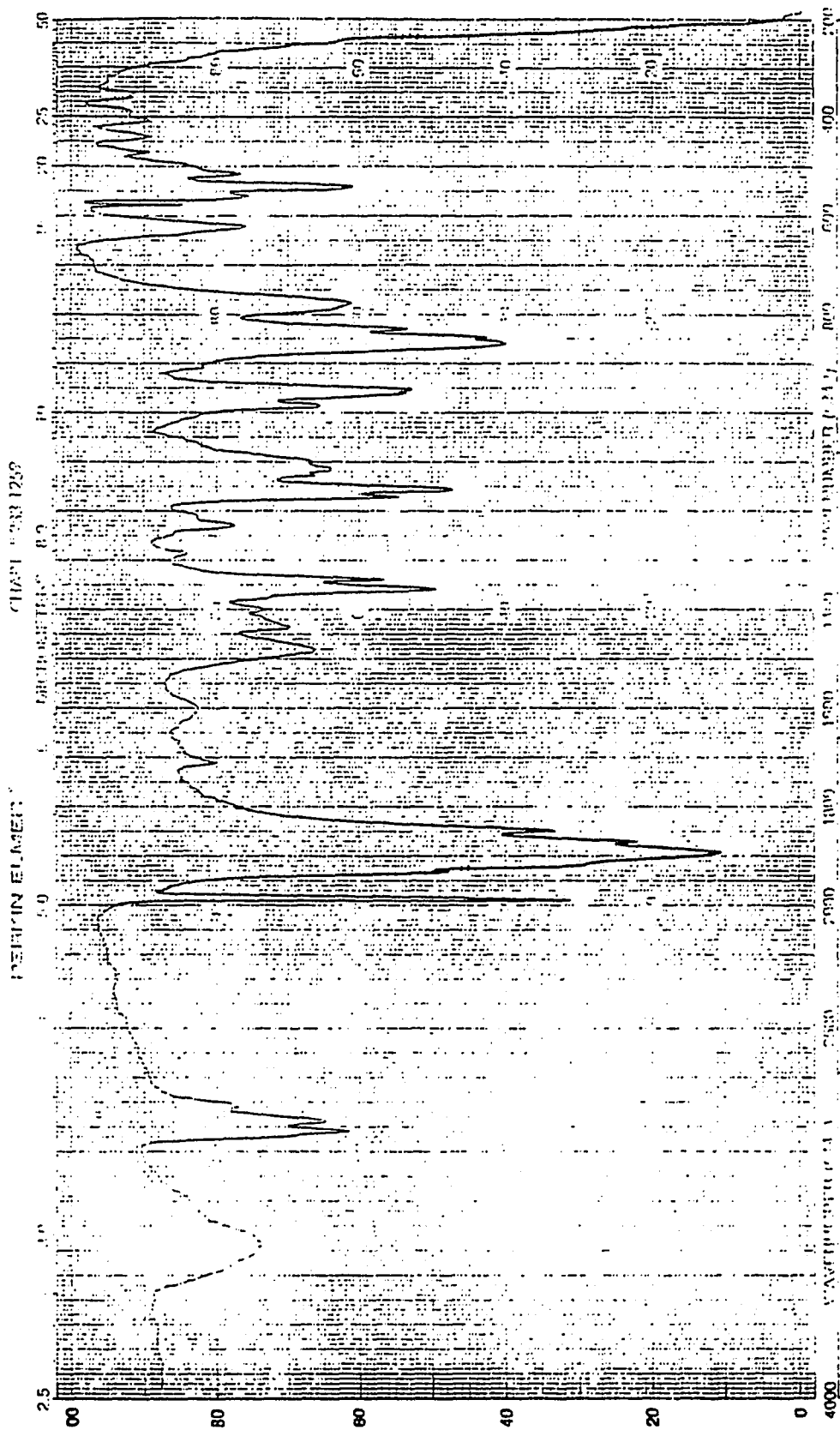
$^{31}\text{P}\{^1\text{H}\}$ NMR Spectrum of $(\text{CO})_3\text{Mo}\{^1\text{Pr}_2\text{NPO}\}_4\text{Mo}(\text{CO})_3$



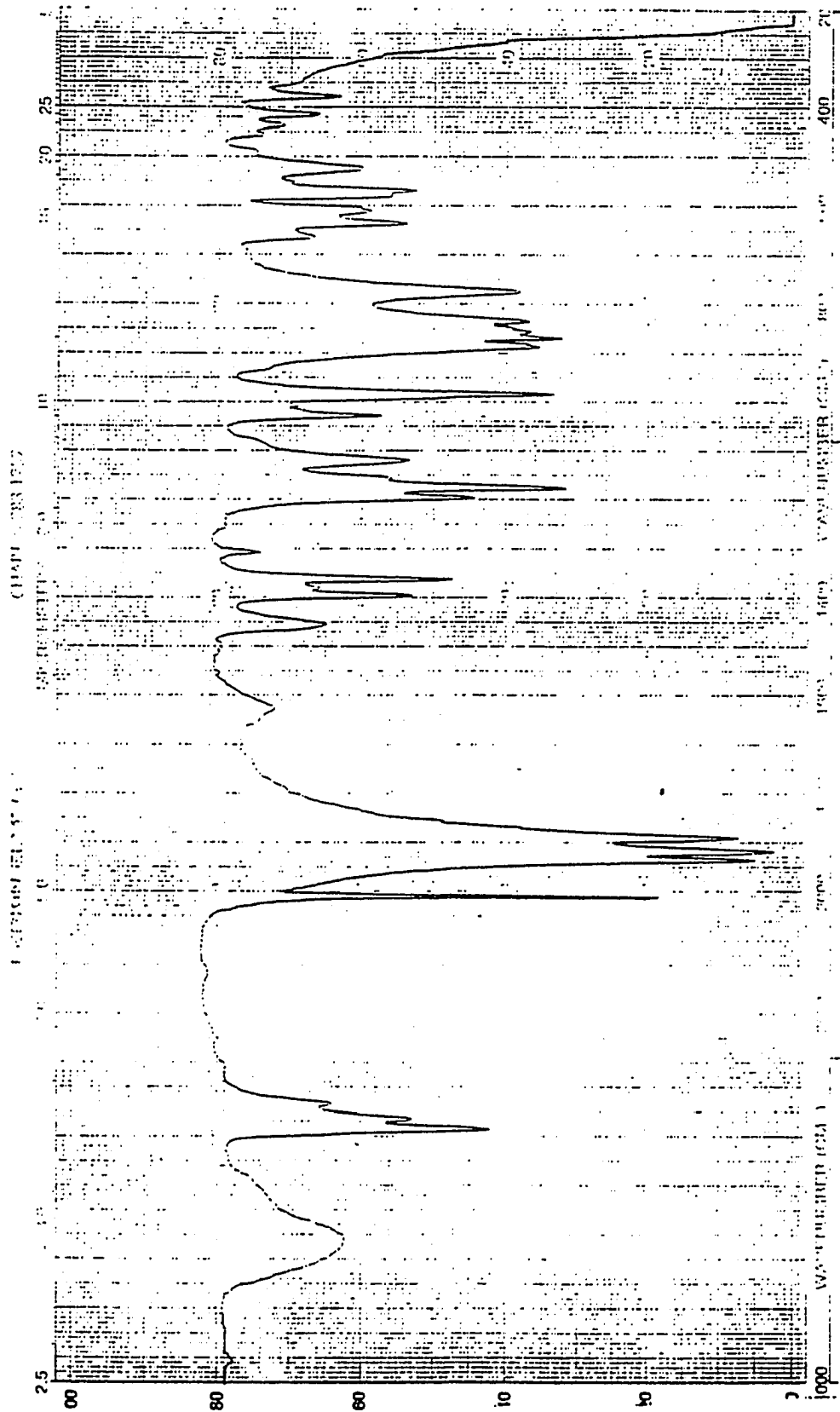
IR Spectrum of $\text{Mo}(\text{CO})_2[\text{S}_2\text{CNMe}_2]_2$



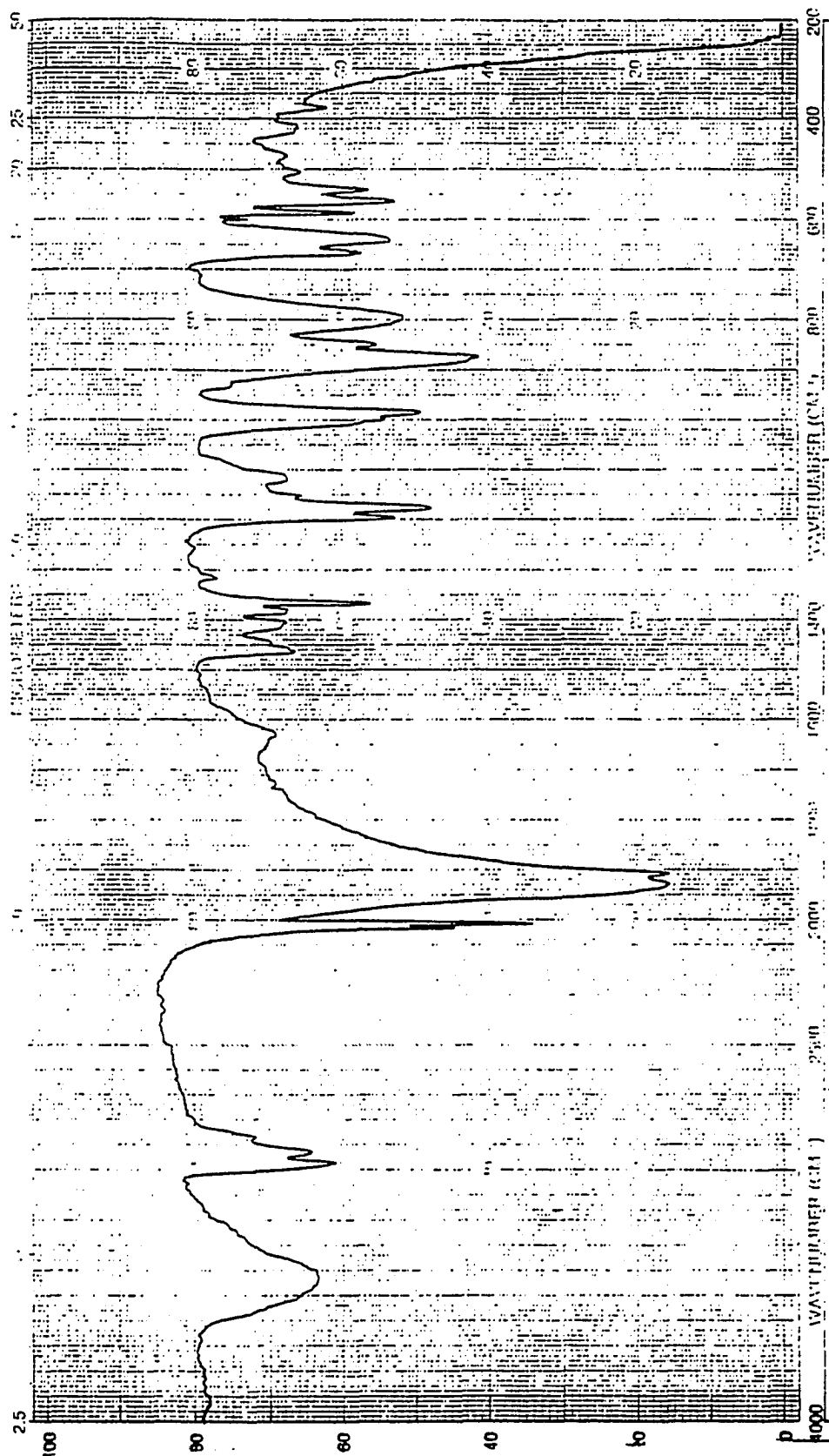
IR Spectrum of $(\text{CO})_4\text{Mo}[\text{Pr}_2\text{NPO}]_4\text{Mo}(\text{CO})_2(\text{S}_2\text{CNMe}_2)_2$



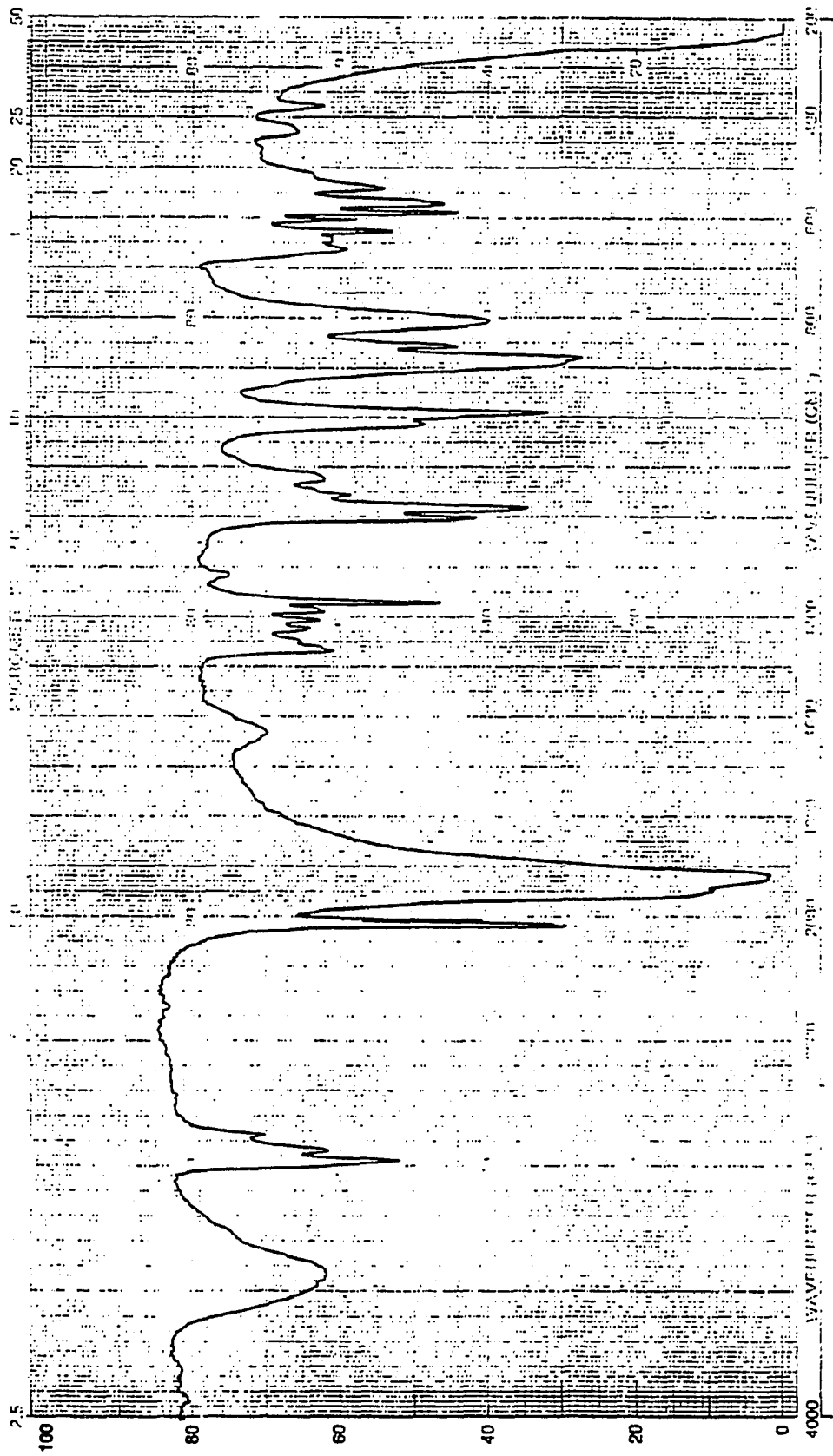
IR Spectrum of $(\text{CO})_4\text{Mo}^{\text{II}}\text{Pr}_2\text{NPO}]_4$



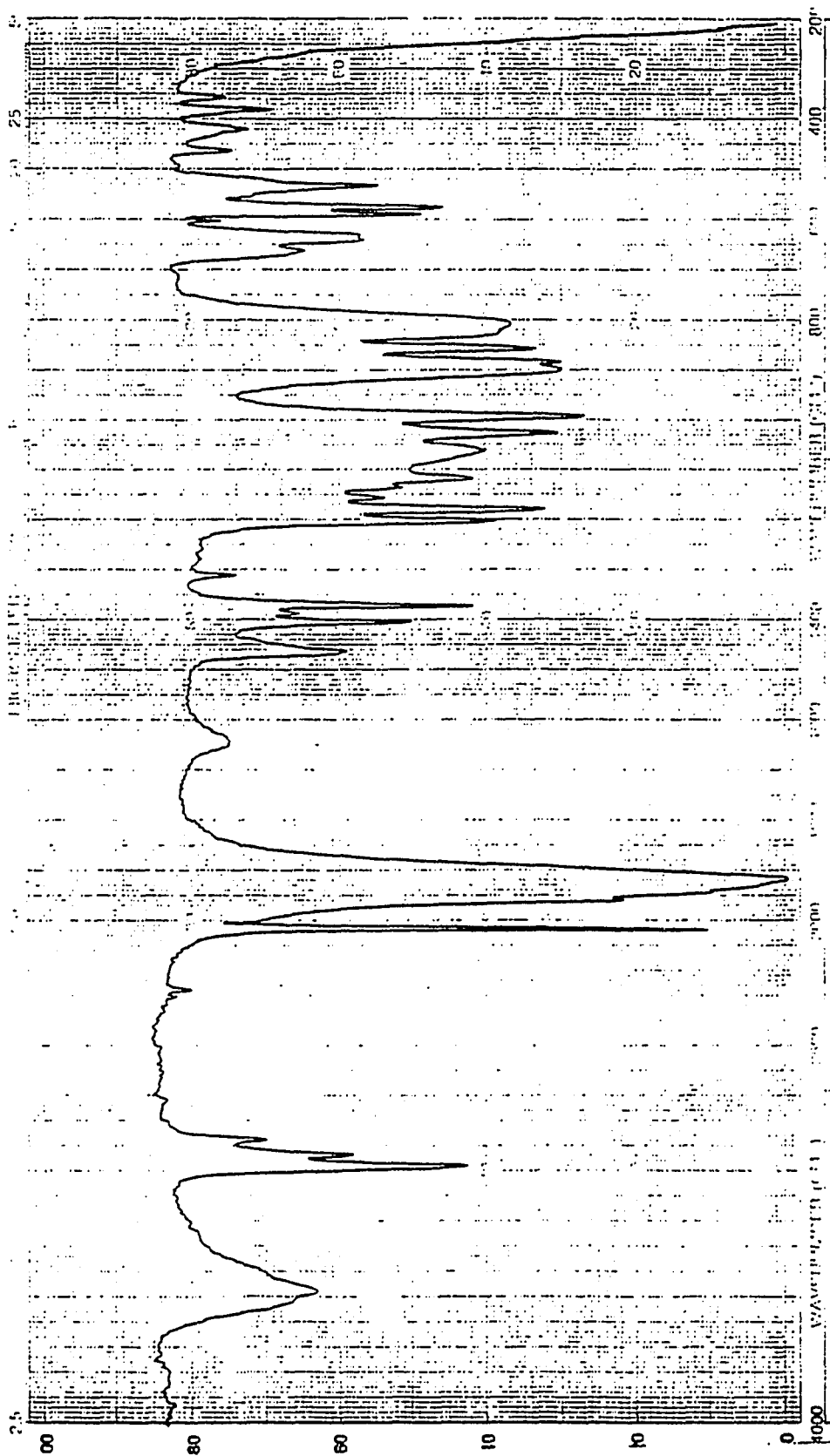
IR Spectrum of $(\text{CO})_4\text{Mo}[\text{iPr}_2\text{NPO}]_4\text{Cr}(\text{CO})_4$



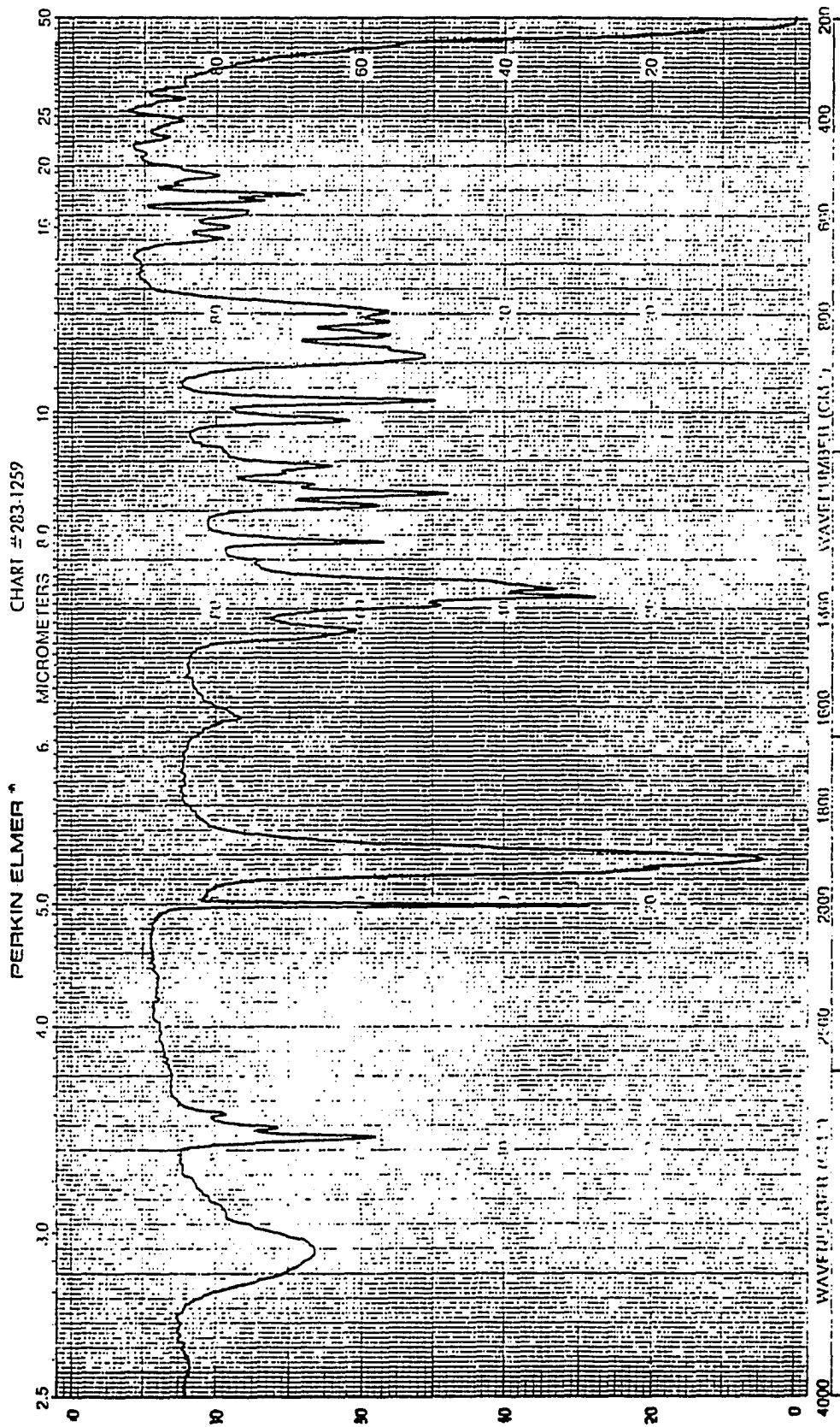
IR Spectrum of $(\text{CO})_4\text{Mo}[\text{Pr}_2\text{NPO}]_4\text{Fe}(\text{CO})_3$



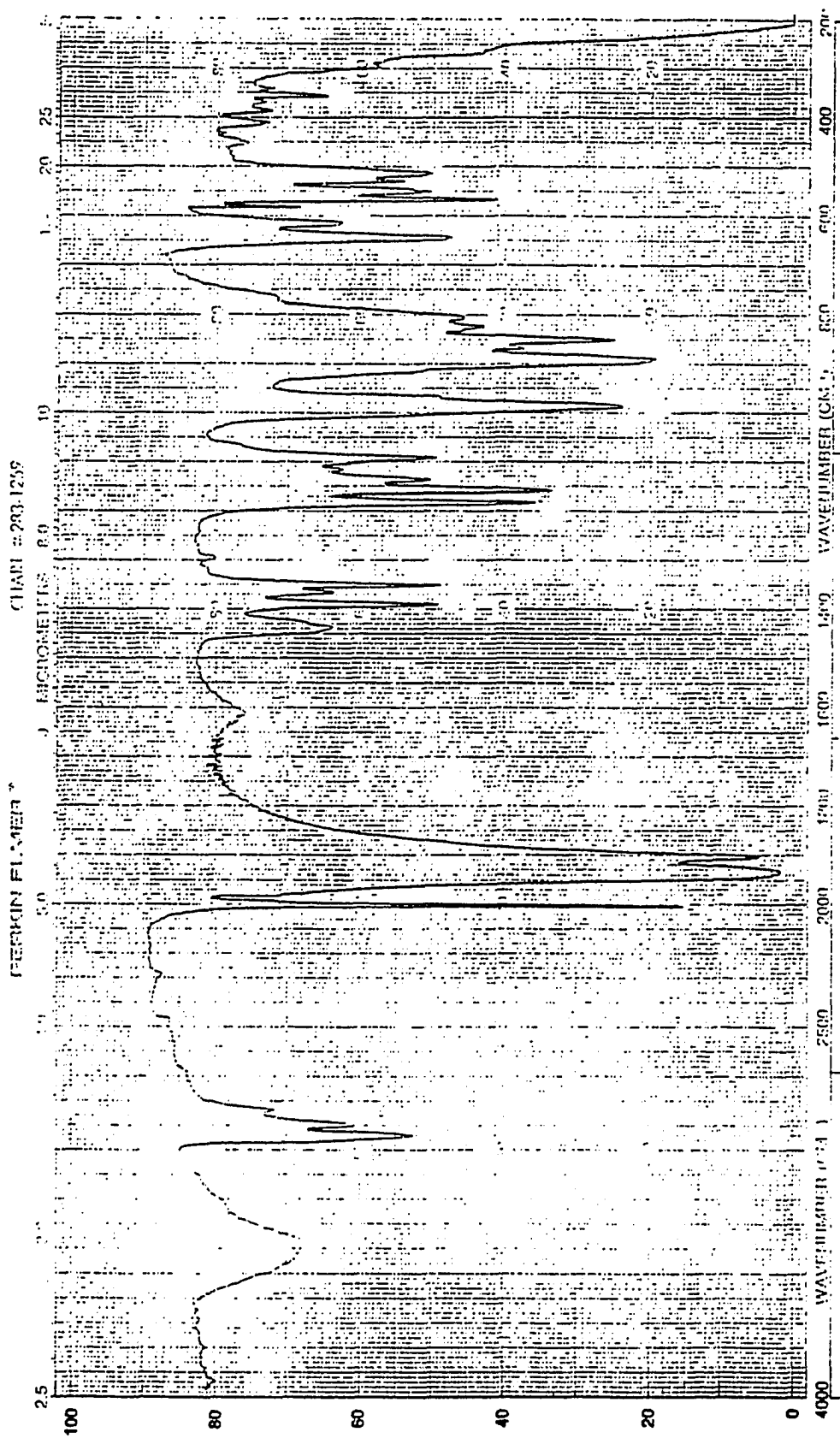
IR Spectrum of $(\text{CO})_4\text{Mo}[\text{Pr}_2\text{NPO}]_4\text{Cu}(\text{CH}_3\text{CN})_2\text{BF}_4$



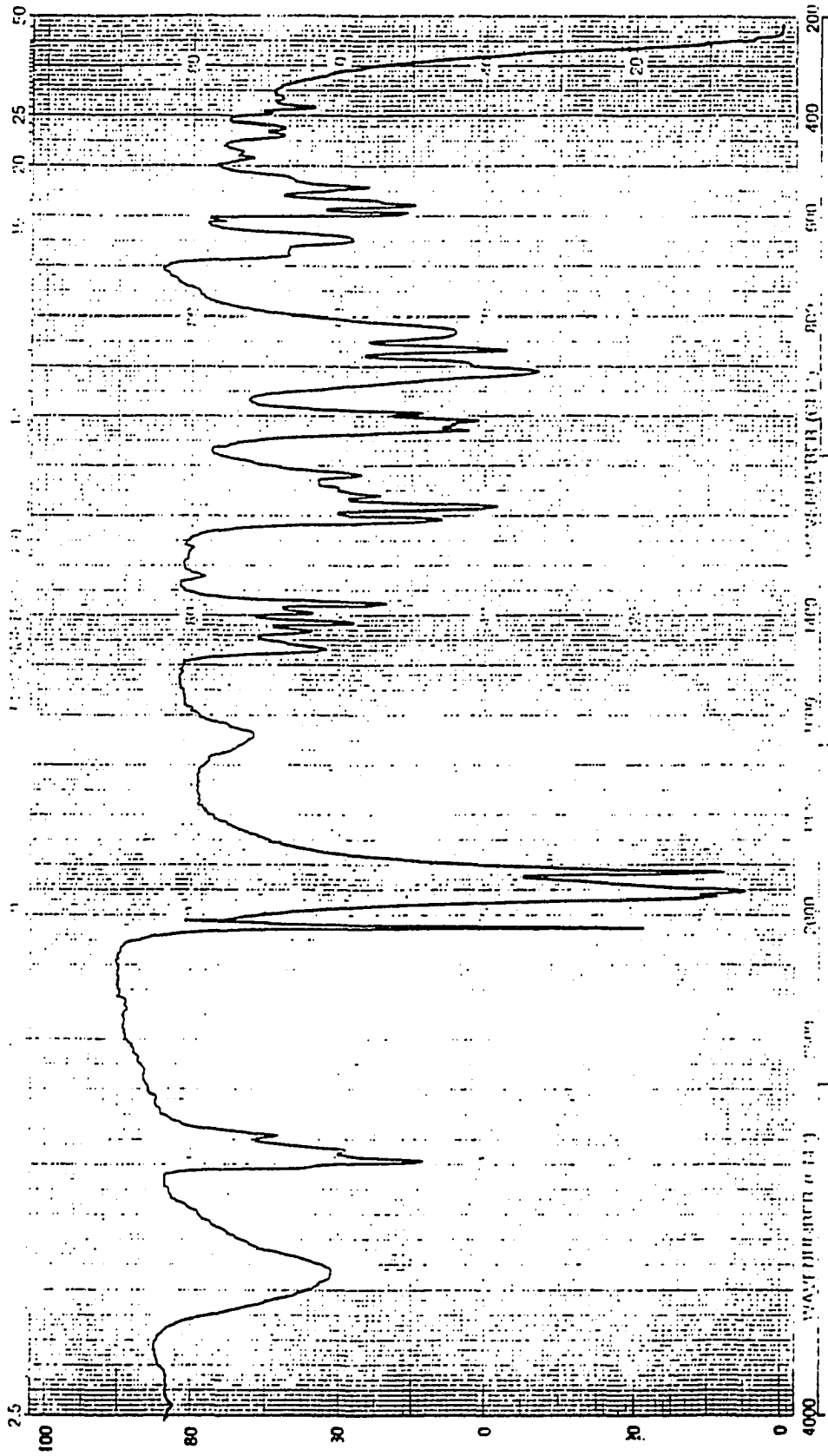
IR Spectrum of $(\text{CO})_4\text{Mo}[\text{Pr}_2\text{NPO}]_4\text{Ag}(\text{NO}_3)$



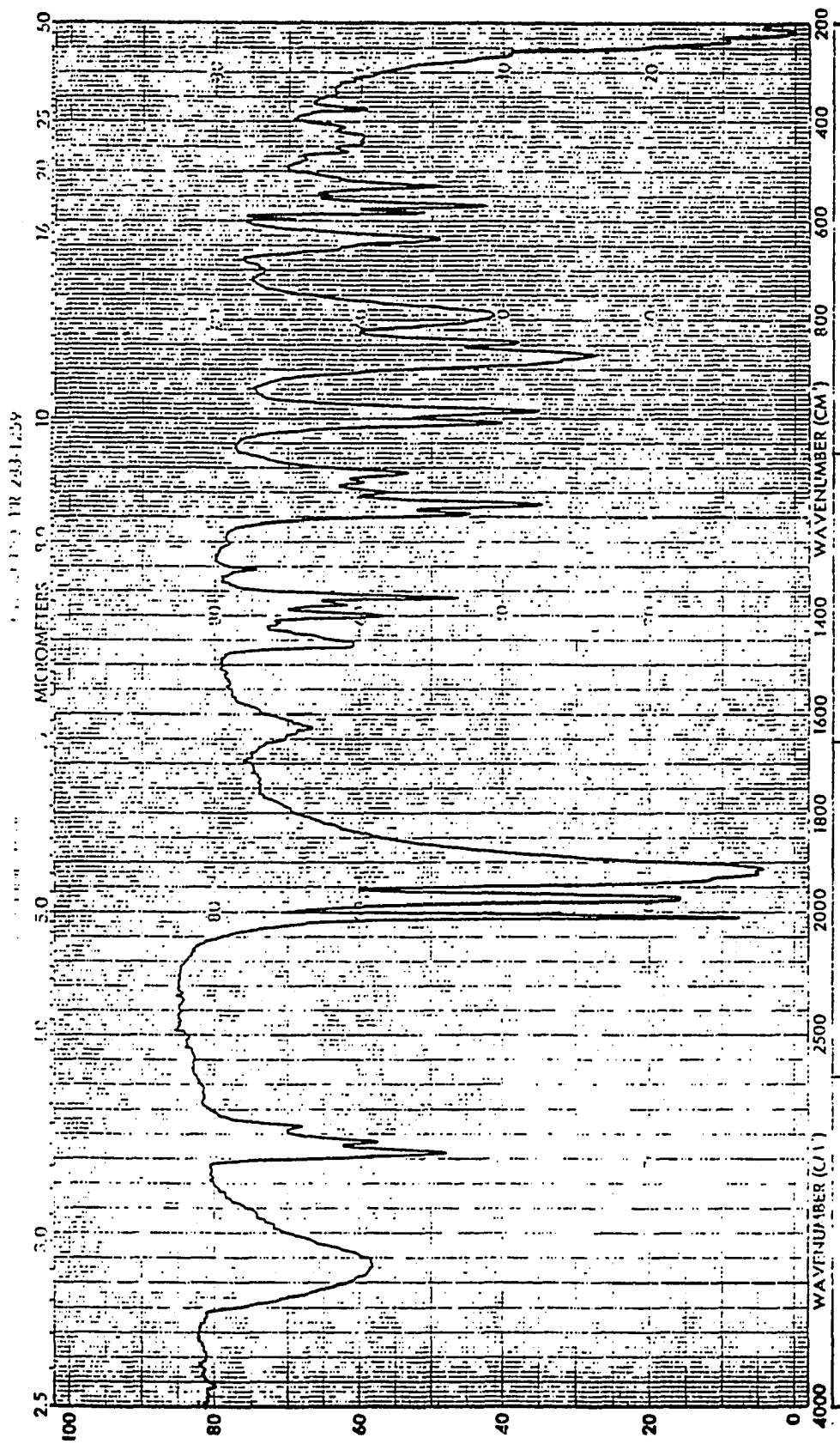
IR Spectrum of $(\text{CO})_4\text{Mo}[\text{iPr}_2\text{NPO}]_4\text{PtCl}_2$



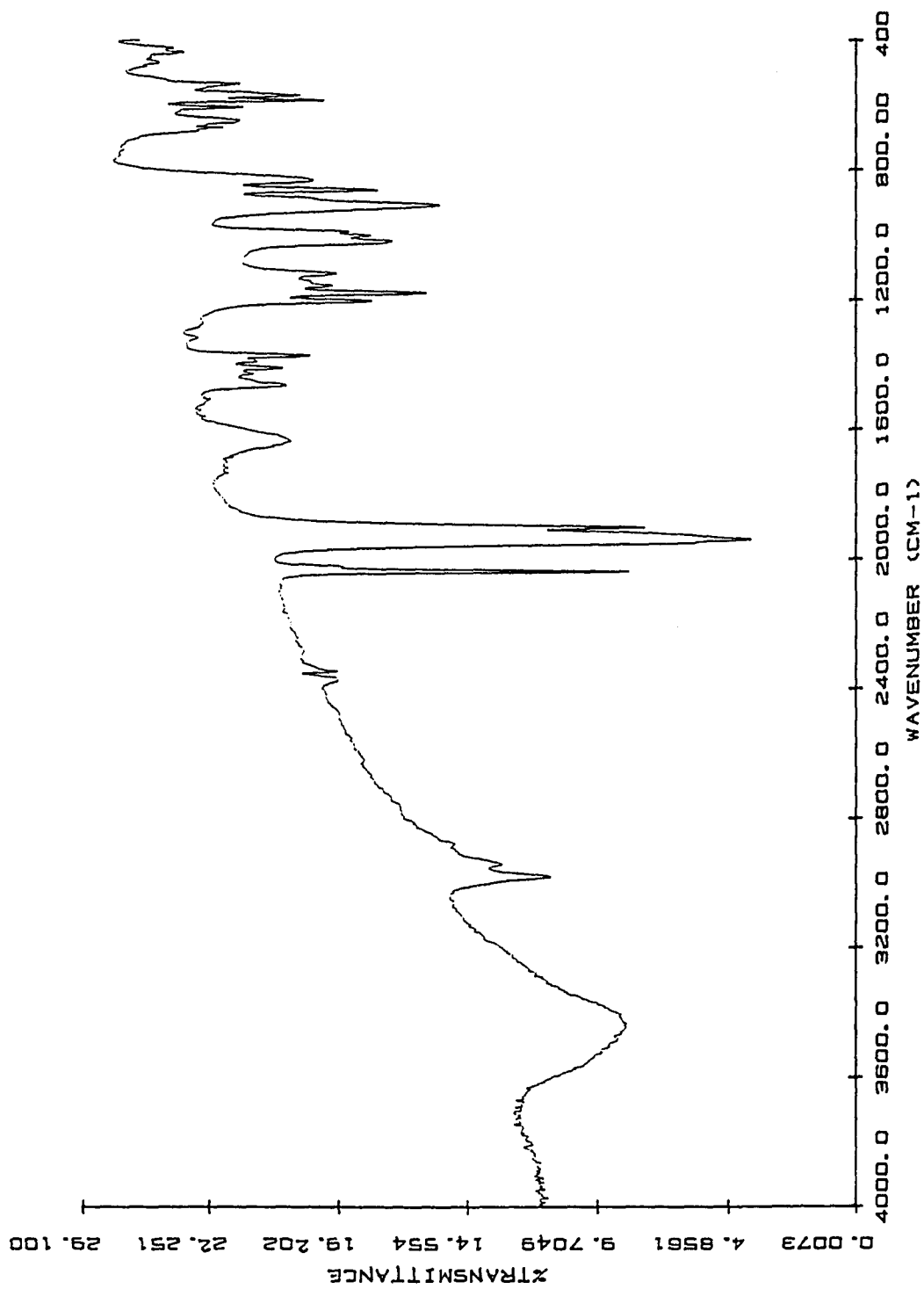
IR Spectrum of $(\text{CO})_4\text{Mo}[\text{Pr}_2\text{NPO}]_4\text{NiBr}_2$



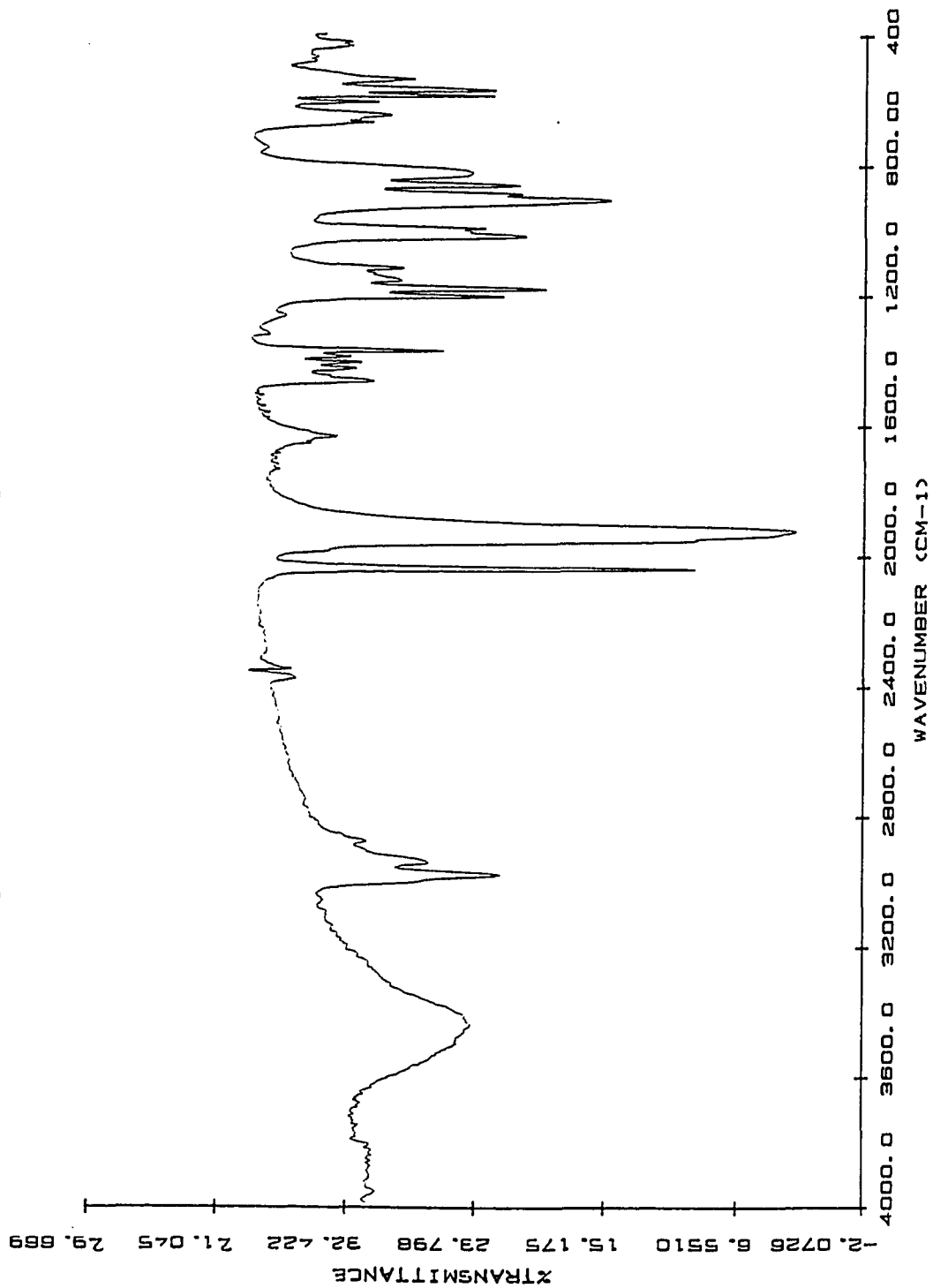
IR Spectrum of $(\text{CO})_3\text{Mo}[\text{iPr}_2\text{NPO}]_5\text{Ni}(\text{CO})_2$



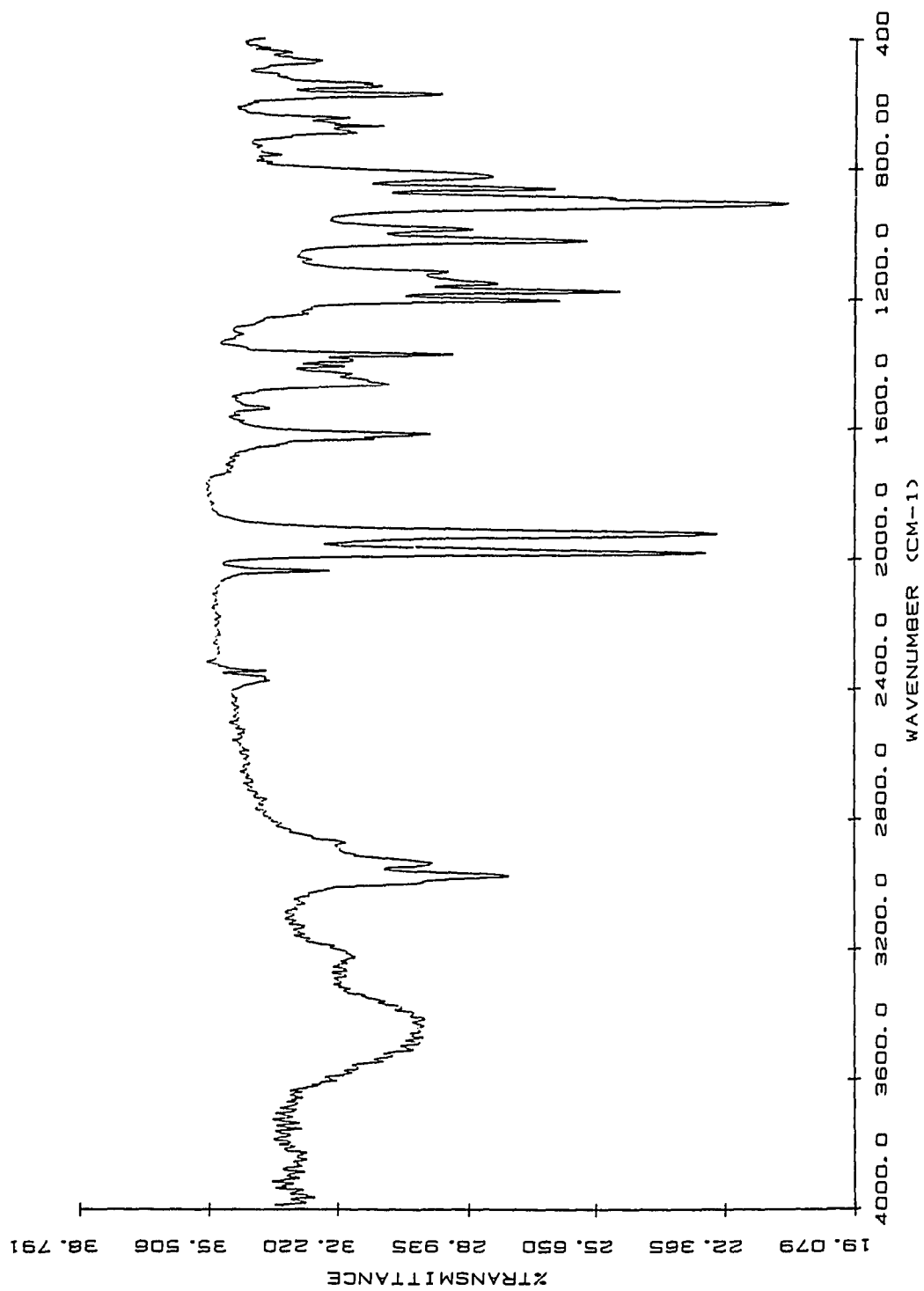
IR Spectrum of $(\text{CO})_4\text{Mo}^i\text{Pr}_2\text{NPO}_4\text{NiCl}_2$



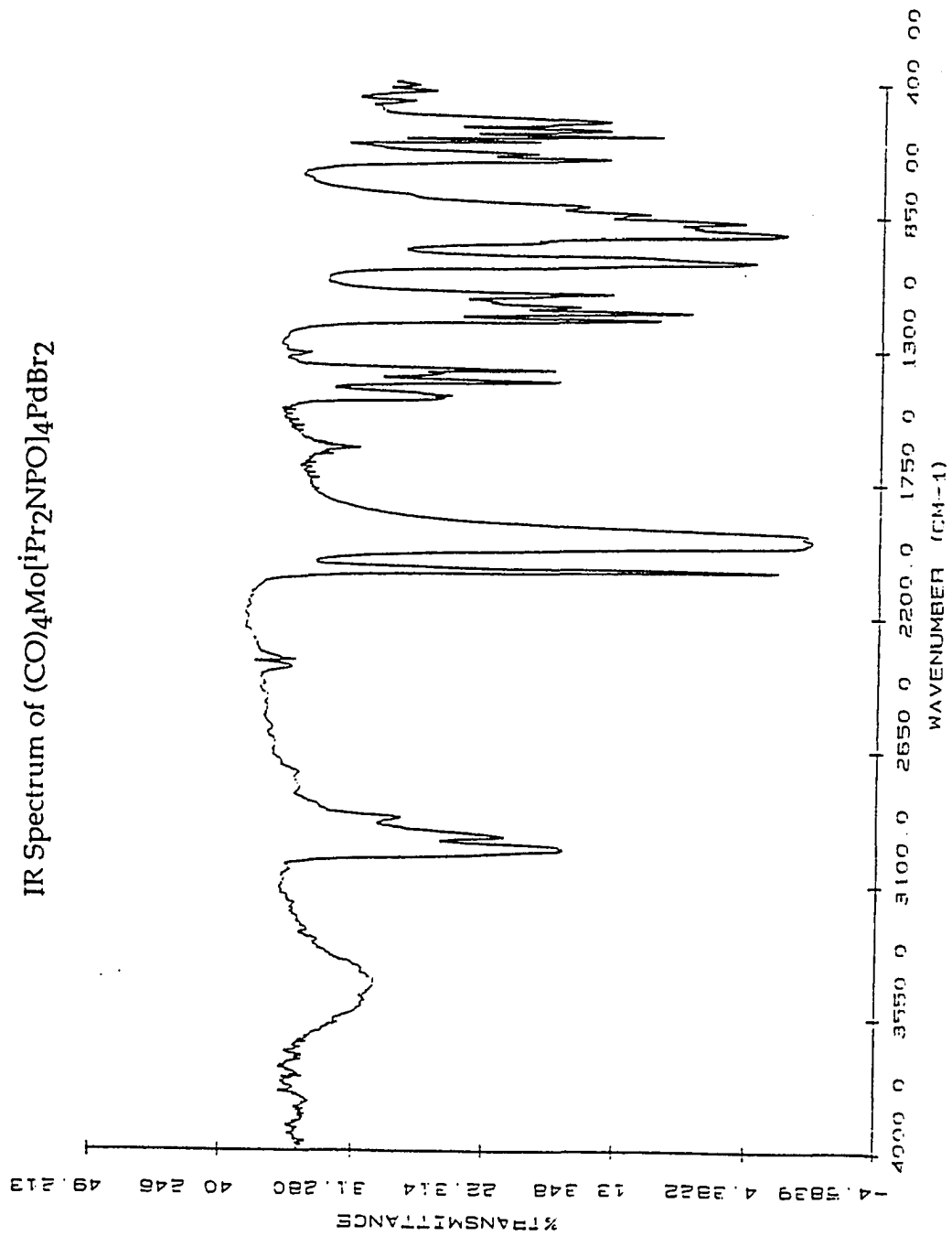
IR Spectrum of $(\text{CO})_4\text{Mo}^{\text{i}}\text{Pr}_2\text{NPO}]_4\text{NiI}_2$



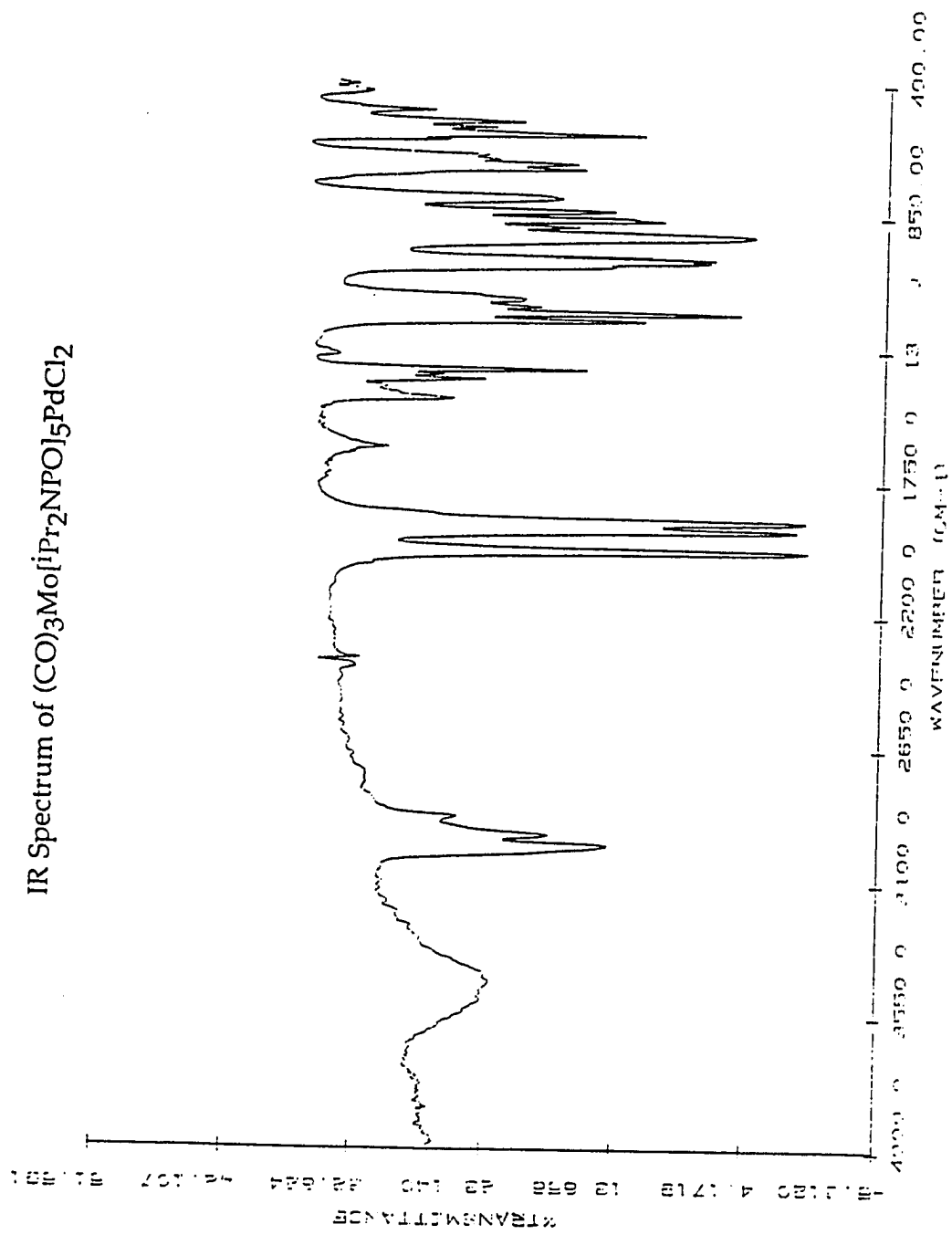
IR Spectrum of $(\text{CO})_2\text{I}_2\text{Mo}[\text{Pr}_2\text{NPO}]_4\text{NiI}_2$



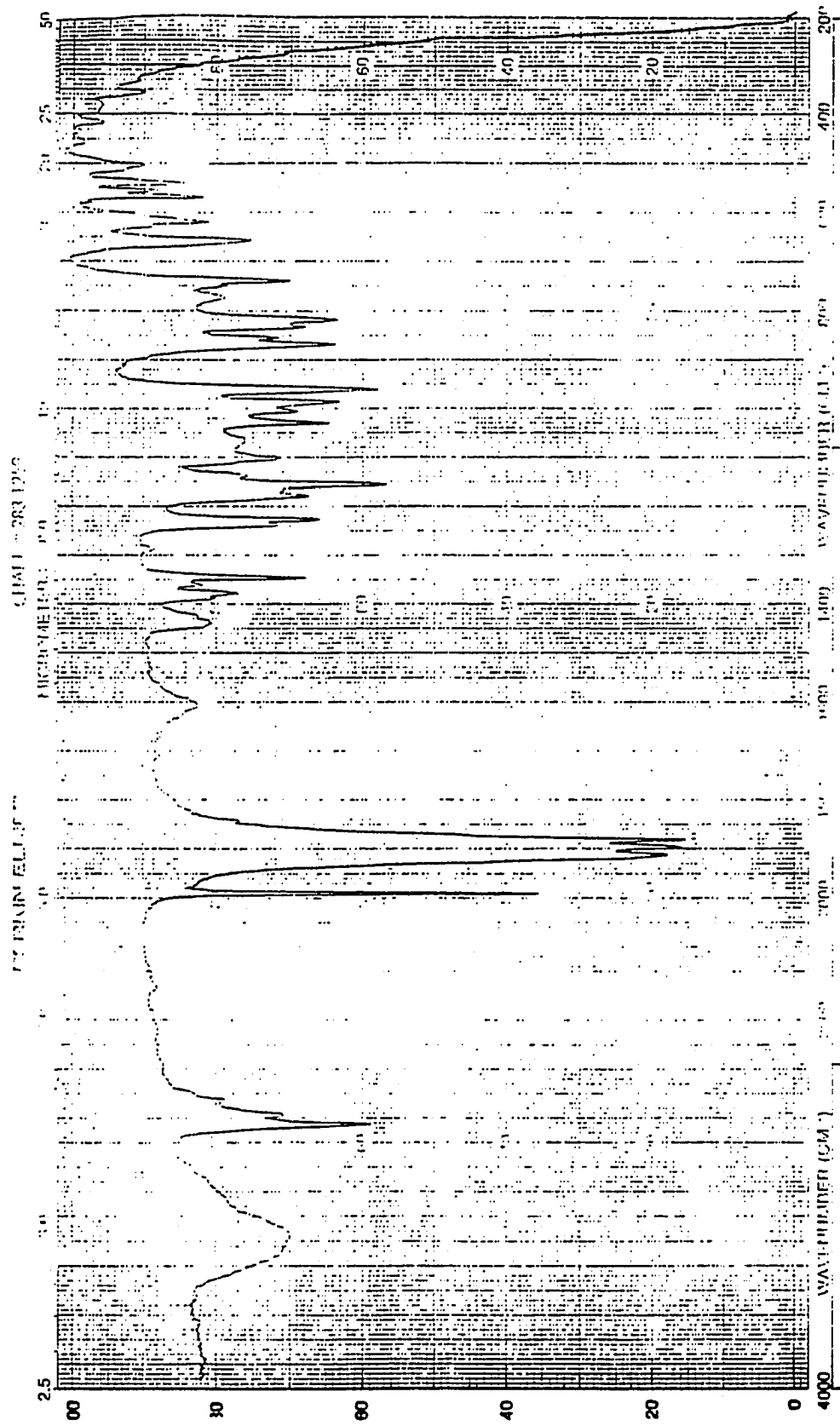
IR Spectrum of $(\text{CO})_4\text{Mo}[\text{iPr}_2\text{NPO}]_4\text{PdBr}_2$



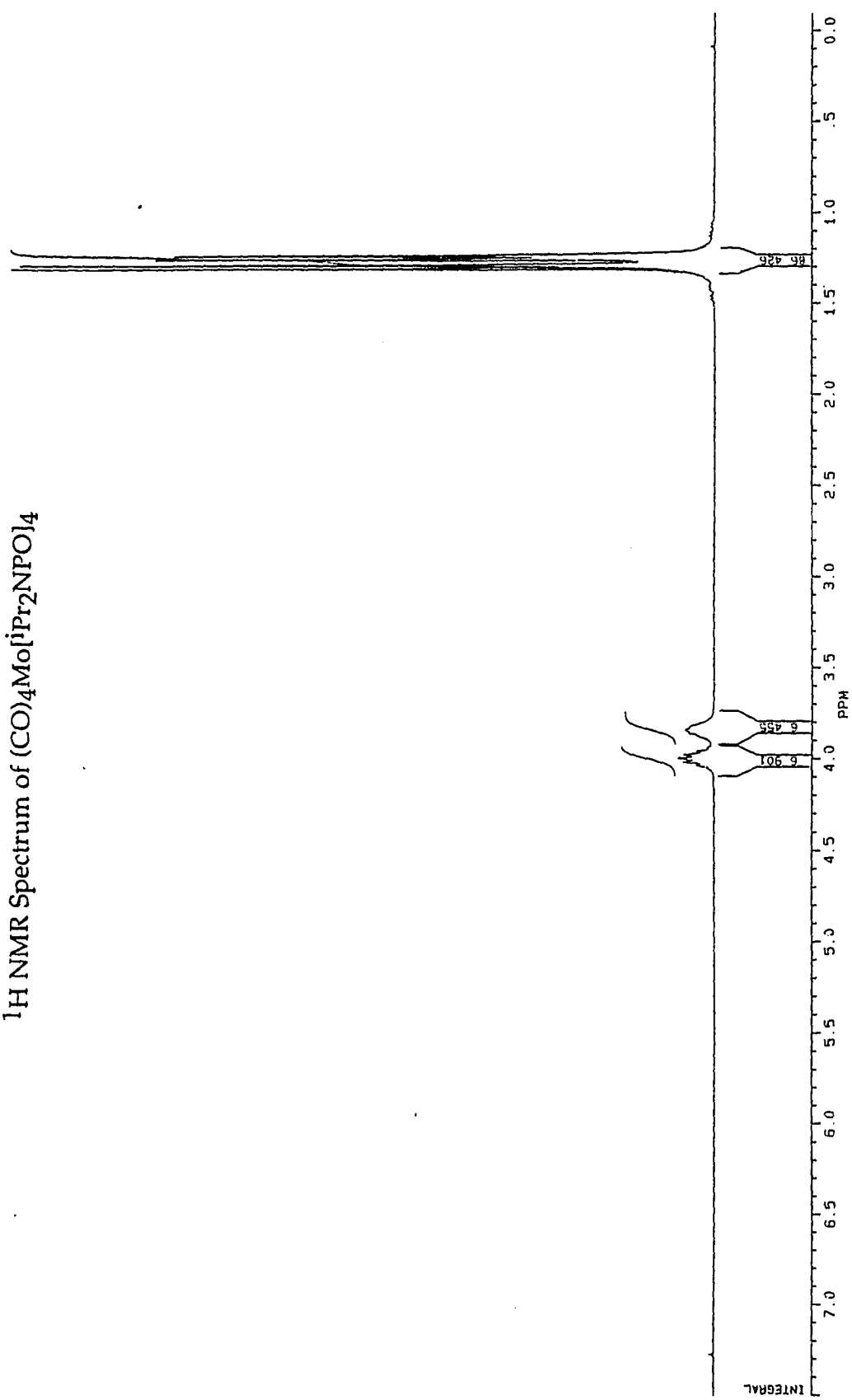
IR Spectrum of $(\text{CO})_3\text{Mo}[\text{iPr}_2\text{NPO}]_5\text{PdCl}_2$



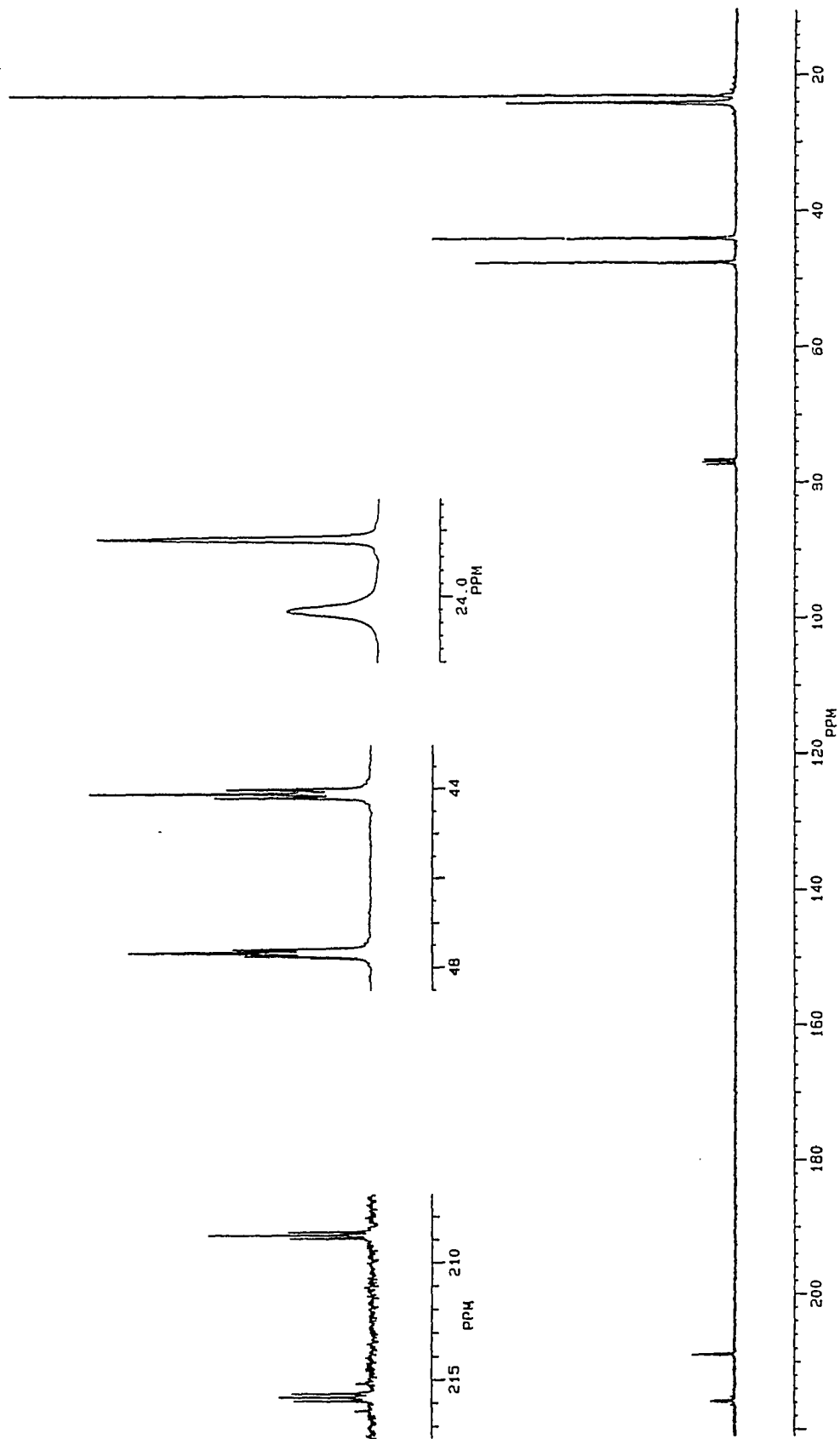
IR Spectrum of $(\text{CO})_4\text{Mo}[\text{iPr}_2\text{NPOMe}]_2(\text{iPr}_2\text{NP(O)H})$



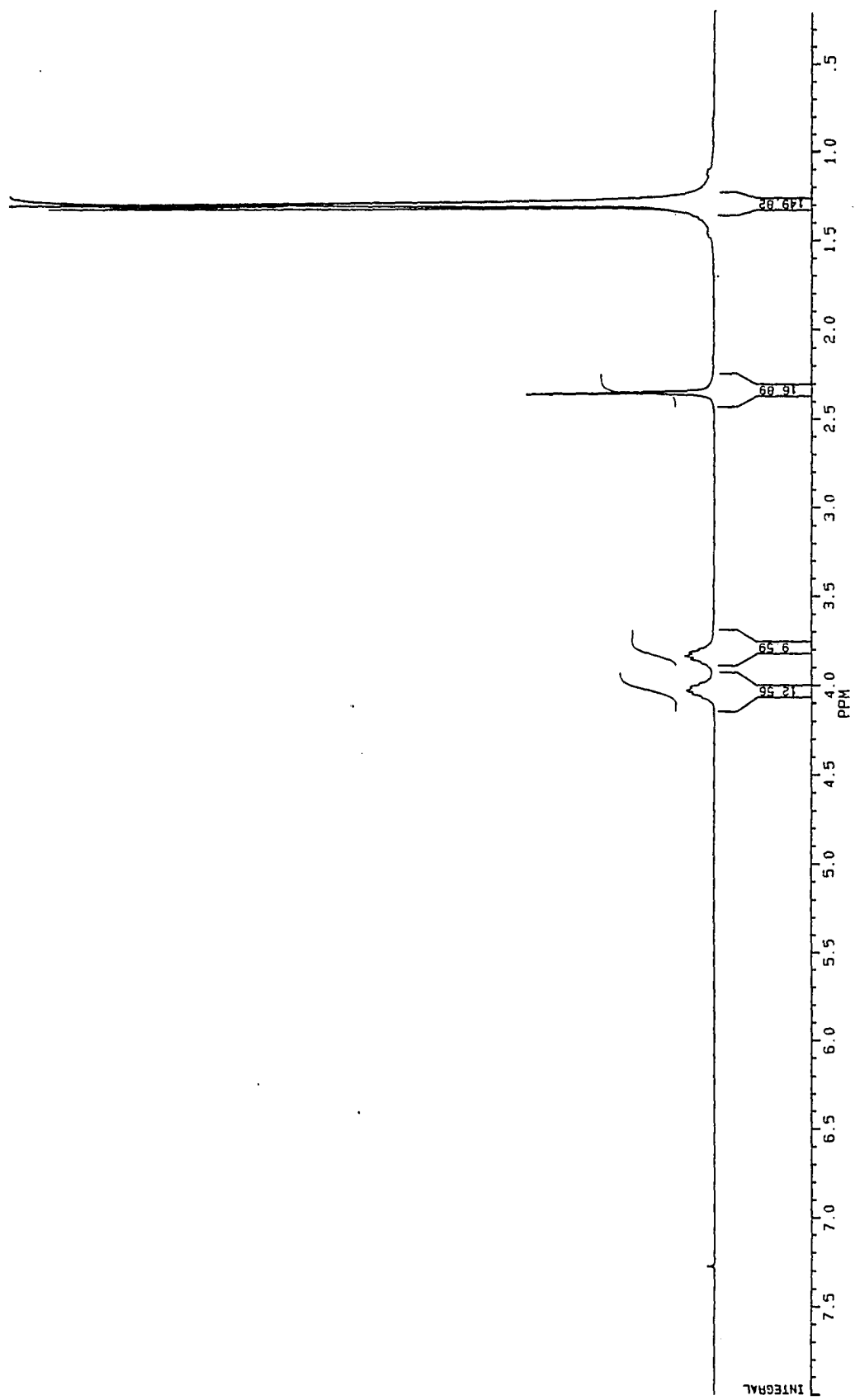
^1H NMR Spectrum of $(\text{CO})_4\text{Mo}[\text{Pr}_2\text{NPO}]_4$



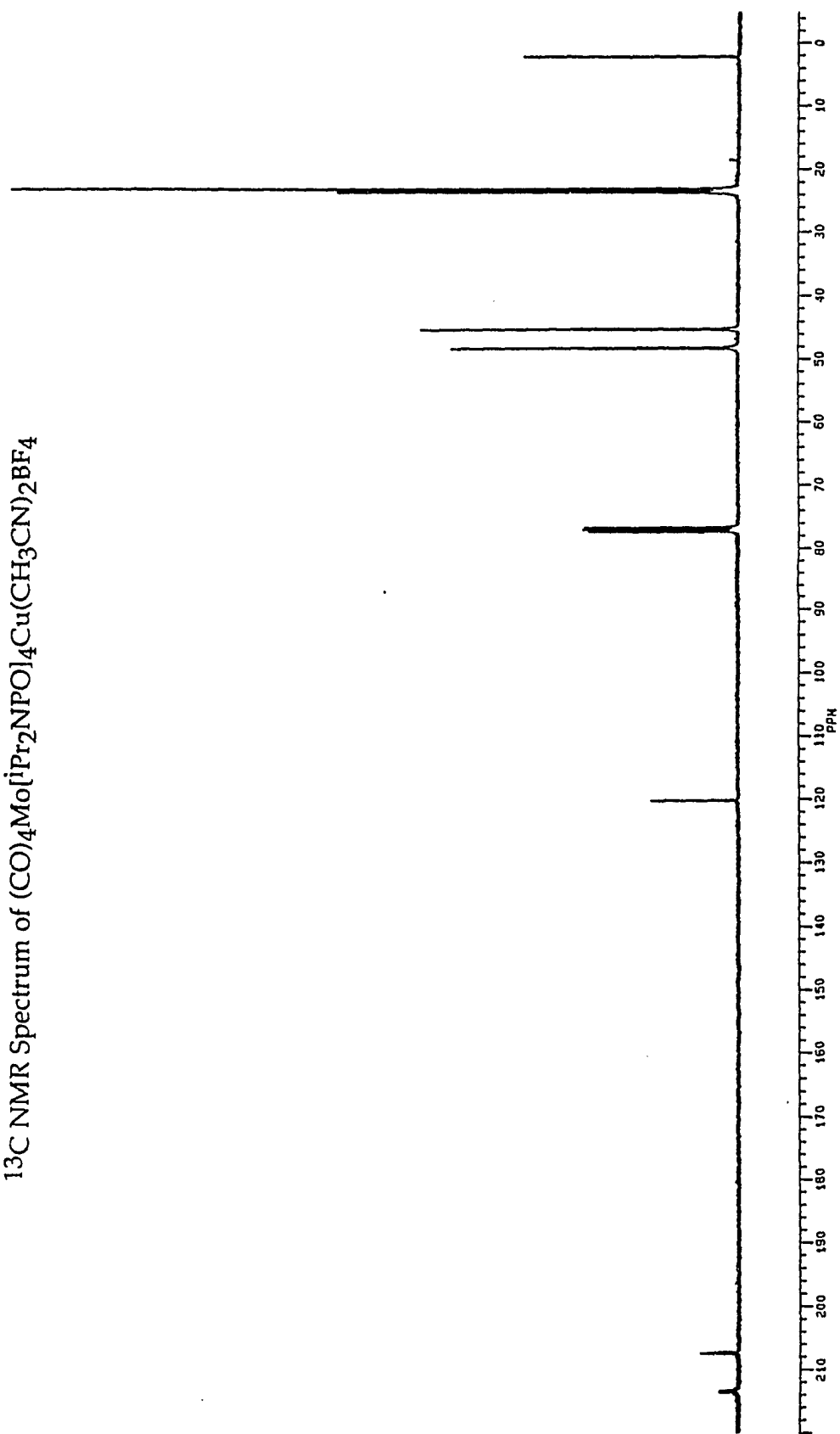
^{13}C (^1H) NMR Spectrum of $(\text{CO})_4\text{Mo}[\text{iPr}_2\text{NPO}]_4$



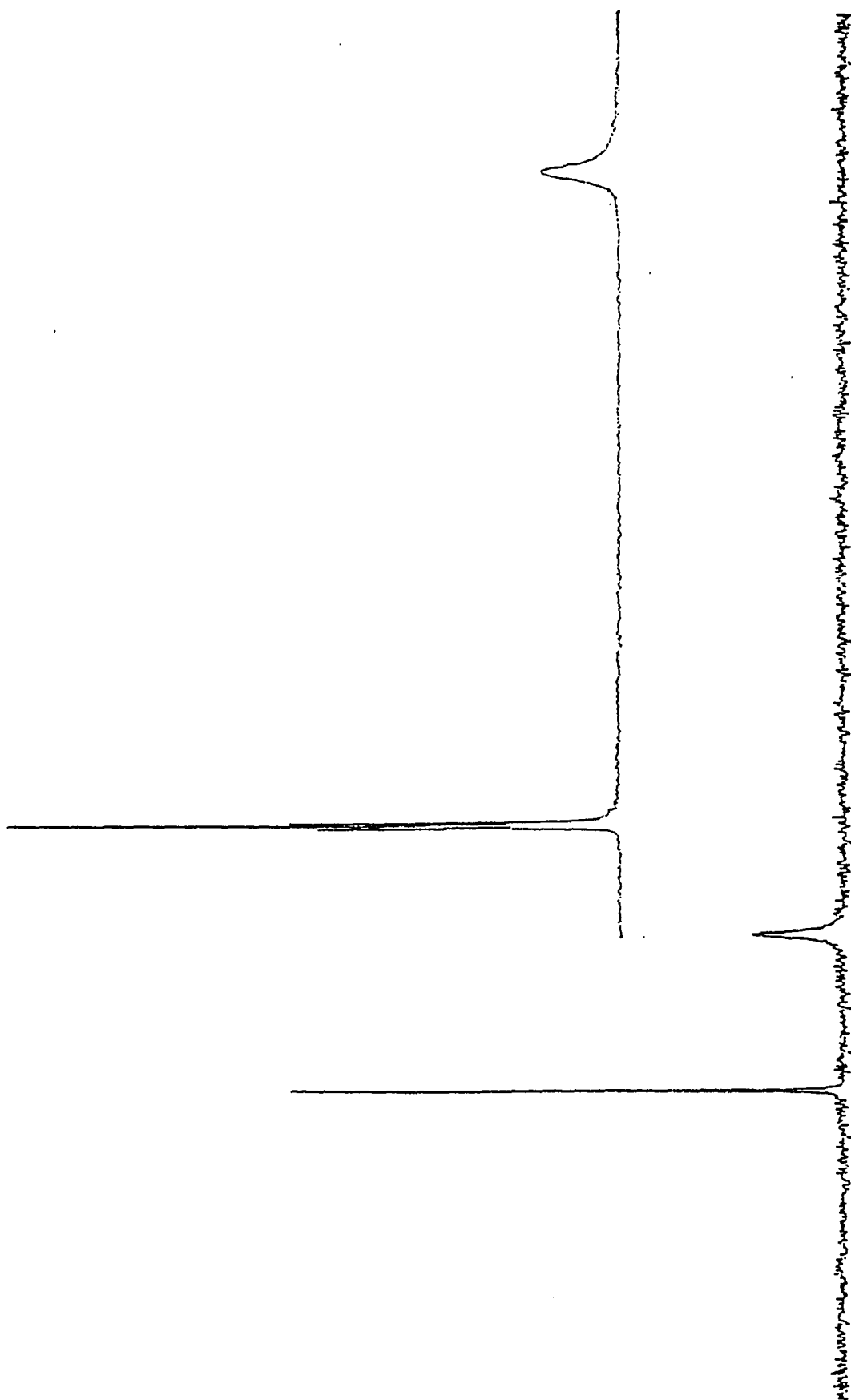
^1H NMR Spectrum of $(\text{CO})_4\text{Mo}[\text{Pr}_2\text{NPO}]_4\text{Cu}(\text{CH}_3\text{CN})_2\text{BF}_4$



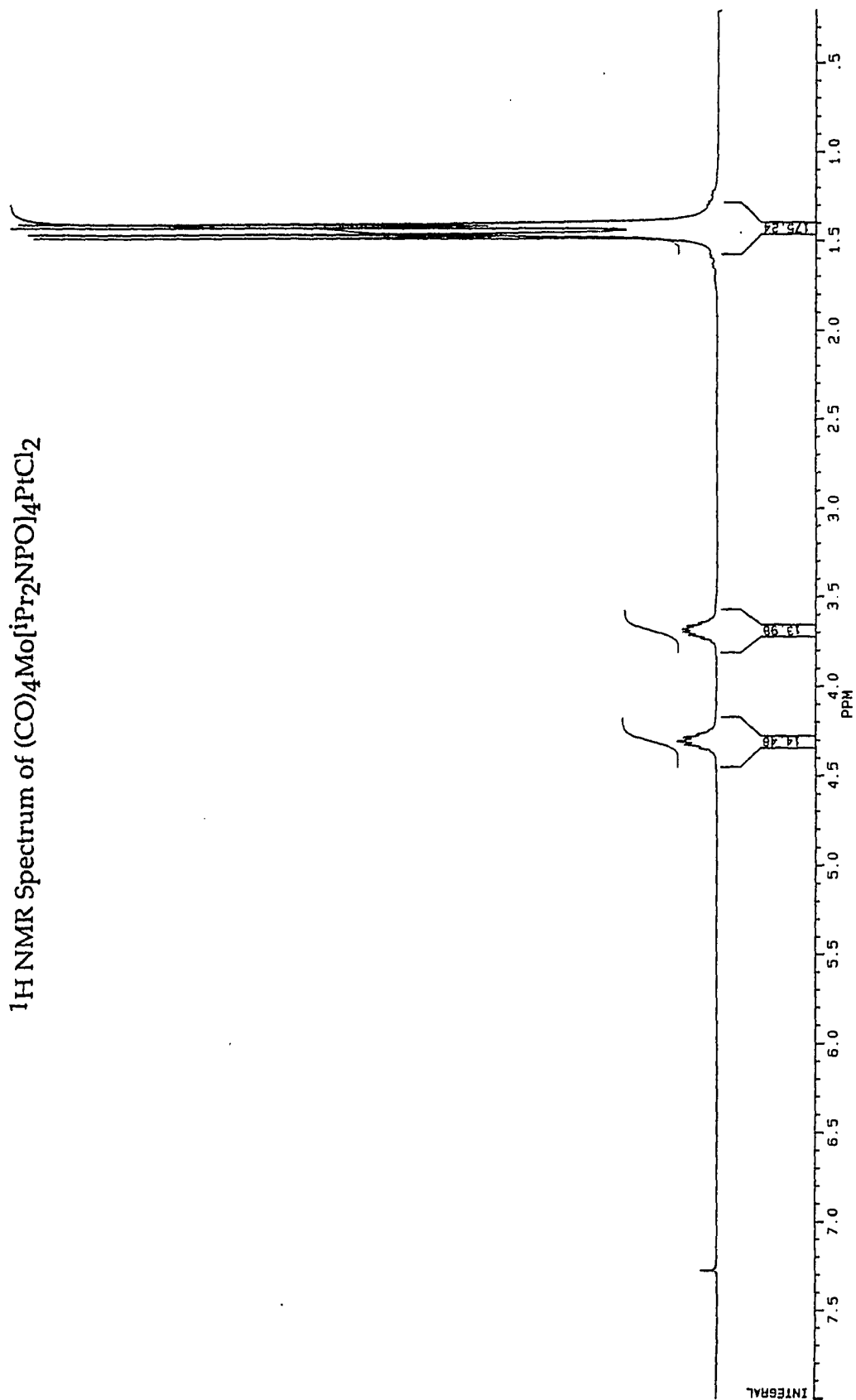
^{13}C NMR Spectrum of $(\text{CO})_4\text{Mo}[\text{Pr}_2\text{NPO}]_4\text{Cu}(\text{CH}_3\text{CN})_2\text{BF}_4$



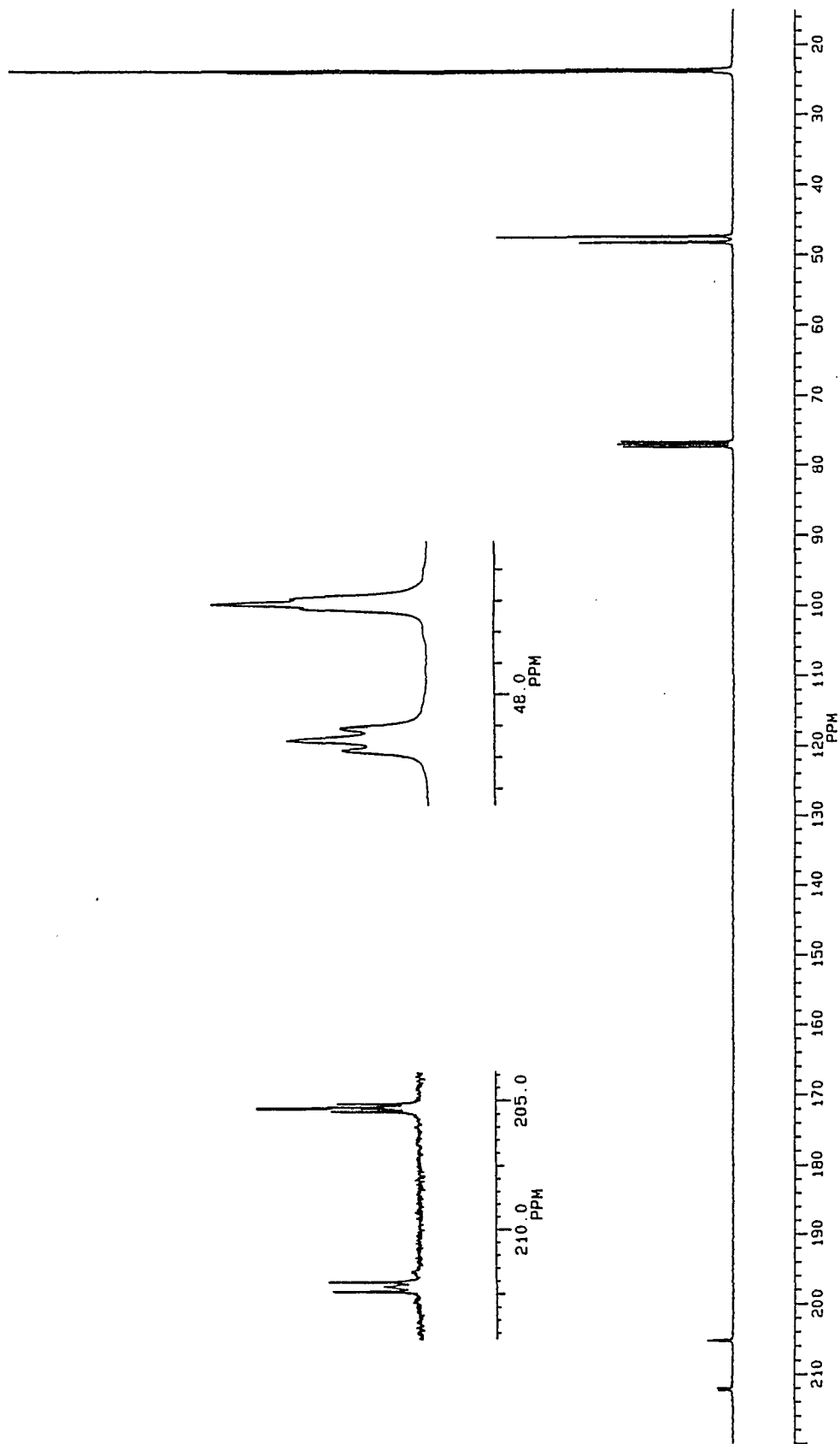
$^{31}\text{P}\{^1\text{H}\}$ NMR Spectrum of $(\text{CO})_4\text{Mo}\{\text{Pr}_2\text{NPO}\}_4\text{Cu}(\text{CH}_3\text{CN})_2\text{BF}_4$



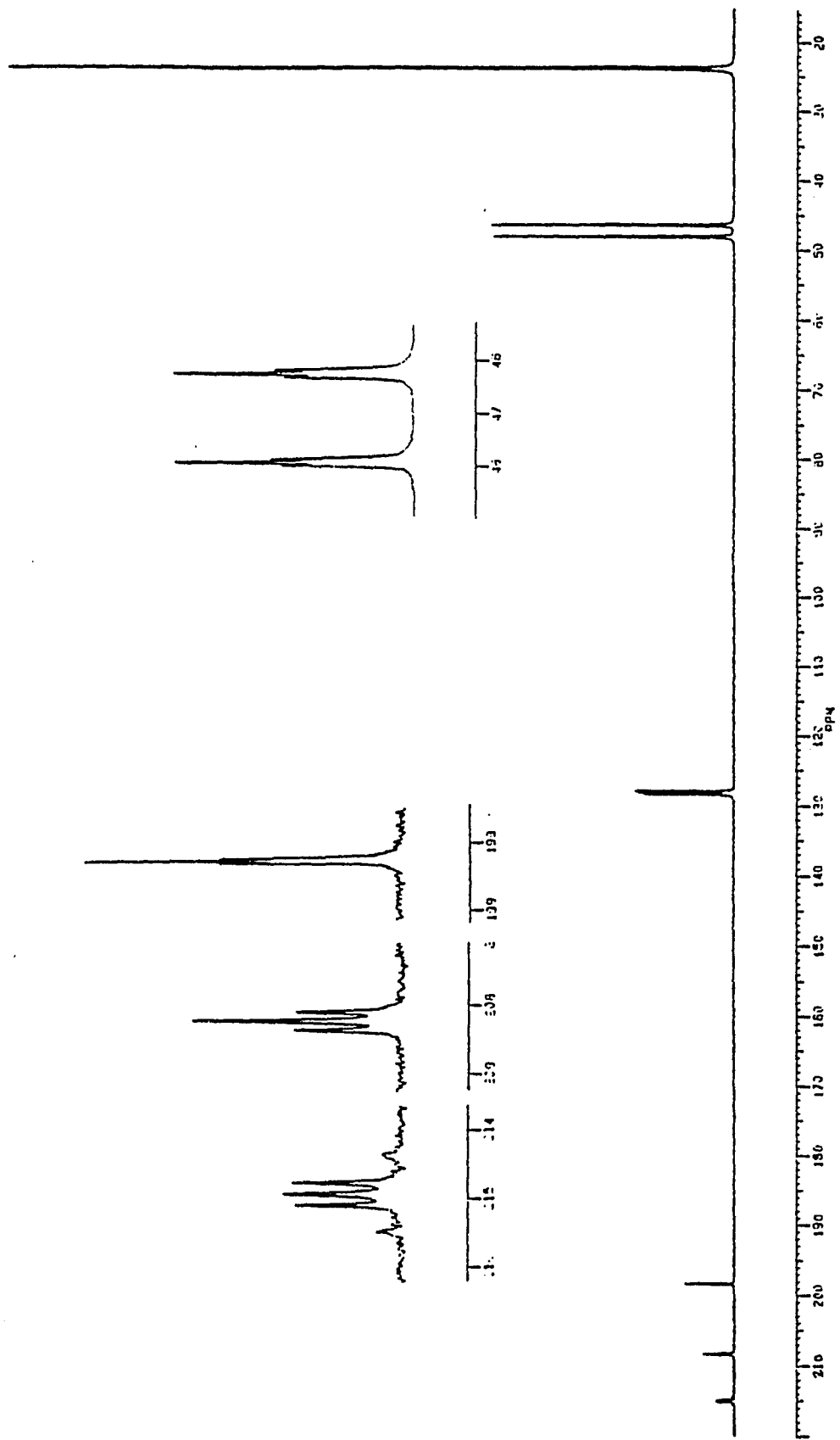
^1H NMR Spectrum of $(\text{CO})_4\text{Mo}[\text{iPr}_2\text{NPO}]_4\text{PtCl}_2$



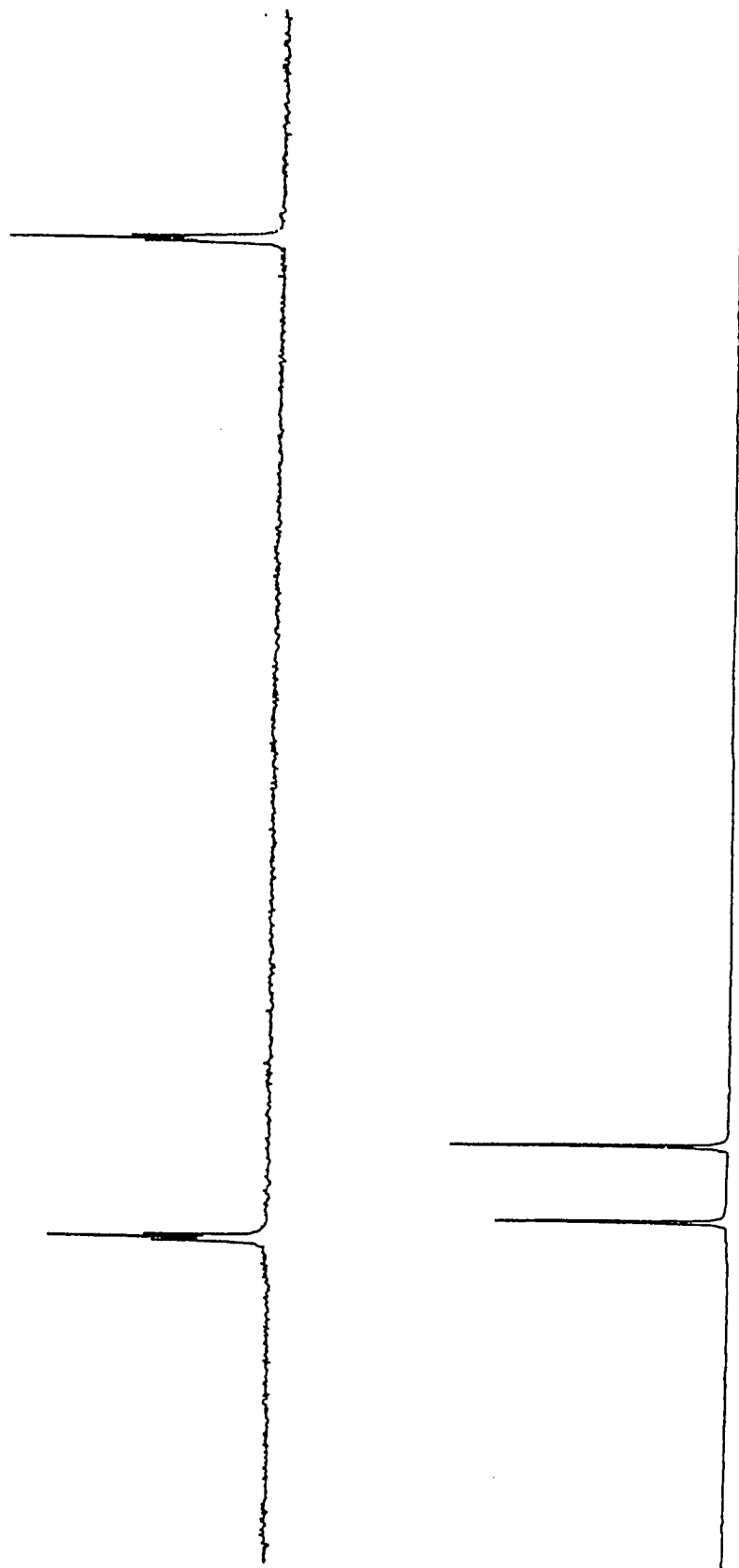
$^{13}\text{C}\{^1\text{H}\}$ NMR Spectrum of $(\text{CO})_4\text{Mo}[\text{Pr}_2\text{NPO}]_4\text{PtCl}_2$



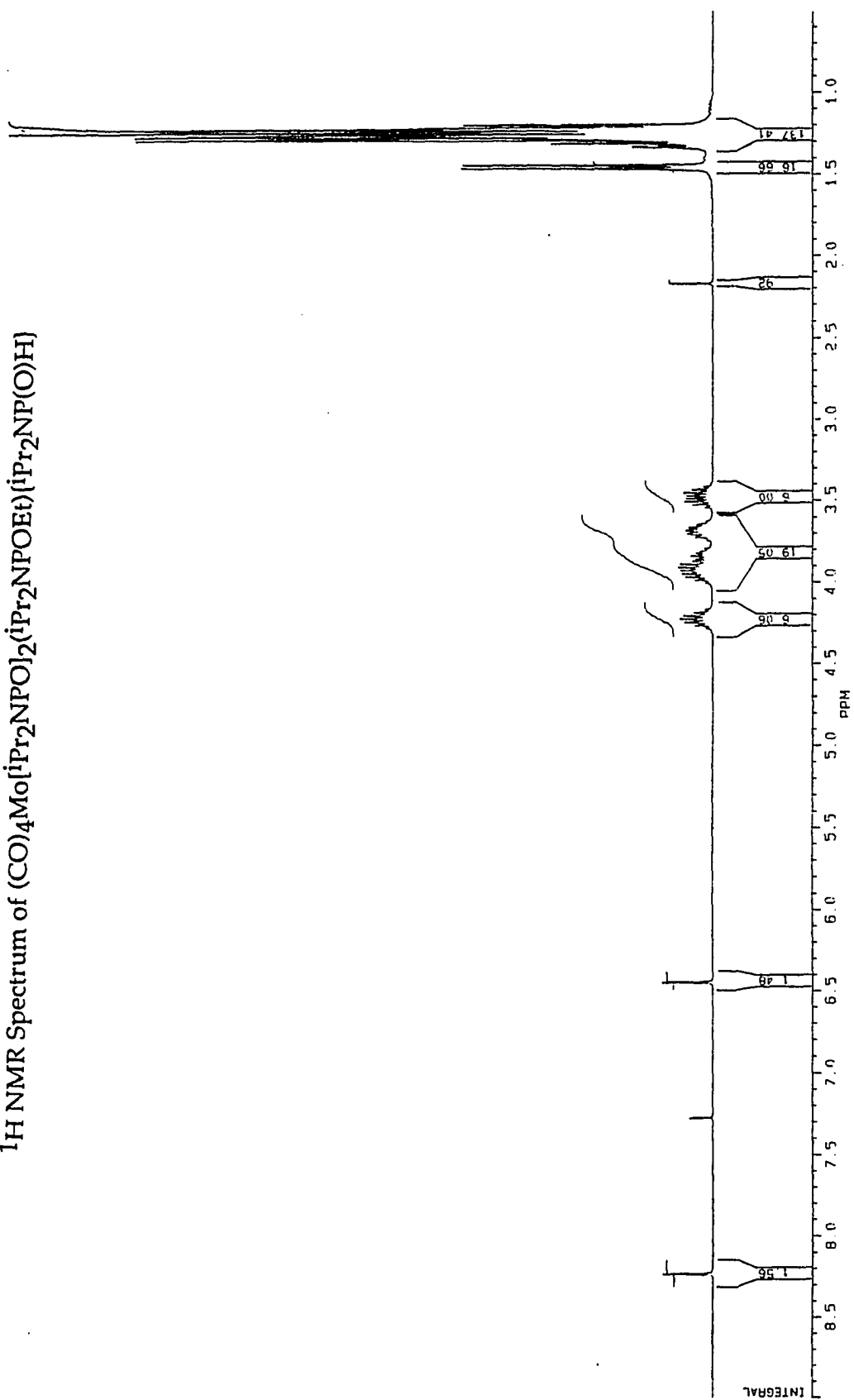
^{13}C NMR Spectrum of $(\text{CO})_4\text{Mo}[\text{iPr}_2\text{NPO}]_4\text{Ni}(\text{CO})_2$



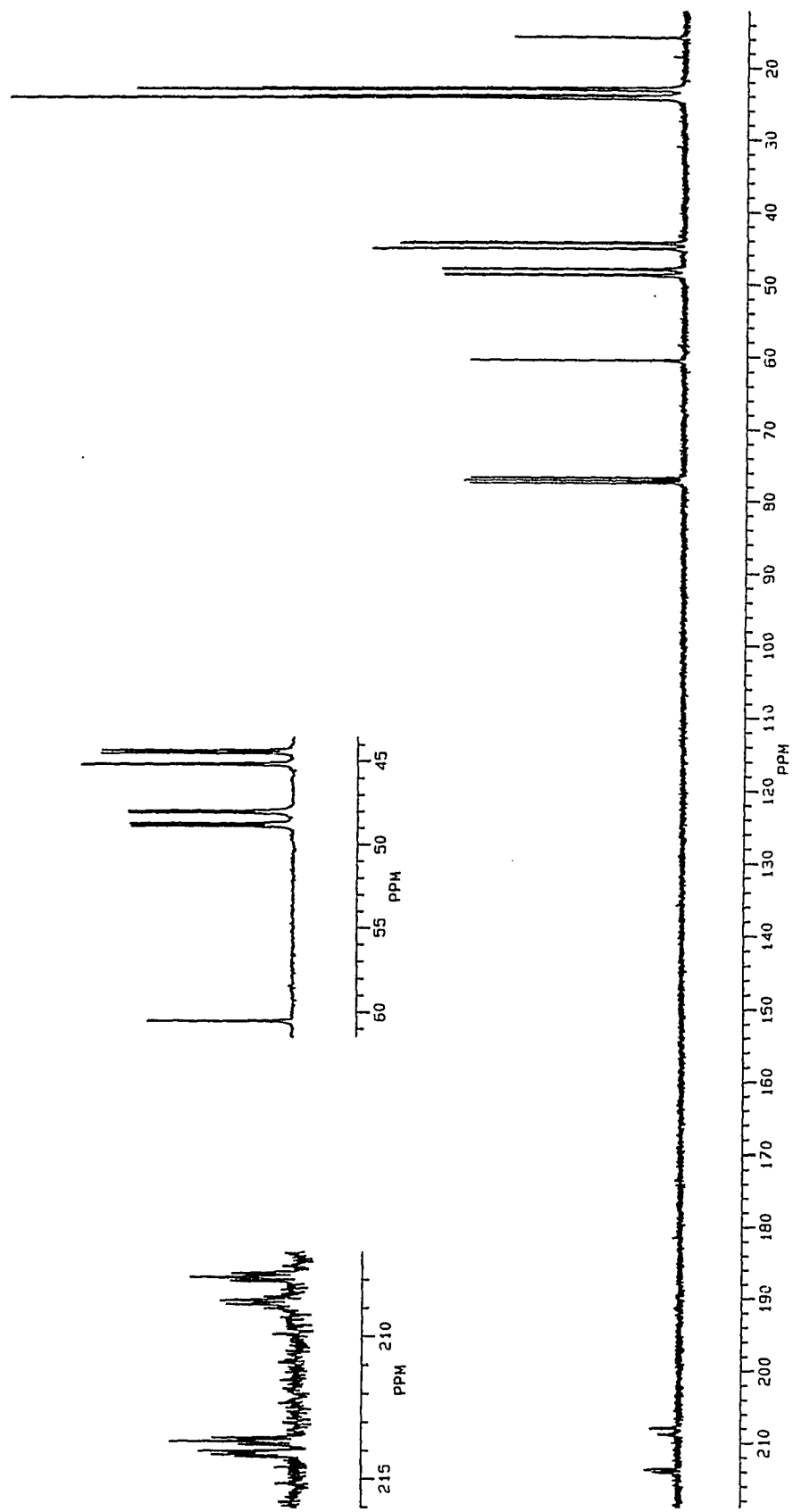
$^{31}\text{P}\{^1\text{H}\}$ NMR Spectrum of $(\text{CO})_3\text{Mo}[\text{iPr}_2\text{NPO}]_5\text{Ni}(\text{CO})_2$



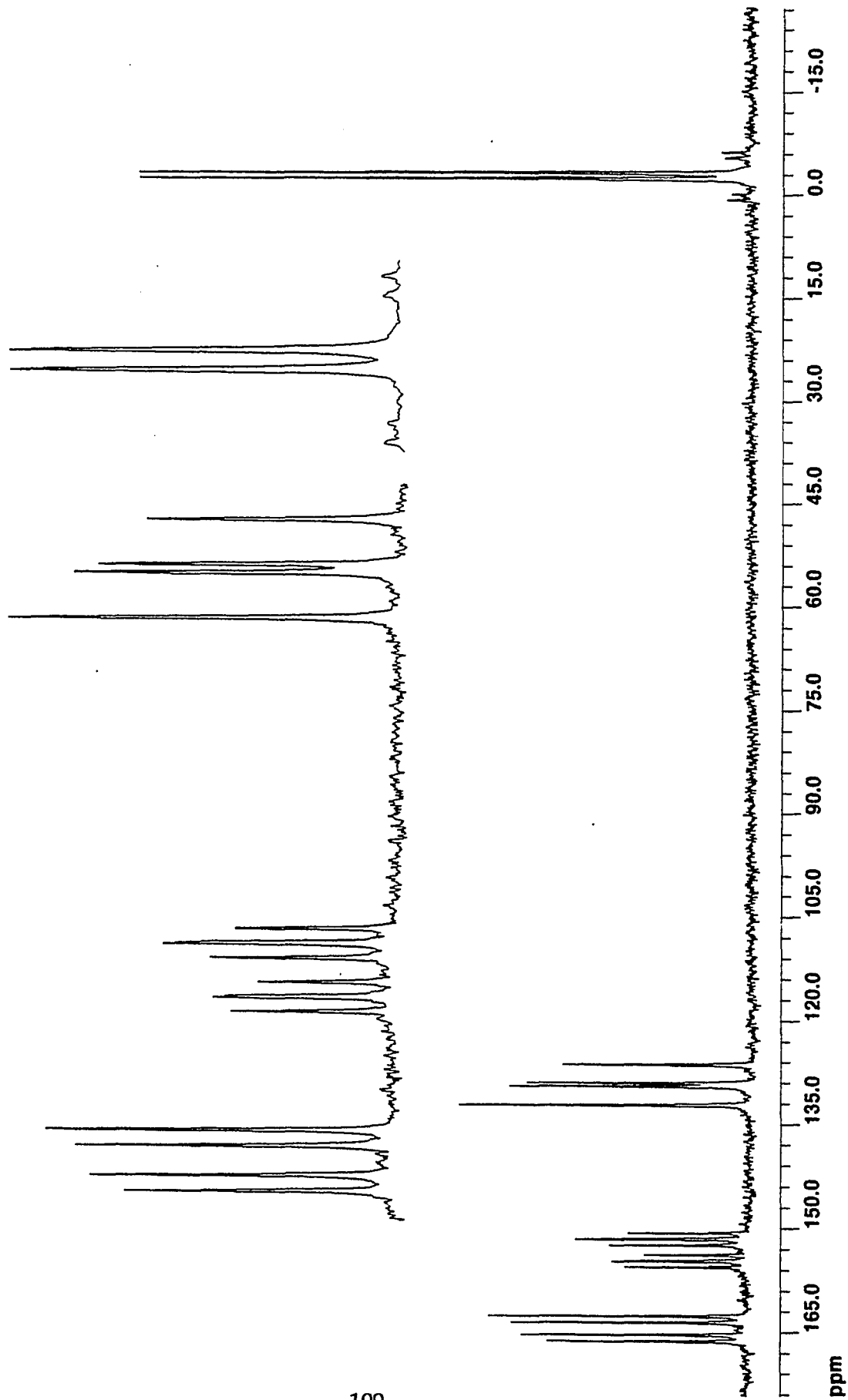
^1H NMR Spectrum of $(\text{CO})_4\text{Mo}(\text{iPr}_2\text{NPOEt})_2(\text{iPr}_2\text{NPOEt})(\text{iPr}_2\text{NP(O)H})$



$^{13}\text{C}\{^1\text{H}\}$ NMR Spectrum of $(\text{CO})_4\text{Mo}(\text{iPr}_2\text{NPO})_2(\text{iPr}_2\text{NPOEt})(\text{iPr}_2\text{NPOEt})\{\text{iPr}_2\text{NP}(\text{O})\text{H}\}$



$^{31}\text{P}\{^1\text{H}\}$ NMR Spectrum of $(\text{CO})_4\text{Mo}[\text{iPr}_2\text{NPO}_2]_2(\text{iPr}_2\text{NPOEt})(\text{iPr}_2\text{NP(O)H})$



^{31}P NMR Spectrum of $(\text{CO})_4\text{Mo}[\text{iPr}_2\text{NPO}]_2(\text{iPr}_2\text{NPOEt})(\text{iPr}_2\text{NP}(\text{O})\text{H})$

